Radboud Repository

Radboud University Nijmegen

PDF hosted at the Radboud Repository of the Radboud University Nijmegen

The following full text is a publisher's version.

For additional information about this publication click this link.
http://hdl.handle.net/2066/18801

Please be advised that this information was generated on 2017-12-05 and may be subject to change.

From Crystal Structure to Morphology

The Implications of Multiple Connected Nets

Reinier Grimbergen

Grimbergen, Reinier Franciscus Petrus
From Crystal Structure to Morphology
The Implications of Multiple Connected Nets
Thesis Nijmegen - with ref. - with summary in Dutch
ISBN 90-9011546-3
Subject Headings: crystallization / morphology / modelling

The work presented in this thesis was financially supported by the Dutch Technology Foundation (SON/STW) under project nr. 349-3166.

From Crystal Structure to Morphology
The Implications of Multiple Connected Nets

een wetenschappelijke proeve op het gebied van
de Natuurwetenschappen

Proefschrift

ter verkrijging van de graad van doctor
aan de Katholieke Universiteit Nijmegen,
volgens besluit van het College van Decanen
in het openbaar te verdedigen op
maandag 25 mei 1998,
des namiddags om 3.00 uur precies

door

Reinier Franciscus Petrus Grimbergen

geboren op 8 december 1969
te Nijmegen

Promotor:	Prof. Dr. P. Bennema
Co-promotor:	Dr. H.L.M. Meekes
Manuscriptcommissie:	Prof. Dr. J.P.J.M. van der Eerden (UU) Prof. Dr. E. Vlieg Dr. R.M. Geertman (Akzo-Nobel, Arnhem)

aan mijn ouders,
voor Carlijn

Voorwoord

Met het gereedkomen van dit proefschrift is niet alleen een einde gekomen aan vier jaar onderzoek, maar ook aan vier mooie jaren op "de afdeling". Met name de goede sfeer bij Vaste Stof Chemie heeft ervoor gezorgd dat ik geen dag met tegenzin naar het lab ben gegaan. Daarvoor wil ik allereerst al mijn collega's van de afgelopen jaren bedanken. De aanzet tot deze prettige atmosfeer werd gemaakt door prof. Bennema. Beste Piet, jouw enthousiasme en openheid zouden een voorbeeld moeten zijn voor andere "hooggeleerden". Met de komst van Elias is er wat dat betreft in ieder geval in de toekomst ook veel goeds te verwachten.

De dagelijkse begeleiding van mijn project lag in handen van dr. "H.K.L.M." Meekes. Van Hugo heb ik veel (ook over mezelf) geleerd. Onze gesprekken over muziek en het "ad mensam ire" op dinsdag zal ik niet snel vergeten, net als de koffieclub bij Jan iedere morgen. De (overigens gezonde) kritische houding van Willem van Enckevort t.o.v. connected netten en PBC's heeft voor mij stimulerend gewerkt om het nut ervan steeds weer opnieuw aan te tonen. Het doet mij dan ook deugd te zien dat hij F-en S- en K-faces nu heeft vertaald naar f- en k-steps [1].

Vanaf deze plaats wil ik ook de leden van de gebruikerscommissie te weten Jan van der Eerden (UU), Jan Meier (Akzo-Nobel), Rob Geertman (Akzo-Nobel), Joost Moonen (DSM), Hans Human (Unilever), Gertjan Witkamp (TU Delft) en Tanja Kulkens (SON-STW) bedanken voor hun interesse in het project en de nuttige tips tijdens de regelmatige bijeenkomsten. De leden van de manuscriptcommissie Jan van der Eerden, Elias Vlieg en Rob Geertman dank ik voor het kritisch lezen van het manuscript en de suggesties voor verbeteringen.

Natuurlijk is er ook veel wetenschappelijke samenwerking geweest. Op de eerste plaats wil ik alle leden van de Graph Club bedanken voor de vele (vaak langdurige) interessante discussies over de fundamenten van de Hartman-Perdok theorie. Deze hebben uiteindelijk geresulteerd in hoofdstuk 2,3 en 4. Een vervolg daarop waren een aantal sessies met Hubert Knops en Marcel den Nijs met als resultaat hoofstuk 5. Marianne Reedijk wil ik bedanken voor haar inzet tijdens haar hoofdvakstage, hetgeen heeft geresulteerd in een mooie paper [Grimbergen et al., 1998c] (hoofdstuk 5). De hoofdstukken 6 en 7 zijn tot stand gekomen in een prettige samenwerking met Peter van Hoof. Met Erwin van den Berg heb ik nog gewerkt aan de morfologie ϵ-caprolactam kritallen in vervolg op het werk van Rob Geertman (hoofdstuk 9). Het ongetwijfeld meest langdurige project is dat van de morfologie van lysozyme (hoofdstuk 10). Zover ik me kan herinneren is Edo er bijna vijf jaar geleden ooit aan begonnen. Dat brengt me tenslotte bij het "geweldige" cesium halide project met Gertjan Bögels, ook wel bekend als "master of twinning" (hoofdstuk 11). Ondanks het feit dat hij al meer dan genoeg publicaties heeft om te promoveren, was hij bereid zijn medewerking te verlenen.

Tijdens mijn bezoeken aan MSI in Cambridge i.v.m. de implementatie van FACELIFT [Grimbergen et al., 1997] in Cerius^2 [MSI,] was er ook altijd een bezoek aan Edo en

[1] *Facets of 40 years of crystal growth, a tribute to Piet Bennema' on the occasion of his retirement*, Ed. W.J.P. van Enckevort, H.L.M. Meekes en J.W.M. van Kessel, p. 51-70

Corinne gepland. De lange discussies over het leven, muziek en wetenschap onder het genot van een sigaar en een smakelijke malt whisky wil ik nog graag blijven voortzetten in de toekomst. I would like to thank Frank Leusen, Steffen Wilke and Gerhard Engel of Molecular Simulations Inc. for the fruitful cooperation in the implementation of the FACELIFT program in the Cerius[2] environment. Verder wil ik Steef Boerrigter bedanken voor het introduceren van een aantal nuttige verbeteringen en extra functionaliteit in FACELIFT. Tenslotte is er nog een vruchtbaar uitstapje gemaakt naar de wereld van de monolagen op goud door een succesvolle samenwerking met Joeri Voets en Jan Gerritsen [Voets et al., 1998].

Naast de afdeling waren er gedurende de afgelopen vier jaar ook nog een aantal andere mensen met wie ik buiten het lab ben opgetrokken. Daarbij denk ik op de eerste plaats aan mijn roeimaten van NTNT: Arthur, Bert en Marc die ervoor hebben gezorgd dat er méér was dan wetenschap alleen. Verder waren de wekelijkse repetities bij het Nijmeegs Studentenkoor Alphons Diepenbrock een ware verademing na een lange dag werken. Een aardige bijkomstigheid is dat Piet van Kalmthout, tevens lid van het koor, mij heeft laten zien dat kristallen ook zeer fraai kunnen zijn [2].

Tot slot wil ik mijn broer Joris bedanken voor zijn mentale steun en zijn correcties van het manuscript en mijn ouders voor de nooit aflatende interesse en steun met name in de laatste maanden. Mijn liefste Carlijn heeft bewezen dat de stelling: *de vrouw is de zandbank der wetenschap* [3], zeker niet altijd opgaat. Zij is mijn veilige haven gebleken!

Reinier

[2] *Laurion, the minerals in the ancient slags*, Piet Gelaude, Piet van Kalmthout en Christiaan Rewitzer
[3] *Cicero*

Contents

1 Introduction **1**

2 On the Prediction of Crystal Morphology I: The Hartman-Perdok Theory revisited **7**

2.1 History of crystallography and morphology 9
2.1.1 Bravais, Friedel, Donnay and Harker (BFDH) 9
2.1.2 Hartman-Perdok theory 10
2.1.3 Equilibrium forms and growth forms 12
2.1.4 Theory of roughening transition 12
2.2 Derivation of F-faces based on crystallography and the concept of roughening 14
2.2.1 Definition of F-face 14
2.2.2 Discussion of connected nets and F-faces 16
2.3 Symmetry of connected nets 22
2.3.1 Broken bond description 22
2.3.2 Influence of a mother phase 23
2.4 Discussion and conclusion 24

3 On the Prediction of Crystal Morphology II: Symmetry Roughening of Pairs of Connected Nets **27**

3.1 Introduction 28
3.2 Symmetry roughening 29
3.3 Possible cases of symmetry roughening 31
3.3.1 Relevant symmetry 31
3.3.2 Orientation 32
3.3.3 Orientation conserving symmetries ($\boldsymbol{k}' = \boldsymbol{k}$) 33
3.3.4 Orientation inverting symmetries ($\boldsymbol{k}' = -\boldsymbol{k}$) 36
3.4 The presence of a mother phase 38
3.5 More complicated crystal graphs 39
3.6 Discussion 41
3.7 Conclusion 43

4 On the Prediction of Crystal Morphology III: Equilibrium and Growth Behaviour of Crystal Faces containing Multiple Connected Nets **47**
4.1 Introduction . . . 48
4.2 Model crystal graphs . . . 49
4.3 Connected net analysis . . . 51
4.3.1 Types I and II . . . 51
4.3.2 Type III . . . 51
4.3.3 Type IV . . . 53
4.4 Monte Carlo simulations . . . 53
4.4.1 Simulation setup . . . 53
4.4.2 Equilibrium results . . . 56
4.4.3 Off-equilibrium results . . . 59
4.5 Implications for the morphology . . . 64
4.6 Discussion and Conclusion . . . 67

5 Preroughening in Organic Crystals **69**
5.1 Introduction . . . 70
5.2 Description of the model . . . 71
5.3 The Phase Diagram . . . 74
5.4 MC simulations . . . 78
5.4.1 Computational Method . . . 78
5.4.2 Surface Transitions . . . 79
5.4.3 Dynamics . . . 82
5.5 Discussion and Conclusion . . . 84

6 Growth behaviour of Crystal Faces containing Symmetry Related Connected Nets: a Case Study of Naphthalene and Anthracene **87**
6.1 Introduction . . . 88
6.2 Theoretical morphology . . . 90
6.2.1 Crystal Graph . . . 90
6.2.2 Connected nets of naphthalene and anthracene . . . 92
6.2.3 Multiple connected nets . . . 94
6.3 Experimental . . . 96
6.3.1 Vapour growth . . . 96
6.3.2 Solution growth . . . 97
6.3.3 Results . . . 98
6.4 Discussion . . . 103
6.5 Conclusions . . . 105

7 Morphology of Orthorhombic n-Paraffin Crystals I: the Influence of Multiple Connected Nets **107**
7.1 Introduction . . . 108
7.2 Connected net analysis and roughening . . . 109
7.2.1 Thermal roughening . . . 110
7.2.2 Kinetic roughening . . . 110
7.2.3 Construction of the morphology . . . 111
7.3 Crystal graph of orthorhombic paraffin . . . 112
7.4 Connected nets and symmetry relations . . . 114
7.4.1 The {001} form . . . 114
7.4.2 The {100} form . . . 116
7.4.3 The {110} form . . . 117
7.4.4 The {111} form . . . 119
7.4.5 The {010} form . . . 119
7.4.6 The {112}, {211} and {210} form . . . 120
7.4.7 The {102}, {021}, {120} and {121} form . . . 120
7.4.8 The {011} and {101} form . . . 120
7.4.9 Anisotropy and roughening temperatures T^R_{hkl} . . . 121
7.5 Predicted morphology . . . 122
7.6 Discussion . . . 124
7.7 Conclusion . . . 126

8 Morphology of Orthorhombic n-Paraffin Crystals II: a Comparison between Theory and Experiments **127**
8.1 Introduction . . . 128
8.2 Predicted morphology . . . 129
8.2.1 Introduction . . . 129
8.2.2 Growth morphology . . . 131
8.3 Experimental setup . . . 133
8.3.1 Vapour growth . . . 133
8.3.2 Solution growth . . . 134
8.3.3 Melt growth . . . 134
8.4 Experimental results . . . 135
8.4.1 Vapour growth . . . 135
8.4.2 Solution growth . . . 137
8.4.3 Melt growth . . . 138
8.5 Discussion . . . 139
8.5.1 Morphology of vapour grown crystals . . . 139
8.5.2 Morphology of solution grown crystals . . . 140
8.5.3 Morphology of melt grown crystals . . . 141
8.6 Conclusions . . . 141

9 Theoretical Morphology of ϵ-Caprolactam: Monomer versus Dimer Analysis **143**
9.1 Introduction . . . 144
9.2 Connected net analysis . . . 144
9.3 Crystal graph . . . 146
9.3.1 Crystal structure . . . 146
9.3.2 Calculation of the bonds . . . 146
9.3.3 The monomer graph . . . 148
9.3.4 The dimer graph . . . 148
9.4 Results . . . 149
9.5 Comparison with previous PBC analyses . . . 149
9.6 Discussion . . . 151
9.7 Conclusions . . . 153

10 Explanation for the Supersaturation Dependence of the Morphology of Lysozyme Crystals **155**
10.1 Introduction . . . 156
10.2 Connected net analysis . . . 158
10.3 Step energy analysis . . . 160
10.4 Disordered flat phases . . . 162
10.5 Discussion . . . 163
10.5.1 Growth rates . . . 164
10.5.2 Surface structure . . . 167
10.6 Conclusions . . . 167

11 The Growth Morphology of Cesium Halide Crystals Evidence for Surface Phase Transitions **169**
11.1 Introduction . . . 170
11.2 Connected net analysis . . . 171
11.2.1 The (001) orientation . . . 172
11.2.2 The (110) orientation . . . 173
11.2.3 The (111) orientation . . . 173
11.2.4 Surface reconstruction . . . 174
11.2.5 Theoretical growth morphology . . . 175
11.3 Monte Carlo simulations . . . 176
11.3.1 Setup . . . 176
11.3.2 Equilibrium . . . 179
11.3.3 Dynamics . . . 180
11.4 Experimental . . . 181
11.5 Experimental results . . . 183
11.5.1 Morphology as a function of driving force . . . 184
11.5.2 Morphology as a function of the furnace temperature . . . 185
11.6 Discussion . . . 186
11.7 Conclusion . . . 187

References 195

Summary 200

Samenvatting 204

List of Publications 207

Curriculum Vitae 207

Chapter 1

Introduction

Introduction

Mankind has always been intrigued by the very beautiful flat shiny facets on various mineral crystals found in nature. In the eighteenth century the science of crystallography started when Haüy discovered that these facets could be described with rational indices [Haüy, 1792]. Theory was developed further in the nineteenth century when Auguste Bravais found that crystals could be considered as a simple assemblage of points. He stated that the importance of the directions of planes (i.e. faces (hkl)) is proportional to their reticular area [Bravais, 1849]. In these days this is known as Bravias' law which states that the morphological importance is proportional to the interplanar distance d_{hkl}.

In 1878 Gibbs expressed the conditions for thermodynamic equilibrium for a crystal surface. Pierre Curie derived Gibbs' relation from Gauss' principle of virtual velocities [Curie, 1885]. This work was the point of departure for the studies of Wulff who discovered that during the growth of a crystal the growth rates are a function of the growth direction [Wulff, 1901]. He formulated a way to construct the crystal morphology assuming that the faces of a polyhedron are determined by the normal vectors having a length proportional to the surface free energy of that direction. This plot is known as the Wulff plot.

Apart from the development of crystal growth theory important encyclopedic works containing morphological data were published at the beginning of the twentieth century like *Chemische Kristallographie* by P. Groth [Groth, 1906] and the famous *Atlas der Kristallformen* of Victor Goldschmidt [Goldschmidt, 1923]. An example of a page from *Atlas der Kristallformen* is shown in figure 1.1. These impressive series of books were used by theoreticians to develop new ideas about the relation between growth forms and the internal structure of crystals. Niggli made a start to link the relative growth rates of crystal faces to the interactions in the crystal lattice [Niggli, 1920].

To establish the lattice theory of Bravais as an empirical law of mineralogy, George Friedel undertook statistical studies of hundreds of species. According to Friedel the interplanar distance has to be corrected for non-primitive cells [Friedel, 1911]. Later Donnay and Harker stated that the interplanar distance d_{hkl} should also be corrected for screw axes and glide planes of the space group of the crystal structure. The combined result of Bravais' law and the extension of Friedel, Donnay and Harker are nowadays known as the BFDH law. Donnay and Donnay extended the BFDH law even further by introducing an intuitive correction for pseudo symmetric cases [Donnay and Donnay, 1961].

During World War II, Max von Laue proved the validity of Wulff's theorem for the equilibrium form of crystals from thermodynamics. This work drew the attention of Wells who intended to establish a link between the atomic internal structure of a crystal and the external form. In the introduction of his paper he writes: *Classical crystallography was restricted to the study of the external forms of crystals and their physical properties. With the development of X-ray crystallography it has become possible in many cases to determine the atomic arrangement in the interior of the crystal, and in recent years attention has been largely concentrated on this aspect of the subject. It should now be possible to begin to fuse these two aspects of the subject* [Wells, 1946].

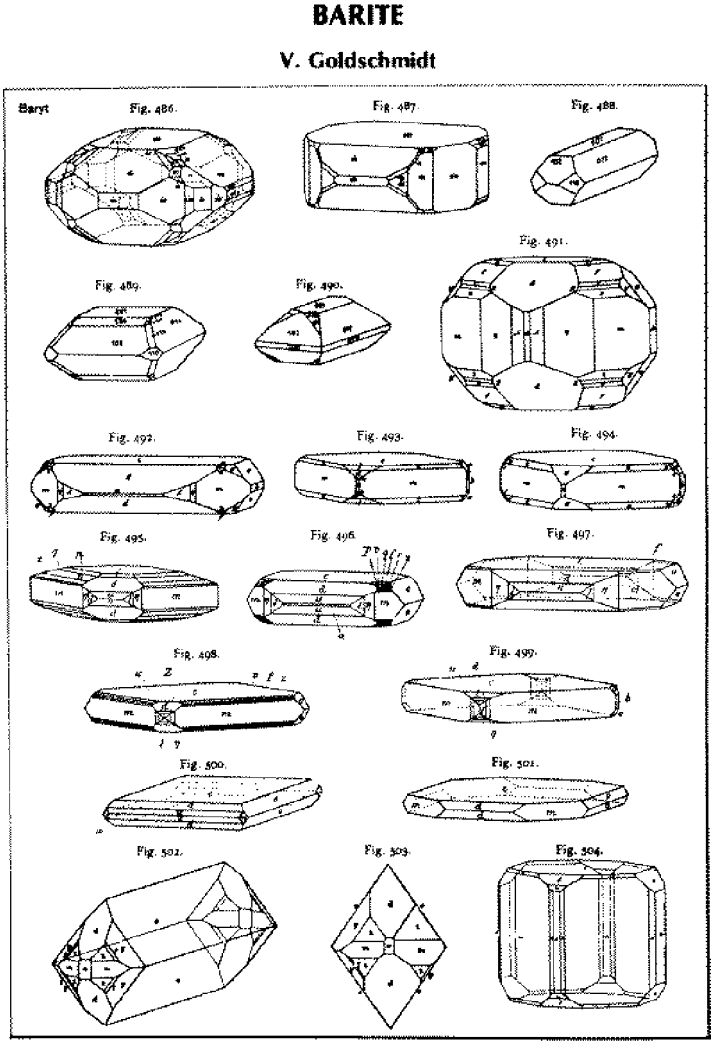

Figure 1.1: Observed morphologies for Barite as shown in *Atlas der Kristallformen*

The X-ray crystallographer Martin Buerger attempted to give a physical explanation for the success of the BFDH law [Buerger, 1947] in terms of surface energies of the faces (hkl).

In 1951 the famous paper of Burton, Cabrera and Frank (BCF) was published [Burton et al., 1951]. It was a culmination of many years of research by people like Kossel [Kossel, 1927], Stranski [Stranski, 1928, Stranski and Kaischew, 1934], Volmer and Weber [Volmer and Weber, 1926] and Kaischew [Kaischew and Stranski, 1934] who had already developed the two dimensional nucleation theories. However, they were not able to explain the experimental fact that many crystal faces already grow at very small supersaturations. In the BCF paper this phenomenon was explained by the presence of screw dislocations which circumvent the need for a nucleation process. An example of a screw dislocation is shown in figure 1.2. Later spirals were found experimentally by Sunagawa using phase-contrast microscopy [Sunagawa, 1977].

Apart from the introduction of dislocation driven growth, in the BCF paper a connection with the world of surface phase transitions as descibed by Onsager [Onsager, 1944] was made.

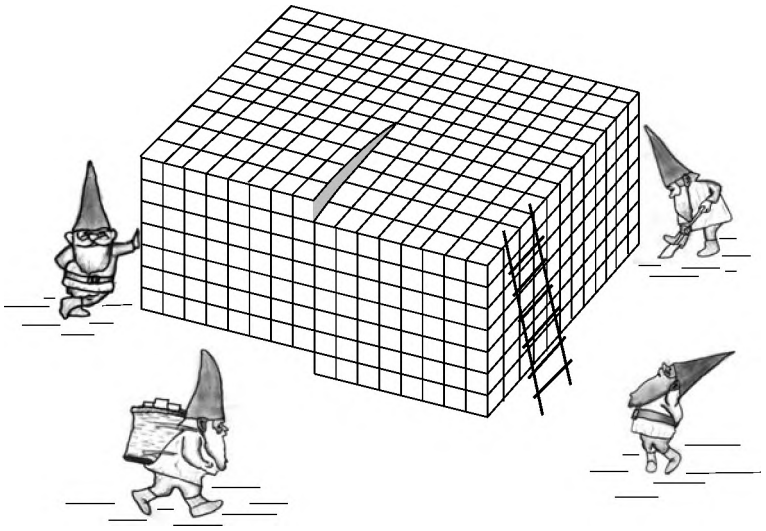

Figure 1.2: Example of a screw dislocation as shown on the frontcover of the reader for the course solid state chemistry I for students at the university of Nijmegen

In 1955 Hartman and Perdok published a series of three papers that employed the kinetic considerations of BCF for the identification of stable crystal faces [Hartman and Perdok, 1955a, Hartman and Perdok, 1955b, Hartman and Perdok, 1955c]. They introduced the concept of periodic bond chain (PBC). Depending on the presence of two or more PBC vectors, a single PBC vector, or none, respectively F- (flat), S- (stepped) or K-faces (kinked) were defined. The F-faces represent the flat faces which are observed on crystals.

In the seventies much effort was put in understanding phase transitions of crystal surfaces. The work of Onsager [Onsager, 1944] was developed further by Kosterlitz and Thouless [Kosterlitz and Thouless, 1973, Kosterlitz and Thouless, 1974], Leamy and Gilmer [Leamy and Gilmer, 1974], van Beijeren [van Beijeren, 1977], Swendsen [Swendsen, 1978] and Müller-Krumbhaar [Müller-Krumbhaar, 1978].

At the same time computers became available and Monte Carlo simulations of the equilibrium and growth behaviour of simple cubic Kossel models were performed to study both thermal phase transitions [Leamy and Gilmer, 1974] but also the growth process of (imperfect) crystals [Gilmer and Bennema, 1972a, Gilmer and Bennema, 1972b, Gilmer, 1976].

Hartman and Bennema showed in 1980 [Hartman and Bennema, 1980] that the relative growth rates of crystal faces R_{hkl} are proportional to the attachment energy E^{att}_{hkl} for moderate supersaturations. This proportionality would become the most widely used recipe to construct theoretical growth morphologies. Later, the classical Hartman-Perdok theory was integrated with the theory of roughening transitions using the concept of connected net. It was shown that the 2-dimensional Ising transition temperature T^C_{hkl} can be calculated for (even rather complicated) connected nets (hkl) [Rijpkema et al., 1982].

The 2-D Ising transition temperature can be used as an approximation for the roughening temperature T^R_{hkl} of a crystal face (hkl).

In 1989 a new type of surface phase called a disordered flat (DOF) phase was introduced by Rommelse and den Nijs [Rommelse and den Nijs, 1987, den Nijs and Rommelse, 1989]. This phase was found in a very simple restricted SOS model with next-nearest neighbour interactions. Mazzeo et al. found the same phase in the so-called staggered BCSOS model [Mazzeo et al., 1995]. Recently, DOF phases were also identified for the (111) [Woodraska and Jaszczak, 1997a, Woodraska and Jaszczak, 1997b] and (100) [den Nijs, 1997] faces of silicon.

The work presented in this thesis starts from the Hartman-Perdok theory integrated with the theory of surface phase transitions. It is the aim of this work to show that, in order to predict the equilibrium and growth behaviour of a face (hkl), the bonding topology at the surface plays a very important role. This is achieved by studying very simple surface models based on the simple cubic SOS model and the BCSOS model. The introduction of anisotropy in those models transforms them from single layered into AB-layered surface models which are generic models for many crystal surfaces of rather complicated crystal structures. In many cases these AB-layered models show a rich phase diagram consisting of flat, disordered flat and rough phases. Also the growth behaviour differs significantly from the well-studied simple cubic Kossel model. It is shown for some specific cases that the presence of AB-layered structures may have a dramatic effect on the predicted growth morphology as well.

The effect of the surface bonding structure on the morphology of crystals is studied from three points of view. First, some extensions were added to the classical Hartman-Perdok theory to account for the presence of multiple surface configurations or connected nets. It is shown that the presence of multiple connected nets for a single crystallographic orientation (hkl) may result in a very low or even zero step free energy. This has major implications for the roughening transition temperature and relative growth rates of these faces (chapter 2 and 3).

Second, in chapter 4 Monte Carlo (MC) simulations are performed to show that the growth morphology may depend very strongly on the supersaturation. Especially the growth rate of faces containing multiple (symmetry related) connected nets are very sensitive to the applied supersaturation. It is shown that the combination of a modern connected net analysis and MC simulations leads to a prediction of the growth morphology as a function of supersaturation.

Third, experiments are presented that confirm the theoretical results. As an example the interesting case of the {011} faces of naphthalene is presented. Both theoretical and experimental evidence was found for the presence of a DOF phase for this crystal face resulting in an anomalous growth behaviour (chapter 5 and 6).

A rigorous connected net analysis of orthorhombic n-paraffin is presented in chapter 7. It is demonstrated that analysis of all connected nets may help to predict the growth morphology as a function of supersaturation. Moreover, the side face structure is studied in detail and the presence of {111} faces is predicted. In the subsequent chapter 8 the results of experimental crystal growth of n-paraffins are presented. For the first time flat

{100}, {010} and {111} faces have been observed in correspondence with the theoretical prediction.

Chapter 9 describes the theoretical morphology of ϵ-caprolactam. Due to the presence of hydrogen-bonded dimers in the crystal structure, the connected net analysis is done assuming both monomers and dimers as the actual growth units. The results of the two analyses do not differ very much. It is shown that, for both the monomers and dimers, the {110} faces may grow with half layers d_{220} depending on the growth conditions such as the solvent and supersaturation.

In order to demonstrate that a modern connected net analysis is generally applicable, the growth morphology of the protein lysozyme is derived from the crystal structure in chapter 10. The experimentally observed dependence of the morphology on the supersaturation and the surface morphology can be explained directly with the results of the analysis.

In the last chapter the morphology of cesium halides is studied both theoretically and experimentally. The growth morphology appears to depend strongly on the growth temperature. At low temperatures the morphology is bounded by {110}, whereas at higher temperatures it is bounded by {001}. The transition between the two morphologies is very distinct. This phenomenon can be explained by a phase transition of the {001} faces from a c2x2 reconstructed phase into a DOF or deconstructed rough phase. In a sense this is an example where the classical connected net analysis fails, because it excludes the possibility of surface reconstructions.

All connected net analyses described in this thesis were performed using a specially designed computer C-program called FACELIFT based on the graph theoretic method described by Strom [Strom, 1980, Strom, 1981, Strom, 1985]. [1]

The work presented in this thesis was financially supported by the Dutch Technology Foundation (SON/STW) under project nr. 349-3166.

[1] A commercial version of the program will be available in a future release of the Cerius^2 molecular modelling program [MSI,]. For academic users the program may be obtained from the department of Solid State Chemistry of the University of Nijmegen (e-mail: hugom@sci.kun.nl).

Chapter 2

On the Prediction of Crystal Morphology I: The Hartman-Perdok Theory revisited

On the Prediction of Crystal Morphology I: The Hartman-Perdok Theory revisited

R.F.P. Grimbergen, H. Meekes, P. Bennema, C.S. Strom and L.J.P. Vogels [1] [2]

Dedicated to P. Hartman

Abstract

The more than forty years old Hartman-Perdok (HP) theory for predicting crystal morphology is reconsidered. The new approach which gives a physical foundation to the theory is based on F-faces having a roughening transition temperature larger than zero Kelvin. The aim of the paper is to confront the field of crystal growth and in particular the classical HP theory with modern statistical thermodynamical treatments of surface models of relatively simple crystal structures. It is shown that crystal faces (hkl) containing multiple connected nets with a relatively high energy content may have a very low roughening temperature and an unexpectedly high growth rate. In some cases crystal faces become rough at zero Kelvin because of multiple connected nets related by symmetry giving rise to symmetry roughening. The use of connected nets in the HP theory offers the possibility to extrapolate results of statistical thermodynamical models of simple crystal surfaces to more complex crystals as encountered in practice. The role of the step free energy in understanding crystal morphology is emphasized.

Introduction

In 1951 Burton, Cabrera and Frank published a famous paper about the growth of crystals and the equilibrium structure of their surfaces [Burton et al., 1951]. They introduced the spiral growth mechanism for imperfect crystal surfaces in addition to the already known two dimensional nucleation mechanism for perfect crystal surfaces. Furthermore they discussed the phenomenon of surface roughening using two dimensional statistical thermodynamical models of Onsager [Onsager, 1944].

A few years later Hartman and Perdok formulated the Hartman-Perdok (HP) theory, also known as the Periodic Bond Chain (PBC) theory, for deriving the crystal morphology from the crystal structure [Hartman and Perdok, 1955a, Hartman and Perdok, 1955b, Hartman and Perdok, 1955c]. Hartman and Perdok did not explicitly take the effect of surface phase transitions, like the roughening transition, into account.

[1] Present address: MOS4YOU, Philips Semiconductors, Gerstweg 2, 6534 AE Nijmegen, The Netherlands

[2] The work presented in this chapter has been accepted for publication in Acta Cryst. A

Since Onsager, statistical thermodynamical surface models have become applicable to more complex crystal surfaces and many surface phases like the normal flat, reconstructed flat, disordered flat (DOF) and rough phase have been found [Leamy and Gilmer, 1974,van Beijeren, 1977,Rommelse and den Nijs, 1987,den Nijs and Rommelse, 1989,Mazzeo et al., 1995]. Nevertheless, many practically grown crystals are too complex to describe with an accurate statistical thermodynamical model.

In this paper it will be shown that integration of the crystallographic HP theory and statistical thermodynamical surface models can be used to derive the equilibrium and growth morphology qualitatively and in many cases quantitatively, of a very wide range of crystals. For this, the F-face defined by Hartman and Perdok will be redefined as a crystal face having a roughening temperature larger than zero Kelvin. F-faces can be determined from a crystal structure by determination of all connected nets. Analysis of all connected nets for a single orientation (hkl) in terms of relatively simple statistical thermodynamical surface models yields information about equilibrium and growth behaviour of the specific face. It will be shown that certain combinations of connected nets cause a an unexpectedly high growth rate in case the step energy is very small. As a special case of the latter, combinations of symmetry related connected nets may result in a zero step energy. These situations give rise to symmetry roughening.

The paper is organized as follows. First, a historical overview of morphological theories is given in which the HP theory and the statistical thermodynamical theory of roughening transitions are emphasized. Next, in section 2.2 an F-face will be redefined and the relation between connected nets and statistical thermodynamical models of interface roughening will be explained. Symmetry of connected nets in the broken bond description and the influence of a mother phase taking the crystal symmetry and destruction of symmetry into account will be treated in section 2.3. We end with a discussion and conclusion.

2.1 History of crystallography and morphology

2.1.1 Bravais, Friedel, Donnay and Harker (BFDH)

The science of crystallography started when Haüy discovered the law of rational indices [Haüy, 1792]. From a modern point of view this law can be stated as follows: Faces occurring on crystals are parallel to netplanes that are perpendicular to a reciprocal lattice vector:

$$\boldsymbol{k}(hkl) = h\boldsymbol{a}^* + k\boldsymbol{b}^* + l\boldsymbol{c}^* \quad h,k,l \in Z, \tag{2.1}$$

where $\boldsymbol{a}^*$, $\boldsymbol{b}^*$ and $\boldsymbol{c}^*$ are the reciprocal lattice vectors. Only the orientation of a face, occurring on a crystal is relevant. This orientation is adequately described by three integers (hkl) which are prime in reference to each other. In the period of 1880 to 1939 the following law of the relative morphological importance of faces (hkl) was formulated by Bravais, Friedel, Donnay and Harker (this is called nowadays the BFDH law). The larger the interplanar distance d_{hkl}, the larger the MI (Morphological Importance) of (hkl) or

$$d_{h_1k_1l_1} > d_{h_2k_2l_2} \rightarrow MI_{h_1k_1l_1} > MI_{h_2k_2l_2}. \tag{2.2}$$

The MI of a face (hkl) is defined as the relative statistical frequency of occurrence of the face (hkl) or the relative size of the face (hkl) occurring on a set of crystals of a certain compound. According to Bravais and Friedel the values of d_{hkl} ought to be corrected for non primitive cells, if these cells are used to calculate d_{hkl}'s [Friedel, 1911]. These corrections may lead to integers h, k and l that are mutually non-prime. According to Donnay and Harker d_{hkl}'s need to be corrected for screw axes and glide planes of the spacegroup of the crystal stucture, because exactly the same crystal surfaces are separated by d_{nhnknl} with $n \in N$ [Donnay and Harker, 1937]. An intuitive extension of the Donnay-Harker law was given by Donnay and Donnay for the case that surfaces separated by d_{nhnknl} are almost the same [Donnay and Donnay, 1961].

In general d_{hkl} has, at least, to be corrected by the crystallographic selection rules as given in ref. [Tables, 1969]. For a treatment of the BFDH law see ref. [Hartman, 1973, Hartman, 1978]. In order to get an impression how crystal (growth) forms look like according to the BFDH law, the ad hoc assumption may be introduced that the relative growth rate $\boldsymbol{R}_{hkl}$ of faces (hkl) is inversely proportional to d_{hkl} or proportional to $k = |\boldsymbol{k}_{hkl}|$. By plotting vectors with a length $R = |\boldsymbol{R}_{hkl}|$ from an origin and erecting faces (hkl) perpendicular to the vectors $\boldsymbol{R}_{hkl}$, a crystal form is obtained. Using this so-called Wulff construction [Wulff, 1901] crystal forms are obtained, which are dominated by faces (hkl) with the highest d_{hkl} and thus the smallest $|\boldsymbol{k}_{hkl}|$. If the space group and elementary cell of a given structure is known all d_{hkl} values can be calculated and crystal forms can be constructed.

2.1.2 Hartman-Perdok theory

The BFDH law often gives a satisfying description of the morphology of crystals. However, there are striking discrepancies between predicted and observed morphologies. The drawback of the BFDH law is its purely geometrical character. Neither the real crystal structure, nor the concept of chemical bond and statistical thermodynamics of interfaces or crystal growth mechanisms are taken into account. In 1955 Hartman and Perdok published three papers, which can be considered as a breakthrough in the theory of morphology, a subscience of crystal growth theory [Hartman and Perdok, 1955a, Hartman and Perdok, 1955b, Hartman and Perdok, 1955c]. In the original HP theory the concept of Period Bond Chain (PBC) plays a key role. A PBC is an uninterrupted chain of bonds representing strong interactions between growth units with an overall periodicity $[uvw] = u\boldsymbol{a} + v\boldsymbol{b} + w\boldsymbol{c}$, $(u, v, w \in Z)$ of the direct primitive lattice and contains no other lattice translation. Moreover, a PBC is stoichiometric with regard to the unit cell contents. In the classical HP theory three types of faces were distinguished:

- F-faces parallel to at least two non parallel intersecting PBCs
- S-faces parallel to only one PBC
- K-faces not parallel to any PBC

Due to the periodicity of the structure two PBCs constituting an F-face determine the composition of an F-slice parallel to (hkl).

Strom has developed a computerprogram for automatic derivation of F-slices. She has shown that it is conceptually more simple and computationally more straightforward to derive the F-slices by determining and combining direct chains (DCs) instead of PBCs [Strom, 1985]. A direct chain is defined as a sequence of strongly bonded growth units of which only the endpoints are identical (i.e. related by a lattice translation) [Strom, 1980]. In contrast to PBCs, DCs need not be stoichiometric with regard to the chemical composition of the crystal (see figure 2.1). Note that each PBC consists of at least one DC and that a stoichiometric DC is also a PBC.

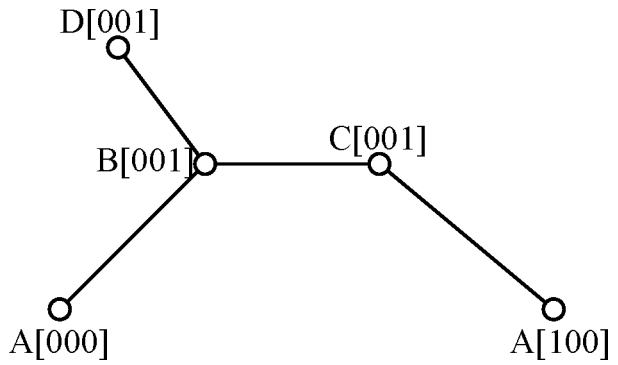

Figure 2.1: Schematic drawing of a PBC with an overall translation [100] consisting of growth units A[000], B[001], D[001], C[001] and A[100]. The DC [100] consists of A[000], B[001], C[001] and A[100]. The chemical composition of the crystal is ABCD. Note that growth unit D is not needed to connect A[000] with A[100].

F-slices can be considered as growth layers or surface configurations . In order to determine which surface configuration will be most pronounced on the growth form in the absence of external factors, the slice energy values associated with the various F-slices in (hkl) are often calculated.

Within the framework of the HP theory it is assumed (and this can be justified [Hartman and Bennema, 1980]) that the rate of growth R_{hkl} of a face (hkl), increases with the attachment energy. This implies that for two faces $(h_1k_1l_1)$ and $(h_2k_2l_2)$ the following relation holds:

$$|E^{att}_{h_1k_1l_1}| > |E^{att}_{h_2k_2l_2}| \;\rightarrow\; R_{h_1k_1l_1} > R_{h_2k_2l_2}. \tag{2.3}$$

Quite often, in order to get an impression of the habit of crystals the ad hoc assumption is introduced that R_{hkl} is proportional to $|E^{att}_{hkl}|$ or

$$R_{hkl} = CE^{att}_{hkl}, \tag{2.4}$$

where C is a constant. E^{att}_{hkl} is defined as the energy released per growth unit when a complete growth layer is attached to a surface (hkl). It is complementary to E^{slice}_{hkl}. E^{att}_{hkl} and E^{slice}_{hkl} together give the crystallization energy E^{cr} or

$$E^{cr} = E^{att}_{hkl} + E^{slice}_{hkl} \tag{2.5}$$

It follows that in principle crystals will be bounded by F-slices having the lowest R_{hkl} or the lowest $|E^{att}_{hkl}|$ and the highest $|E^{slice}_{hkl}|$ [Hartman and Perdok, 1955a, Hartman and Perdok, 1955b, Hartman and Perdok, 1955c, Hartman and Bennema, 1980, Hartman, 1973, Hartman, 1987]. Faces (hkl) with the highest $|E^{slice}_{hkl}|$ will have in most cases the largest d_{hkl}. This explains the success of the BFDH law [Hartman, 1978]. The HP theory has been applied with large success to numerous crystalline structures both organic and inorganic [Hartman, 1987, Bennema and van der Eerden, 1987, Bennema, 1993]. The theory was extended to ionic crystals and Madelung and Ewald methods were used to calculate E^{att}_{hkl} and E^{slice}_{hkl} [Hartman, 1987, Woensdregt, 1990, Strom and Hartman, 1989].

2.1.3 Equilibrium forms and growth forms

The theory of equilibrium forms, firmly rooted in thermodynamics, leads to a logical recipe to construct an equilibrium form. This recipe is given by [Wulff, 1901, Herring, 1953]

$$D_{hkl} = A\sigma_{hkl} \tag{2.6}$$

where D_{hkl} is the distance from the origin of the coordinate system to the face (hkl). It is proportional to the surface free energy σ_{hkl} of the face (A is a constant). An equilibrium form can be obtained using the Wulff construction. A review on equilibrium forms is given by Kern [Kern, 1987].

In order to obtain growth forms, in eq. (2.6) σ_{hkl} has to be replaced by the relative growth rates R_{hkl}. Expressions for R_{hkl} may be given by $R_{hkl} \propto (d_{hkl})^{-1}$, $R_{hkl} \propto E_{att}$ or more sophisticated expressions derived from the modelled fluid part of the interface and kinetic crystal growth models [Liu et al., 1995a, Liu et al., 1995b].

The spread in growth rates of experimentally observed crystals may be very high even in the case of symmetrically equivalent faces (of one form $\{hkl\}$), due to different growth histories of different faces caused by different dislocations, hydrodynamics or absorption of impurities.

2.1.4 Theory of roughening transition

Around 1950 Burton, Cabrera and Frank described the transition of flat crystal faces at equilibrium to roughened faces as a function of temperature [Burton et al., 1951]. At that time, an exact calculation of the roughening transition was restricted to a rectangular two dimensional lattice with equal or different interactions in the two crystallographic directions [Onsager, 1944]. The allowed height differences in this model were $|\Delta h| \pm 1$ (unit cell). For this model the step free energy decreases linearly with increasing temperature T and vanishes at $T = T^C$, the transition temperature. This type of surface transition is known as the Ising transition.

The theory of roughening transitions was developed further in the seventies by Kosterlitz and Thouless [Kosterlitz and Thouless, 1973, Kosterlitz and Thouless, 1974], Leamy and Gilmer [Leamy and Gilmer, 1974], van Beijeren [van Beijeren, 1977], Swendsen [Swendsen, 1978], Müller-Krumbhaar [Müller-Krumbhaar, 1978] and Shugard, Weeks and

Gilmer [Shugard et al., 1978]. For these models the height differences Δh were not restricted to $|\Delta h| \pm 1$. It was shown that the cubic faces of a simple cubic solid-on-solid (SOS) model and the body centered solid-on-solid (BCSOS) model show a roughening transition of infinite order, which is characterized by a critical (dimensionless) temperature θ^R_{hkl} such that

$$\begin{aligned} \theta < \theta^R_{hkl} &\rightarrow \gamma_{hkl} > 0 \\ \theta \geq \theta^R_{hkl} &\rightarrow \gamma_{hkl} = 0, \end{aligned} \tag{2.7}$$

where γ_{hkl} represents the step free energy of a step on the face (hkl). The dimensionless roughening temperature for a face (hkl) is defined by

$$\theta^R_{hkl} = \left(\frac{2\mathrm{k}T^R_{hkl}}{\Phi_{str}} \right) \tag{2.8}$$

where Φ_{str} represents an arbitrary reference bond which in this case is the strongest bond of the crystal and the factor 2 is conventional. T^R_{hkl} is the absolute roughening temperature of the face (hkl). It was shown that for these models the step free energy γ vanishes continuously as

$$\gamma \sim \exp[-\alpha(T^R - T)^{-1/2}], \quad T \leq T^R \tag{2.9}$$

where T is the actual temperature and α is a coefficient depending on the system. In general the roughening temperature T^R is somewhat higher than the Ising transition temperature T^C.

Within the framework of cell models the bond energies at the interface have the shape [Bennema and van der Eerden, 1987, Bennema, 1993, Bennema, 1996]

$$\Phi_i = \Phi_i^{sf} - \frac{1}{2}(\Phi_i^{ss} + \Phi_i^{ff}), \tag{2.10}$$

where sf refers to a solid-fluid bond, ss to a solid-solid and ff to a fluid-fluid bond. Here fluid means any motherphase, including a very dilute vapour. Φ_i corresponds to the broken bond energy of the i-th bond of the crystal.

As shown above, the concept of roughening transition was derived for simple crystals like the simple cubic SOS and BCSOS models. For real crystal faces simplified to somewhat more complex Kossel like structures, van der Eerden [van der Eerden, 1976], Rijpkema and Knops [Rijpkema et al., 1982] showed that the 2-D Ising transition temperature T^C_{hkl} may be used as an (usually lower bound) estimate for the roughening temperature T^R_{hkl}.

We note that during the past ten years a lot of effort has been put in understanding more complex interface models from a statistical thermodynamical point of view. Rommelse and den Nijs found a pre-roughening transition to a so-called disordered flat phase (DOF), for SOS models with next nearest neighbour interactions [Rommelse and den Nijs, 1987, den Nijs and Rommelse, 1989]. Mazzeo et al. calculated a phase diagram for the two component BCSOS model [Mazzeo et al., 1995]. The latter phase diagram, which is applicable to cesium chloride type of structures, exhibits flat, reconstructed flat, disordered flat and rough phases.

The implication of the roughening transition for crystal faces (hkl) is that these faces will, in essence, remain flat in thermodynamic equilibrium at a temperature below the roughening temperature. Even if this surface is exposed to a driving force for crystallization the surface will grow by a layer mechanism (2D nucleation or spiral growth) keeping in principle the orientation (hkl). Note that a crystal face may become rough below the roughening temperature because of a high driving force. This phenomenon is known as kinetic roughening [Elwenspoek and van der Eerden, 1987, Jetten et al., 1984]. If in equilibrium the surface has a temperature above its roughening temperature, it will no longer keep its orientation (hkl) and in case of growth, it will grow as a macroscopically rounded-off surface without orientation (hkl) [van Veenendaal et al., 1998]. This is because the step free energy has become zero.

It has been shown by Prestipino et al. that the disordered flat phase may have major implications for the growth behaviour of crystal faces [Prestipino et al., 1995].

2.2 Derivation of F-faces based on crystallography and the concept of roughening

In this section a new definition for an F-face will be given based on the concept of roughening. Using a model crystal graph, it will be shown that specific combinations of connected nets result in very low or even zero step energy. This may have major implications for the equilibrium and growth behaviour of a crystal face (hkl).

2.2.1 Definition of F-face

In the HP theory, the definition of an F-face still includes faces which, despite the presence of two intersecting non-parallel PBCs, have a roughening temperature of zero Kelvin. In order to include such cases we will use a definition of an F-face based on the theory of roughening transition. An F-face (hkl) is defined as a crystal face (hkl) with a roughening temperature larger than zero Kelvin ($T^R_{hkl} > 0$K).

Van Beijeren and Nolden [van Beijeren and Nolden, 1986] have shown that a flat face (i.e. a crystal face below the roughening temperature) with normal $\boldsymbol{k}$ has the property that for all crystallographic directions $\boldsymbol{u} = u\boldsymbol{a} + v\boldsymbol{b} + w\boldsymbol{c}$ labeled by $[uvw]$ $(u, v, w \in Z)$ that are coplanar with the face (i.e. $\boldsymbol{u} \cdot \boldsymbol{k} = 0$) the sum of the step free energies of a step in the $\boldsymbol{u}$ and $-\boldsymbol{u}$ direction is larger than zero, or

$$\gamma(\boldsymbol{u}) + \gamma(-\boldsymbol{u}) > 0 \quad \forall \boldsymbol{u}, \boldsymbol{u} \cdot \boldsymbol{k} = 0 \tag{2.11}$$

If one aims to predict and understand crystal morphology and crystal growth, one needs to determine all F-faces (i.e. crystal faces with $T^R > 0$) from the crystal structure. As argued before it is almost impossible for practical crystals to determine all these faces on the basis of statistical thermodynamical models. A convenient solution to this problem is to derive all connected nets of a crystal structure and subsequently analyze these on the basis of relatively simple statistical thermodynamical models.

A connected net is defined as the combination of at least two intersecting non-parallel direct chains (DCs). Equivalent connected nets are separated by the interplanar distance

d_{hkl} according to the BFDH law. This is the distance that separates physically identical surfaces. All equivalent growth units in all DCs constituting a connected net differ by a translation $\boldsymbol{u}$ perpendicular to $\boldsymbol{k}$. This is called the flatness criterion.

Note that there is a difference between a connected net and an F-slice defined earlier by Strom. She defined an F-slice as the combination of at least two intersecting non-parallel PBCs [Strom and Heijnen, 1981]. All equivalent growth units in all PBCs constituting an F-slice differ by a translation $\boldsymbol{u}$ perpendicular to $\boldsymbol{k}$ (flatness criterion). The definition implies that the F-slices are stoichiometric with respect to the chemical composition of the unit cell. In contrast, connected nets need not be stoichiometric. A further difference between the HP theory and the present approach is that Hartman does not allow polar F-slices for centrosymmetric crystals whereas polar connected nets are allowed in the present analysis [Hartman, 1973].

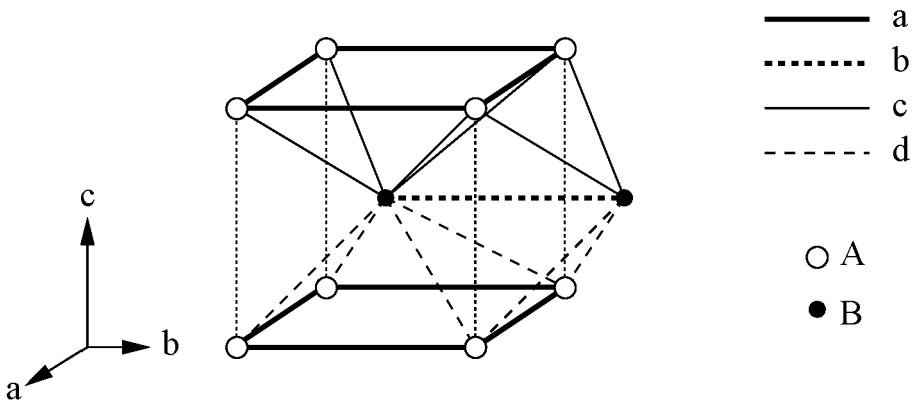

Figure 2.2: Basic model crystal graph. The b bond is present in both the [100] (not drawn) and [010] direction.

For the determination of connected nets from a crystal structure it is convenient to reduce growth units in the crystal lattice to their geometrical centers (or centres of gravity if preferred) and represent strong interactions between the growth units by bonds between these centers. In this way an infinite set of points inter-connected with bonds is formed. Inspired by graph theory, we define this as the *crystal graph*. It must be emphasized that in general the crystal graph has a higher symmetry than the corresponding crystal. In all cases the actual spacegroup symmetry of the crystal has to be considered.

The proposed model crystal graph is presented in figure 2.2. Note, that for reason of clarity we have drawn more than the unit cell. The crystal graph consists of two types of growth units A and B, which are indicated by their centres of gravity. The stoichiometry of the crystal is AB. Growth units A are situated at the corners and growth units B in the centre of the elementary cell. Note that the actual positions of the growth units in the crystal can have a lower symmetry. Between growth units A and B bonds c and d are present. In the [100] and [010] direction two neighbouring growth units A are connected to each other by the bonds a. In the same way two adjacent growth units B are connected by bonds b in the [100] and [010] direction.

In the discussion of different types of F-faces, different crystal graphs will be derived from the model crystal graph in figure 2.2 by redefining the a, b, c and d bonds and growth units A and B.

2.2.2 Discussion of connected nets and F-faces

In this section some properties of F-faces and connected nets will be explained and illustrated using the model crystal graph depicted in figure 2.2.

For simplicity, all bond energies used in the analysis are so-called broken bond energies which are defined as the energy needed to break the bond between the growth units. Thus, per growth unit the broken bond energy is half the bond energy of the bond between two growth units. In the following step energies will be calculated on the basis of these broken bonds. Therefore step energies instead of step free energies are used. Such an approach can still be used to determine whether a face is an F-face as the entropy contribution to the free energy vanishes at zero Kelvin.

The broken bond energies of the bonds a, b, c and d will be indicated with Φ_a, Φ_b, Φ_c and Φ_d respectively. It is assumed that there are no other interactions in the crystal lattice apart from the bonds defined in the crystal graph. The effect of long range interactions, surface relaxations, polarity and interactions between the crystal and the mother phase will be ignored at this stage but will be discussed in section 2.3.2.

2.2.2.1 Illustration of the BFDH law for connected nets

Consider the crystal graph of figure 2.2 with $b = a$, $d = c$ and B=A. The [100] projection of the (001) face is shown in figure 2.3. The unit cell is an I-centered cell. Application of the BFDH law will result in a halving of the interplanar distance separating exactly equivalent surfaces.

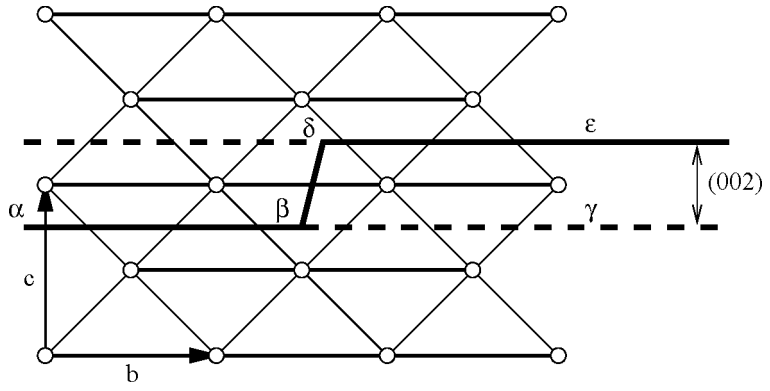

Figure 2.3: [100] Projection of the (001) face of the crystal graph of figure 2.2 with $b = a$, $d = c$ and B=A. The indicated step along [010] is equivalent to a step along [100].

In that case there is a single connected net (002) presented in figure 2.3. The step energy for the orientation (001) can be calculated comparing the surface energies of a flat surface bounded by $\alpha\beta\gamma$ with the surface energy of a surface with a step bounded

by $\alpha\beta\delta\epsilon$. Counting the broken bonds results in a step energy of Φ_a. This illustrates the law of Bravais and Friedel for non primitive cells. The general BFDH law is illustrated by the same figure if it were the crystal graph of the crystal of figure 2.2 with spacegroup symmetry $P112_1$.

Under growth conditions ($\Delta\mu > 0$), this type of crystal face will grow with layers of thickness d_{002} at a temperature below the roughening temperature ($T < T^R$) and at a low driving force not causing kinetic roughening.

2.2.2.2 Multiple connected nets

Consider the (001) face of the crystal graph in figure 2.2 with $\Phi_a = \Phi_b = 0$. In this case two different connected nets $(001)_1$ and $(001)_2$ are present as indicated in figure 2.4. The step energy can be calculated by taking the difference in surface energy for $(001)_1$ between the surface bounded by $\alpha\beta\gamma$ and the surface bounded by $\alpha\beta\delta\epsilon$ is equal to the difference in bond energy $2(\Phi_d - \Phi_c)$. As a result the roughening temperature for the F-face (001) is larger than zero Kelvin. At equilibrium conditions the face would be flat and bounded by the surface with the lowest surface energy. If the c bond is stronger than the d bond, the surface would be bounded by the A growth units. Under growth conditions ($\Delta\mu > 0$) at a temperature $T < T^R$, the surface would then grow with layers $(001)_2$.

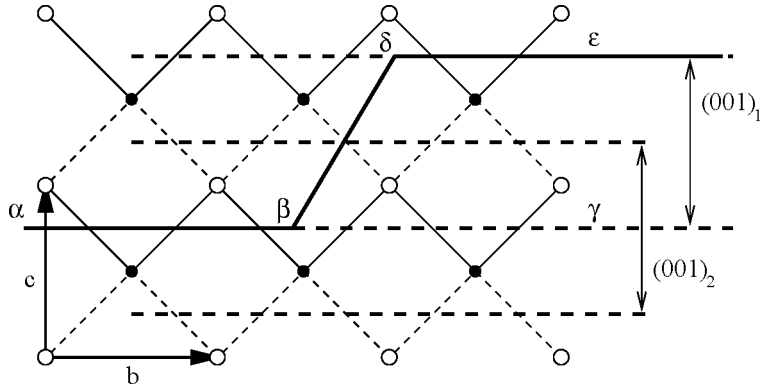

Figure 2.4: [100] Projection of the crystal graph of figure 2.2 without a and b. The indicated step along [010] is equivalent to a step along [100].

In figure 2.5 the [100] projection of the (001) face of the model crystal graph of figure 2.2 is drawn, now including all bonds. For this orientation four connected nets indicated with $(001)_1$, $(001)_2$, $(001)_3$ and $(001)_4$ can be found. The connected nets $(001)_1$ and $(001)_2$ each consist of the two connected nets $(001)_3$ and $(001)_4$. In case $(001)_1$ represents the preferred surface configuration, the step energy can be calculated, as shown before, by calculation of the surface energy difference between interface $\alpha\beta\gamma$ and $\alpha\beta\delta\epsilon$. In this case the step energy is equal to $(2\Phi_d - 2\Phi_c) + \Phi_a + \Phi_b$.

In case of growth below the roughening temperature, the crystal will grow layer by layer preferring the lowest energy surface at the interface. Assuming that $\Phi_c < \Phi_d$ the crystal will grow with layers $(001)_1$.

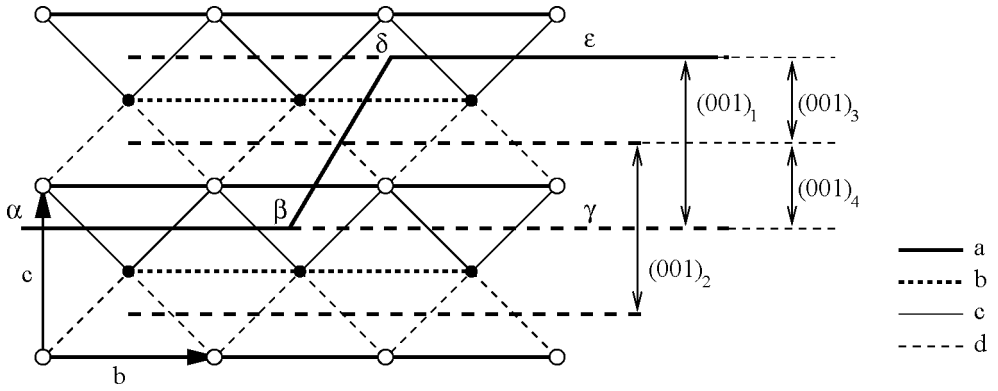

Figure 2.5: [100] Projection of the (001) face of the crystal graph of figure 2.2. The indicated step along [010] is equivalent to a step along [100].

Under certain conditions it is more favorable to grow effectively with half layers by alternating layer $(001)_3$ and $(001)_4$. The growth behaviour of faces containing multiple connected nets will be subject of a future paper [Grimbergen et al., 1999a].

2.2.2.3 Symmetry roughening

We now consider a limiting case of the (001) face as presented in figure 2.4 for which $\Phi_a = \Phi_b = 0$ and $c = d$. Note that still growth unit A differs from growth unit B. A [100] projection of the crystal graph is shown in figure 2.6. Again, two different connected nets can be distinguished indicated with $(001)_1$ and $(001)_2$. The topology of the two connected nets is identical, but the difference is that for $(001)_1$ B growth units while for $(001)_2$ A growth units are at the surface.

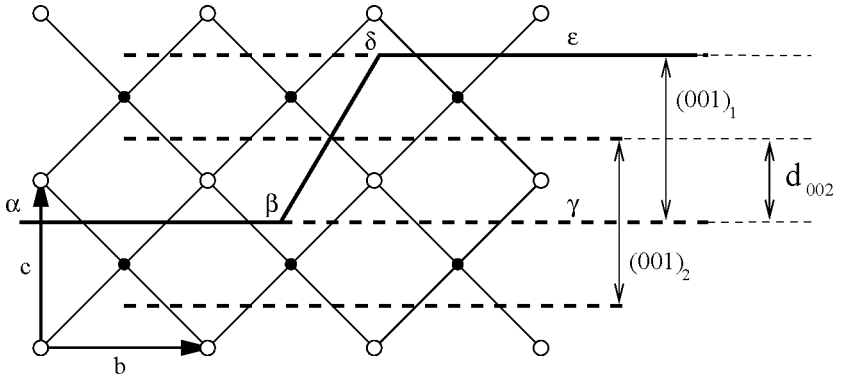

Figure 2.6: [100] Projection of the (001) face of the crystal graph of figure 2.2 with $a = b = 0$ and $c = d$. A step along [100] is equivalent to the indicated step [010].

In figure 2.6 it can be seen that starting from a surface with B on top, the difference in broken bond energy of a flat surface bounded by $\alpha\beta\gamma$ and a surface with one step bounded by $\alpha\beta\delta\epsilon$ is equal to zero resulting in a zero step energy. This implies that this face would be rough at zero Kelvin ($T^R = 0$). The same holds if one starts with the A growth units

on top. This special situation will be referred to as *symmetry roughening*. Symmetry roughening will be treated extensively in a forthcoming paper [Meekes et al., 1998].

If the unit cell is an I-centered cell and consequently A=B, there would not be a valid connected net for the face (001). This is trivial, because the layer thickness d_{001} would become d_{002} according to the crystallographic BFDH law and there are no connected nets (002) (see figure 2.6). The consequence is that the face would be rough at $T = 0K$ and thus not be a valid F-face. This has also been found for the body centered solid-on-solid (BCSOS) model. For the BCSOS model without next nearest neighbour interactions the roughening temperature of the (001) face is zero Kelvin [van Beijeren, 1977].

2.2.2.4 Illustration of the general roughening criterion

In some specific cases the step energy for a step in a direction $\boldsymbol{u}$ may not be equivalent to a step in the opposite direction -$\boldsymbol{u}$. This is illustrated in figure 2.7. The c and d bonds have been divided in c_1, c_2, d_1 and d_2 bonds.

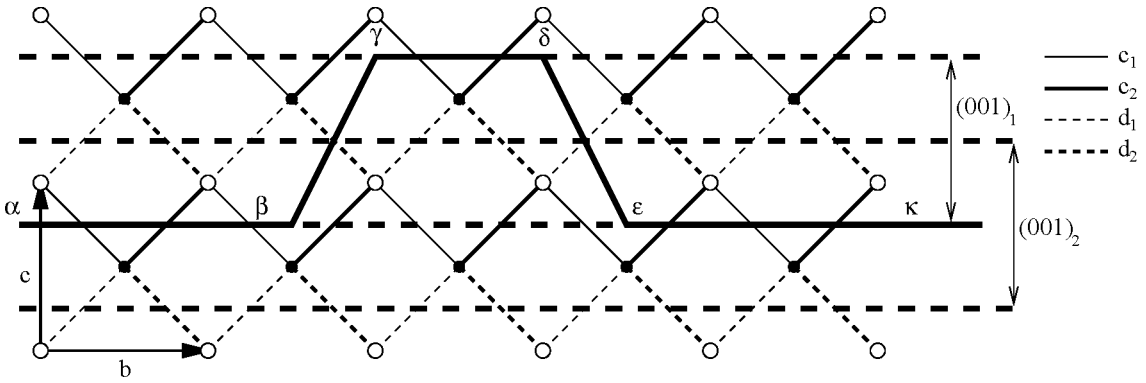

Figure 2.7: [100] Projection of the (001) face of the crystal graph of figure 2.2 with bonds c_1, c_2, d_1, d_2 and $a = b = 0$. Steps along [100] and [010] are equivalent.

Two connected nets can be distinguished indicated with $(001)_1$ and $(001)_2$. Calculation of the the step energy for the step $\alpha\beta\gamma\delta$ on the $(001)_1$ face yields $(2\Phi_{d_2} - 2\Phi_{c_2})$ and for the step $\kappa\epsilon\delta\gamma$ $(2\Phi_{d_1} - 2\Phi_{c_1})$. Assuming that $(\Phi_{c_1} + \Phi_{c_2}) < (\Phi_{d_1} + \Phi_{d_2})$ different situations may occur:

- $(\Phi_{c_1} < \Phi_{d_1}) \wedge (\Phi_{c_2} < \Phi_{d_2})$
- $(\Phi_{c_1} > \Phi_{d_1}) \wedge (\Phi_{c_2} < \Phi_{d_2})$
- $(\Phi_{c_1} < \Phi_{d_1}) \wedge (\Phi_{c_2} > \Phi_{d_2})$.

In the first case both step energies are positive. In the second situation the step energy for the step $\alpha\beta\gamma\delta$ is positive while the step energy for the step $\kappa\epsilon\delta\gamma$ is negative! The third situation corresponds to the reverse. In all situations mentioned, relation (2.11) holds. Therefore the face is a genuine F-face having a roughening temperature larger than zero Kelvin. Obviously, the face would become rough in case $(\Phi_{c_1} + \Phi_{c_2}) = (\Phi_{d_1} + \Phi_{d_2})$. If $(\Phi_{c_1} + \Phi_{c_2}) > (\Phi_{d_1} + \Phi_{d_2})$, the $(001)_2$ connected net would give the surface configuration with the lowest surface energy.

2.2.2.5 Disordered flat faces

For some time interface models were based on first nearest neighbour bonds and it has been shown that some specific models like the SOS, RSOS and BCSOS models [Leamy and Gilmer, 1974, van Beijeren, 1977, Swendsen, 1978, Müller-Krumbhaar, 1978, Shugard et al., 1978] reveal a roughening transition. Later Rommelse and den Nijs found a new phase of crystal surfaces, a so-called disordered flat (DOF) phase by taking next nearest neighbour interactions into account [Rommelse and den Nijs, 1987, den Nijs and Rommelse, 1989]. In their model this phase occurs in between the flat and the rough phases of a crystal face.

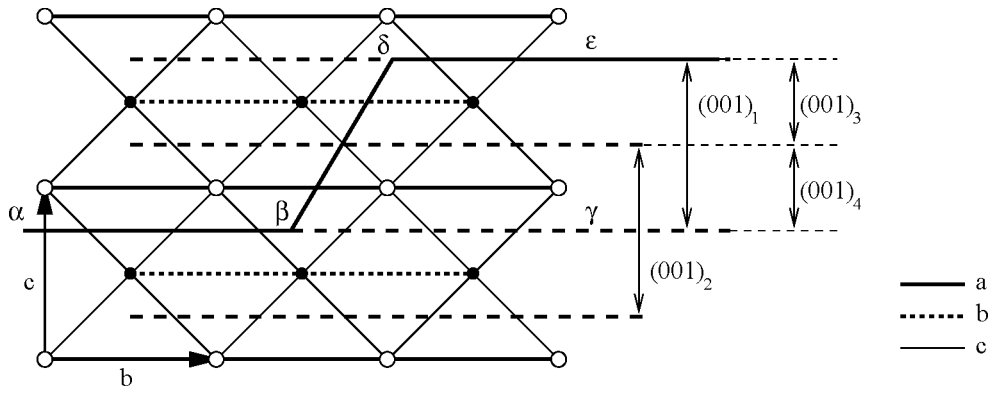

Figure 2.8: [100] Projection of the (001) face of the crystal graph of figure 2.2 with $d = c$. Steps along [100] and [010] are equivalent.

In our description of crystal faces based on connected nets, the DOF phase can also be identified. This can be illustrated looking at figure 2.8. In case the bonds c and d are considered as first nearest neighbour solid-on-solid bonds, and the a and b next nearest neighbour bonds are not equivalent ($\Phi_a \neq \Phi_b$) , this model is identical to the staggered BCSOS model described by Mazzeo et al. for which the phase diagram is known and a disordered flat phase has been identified [Mazzeo et al., 1995]. Apart from the connected nets $(001)_1$ and $(001)_2$, two connected nets $(001)_3$ and $(001)_4$ can be identified. Of the latter two connected nets, each has its own 2-D Ising transition temperature $T^C_{001_3}$ and $T^C_{001_4}$ respectively. In figure 2.8 it can be seen that the step energy for this crystal face is $(\Phi_a + \Phi_b)$ independent of whether connected net $(001)_1$ or connected net $(001)_2$ is chosen as surface configuration. This is a consequence of the broken bond description. Thus the crystal face will have a roughening temperature larger than zero Kelvin.

At temperatures lower than the Ising temperatures of the two individual connected nets $(001)_3$ and $(001)_4$, the surface will be flat. For the moment it will be assumed that $\Phi_a > \Phi_b$ and consequently $T^C_{001_3} < T^C_{001_4}$. When the temperature becomes higher than the 2-D Ising temperature of the $(001)_3$ connected net $((T > T^C_{001_3}) \wedge (T < T^R_{001_1}))$, the crystal face will show an Ising transition to a DOF phase. Consequently, the crystal face will be essentially flat, because of the connected net $(001)_4$ with the highest Ising temperature. However, the $(001)_3$ connected net will not be ordered anymore. When the temperature is increased furher $(T > T^R_{001_1})$, one would expect that the crystal face will

show a roughening transition from the DOF phase to a rough phase. However, it was proven for the two component BCSOS model that there is no roughening transition and the crystal face will stay in the DOF phase as long as $\Phi_a \neq \Phi_b$ [Mazzeo et al., 1995]. This behaviour may be due to the strict BCSOS condition of the model [van Beijeren and Nolden, 1986]. For real crystals such type of faces will probably have a roughening transition at higher temperatures.

The implication for crystal morphology is that flat and DOF phases will result in well-defined flat crystal facets on a macroscopic scale, while a rough face would be observed as a macroscopically rounded-off face. Futhermore, a DOF phase may result in anomalous growth behaviour as compared to a normal flat face. Prestipino et al. have shown for the FCSOS model, using Monte Carlo simulations, that exactly at the preroughening temperature the crystal face grows continuously and has a very high growth rate, whereas just above and below this critical temperature the crystal grows layer by layer and the growth rate is lower [Prestipino et al., 1995].

2.2.2.6 Reconstructed flat faces

The connected net analysis is principally based on attractive bonds. In case strong repulsive interactions are added to the crystal graph, the situation may occur that energetically a reconstructed face, having a larger surface periodicity, is favoured. An example is the (001) face of the cesium chloride structure. This crystal face has been modelled using the two component BCSOS model with repulsive next nearest neighbour interactions [Mazzeo et al., 1995]. They find a c2x2 reconstructed flat phase for the (001) face.

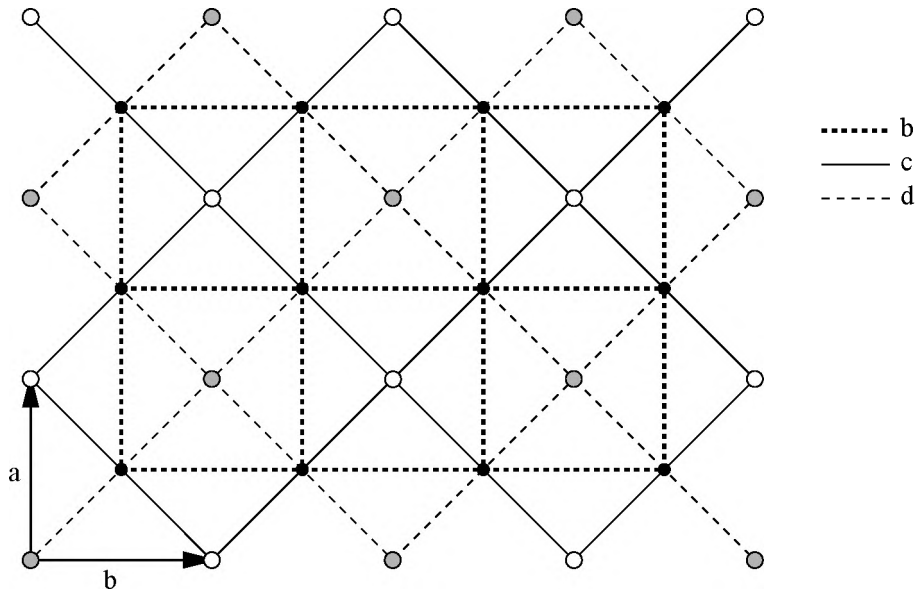

Figure 2.9: [001] Projection (top view) of one of the two (001) connected nets violating the flatness criterion. The black dots: B growth units; grey dots: A growth units at z=0; white dots: A growth units at z=1. $\Phi c = \Phi_d$.

In our model graph this situation corresponds to repulsive a and b bonds and SOS bonds c and d. The resulting c2x2 reconstruction can be derived from a connected net analysis in case the flatness criterion (see section 2.1) is suspended. Then, the connected net as depicted in figure 2.9 is a valid connected net. Note that the c and d bonds are drawn although the bond energies are similar. The connected net shown has a symmetry related connected net translated over [100]. These two connected nets do not cause symmetry roughening because there is a step energy to go from one connected net to the symmetry equivalent one. In this case the step energy corresponds to the formation of a domain wall between the two reconstructed surface configurations and implies the formation of a repulsive a bond.

It is interesting that depending on the ratio of the bond energies, the crystal face will behave differently when the temperature is increased. This can be seen in the phase diagram for this model in ref. [Mazzeo et al., 1995]. It is shown that for some specific ratio of bond energies $\frac{\Phi_a}{\Phi_b}$, the crystal surface is reconstructed flat at low temperatures, rough at higher temperatures and will become disordered flat at very high temperatures. This implies that the crystal face becomes flat at high temperatures instead of rough! Mazzeo et al. refer to this situation as an *inverse roughening* transition [Mazzeo et al., 1995].

2.3 Symmetry of connected nets

2.3.1 Broken bond description

A connected net analysis of a crystal structure often yields a series of connected nets for a single orientation (hkl) which may also be interpreted as a number of different surface configurations. We will denote a connected net by $\mathbf{k}^n_{hkl}$, where the superscript n labels the different connected nets for the orientation (hkl) having a normal $\mathbf{k}_{hkl}$ with $|\mathbf{k}_{hkl}| = \frac{1}{d_{hkl}}$. In case a crystal has the lowest possible symmetry P1 all the connected nets are unique surface configurations, but for crystals with higher symmetry connected nets may be related by symmetry.

In general, a symmetry operator R_i of the spacegroup of the crystal transforms a connected net $\mathbf{k}$ into itself or in another connected net $\mathbf{k}'$ with a different orientation. In the discussion of symmetry related connected nets for a crystal face (hkl), we will consider all symmetry elements that conserve the orientation. In that case two different situations may occur: $\mathbf{k}' = \mathbf{k}$ and $\mathbf{k}' = -\mathbf{k}$. The latter situation will be referred to as *boundary swapping*. Note that boundary swapping gives rise to a pair of connected nets with opposite surfaces.

An example of boundary swapping is shown in figure 2.6. In case the spacegroup symmetry of the graph in figure 2.2 is Pmmm, the $(001)_1$ and the $(001)_2$ connected nets would be related by symmetry elements causing $\mathbf{k}' = -\mathbf{k}$. Based on broken bonds the surface energies of the two connected nets are equal and the step energy for the face is zero. Because of the symmetry this face will have a roughening temperature of zero Kelvin. This type of roughening we have called symmetry roughening.

It will be shown in a forthcoming paper that a thorough analysis of symmetry relations between connected nets leads to the already known BFDH selection rules and,

complementary to those, conditions at which symmetry roughening can occur [Meekes et al., 1998].

2.3.2 Influence of a mother phase

The connected net analysis is essentially based on bonds between growth units defined in the bulk crystal lattice. Furthermore, the assumption is made that the positions of growth units at an interface are exactly the same as their positions in the bulk crystal. In this section we consider very briefly the situation beyond the broken bond description, including the effect of a mother phase, relaxation and reconstruction.

Taking the possibility of surface reconstruction into account, the original HP theory has to be reconsidered to some extent. This was already realized by Hartman and Sun et al. [Hartman, 1989, Sun et al., 1990] for corundum, hematite and $YBa_2Cu_3O_{7-x}$. Including surface reconstruction implies either allowing a larger periodicity at the surface as compared to the bulk or relaxing the flatness criterion when one sticks to the periodicity of the bulk lattice.

In case of surface relaxation, the mesh area M_{hkl} is not changed with respect to the unrelaxed bulk structure. In this case the following symmetry elements will be conserved at the crystal - mother phase interface

- All n-fold rotation axes parallel to **k**.
- All mirror planes and glide planes parallel to **k** with a glide component perpendicular to **k**.

In case of reconstruction, more symmetry elements will be lost depending on the actual reconstruction. It can be concluded that the symmetry elements causing boundary swapping are lost at the interface. This implies that faces containing symmetry related connected nets giving rise to boundary swapping and symmetry roughening, will formally not roughen at zero Kelvin. In figure 2.6 it can be observed that the two alternative connected nets have either A growth units or B growth units at the interface. In the broken bond description this situation results in equivalent surface energies, but it is obvious that these two surfaces will have different surface free energies. However, the free energy difference might be very small and the crystal face will become rough already at very low temperatures.

In general, the interaction of a mother phase with the crystal face may either increase or decrease the surface free energy and the step free energy for a crystal face (hkl). This is due to adsorbed solvent molecules, the presence of complexes or a preordering effect of the mother phase just at the interface. In any case the effect can be very complex. Nevertheless, we will assume that the effect of a mother phase only influences bond energies as long as there is no reconstruction. Relaxation, as argued before, can destroy some symmetry elements.

In general the effect of a mother phase can change the relevant parameters for crystal growth namely the attachment energy, the step free energy and consequently the roughening temperature. Calculations of the effect of a solvent on the crystal morphology have been performed by several authors; see for example refs. [Berkovitch-Yellin, 1985, van der Voort, 1991a, van der Voort, 1991b, Liu et al., 1995a].

2.4 Discussion and conclusion

The present definition of an F-face originates from the idea to integrate the statistical thermodynamical theories of surface phase transitions and the classical Hartman-Perdok theory for derivation of crystal morphology from the crystal structure. It is very important to bring these disciplines of science together in order to improve the understanding of the behaviour of crystals either in thermodynamic equilibrium with their mother phase or under growth conditions.

Statistical thermodynamical surface models have become more and more applicable to complex crystals and have revealed many surface phases like the normal flat, reconstructed flat, disordered flat (DOF) and rough phase. These phases will influence not only the equilibrium but also the growth morphology of crystals.

These models have to be generalized in order to be applicable to a wider range of experimental crystal structures. In this paper we have shown that by derivation and subsequent analysis of all connected nets of a crystal structure, the surface phases found by the more sophisticated statistical thermodynamical models can be identified qualitatively.

Analysis of combinations of connected nets is the key to understand equilibrium and growth behaviour of more complex crystal faces. In the classical HP theory, the slice energy and attachment energy are the most important parameters for the description of the morphology. In our opinion, both the step free energy and the attachment energy are key parameters for understanding the equilibrium and growth behaviour of crystal faces. We have shown that step energies of a crystal face (hkl) can become very small for specific combinations of connected nets even in the case of very high slice energies. In such cases the roughening temperature of the crystal face can be much lower than expected on the basis of calculated Ising transition temperatures of individual connected nets. Moreover, the growth rate for this type of faces will be high already at low driving forces due to a two dimensional low nucleation barrier. This is in contrast with the usual assumption that the growth rate depends on the attachment energy only.

For small step free energies in a single direction $[uvw]$ of a Kossel-like crystal it has been shown by Burton, Cabrera and Frank that the roughening transition temperature is very low. Consequently, those crystal faces will become rough even at low driving forces. Such an anisotropy can be amplified drastically by pairs of connected nets giving rise to very low step free energies for which the slice energies can still be very high. Crystal faces having a very low step free energy in a single direction $[uvw]$ and simultaneously high slice energies, have been found for triacylglyceride and paraffin crystals [Hollander et al., , van Hoof et al., 1998a].

Eq. (2.11) implies that crystal faces having a step free energy of zero in a single direction $[uvw]$ are already rough at zero Kelvin. In this special case of symmetry roughening the step energy for a crystal face (hkl) is zero despite the presence of connected nets containing very strong bonds. The roughening temperature of such faces is zero Kelvin and the growth rate will be very high. An example of symmetry roughening is found for naphthalene and anthracene crystals [Grimbergen et al., 1998c]. A complete overview of symmetry relations between connected nets can be found in ref. [Meekes et al., 1998].

Note that in the analysis of the connected nets calculated energies are not free energies. The statistical thermodynamical models show that the entropic contribution is

essential for exact calculation of the roughening transition temperatures and the presence of different types of surface phases. It is a challenge for the future to develop general applicable methods for calculation of step free energies and surface free energies of crystal surfaces in contact with a mother phase.

In a forthcoming paper the growth behaviour of crystal faces containing multiple connected nets will be studied using the connected net analysis and Monte Carlo (MC) simulation techniques [Grimbergen et al., 1999a]. The effect of anisotropy in the growth layer will be studied in detail on the basis of the connected nets. A combination of a connected net analysis and subsequent MC crystal growth simulations offers the possibility to predict crystal morphology as a function of driving force.

Acknowledgements

The authors would like to thank E.S. Boek, X.Y. Liu, M.A. Verheijen, J.P. van der Eerden, H. Knops and P. Hartman for valuable discussions. Two of us (C.S. Strom and R.F.P. Grimbergen) would like to acknowledge financial support of the Dutch Technology Foundation (STW).

Chapter 3

On the Prediction of Crystal Morphology II: Symmetry Roughening of Pairs of Connected Nets

On the Prediction of Crystal Morphology II: Symmetry Roughening of Pairs of Connected Nets

H. Meekes, P. Bennema and R.F.P. Grimbergen [1]

In commemoration of J.D.H. Donnay (1902-1994)

Abstract

Within the framework of the Periodic Bond Chain analysis for the prediction of crystal morphology connected nets play a crucial role. For a face (*hkl*) often more than one connected net is found. Symmetry relations between such connected nets can give rise to symmetry roughening of nets. In this paper all cases where symmetry may lead to symmetry roughening are derived. The role of a mother phase in contact with the crystal is explicitly taken into account. It turns out that cases of symmetry roughening are, in a sense, complementary to situations where the classical Bravais-Friedel-Donnay-Harker selection rules apply.

3.1 Introduction

In part I of this series of papers a physical basis was given for the classical Hartman-Perdok or periodic bond chain (PBC) analysis which is used to predict the morphology of a crystal from the crystal structure in terms of bonds between growth units [Grimbergen et al., 1998b]. So far, the bond energies have only played a minor role in the treatment. Nevertheless, they will be dealt with in a following part. In part I mainly the determination of F-faces, i.e. those (flat) faces that may occur on an equilibrium or growth form of a crystal in terms of connected nets, has been treated. An F-face (*hkl*) was defined as a crystal face (*hkl*) with a roughening temperature larger than zero Kelvin. The derivation and analysis of all connected nets of a crystal face offers a convenient way to determine whether a face is an F-face or not.

Statistical thermodynamic models of surfaces of relatively simple crystal structures play a key role in this analysis. As explained in part I a connected net (*hkl*) is a graph made up of points (representing the growth units) connected by bonds formed by the combination of at least two intersecting non-parallel so-called direct chains. A connected net (*hkl*) is repeated over a distance d_{hkl} which is the interplanar distance of faces (*hkl*). The effect of a mother phase on the stability of an F-face was explicitly taken into account. References to survey papers on the PBC-analysis can be found in part I.

A kind of roughening, namely symmetry roughening, which is typical for certain pairs of equivalent connected nets was also introduced. One often finds pairs of connected nets for a face (*hkl*) that are mutually equivalent according to the spacegroup symmetry. Some of these pairs turn out to give rise to symmetry roughening of the corresponding

[1] The work presented in this chapter has been accepted for publication in Acta Cryst. A

crystal face at $T = 0$K. In this paper symmetry roughening is investigated in more detail. Another more practical reason for studying the effect of symmetry relations between connected nets of a crystal face is the large amount of connected nets that may be found for a single face. To avoid a superfluous energy calculation for such pairs, rules based on symmetry arguments and the physics of the roughening transition are derived in order to predict such a roughening in advance. This will be even more important for F-faces that merely have such pairs of connected nets, because such faces will not show up on a crystal form despite the presence of connected nets.

All cases where symmetry may lead to symmetry roughening are derived. A distinction is made between pairs of connected nets giving rise to microscopic symmetry roughening, leading to a macroscopically flat face, and pairs giving rise to macroscopic symmetry roughening for which the face gets rough even macroscopically. Analogous to part I, the role of a mother phase in contact with the crystal is explicitly taken into account.

This paper is organized as follows. First, the phenomenon of symmetry roughening will be explained and illustrated for one specific example. In the next section all symmetry elements that may lead to symmetry roughening will be derived and studied neglecting the effect of a mother phase. Such cases are referred to as a broken bond description [Grimbergen et al., 1998b]. The effect of the presence of a mother phase will then be treated. The generalization to any crystal graph completes the classification. In the discussion the findings are summarized and put in a broader perspective. Finally a conclusion is given.

3.2 Symmetry roughening

An example is given of an F-face having a pair of connected nets that gives rise to symmetry roughening. Consider the crystal graph presented in figure 3.1.

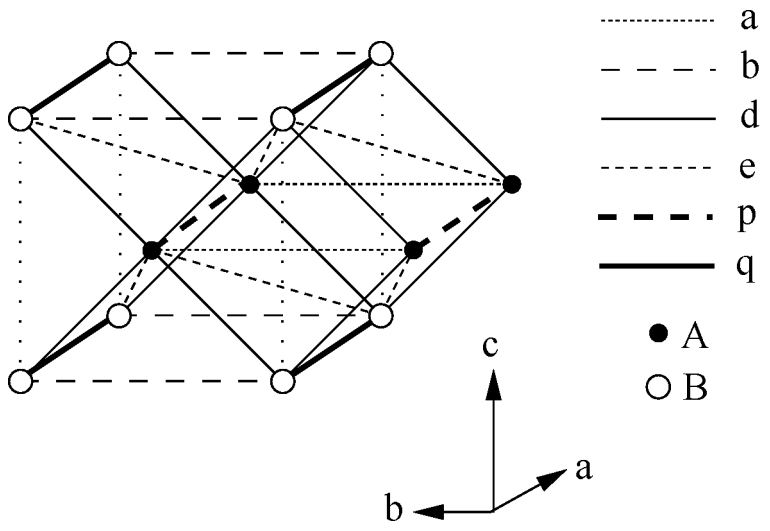

Figure 3.1: Model crystal graph. The spacegroup is P1; bonds d actually consist of bonds d_1 to d_4 in the (100)-face (not indicated); also bonds e consist of four different bonds.

The unit cell contains one growth unit A and one growth unit B. This graph differs from the model graph used in part I. The stoichiometry is still AB, though the symmetry is drastically reduced as a starting point for each example treated and it is assumed that the symmetry of the corresponding crystal is P1. Labeling of bonds and growth units is also different as compared to part I. Furthermore, bonds e are added. As a consequence of the absence of symmetry, the bonds d actually consist of four different bonds d_1 to d_4 in the (100)-face of the unit cell. Also bonds e consist of four different bonds. In figure 3.1 we do not make this distinction for clarity sake.

In the examples to follow, sometimes some of the bonds are neglected although always a connected crystal graph is considered. Mainly the [100] and [001]-projection of the graph for different symmetry elements which are added temporarily, resulting in triclinic or monoclinic spacegroups are studied. As a result spacegroups which do not conform to the standard settings are mentioned frequently . This is a result of the choice to treat all cases within the same crystal graph for clarity sake. In all cases the space group symbols explicitly give the setting and the orientation of a mirror or rotation axis.

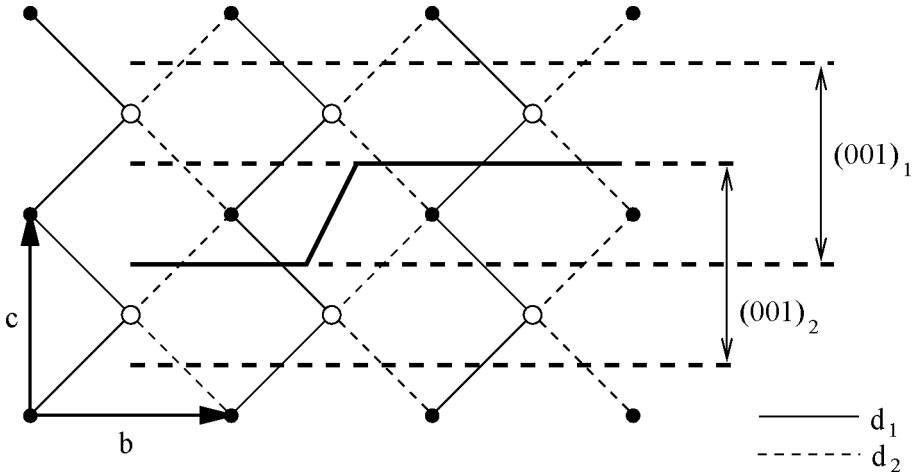

Figure 3.2: Symmetry roughening for the (001) connected nets. The [100]-projection is drawn. Note that a homogeneous horizontal mirror plane runs through the growth units. The solid line follows a path from $(001)_1$ to $(001)_2$ without cost of energy

It has to be noted that when drawing (crystal) graphs only the topology is relevant and actual crystallographic angles may differ from 90° depending on the spacegroup symmetry of the crystal considered. An important distinction has to be made between symmetry elements with and without a non-primitive translation. Homogeneous symmetry elements such as a mirror, an n-fold rotation axis and the inversion have no non-primitive translation and are elements of point groups. The term inhomogeneous symmetry element is used for glide planes and screw axes having a non-primitive translation. Later the symmetry of the crystal in general is discussed.

As an example of symmetry roughening consider the case that there is a horizontal mirror plane m_z through the layers of growth units A (and B). As a result the four different bonds d_1 to d_4, now, are equivalent in two pairs denoted d_1 and d_2, respectively. For the

moment, the bonds a, b and e are neglected. The mirror symmetry is destroyed for a semi-infinite crystal in contact with a mother phase as was discussed in part I. For the moment, however, the effect of a mother phase is neglected, implying that also any surface reconstruction is ruled out, analogously to part I.

Figure 3.2 shows that for the orientation (001) two connected nets can be identified which are related by the horizontal mirror plane. Bonds p and q make the nets of the figure connected in two dimensions. The figure also shows a cut which starts along the connected net $(001)_1$, making a step to the connected net $(001)_2$ and following the latter one. Such a profile corresponds to the same broken bond energy per surface mesh area as a pure $(001)_1$ or $(001)_2$ connected net. In other words, the step energy of the artificial step is zero. Although there are two connected nets present the face (001) always gets rough as the step energy equals zero. The (001) face can have many such steps, both from $(001)_1$ to $(001)_2$ and from $(001)_2$ to $(001)_1$ without any difference in broken bond energy. Such a face is rough as long as there is no other connected net possible for that orientation. In the example this is the case as $(001)_1$ and $(001)_2$ are the only connected nets possible according to the definition.

This example of roughening related to the presence of a symmetry element, was already mentioned by Bennema and van der Eerden [Bennema and van der Eerden, 1987]. The example in figure 3.2 shows a case where the connected nets of the symmetry pair are situated at different heights along the face normal. This results in a roughening in the sense that on a macroscopic scale the face rounds off. It is also possible that the connected nets are at the same height, for example due to a mirror perpendicular to the face. In such a case, the pair gets rough in the sense that no distinction can be made between the two connected nets. The face then stays flat on a macroscopic scale. The distinction between these two kinds of symmetry roughening is discussed furtheron in more detail.

3.3 Possible cases of symmetry roughening

3.3.1 Relevant symmetry

The relevant symmetry is the space group symmetry of the crystal. This is the complete symmetry for an infinite crystal. There are two important restrictions that lower the symmetry:

- The symmetry of a semi-infinite crystal (i.e. a crystal bounded on one side by a (flat) face) is generally lower. As will be seen, only the local symmetry of the connected nets is relevant for symmetry roughening. Nevertheless, surface reconstruction can affect this local symmetry severely. The presence of a mother phase can put even more restrictions on the symmetry considerations. This symmetry reduction has been treated in part I. For the moment it is assumed that if a mother phase is present, its effect, as symmetry is concerned, is negligible and also surface reconstruction is neglected.

- In order to find the connected nets, the crystal is reduced to the crystal graph, which is defined by points made up of the growth units of the crystal, together with

the bonds. Generally, the points are at the centre of mass of those growth units. Therefore, for a connected net (and also for the crystal graph) the symmetry is generally higher than for the corresponding connected net (crystal), defined on the positions of all atoms or ions of the crystal. As a result, sometimes the actual space group symmetry of the crystal has to be reconsidered.

In general, the space group G is the group $\{R_i||g_i\}$, where R_i are all elements of the point group K. The translations g_i consist of primitive translations of the lattice Λ together with the relevant non-primitive translations. The non-primitive translations depend on the choice of the origin. The primitive translations are only needed for the symmetry group of the unit cell and depend also on the growth unit or bond under consideration. Using this convention allows one to restrict oneselve to the R_i together with the non-primitive translations modulo primitive translations when considering the symmetry restrictions on the connected net. One has to bear in mind however, that the primitive translations of R_i, in the case of a connected net, are those that bring the growth units and bonds back into the connected net. In other words, the unit cell of the connected net as determined by the interplanar distance $\boldsymbol{d}_{hkl}$ and a mesh area $\boldsymbol{M}_{hkl}$ is considered. The mesh area is defined by $\boldsymbol{d}_{hkl} \cdot \boldsymbol{M}_{hkl} = V$, where V is the volume of the unit cell of the crystal. To be more precise, the symmetry G_s of the *slice* corresponding to the connected net will be the relevant one. The subscript s is dropped in the following. A connected net is denoted by $\boldsymbol{k}^n_{hkl}$, where the superscript n labels the different connected nets possible for the F-face (hkl) having a normal $\boldsymbol{k}_{hkl}$, where $|\boldsymbol{k}_{hkl}| = \frac{1}{d_{hkl}}$. If not leading to confusion the indices hkl or the label n are suppressed.

In general, $R \in G$ transforms a connected net $\boldsymbol{k}$ into another connected net $\boldsymbol{k}'$. Note that growth units at the end position $\boldsymbol{c}_j{}^e \in \boldsymbol{k}$ of a bond j are equivalent (symmetry related) to those at $\boldsymbol{c}_j{}^{e'} \in \boldsymbol{k}'$ and that this also holds for starting positions of the bond at $\boldsymbol{c}_j{}^s$ and $\boldsymbol{c}_j{}^{s'}$. Therefore also the bonds $\boldsymbol{b}_j \in \boldsymbol{k}$ and $\boldsymbol{b}'_j$ are equivalent. Thus, the bond energies of $\boldsymbol{b}_j$ and $\boldsymbol{b}'_j$ are equal and even the connected net energy $E^{\text{slice}} = \sum_j E(\boldsymbol{b}_j)$ is the same for $\boldsymbol{k}$ and $\boldsymbol{k}'$.

3.3.2 Orientation

A general transformation $R \in K$ transforms a connected net $\boldsymbol{k}$ into another connected net $\boldsymbol{k}'$ with a different orientation. Note that a different orientation is also found if $\boldsymbol{k}' = -\boldsymbol{k}$. The latter case has been referred to as *boundary swapping* in part I. In case of a different orientation the symmetry element R only implies that if the net $\boldsymbol{k}$ leads to a stable F-face $\boldsymbol{k}$, the face $\boldsymbol{k}' = R\boldsymbol{k}$ is as stable. For example, a 4-fold rotation axis parallel to the c-axis ensures that the faces (and all of its connected nets) (100), ($\bar{1}$00), (010) and (0$\bar{1}$0) are equivalent and have the same slice energy E^{slice}.

Symmetry elements that change the orientation of the connected net such that $\boldsymbol{k}' \neq \pm\boldsymbol{k}$, can not give rise to symetry roughening. One can, and it is usually more efficient to do, apply the symmetry elements that transform a connected net into one with a different orientation in advance, thereby decreasing the number of nets that have to be checked on connectedness or for which the energy has to be calculated.

3.3.3 Orientation conserving symmetries ($\boldsymbol{k}' = \boldsymbol{k}$)

One can, in the case that $\boldsymbol{k}' = \boldsymbol{k}$, limit the discussion to symmetry elements that conserve the orientation of a connected net. The special case of boundary swapping, that is $\boldsymbol{k}' = -\boldsymbol{k}$ will be treated furtheron. For this purpose a certain connected net $\boldsymbol{k}$ is considered. The symmetry elements R that leave its orientation invariant are (glide) mirror planes and (2, 3, 4 and 6-fold) rotation (screw) axes that are perpendicular to the net and thus parallel to $\boldsymbol{k}$. For these symmetry operations one can distinguish four different situations.

3.3.3.1 Singlet due to a homogeneous symmetry element

Consider the case that the symmetry operation R is a homogeneous mirror plane or a homogeneous 2, 3, 4 or 6-fold axis perpendicular to the connected net. If the connected net is transformed into itself it is called a singlet and there is no symmetry roughening.

3.3.3.2 Doublet due to a homogeneous symmetry element

The second situation considered, refers to the case that the net is not transformed into itself by a homogeneous symmetry operation. Then, the symmetry element gives rise to equivalent connected nets that are at the same height with respect to $\boldsymbol{d}_{\boldsymbol{k}}$. A doublet, triplet, quadruplet or sextet of equivalent connected nets is found for a 2, 3, 4 or 6-fold rotation axis respectively. A mirror plane gives rise to a doublet. All multiplets can be reduced to sets of doublets. In these cases it is, sometimes, possible to make a path via bonds from one connected net to the other without cost of energy. The consequences of this will be worked out in section 3.3.3.4.

3.3.3.3 Doublet due to an inhomogeneous symmetry element; BFDH

The case of a screw axis or a glide plane perpendicular to the connected net $\boldsymbol{k}$ always imposes restrictions. In the case of the repeated action of an n-fold screw axis one obtains n mutually equivalent connected nets with thickness $d_{\boldsymbol{k}}/n$ that differ in height as seen along the screw axis. In case the mutual shift between the connected nets is an integer times $d_{\boldsymbol{k}}$ the situation is equivalent to the case of section 3.3.3.1; otherwise the n mutually equivalent connected nets $\boldsymbol{k}^n_{hkl}$ lead to a 'selection rule' for the face $\boldsymbol{k}_{hkl}$. For example, an n-fold screw axis parallel to the c-axis leads to the selection rule that $(00l)$ can only be an F-face if $l = nm$ $(m \in Z)$.

Similarly, the case of a glide plane perpendicular to the connected net $\boldsymbol{k}$ with the glide direction not perpendicular to $\boldsymbol{k}$ is considered. Now, one finds two equivalent connected nets which are mutually translated along the glide direction, which imposes restrictions on the Miller indices corresponding to the glide direction. For example, a glide plane a perpendicular to the $\boldsymbol{b}$-axis gives rise to the selection rule that $(h0l)$ can only be an F-face if $h = 2m$ $(m \in Z)$. These restrictions are already well-established and are covered by the Bravais-Friedel-Donnay-Harker (BFDH) law [Friedel, 1911, Donnay and Harker, 1937, Hartman, 1973, Hartman, 1978]. Especially the laws derived by Donnay and Harker impose these restrictions on the possible F-faces. The (connected) nets that are restricted by such selection rules consist in case of an n-fold screw axis of n (possibly connected)

nets with thickness $d_{\boldsymbol{k}}/n$ and with mutually the same structure. For a glide plane two equivalent connected nets are obtained that are translated over the non-primitive glide translation. In other words, the connected nets restricted by the BFDH-law need not be checked on connectedness anyway. In such a case, one has to test the nets with smaller thickness according to the selection rules. Bravais and Friedel treated the selection rules due the choice of a non-primitive cell. These are rather straightforward as such a choice has direct impact on the indices (hkl).

In conclusion, in case of a glide plane (with a component of the glide along $\boldsymbol{k}$) or a screw axis, all faces perpendicular to these are restricted by the selection rules, which are the same ones as the limiting reflection conditions used in diffraction. As the BFDH rules have been formulated for complete slices only the general conditions are relevant. The BFDH rules are relevant only for cases where boundary swapping plays no role. For that reason they even apply in the presence of a mother phase. In the modern formalism where the emphasis is laid on the connected nets, the special conditions play a role as well. The latter conditions apply only if all growth units of the connected net are at the corresponding special positions. In that case, one has to be careful and make a distinction between the actual molecule and the centre of gravity. If special conditions appear for a connected net for the inhomogeneous symmetry elements discussed in this section, the BFDH rules already restricts the analysis to one of the two connected nets. However, for other orientations (hkl) that are not restricted by the BFDH rules, one can have pairs of connected nets. All such cases are covered by the other sections of this paper. In other words, the special conditions are automatically taken into account as the symmetry group of the slice corresponding to the connected net is considered. The connected nets which obey the BFDH-law still might lead to symmetry roughening due to other symmetry elements.

3.3.3.4 Doublet due to an inhomogeneous symmetry element; non-BFDH

For the connected nets that fulfill the conditions imposed by the BFDH-law one can still find pairs of connected nets for which the nets are mutually equivalent via one of the orientation conserving symmetry operations. As the symmetry elements relevant for the BFDH selection rules can give no further restrictions on the nets obeying these rules, one is left with the case of a glide plane perpendicular to the connected net with the glide perpendicular to $\boldsymbol{k}$. This symmetry element can give rise to symmetry roughening. Note that the connected nets of such a pair are at the same height with respect to $d_{\boldsymbol{k}}$. The situation is somewhat comparable to that of section 3.3.3.2. An example can be found in figure 3.3. In this figure the [100]-projection of the model graph of figure 3.1 is drawn again. Bonds b and e are neglected and bonds p and q run along the projection direction. A b-glide plane perpendicular to the $\boldsymbol{a}$-axis is added and the space group becomes Pb11. As a result the number of atoms in the unit cell is doubled which is indicated by the dashed net in the figure. The bonds d still consist of four different bonds each being doubled by the mirror. Horizontal bonds between the growth units A are maintained in order to have the whole crystal graph connected. The solid wavy lines represent a slice of one of the connected (001) nets of a pair. The second one is partly drawn with a dashed wavy line. A transition over a distance d_{001} results in a non-zero step energy, ensuring a finite

Ising transition temperature for the individual connected nets [Grimbergen et al., 1998b]. This pair of connected nets gets rough due to the fact that a transition between the two nets can be made without cost of energy as the same bonds are broken per mesh area. Therefore, the roughening does not result in a rounding of the face; the two connected nets are at the same height.

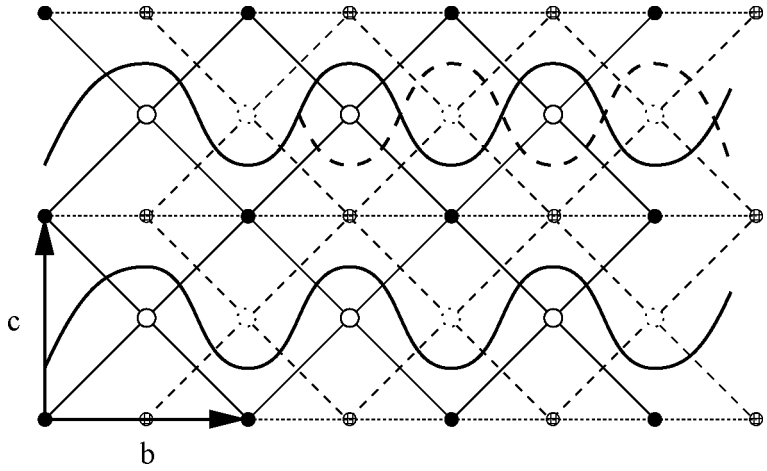

Figure 3.3: Symmetry roughening for a pair of (001) connected nets due to a glide plane perpendicular to the face for which the glide is perpendicular to $\boldsymbol{k}$. The [100]-projection is drawn. The mirror plane is in the plane of the figure and the dashed net is translated over [0 $\frac{1}{2}$ 0] with respect to the solid net; the space group is Pb11. Bonds b and e are neglected. The symmetry roughening is microscopic.

Figure 3.3 alternatively represents the situation for space group P1a1. The most simple example as the crystal is concerned, however, is that of a glide plane that transforms growth unit A into B. Consider, for instance, the (100) connected net in the [001]-projection of figure 3.1 as presented in figure 3.4. In this example bonds a, b and d are neglected. As this graph is a little complicated also the [010]-projection showing the zig-zag pattern of the bonds e for the two connected nets is drawn. The relevant space groups are P1c1 and P11b. Bonds p and q, which are now symmetry related, make the nets connected. Due to the glide plane the four different bonds e are grouped into two sets of bonds denoted e_1 and e_2. Once more we are dealing with two connected nets which are at the same height as indicated in the figure. Again, a transition between the two nets can be realised without cost of energy. As mentioned before the situation dealt with in section 3.3.3.2 is comparable to that of this section. In fact, besides some minor details figures 3.3 and 3.4 also illustrate the situations of space group P1m1 or P112 and of space group P211 respectively. In order to understand this one has to keep in mind that in the basic crystal graph of figures 3.1 the position of growth units A is arbitrary as the space group for this figure is P1.

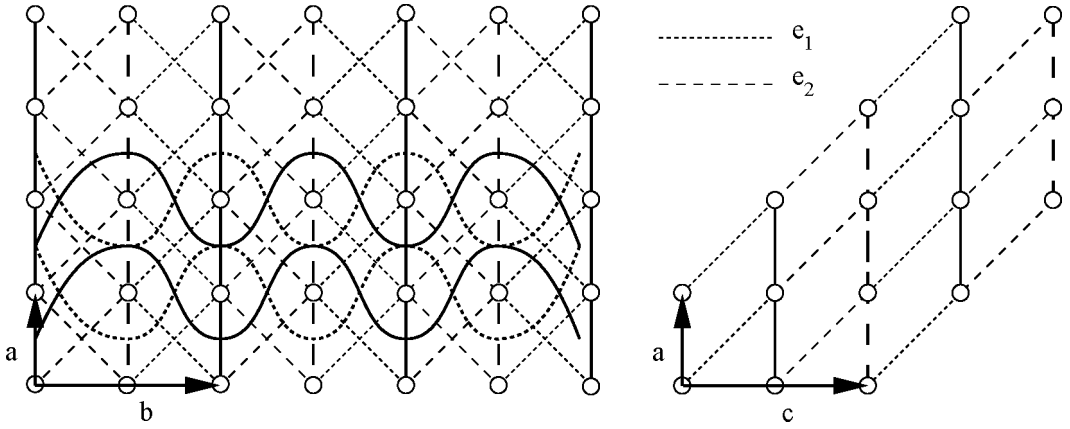

Figure 3.4: Symmetry roughening for a pair of (100) connected nets due to a glide plane perpendicular to the face for which the glide is perpendicular to $\boldsymbol{k}$. The space group is P1c1 or P11b. Both the [001]-projection (left) and the [010]-projection (right) are drawn. The vertical bonds are p and q bonds; they are symmetry related in this case but still indicate the rows of former growth units A and B respectively.

In conclusion, one finds that for orientation conserving symmetry elements ($\boldsymbol{k}' = \boldsymbol{k}$) the BFDH selection rules are complementary to the situations where symmetry roughening can take place. Symmetry roughening is limited to the following two situations:

- a glide plane perpendicular to the connected net with the glide perpendicular to $\boldsymbol{k}$
- a homogeneous plane or a homogeneous 2, 3, 4, or 6-fold axis perpendicular to the connected net giving rise to doublets

In all these cases the two connected nets which are symmetry related are at the same height. Obviously, no symmetry roughening is found for singlets.

3.3.4 Orientation inverting symmetries ($\boldsymbol{k}' = -\boldsymbol{k}$)

A new case arises when one considers the symmetry elements that invert the orientation of a connected net. These are a mirror or 2-fold axis parallel to the connected net and the inversion. In this case, the upper and lower sides of the connected net are interchanged and one can speak of boundary swapping. Now, four situations can be distinguished. The different cases are distinguished by the presence of a non-primitive translation but also by the position of the symmetry element along the face normal. If the net is transformed into itself special positions of a connected net exist for a symmetry element modulo primitive translations. Such singlets are non-polar, that is, despite the boundary swapping, the mother phase interacts in the same way with the two surfaces [Grimbergen et al., 1998b]. If the symmetry element is not at a special position of the connected net, the transformed net will be displaced along the face normal and the corresponding members of the doublet will differ in height and (or) lateral position. A polar connected net can not be a singlet under orientation inverting symmetries. Note that the special positions of a connected net generally differ from those of the unit cell.

3.3.4.1 Singlet due to a symmetry operation at a special position

For a two-fold (screw) axis or a (glide) mirror plane parallel to the connected net or the inversion, the symmetry operation transforms the net into itself modulo a primitive translation in case the symmetry operation is at a special position of the connected net. In this case we are again dealing with a singlet. Despite the fact that one can formally speak of boundary swapping, effectively there is no difference in the surface structure. In such a case, the (single) net is non-polar and there is no restriction.

3.3.4.2 Doublet due to a homogeneous symmetry operation

For a homogeneous symmetry element giving rise to boundary swapping, symmetry roughening can occur, namely when the element is not at a special position of the connected net. The net can be either polar or non-polar. In such a case the two connected nets of the pair have a height difference. An example can be found in figure 3.5.

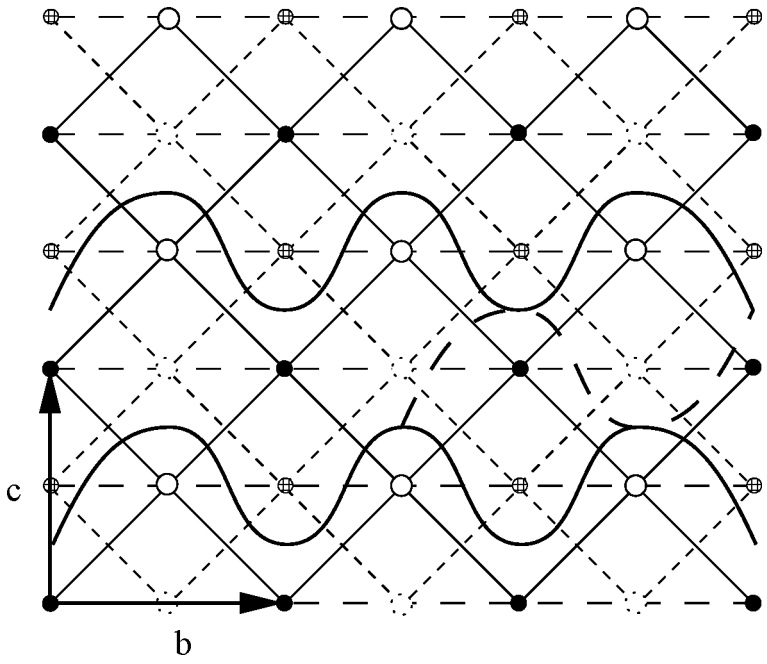

Figure 3.5: Symmetry roughening for a pair of (001) connected nets. The space group is P11m, P211 or P121. The [100]-projection is depicted. The dashed cut is the symmetry image of the solid cut.

The graph in this figure represents again the [100]-projection of the graph of figure 3.1. Bonds e are neglected. It illustrates a situation for which the space group is P11m, P211 or P121. Therefore, also the space group $P\bar{1}$ is covered by this example. The unit cell content is doubled. Still, the bonds d consist of four different bonds, each doubled by the symmetry operation. A horizontal bond between the growth units is added in order to have the whole crystal graph connected. The graph suggests a smaller unit cell due to the symmetry imposed. This is a case where the symmetry of the graph is higher than that of the crystal. The centres of gravity represent for example a polar molecule

with a dipole moment parallel to $\boldsymbol{k}$. The wavy solid line represents a slice of one of the connected nets of a pair. The second net symmetry related to the first one is represented by the dashed wavy cut. Again the figure shows a transition between the two nets can be made without cost of energy. Hence, the pair gives rise to macroscopic symmetry roughening when broken bonds are considered. Note, that as in the case of figure 3.2, the two connected nets of the pair already would give rise to roughening due to the fact that the transition from the solid to the dashed net in figure 3.5 can be continued to the solid net one interplanar distance higher, again without cost of energy.

3.3.4.3 Doublet due to an inhomogeneous symmetry operation not at a special position

Next, the case of an inhomogeneous symmetry element not at a special position of the connected net is considered. First, the case is treated for which the symmetry operation gives rise to two equivalent connected nets translated along a non-primitive translation parallel to the net. There is no height difference for the doublet. In fact, figure 3.3 can be interpreted to serve as an example for this case as well. For this, the spacegroup is assumed to be P11b or $P12_11$. However, in contrast to the situation dealt with in the corresponding section, in this situation there is boundary swapping. Note, that the symmetry element acts on the growth units and not on the boundary of the cuts. There is no difference in broken bond energies and even a path from one of the nets to the other does not cost any energy. Therefore, the pair still gives rise to microscopic symmetry roughening.

Secondly, the situation of a glide plane or two-fold screw axis perpendicular to $\boldsymbol{k}$ but not at a special position of the connected net, giving rise to two nets also differing in height along the face normal will be treated. Figure 3.5 can now serve as an illustration for the space group $P2_111$ or P11a. Also in this case, a transition between the two nets can be made without cost of energy. Hence, the pair gives rise to macroscopic symmetry roughening in a broken bond treatment.

3.4 The presence of a mother phase

The situations described above change when one considers a crystal in contact with a mother phase. Then, the description in terms of broken bonds, in principle, does not longer hold. As discussed in part I only a few symmetry elements of the crystal survive in the situation of a semi-infinite crystal in contact with a mother phase in absence of reconstruction and assuming that at least topologically, the outer layers of the surface are comparable to the bulk structure. These symmetry elements are the rotation axes perpendicular to the face and a mirror or glide plane perpendicular to the face with the glide along the face. This severe symmetry reduction is due to the fact that successive layers in the crystal near the surface will interact differently with the mother phase. Of course, the interaction can be extremely complicated due to adsorbed complexes, reconstruction, etcetera. For the problem of symmetry roughening however, it is assumed that only the symmetry properties are relevant of the most outer layer which determine the degeneracies in energy. Topologically, this layer will be comparable with a corresponding

bulk layer in case no reconstruction is present. Therefore, energies may differ but the symmetry properties remain in tact up to the polarity of a layer. In other words, it is assumed that when a step is realised on a surface, the vanishing of the step free energy due to symmetry is determined by the symmetry of the bulk crystal. Nevertheless, for polar cuts there will be a difference in surface energy due to the mother phase in case of boundary swapping. As an example the first case of figure 3.2 is reconsidered. The two alternative connected nets $(001)_1$ and $(001)_2$ will interact differently with the mother phase. Therefore, the mirror symmetry will be lost for, at least, the most outer layer, be it $(001)_1$ or $(001)_2$. Hence, the surface energies for the two will be different. Thus, the symmetry roughening caused by this pair vanishes when a mother phase is present.

In case the symmetry element which gives rise to boundary swapping is at a special position of the connected net, the two boundaries will be equivalent. In such a case the interaction with the mother phase will be the same for the two boundaries and the pair still gives rise to symmetry roughening.

3.5 More complicated crystal graphs

The question arises whether the classification in terms of symmetry presented in the previous sections also holds for more complicated connected nets. In order to study this, one can simply add bonds to the nets studied up to now. As an example, reconsider the case of figure 3.5. If one adds an arbitrary bond to the graph the symmetry operation generates equivalent bonds.

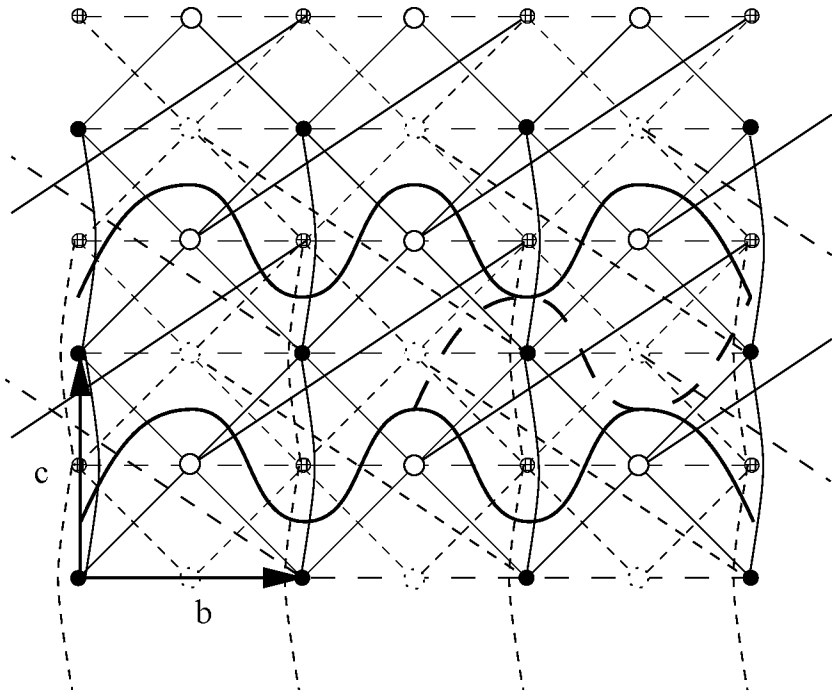

Figure 3.6: Symmetry roughening for the pair of (001) connected nets of figure 3.5. Two new bonds have been added. The dashed bonds are the symmetry image of the solid ones.

In figure 3.6 the situation is drawn. Any such equivalent bond is again cut as many times by the solid wavy boundary as it is by the dashed wavy boundary. There is one type of bond, however, that can destroy symmetry roughening. If one reconsiders the case of figure 3.3 one can, again, add any bond and its symmetry equivalent ones. In this case however, there is one kind of bond which is not cut as often on making a transition from one of the two equivalent connected nets to the other. Such a bond is a horizontal bond cut by the boundary. The situation is illustrated in figure 3.7.

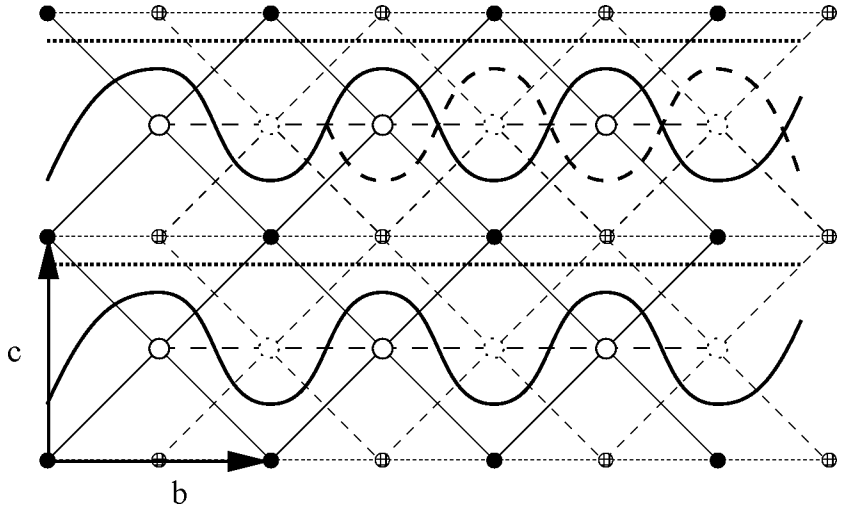

Figure 3.7: Symmetry roughening for the pair of (001) connected nets of figure 3.3. The added horizontal bond between the growth units B, cut by the wavy boundary is omitted once on a transition from the solid to the wavy boundary. An alternative flat connected net in this situation is indicated.

As a result, such a transition in the presence of a horizontal bond which is cut by the two connected nets, always favours a repeated jump from one connected net of the pair to the other. It is easily verified that an alternative connected net exists for a situation for which symmetry roughening occurs for a pair of connected nets with no height difference combined with a horizontal bond cut by the boundaries due to a repeated jump between the nets. The alternative net can be less stable than each of the pairs of connected nets as the horizontal bond energy can be (very) small as compared to the difference between the lower d-bonds and the upper ones in figure 3.7. In spite of this, the symmetry roughening of the pair is lifted in any such case. In conclusion, one finds that the minimum demand for the phenomenon of symmetry roughening is the excistence of a doublet. If any bond perpendiclar to $\boldsymbol{k}$ would destroy the symmetry roughening, there exists an alternative surviving connected net.

3.6 Discussion

The results obtained up to now are summarised in table 3.1. Symmetry roughening covers different kinds of roughening for which an step (free) energy is zero already at $T = 0$K. The major difference between symmetry roughening and well-known kinds of roughening such as thermal roughening and kinetical roughening is that the latter kinds of roughening take place for temperatures $T > 0$K. Symmetry roughening can occur in case of doublets of connected nets. From this perspective, only connected nets which are singlets and have a thickness d_{hkl} according to BFDH give rise to F-faces.

This definition is appropriate when referencing to crystal graphs because in such cases the relevant bonds are already chosen. With respect to the actual crystal one has to realize that at low temperatures more and more weak bonds become relevant for the stability of the crystal and its faces. Strictly spoken such additional bonds could destroy the symmetry roughening at lower temperatures.

In a sense, symmetry roughening is an artifact as a result of the pursuit of F-faces in terms of connected nets and the definition of an F-face as a crystal face (hkl) with a roughening temperature larger than zero. The exhaustive determination of all F-faces for any crystal in terms of that definition, however, is at the moment only feasible via a determination of all connected nets, as discussed in part I. An analysis of all connected nets simply implies the rejection of appropriate pairs for which symmetry roughening occurs. A kind of symmetry roughening can also occur in a situation for which the symmetry between the relevant bonds has an accidental nature.

Note that while symmetry roughening imposes restrictions on the F-faces as they are rough at zero Kelvin, the BFDH rules impose restrictions on the choice of faces (and thus connected nets) because of the existence of a thinner slice with the same surface energy. As the symmetry elements relevant for BFDH never cause boundary swapping, the corresponding rules always hold, even in the presence of a mother phase.

Coming back to symmetry roughening, an important distinction has to be made between cases for which the pair consists of connected nets at the same height and ones for which they differ in height with respect to the direction of $\boldsymbol{k}$. If the nets only have a zero step (free) energy for transitions between nets at the same height, the corresponding face does not get rough macroscopically. The only result is that it is impossible to make a distinction between the nets on a microscopic scale. In such a case, the steps can be considered as domain walls between surface domains having a configuration corresponding to the two connected nets. The free energy corresponding to a step with height d_{hkl} is still finite. Therefore, these nets lead to a stable F-face. Microscopic roughening is related to the situation of so-called disordered flat (DOF) phases found in statistical thermodynamical Solid On Solid models with next nearest neighbour interactions [Rommelse and den Nijs, 1987, den Nijs and Rommelse, 1989]. Such a situation can lead to increased growth rates [Grimbergen et al., 1998b, Grimbergen et al., 1999a].

For symmetry roughening of a pair of connected nets at different height, the face gets rough macroscopically if there is no alternative singlet connected net present. Looking at Table 3.1 one finds that the only cases where macroscopic symmetry roughening can take place are those for which boundary swapping occurs due to symmetry elements not at special positions of the connected net. The same table shows that such a macroscopic

Table 3.1: Cases of symmetry roughening for a crystal in the broken bond description and for a crystal in contact with a mother phase.

	R		vacuum	mother phase
$\boldsymbol{k}' \neq \pm\boldsymbol{k}$			no restrictions	no restrictions
$\boldsymbol{k}' = \boldsymbol{k}$	m $\parallel \boldsymbol{k}$	homogeneous	singlet or SR; sh	singlet or SR; sh
		glide$\perp \boldsymbol{k}$	SR; sh	SR; sh
		glide not$\perp \boldsymbol{k}$	BFDH	BFDH
	$2,3,4,6 \parallel \boldsymbol{k}$	homogeneous	singlet or SR; sh	singlet or SR; sh
		screw	BFDH	BFDH
$\boldsymbol{k}' = -\boldsymbol{k}$	m $\perp \boldsymbol{k}$	homogeneous or glide at sp, np	singlet	singlet
		homogeneous not at sp,	SR; dh	no restrictions
		glide not at sp,	SR; sh or dh	no restrictions
	$2 \perp \boldsymbol{k}$	homogeneous or screw at sp, np	singlet	singlet
		homogeneous not at sp,	SR; dh	no restrictions
		screw not at sp,	SR; sh or dh	no restrictions
	$\bar{1}$	at sp, np	singlet	singlet
		not at sp	SR; sh or dh	no restrictions

$\boldsymbol{k}' = R\boldsymbol{k}$
m: (glide) mirror plane; 2,3,4,6: (screw) axes
BFDH: Bravais-Friedel-Donnay-Harker applies
SR: symmetry roughening
sh: doublet consisting of nets at the same height
dh: doublet consisting of nets at different heights
sp: special position for the connected net; np: non-polar net

symmetry roughening is, in principle, lifted in the case of a mother phase in contact with the crystal face. In any case, macroscopic symmetry roughening will not appear when the orientation (hkl) has a singlet because the latter ensures that the roughening temperature for the orientation will be larger than zero Kelvin. Microscopic symmetry roughening can still occur even in case a singlet is present.

In general, the symmetry of a crystal can be higher than that of the monoclinic and triclinic cases treated up to now. In order to test the presence of symmetry roughening for any face (hkl) one can select all symmetry elements of the space group that leave $\boldsymbol{k}_{hkl}$ invariant up to a sign and use table 3.1 as a reference. One symmetry element giving rise to symmetry roughening is sufficient to discard the pair of connected nets if no alternative singlet is present. One has to bear in mind, however, that only symmetry roughening with a height difference gives rise to a macroscopic roughening effect and that the presence of a mother phase, in principle, destroys such an effect. Microscopic symmetry roughening is not destroyed in the presence of a mother phase.

The inversion plays a special role. It was not mentioned in section 3.3.4.3 because in that subsection inhomogeneous symmetry elements and $\mathrm{P}\bar{1}$ which is symmorphic were treated. Considering for instance a space group like Pnnn, the inversion has a non-primitive translation $(\frac{1}{2}\frac{1}{2}\frac{1}{2})$ depending on the choice of the origin. For such a space group any face normal $\boldsymbol{k}_{hkl}$ is invariant under the inversion up to a sign and the non-primitive translation assures the presence of a doublet with height difference as long as the inversion is not at a special position of the connected net.

The effect of symmetry on crystal morphology has been treated in this paper on a microscopic scale without taking the actual growth mechanism into account. Microscopic growth mechanisms such as spiral growth are also symmetry determined. An example of such microscopic effects on interlacing as observed for spirals on crystals of e.g. SiC and $NiSO_4{\cdot}6H_2O$ will be treated in ref. [van Enckevort and Bennema, 1998].

3.7 Conclusion

In this paper all possible symmetries in crystals where symmetry roughening of pairs of connected nets can take place, are deduced. The relevant symmetries are the ones which leave the orientation of the face unchanged up to a sign. Within this catagory of symmetry elements, one can distinguish three situations.

- Symmetry elements that leave the connected net invariant (singlet).
- Symmetry elements that relate a doublet covered by the well-established Bravais-Friedel-Donnay-Harker (BFDH) rules.
- Doublets which can cause symmetry roughening.

Singlets have no restriction and BFDH-doublets result in selection rules which are the same as the general reflection conditions used in X-ray crystallography. When a pair of connected nets of the same face (hkl) obeying the BFDH conditions is related by symmetry the face, in principle, gets rough when no alternative singlet is present. This does not always mean that the corresponding face (hkl) also becomes rough on a macroscopic scale.

An important distinction is made between microscopic and macroscopic roughening. If the pair-wise symmetric connected nets are at a different height as seen along the face normal, then the face becomes rough macroscopically, that is, gets rounded off if there is no alternative singlet connected net present. According to the definition of an F-face given in part I such a face is not an F-face.

If the nets are at the same height, the face does not get rounded off but it always becomes rough microscopically unless there is an alternative connected net present. The alternative nets that can destroy symmetry roughening must contain bonds parallel to the face.

The presence of a mother phase does not alter these cases as long as the symmetry element does not invert the boundaries of the connected nets, that is, as long as there is no boundary swapping. In case of boundary swapping, the pair does not get rough if the symmetry element is at a special position of the connected net. In such a case the net is non-polar. If the boundary swapping occurs for a more general position of the symmetry element and a mother phase is present the interaction with the mother phase can destroy the symmetry roughening. All these situations are summarized in table 3.1.

It is clear that symmetry roughening can have severe implications for the morphology of crystals. First of all, the morphological importance of a face can be reduced drastically because a pair of connected nets of the face can get rough due to symmetry roughening leaving a weaker alternative connected net behind. In case there is no alternative, the face will either not show up at all or will be rounded off for macroscopic symmetry roughening. In case of microscopic symmetry roughening, the face stays macroscopically flat.

One of the questions which remains, is whether the growth mechanism of microscopically rough faces is different from that of normal faces. Another point to be studied is the effect of a finite temperature or a finite supersaturation. One can imagine that a pair of connected nets that is not exactly symmetry related but just differs slightly in bond energies will still get rough at a finite temperature or supersaturation. In such a situation one could respectively speak of thermal symmetry roughening or kinetical symmetry roughening, or in more general terms, of pseudo symmetry roughening. In practice one frequently encounters crystals with pairs of connected nets which, though structurally clearly not related by symmetry, have very comparable bond energies. On the other hand, a mother phase interacting with the crystal surface could cause only a small energy difference for a pair of connected nets in case of boundary swapping. In such a case the discriminating effect of the motherphase can be destroyed by a finite superstaturation. Again, the implications of an non-equilibrium situation can have severe implications for the morphology. Such situations will be put into a broader perspective of morphological importance of faces in part III of this series of papers [Grimbergen et al., 1999a].

The effect of a mother phase interacting with the crystal surface has been neglected very often in the past. In this paper as well as in part I the influence of the symmetry of connected nets in the boundary between crystal and mother phase is explicitly taken into account. Further studies into this matter, including modelling studies, will become more and more viable using modern computing power and modelling software. In such studies the implication of symmetry roughening and in particular pseudo symmetry roughening are expected to become apparent, offering a more reliable tool to predict crystal morphology using the Periodic Bond Chain analysis.

Acknowledgements

The authors would like to thank J.P. van der Eerden, P. Hartman and the members of the Nijmegen Graph Club, C.S. Strom, L.J.P. Vogels, X.Y. Liu and E.S. Boek for valuable discussions. R. de Gelder is gratefully acknowledged for critically reading the manuscript. R.F.P. Grimbergen would like to acknowledge the financial support of the Dutch Technology Foundation (STW).

Chapter 4

On the Prediction of Crystal Morphology III: Equilibrium and Growth Behaviour of Crystal Faces containing Multiple Connected Nets

On the Prediction of Crystal Morphology III: Equilibrium and Growth Behaviour of Crystal Faces containing Multiple Connected Nets

R.F.P. Grimbergen, P. Bennema and H. Meekes

Abstract

In this paper the equilibrium and growth behaviour of faces (hkl) with more than one connected net is studied. It is shown that for these types of orientation different surface phases exist under equilibrium conditions as a function of temperature. Depending on the exact bonding topology at the surface, flat, rough or disordered flat (DOF) phases are found. Moreover, the growth rate R_{hkl} of such faces can differ significantly from the usually calculated relative growth rates based on the attachment energy. Monte Carlo (MC) simulations confirm the results from the Hartman-Perdok analyses and offer a tool for the prediction of the crystal habit as a function of supersaturation.

4.1 Introduction

Recently a physical foundation for the description of the stability of faces (hkl) of crystals in terms of connected nets and Periodic Bond Chains (PBCs) was derived [Grimbergen et al., 1998b]. It was shown that application of the PBC theory to a crystal structure often leads to many connected nets for an orientation (hkl) and that specific combinations of connected nets may even cause a face (hkl) to roughen at zero Kelvin (T^R=0). This phenomenon was called symmetry roughening and it can have major implications for crystal morphology.

In a second paper [Meekes et al., 1998] all relevant symmetry relations for pairs of connected nets of a single orientation (hkl) were analysed. It was found that some symmetry relations between connected nets cause symmetry roughening and others result in the classical Bravais-Friedel-Donnay-Harker (BFDH) selection rules. The influence of a motherphase in contact with the crystal was included in the analysis.

In the present paper besides crystal faces containing symmetry related pairs of connected nets also pairs of connected nets for which such a symmetry relation is not present are treated. It will be shown that despite the absence of a symmetry relation the effective step free energy can be very low resulting in what will be called pseudo symmetry roughening. Simple crystal surface models, which are to our opinion generic for many types of crystal, will be used to illustrate the equilibrium and growth behaviour of a crystal face as a function of the connected net structure. In some cases the presence of multiple connected nets gives rise to a very small step energy which results in a roughening temperature for the orientation (hkl) (T^R_{hkl}) lower than the calculated 2-D Ising transition temperature (T^C_{hkl}) based on the connected net with the highest slice energy [Grimbergen et al., 1998b]. For other cases a so-called disordered flat (DOF) phase is found which is

known from simple statistical thermodynamical surface models with next nearest neighbour interactions [Rommelse and den Nijs, 1987,den Nijs and Rommelse, 1989]. Recently, DOF phases were found for the (111) [Woodraska and Jaszczak, 1997a, Woodraska and Jaszczak, 1997b] and (100) [den Nijs, 1997] faces of silicon and there is experimental [Grimbergen et al., 1998c] and theoretical [Grimbergen et al., 1998a] evidence that a DOF phase exists for the (011) faces of naphthalene.

Obviously, the surface phase of a face (hkl) will also affect the growth rate and mechanism of that face. It is well-known that the step free energy is an important parameter that determines the growth rate to a large extent. In the flat phase the step free energy is larger than zero and at low supersaturations layer-by-layer growth occurs, whereas in the rough phase the step free energy has vanished and continuous (rough) growth occurs even at the lowest supersaturations. For a DOF phase the step free energy has vanished, but a difference in energy of crossing steps keeps the surface flat. The effective nucleation barrier in the DOF phase appears to be very small [Woodraska and Jaszczak, 1997a, Woodraska and Jaszczak, 1997b, Grimbergen et al., 1998a].

In general we will show that crystal faces containing multiple connected nets may have a very small effective step energy which results in a growth rate being higher than the traditionally calculated growth rate which assumes a rate proportional to the attachment energy. The qualitative results are verified by Monte Carlo (MC) simulations of these specific orientations under equilibrium and growth conditions. In this way a prediction of the crystal habit as a function of temperature and supersaturation can be achieved. Notice that the morphology based on the attachment energy is by definition independent of the supersaturation [Hartman and Bennema, 1980].

In the next section three model crystal graphs are introduced. For all models the (001) orientation consists of multiple connected nets. In section 4.3 the connected net analysis for the (001) faces of all models is presented and the roughening transition temperatures are estimated. In addition, the growth behaviour will be discussed. In section 4.4 the MC simulation results are presented and in section 4.5 the MC results are compared with the results of the connected net analysis and the growth morphology is derived. Moreover, from the simulation data the growth morphology as a function of supersaturation is predicted. Finally, in section 4.6 some conclusions are drawn.

4.2 Model crystal graphs

In this section three different types of crystal graph are introduced which are generic for many crystals. The attention will be focussed on the (001) orientation of these graphs. All (001) orientations have in common that there are at least two different connected nets present. The number of growth units in the unit cell of all crystal graphs is two (Z=2). Growth units are labelled with A and B to indicate that their position with respect to the (001) orientation may be different. It is assumed that the chemical composition of the growth units is equivalent.

The first crystal graph is drawn in figure 4.1. The (001) orientation can be considered as that of a classical simple cubic or Kossel crystal. However, the difference is that in our model the (001) face is an AB-layered structure.

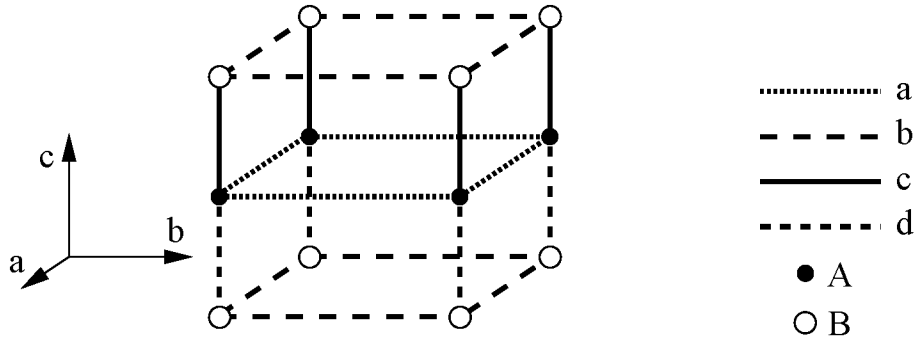

Figure 4.1: Crystal graph for the AB-layered Kossel models (type I and II).

Two different types of crystal surface were studied for the (001) face of this crystal graph. The first type has equivalent horizontal bonds and thus the bond energies are equal ($\Phi_a = \Phi_b$) and the vertical bonds are different ($\Phi_c \neq \Phi_d$), Φ being the bond energy per growth unit. In this case we consider a layered structure with alternating layers A and B with vertical bonds c and d respectively. This surface type will be referred to as type I. Second, the case that the vertical bonds are equivalent ($\Phi_c = \Phi_d$) and the horizontal bonds differ ($\Phi_a \neq \Phi_b$) is considered. This type of crystal face is called type II. Note that in the isotropic case with $\Phi_a = \Phi_b = \Phi_c = \Phi_d$ the two types I and II become equivalent and correspond to the well-studied (001) face of the Kossel model.

The second model graph of which the (001) orientation corresponds to a (110) Kossel-like face is drawn in figure 4.2. Again, it is clear that this orientation is an AB-layered structure.

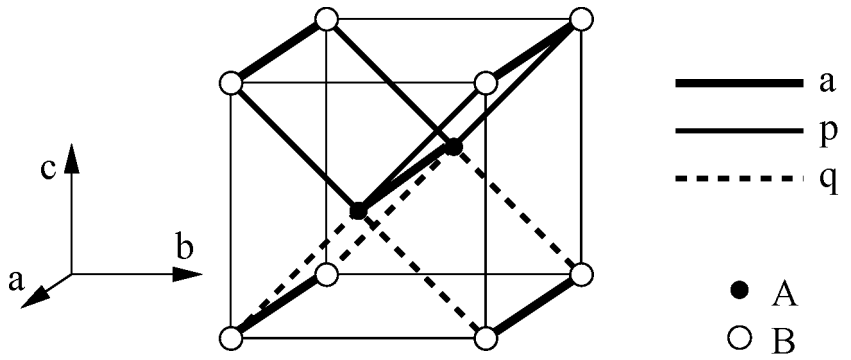

Figure 4.2: Crystal graph for the modified (110) Kossel model (type III). The thin solid lines are drawn to indicate the unit cell edges but do not represent bonds of the crystal graph.

Along the a-direction a horizontal bond a is present, whereas in the b-direction there is no horizontal bond present. The oblique bonds p and q make the crystal graph connected. This type of crystal surface is called type III.

To study (001) AB-layered body centered types of crystal surface the (001) face of a third model graph depicted in figure (4.3) was used. Note that there are no horizon-

tal bonds present for the (001) orientation neither in the a- nor in the b-direction, but exclusively the oblique bonds p and q. This type of crystal facet is called Type IV.

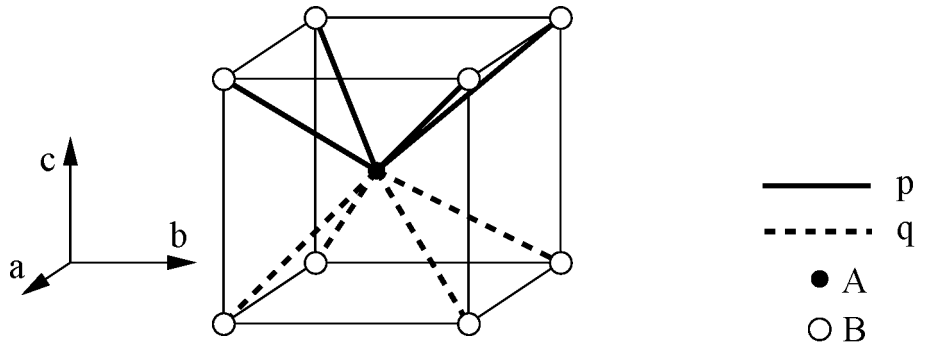

Figure 4.3: Crystal graph for the (001) BCSOS model (Type IV). The thin solid lines are drawn to indicate the edges of the unit cell, but do not represent bonds of the crystal graph.

4.3 Connected net analysis

In the next subsections all connected nets for the (001) orientations of the model crystal graphs will be presented briefly. All connected nets are used to derive the overall broken bond step energies.

4.3.1 Types I and II

Four connected nets can be identified for the (001) orientation of the crystal graph in figure 4.1. A [100] projection of the connected nets is shown in figure 4.4. From the figure it can be clearly observed that the connected nets $(001)_1$ and $(001)_2$ consist of two stacked $(001)_3$ and $(001)_4$ connected nets. The broken bond step energy for this orientation is equal to the step energy of a step $(001)_1$ (or $(001)_2$) for both types I and II and is equal to $(\gamma_1 + \gamma_2)$ both in the a- and b-direction. This step energy determines the roughening transition temperature T^R_{001}. In the special case that $\Phi_a = \Phi_b = \Phi_c = \Phi_d = \Phi$ the roughening temperature will be governed by γ_1 $(=\gamma_2 = \Phi)$. Again, this limiting case corresponds to the (001) face of the simple cubic Kossel model.

A type I facet grows with either $(001)_1$ or $(001)_2$ growth layers depending on the surface free energy of the surface bounded by $(001)_1$ or $(001)_2$. In principle, the orientation can grow alternately with $(001)_3$ and $(001)_4$ growth layers when the energies do not differ too much. Type II surfaces will grow alternately with layers $(001)_3$ and $(001)_4$. Usually it is assumed that the growth rate will be determined mainly by the layer with the lowest growth velocity.

4.3.2 Type III

The (001) face of the crystal graph in figure 4.2 contains two connected nets $(001)_1$ and $(001)_2$. In figure 4.5 the [100] projection of the connected nets is depicted. Assuming that

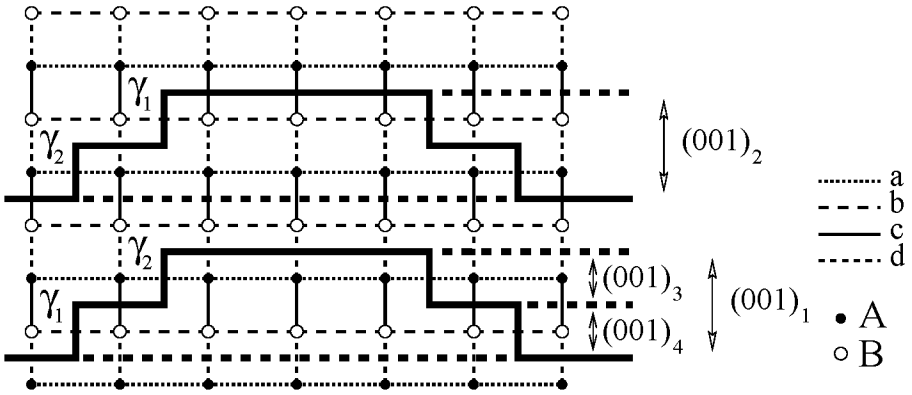

Figure 4.4: Projection along [100] of the crystal graph in figure 4.1. Connected nets are indicated with $(hkl)_n$ with n=1,2,3,4. The broken bond step energies γ_1 and γ_2 are drawn as well.

$\Phi_p < \Phi_q$ the (001) face will be bounded by $(001)_1$. The step energy is equal to the broken bond step energy γ_1. This step energy can be found by calculating the energy difference of the surface bounded by $\alpha\beta\gamma\delta$ and $\alpha\beta\epsilon\phi\gamma\delta$ (figure 4.5) [Grimbergen et al., 1998b]. For this case $\gamma_1 = \Phi_q - \Phi_p$ both for step $\beta\epsilon$ and step $\phi\gamma$. Note that the broken bond step energy along the [010] direction is equal to the broken bond energy Φ_a.

The growth kinetics for these types of crystal facet are governed by the broken bond energy difference $|\Phi_p - \Phi_q|$. If $|\Phi_p - \Phi_q| \rightarrow 0$ the step free energy will become very small. Therefore, it is expected that the crystal facet becomes rough already at very low supersaturations and will grow in a rough (continuous) mode ($R_{hkl} \propto \exp[\Delta\mu]$). A limiting case is the situation where $\Phi_p = \Phi_q$. Then the model reduces to the (110) face of a simple cubic Kossel model which has a roughening temperature of zero Kelvin. Note that for that case formally no valid connected net is present for this orientation [Grimbergen et al., 1998b]. Consequently, such a facet will grow in a continuous (rough) mode and is in fact already rough at zero supersaturation.

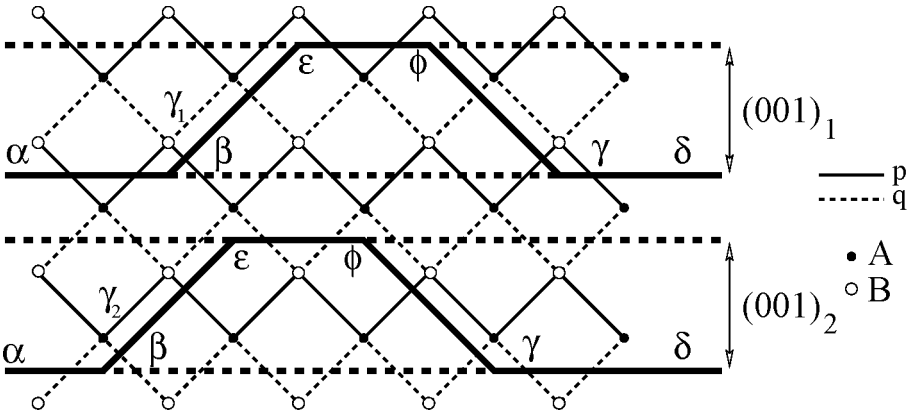

Figure 4.5: Projection along [100] of the crystal graph in figure 4.2 and the crystal graph in figure 4.3. Connected nets are indicated with $(hkl)_n$ with n=1,2.

4.3.3 Type IV

Principally, the same situation described in the previous subsection applies to the (001) orientation of the crystal graph of figure 4.3. The fundamental difference between faces of type III and type IV is that for type IV the broken bond step energies for the [100] and [010] direction are equal to the step energies of type III faces along the [100] direction. This step energy is equal to $|\Phi_p - \Phi_q|$ and determines the roughening transition temperature for type IV facets. Under growth conditions the 2-D nucleation barrier is determined only by the step energy $|\Phi_p - \Phi_q|$.

A well-known limiting case for which ($\Phi_p = \Phi_q$) is described by the isotropic BCSOS model without next nearest neighbour interactions [van Beijeren, 1977]. This model has a roughening transition temperature (T^R) of zero Kelvin.

4.4 Monte Carlo simulations

4.4.1 Simulation setup

For all simulations a standard Metropolis algorithm was implemented according to ref. [Gilmer and Bennema, 1972a]. The rate of attachment of molecules at a site (K^+) is proportional to the supersaturation $\Delta\mu$

$$K^+(\Delta\mu) = K_0^+ \exp[\Delta\mu/\mathrm{k}T] \,, \tag{4.1}$$

where k is the Boltzmann constant and T the absolute temperature. K_0^+ is the attachment rate at equilibrium given by

$$K_0^+ = P_0^+ I_0 A \,, \tag{4.2}$$

where P_0^+ is the probability that a growth unit impinging on a site is correctly positioned to attach to the crystal surface, I_0 is the equilibrium rate of impingement of growth units per unit area and A is the area of a lattice site. In our simulation we assume that P_0^+ is not dependent on the type of bond which is being formed and is taken to be a constant [Gilmer and Jackson, 1977]. For our AB-layered surfaces the rate at which growth units at the surface will detach depends exponentially on the binding energy (E_b^A for layer A and E_b^B for layer B) of the growth unit at the surface which is strongly site dependent:

$$K^-(E_b^A/\mathrm{k}T) = K_0^- \exp[-E_b^A/\mathrm{k}T] \tag{4.3}$$

and

$$K^-(E_b^B/\mathrm{k}T) = K_0^- \exp[-E_b^B/\mathrm{k}T] \,, \tag{4.4}$$

where K_0^- is a constant. At equilibrium the average detachment and attachment rates must be equal. For our layered surface structures we have assumed that the average attachment rate is equal to the average detachment rate of a growth unit with a binding energy of exactly half the average binding energy of a growth unit in the fully occupied lattice, denoted $\bar{\Phi}$:

$$K^+(\Delta\mu = 0) = K^-(\bar{\Phi}/\mathrm{k}T) \,. \tag{4.5}$$

This implies along with eq. (4.1) the relation

$$K_0^+ = K_0^- \exp[\mu_0/\mathrm{k}T] \,, \tag{4.6}$$

where $\mu_0 = -\bar{\Phi}$ is the average chemical potential at equilibrium. In our simulation model the anisotropy (δ) is defined in terms of bondenergies Φ according to:

$$\delta = \Phi_1/\Phi_2 \wedge \frac{\Phi_1 + \Phi_2}{2} = \Phi \,, \tag{4.7}$$

with $0<\delta\leq 1$. Relation (4.7) guarantees a constant lattice energy for simulations with a different anisotropy. The definition of the bonds used in the MC simulations of the four types of crystal facets are listed in table 4.1. Note that for the model types I and II i=0-4 and for type III i=0-2. For model IV the binding energy at a site does not depend on the number of neighbours. The bondenergies are defined per growth unit (Φ) while in the simulation the total energy of a bond (2Φ) is used. Our simulation model has three free (dimensionless) parameters, namely $\Phi/\mathrm{k}T$, δ and $\Delta\mu/\mathrm{k}T$.

Table 4.1: Definitions of bonds used in the MC simulations for the different model types I-IV. In the second and third column the bonds that lead to the anisotropy (Φ_1 and Φ_2) are given for each model. The remaining bonds of each model are shown in the fourth column and have a bondstrength of Φ per growth unit in our simulation model. In the fifth column half the average binding energy of a growth unit in the fully occupied lattice is given and the last two columns contain the binding energies for a growth unit in layer A or B with number of neighbours i within the layer.

Type	Φ_1	Φ_2	Φ	$\bar{\Phi}$	E_b^A	E_b^B
I	Φ_c	Φ_d	Φ_a,Φ_b	6Φ	-2Φ_1-2$i\Phi$	-2Φ_2-2$i\Phi$
II	Φ_a	Φ_b	Φ_c,Φ_d	6Φ	-2Φ-2$i\Phi_1$	-2Φ-2$i\Phi_2$
III	Φ_p	Φ_q	Φ_a	6Φ	-4Φ_1-2$i\Phi$	-4Φ_2-2$i\Phi$
IV	Φ_p	Φ_q	-	8Φ	-8Φ_1	-8Φ_2

The solid-on-solid (SOS) condition was defined differently for the different types of surface. For type I and II faces the standard SOS condition of the simple cubic Kossel model was applied for which all incoming growth units can only be bonded to an underlying growth unit (c or d bond, see figure 4.1). A modified SOS condition has been applied for type III faces. Each incoming growth unit has to make two bonds with the interface (either p or q bonds, see figure 4.2). For the type IV faces four bonds (either p or q, see figure 4.3) have to be formed. This is the well-known BCSOS condition.

Sticking coefficients S for the surfaces were defined as

$$S = \frac{attachments - removals}{attachment\ attempts} \tag{4.8}$$

and crystal growth rates R by

$$R = S d_{hkl} K^+ \,, \tag{4.9}$$

where d_{hkl} is the interplanar distance of the face (hkl).

A convenient unit of time used in MC simulations is the Monte Carlo Sweep (MCS), which equals 1 when the number of attempted moves is equal to the number of matrix sites. In our simulations square matrices with dimensions 30x30 (L=30) and 40x40 (L=40) were used. The equilibration time was typically in the order of $1 \cdot 10^5$-$0.5 \cdot 10^6$ MCS and the subsequent data collection run $0.5 \cdot 10^6$-$1 \cdot 10^6$ MCS. For the anisotropy parameter the values δ=1, 0.8, 0.6 and 0.4 were chosen.

During the simulation several quantities were calculated. A very important quantity is the height-difference correlation function which diverges in case of thermal roughening (for a review see refs. [Weeks, 1986,van Beijeren and Nolden, 1986]). The height-difference correlation function is defined as

$$G(r) \equiv < [h(r) - h(r_0)]^2 > \tag{4.10}$$

and diverges in case of thermal roughening as

$$\lim_{r \to \infty} G(r)/a^2 \to [K_\infty(T)/\pi] \ln(r) \; . \tag{4.11}$$

Here, $h(r_0)$ is the height of a reference position, $r = |r - r_0|$ is the lateral distance parallel to the surface, a is the vertical periodicity and $< ... >$ denotes a thermal average. The roughening temperature can be determined by locating the temperature at which the G(r) function takes on the universal value K_∞=$2/\pi$ [Shugard et al., 1978]. For our models the periodicity is a=2 (eq. 4.11) in case δ<1 due to the AB-layered structure. For δ=1 the periodicity is a single layer and thus a=1 was used in eq. (4.11) to determine the roughening temperature. The height difference simulation data were fitted to the functional form $G(r) = [A/\pi^2]\ln(r) + C$ for L=40 and r =6-16. Note that for δ=1 thermal roughening occurs in case $A \geq 2$ and for δ<1 roughening occurs for $A \geq 8$.

Another quantity that can be calculated easily during the MC simulation is the surface specific heat $c(T)$. The surface specific heat can be calculated from the surface energy fluctuations as

$$c(T) = \frac{1}{N \mathrm{k} T^2} (< E_s^2 > - < E_s >^2) \; , \tag{4.12}$$

where N is the number of matrix sites, k is the Boltzmann constant, T is the absolute temperature and E_s is the surface energy of the complete surface. Because of its sensitivity to energy fluctuations in finite systems, $c(T)$ is a useful tool for indicating phase transitions.

The interface width $\sqrt{< \delta h^2 >}$ provides information about the roughness of a crystal face and is defined as:

$$< \delta h^2 > \equiv \frac{1}{N} \sum_i < (h_i - \bar{h})^2 > \; , \tag{4.13}$$

where N is the number of matrix sites and

$$\bar{h} = \frac{1}{N} \sum_i h_i \; . \tag{4.14}$$

4.4.2 Equilibrium results

In table 4.2 the results of the equilibrium MC simulations for the four types of (001) facets are summarized.

Table 4.2: Results of the Monte Carlo simulations for $\Delta\mu$=0. For all four types of surface the temperatures kT/Φ are listed where the specific heat $c(T)$ has a maximum and the amplitude A of the height-difference correlation function $G(r)$ becomes 2 (δ=1) or 8 (δ<1) as a function of the anisotropy δ.

	Type I		Type II		Type III		Type IV	
δ	$c(T)$ (kT/Φ)	$G(r)$ (kT/Φ)	$c(T)$ (kT/Φ)	$G(r)$ (kT/Φ)	$c(T)$ (kT/Φ)	$G(r)$ (kT/Φ)	$c(T)$ (kT/Φ)	$G(r)$ (kT/Φ)
0.4	1.74	2.22	2.10	2.41	1.40	3.10	1.25	-
0.6	1.60	2.22	1.90	2.35	1.05	2.90	0.67	-
0.8	1.33	2.22	1.74	2.25	0.70	2.65	0.31	-
1.0	1.17	1.29	1.17	1.29	-	-	-	-

4.4.2.1 Types I and II

The results for types I and II are comparable. At low temperatures the facets are perfectly flat whereas at higher temperatures first excitations of single particles appear and eventually the face becomes completely rough at high temperatures. As already mentioned before in the isotropic limit δ=1 type I and II both represent the simple cubic Kossel model. The Monte Carlo results for this case yield a roughening temperature of kT^R/Φ=1.29 which is in good agreement with previously reported values of kT^R/Φ=1.28 [Leamy and Gilmer, 1974]. Moreover, the maximum in the specific heat at kT/Φ=1.17 is in good agreement with the reported value of kT/Φ=1.15 by Swendsen [Swendsen, 1977].

From the connected net analysis in section 4.3 it was concluded that the roughening temperatures T^R of types I and II surfaces are determined by the overall step energy of a complete step (001). With the restrictions of our MC simulations (see eq. (4.7)) this step energy is for both types equal to Φ=2kT in case δ<1. As an estimate for the roughening temperature T^R the 2-D Ising transition temperature T^C of a simple cubic isotropic connected net with a bondstrenght of 2Φ can be calculated. Using the program TCRITIC [Hoeks, 1993] we found kT^C/Φ= 2.27 which is in rather good agreement with the calculated roughening temperatures for the type I and II surfaces determined from the height-difference correlation function $G(r)$ as shown in table 4.2.

At the temperature at which the specific heat has a maximum, the fluctuations of the surface energy are maximal. The specific heat for type II surfaces is plotted against the temperature in figure 4.6. We attribute the increase in fluctuations to a drastic drop in the step free energy of the strongest connected net $(001)_3$ (in case Φ_a>Φ_b, see figure 4.4) which is present at the surface. On the other hand, the roughening temperature has a value which is considerably higher than the maximum in $c(T)$. Moreover, T^R is

less dependent of the anisotropy, at least for type I. The temperature interval between $T(c^{max})$ and T^R is rather small in the isotropic case, takes on the largest value for very small anisotropy and decreases again for larger anisotropies.

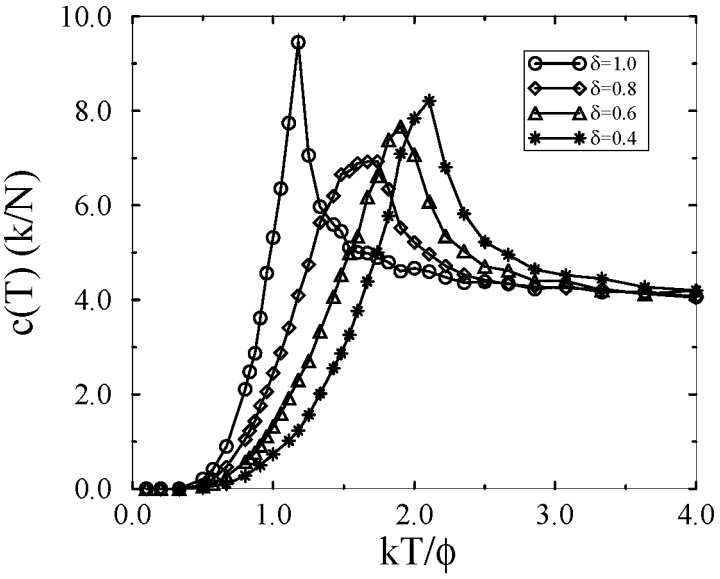

Figure 4.6: The specific heat $c(T)$ for type II surfaces as a function of the temperature kT/Φ for δ=1.0, δ=0.8, δ=0.6 and δ=0.4.

In figure 4.7 the interface width δh for type II surfaces is plotted. Remarkebly, in the anisotropic cases the interface width becomes more or less linear with temperature at T=T^R. Moreover, the deviation for the anisotropic cases from the isotropic surface, starting from $\Delta\mu/kT\approx1$, clearly demonstrates that the anisotropic surfaces maintain their flatness upto higher temperatures. The difference in behaviour of the isotropic surface and the slightly anisotropic surface (δ=0.8) indicates that the introduction of anisotropy has an unexpectedly pronounced effect.

All these observations suggest that for anisotropic AB-layered Kossel-like faces, the surface becomes locally disordered but remains essentially flat at temperatures between $T(c^{max})$ and T^R. This intermediate phase might be compared to that of a DOF phase, although such a phase has not been identified for such types of surface.

In order to get more insight in the behaviour of the step energy as a function of temperature, simulations were done for type II surfaces with and without a complete step along [010]. This was done by a modification in the periodic boundary conditions in such a way that always a complete (001) step (with height 2 due to the AB-layered structure) is present. From these simulations the step energy densities for δ=1.0, δ=0.8 and δ=0.6 were calculated as shown in figure 4.8.

If the results are compared with table 4.2 it is clear that the step energy drops drastically at the temperature $T(c^{max})$ and slowly approaches zero at T^R. Thus, the steepness

of the step energy density drop is a measure for the temperature interval for the intermediate phase. The drop in step energy can also be found in simulated growth curves which will be presented in section 4.4.3.

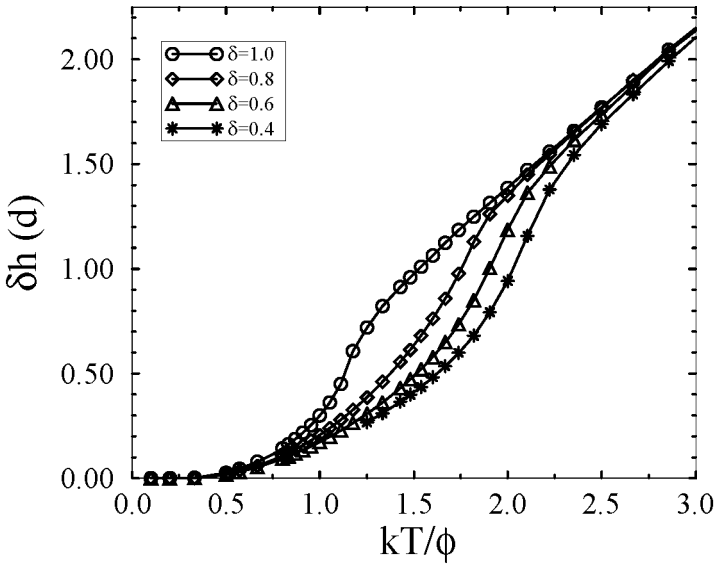

Figure 4.7: Interface width δh for type II surfaces as a function of temperature.

4.4.2.2 Type III

Recently the phase diagram of type III surfaces was derived showing a flat, a disordered flat (DOF) and a rough phase. It was shown that the temperature at which a maximum in the specific heat is found coincides with the preroughening transition temperature T^{pr} [Grimbergen et al., 1998a]. The roughening transition at $T{=}T^R$ was found at the point where the amplitude A became larger than 8. The MC results of the present study are equivalent to those presented in ref. [Grimbergen et al., 1998a]. It can be concluded that type III surfaces are flat for $T{<}T^{pr}$, disordered flat for $T^{pr}{<}T{<}T^R$ and rough for $T{>}T^R$. At $T{=}T^{pr}$ the step energy drops to a very small value. This behaviour of the step energy as a function of temperature can be compared to the results for type II surfaces as shown in figure 4.8. The case of $\delta{=}1$ is absent in table 4.2 because it corresponds to the anisotropic limit of the model for which the step energy along the [100] direction (see figure 4.5) is zero. Therefore, the roughening temperature kT^R/Φ is zero. It is not possible to perform a reliable MC simulation for this limiting case.

4.4.2.3 Type IV

The results for type IV surfaces with $\delta{=}1$ are rather trivial since the step energies for both the [100] and [010] direction are zero. This isotropic case has a roughening temperature

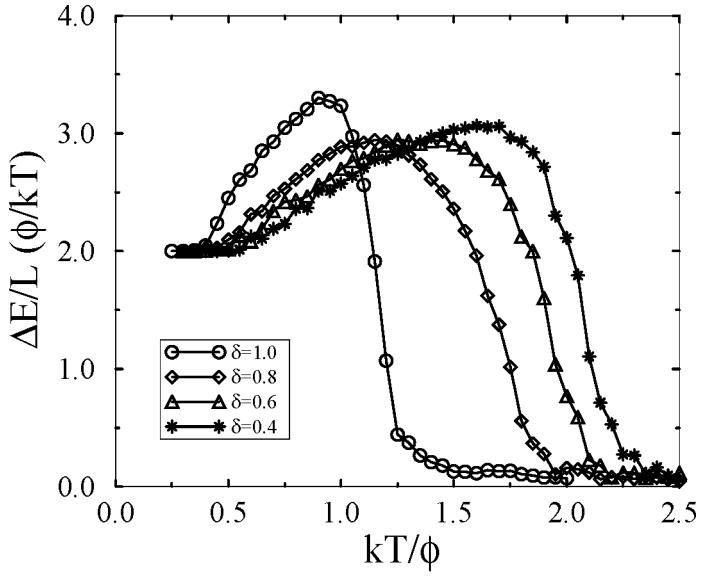

Figure 4.8: Step energy density $\Delta E/L$ for type II surfaces as a function of the temperature kT/Φ for δ=1.0 (kT^R/Φ=1.29) , δ=0.8 (kT^R/Φ=2.25) and δ=0.6 (kT^R/Φ=2.35).

of zero Kelvin [van Beijeren, 1977]. In case δ<1 the step energy is larger than zero. A remarkable feature of the MC results for δ<1 is that the amplitude A does not exceed the critical value of 8, even at the highest temperatures indicating that the surface does not become rough (table 4.2). To our opinion the results of the type IV surface model can be compared to those of the staggered BCSOS model as described in refs. [Mazzeo et al., 1995, Nolden and van Beijeren, 1994] where for anisotropic surfaces with attractive bonds only a flat and DOF phase were found. Therefore, we think that our model has a flat and a DOF phase separated by a preroughening phase transition which causes the maximum in the specific heat. The absence of a rough phase must be attributed to the very strict solid-on-solid condition. The temperatures at which the specific heat is maximal are in good agreement with the calculated 2-D Ising transition temperature of a simple cubic isotropic connected net with a bondstrength equal to the effective step energy ($\Phi_p - \Phi_q$) calculated using the program TCRITIC [Hoeks, 1993]. The calculated 2-D Ising transition temperatures where kT^C/Φ=1.10 (δ=0.4), kT^C/Φ=0.64 (δ=0.6) and kT^C/Φ=0.28 (δ=0.8).

4.4.3 Off-equilibrium results

In order to study the growth behaviour of the different types of crystal face, MC simulations with $\Delta\mu/kT$>0 were done. In the present study we restricted ourselves to simulations of perfect crystal facets without dislocations. Thus, the growth mechanism is 2-D nucleation growth at low supersaturation and continuous (rough) growth at higher supersaturations.

4.4.3.1 Types I and II

For the type I surfaces the surface (or attachment) energies for the two sublayers A and B become different in case δ<1. It is expected that upon increasing the anisotropy ($\delta \to 0$), the growth rate will decrease as the attachment energy for a complete double layer (001) decreases. The results of the MC simulations are shown in figure 4.9. The temperature kT/Φ=0.83 is chosen in such a way that all surfaces are flat at $\Delta\mu$=0. It can be seen very clearly that the nucleation barrier increases with decreasing δ (i.e. increasing anistropy).

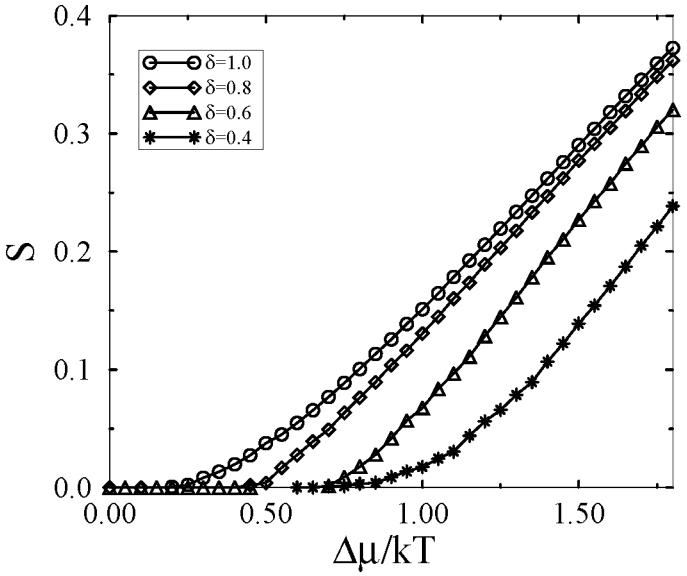

Figure 4.9: Sticking fraction S for type I surfaces as a function of the supersaturation $\Delta\mu$/kT at a temperature of kT/Φ=0.83 and for different anisotropies δ.

An interesting detail in figure 4.9 is the behaviour of the sticking fraction for the isotropic (δ=1) surface as compared to the behaviour of the sticking fraction for small anisotropy (δ=0.8). It is clear that when the anisotropic face starts growing ($\Delta\mu$=0.45kT) it is almost immediately growing linearly with increasing supersaturation. In contrast, the isotropic (δ=1) surface starts growing at much lower supersaturation ($\Delta\mu$/kT=0.17) and becomes linear at much higher supersaturation ($\Delta\mu$/k$T\approx$0.9). At $\Delta\mu$/kT=0.55 the interface width of the anisotropic surface becomes higher than that of the isotropic surface.

Another interesting result of the dynamics simulations for type I surfaces is that at the supersaturation at which the sticking fraction becomes approximately linear, a maximum in the specific heat $c(\Delta\mu)$ is found in case δ<1. The corresponding supersaturations were $\Delta\mu$/kT=0.7 (δ=0.8), $\Delta\mu$/kT=0.9 (δ=0.6) and $\Delta\mu$/kT=1.1 (δ=0.4).

In the case of type II surfaces the situation is somewhat different. The attachment energies are equivalent for both surfaces (A or B on top). On the basis of the attachment energy criterion the growth rate should be the same independent of the anisotropy. In figure 4.10

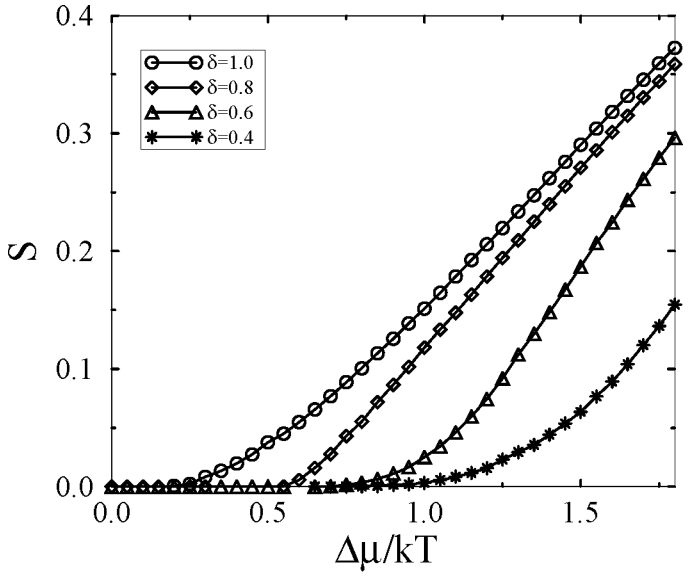

Figure 4.10: Sticking fraction S for type II surfaces as a function of the supersaturation $\Delta\mu/\mathrm{k}T$ for a temperature $\mathrm{k}T/\Phi$=0.83 and different anisotropies δ.

the sticking fraction is plotted versus the supersaturation for a temperature $\mathrm{k}T/\Phi$=0.83. It can be concluded that the anisotropy has the same kind of influence on the nucleation barrier as it has for type I faces. The shape of the curves, however, is different.

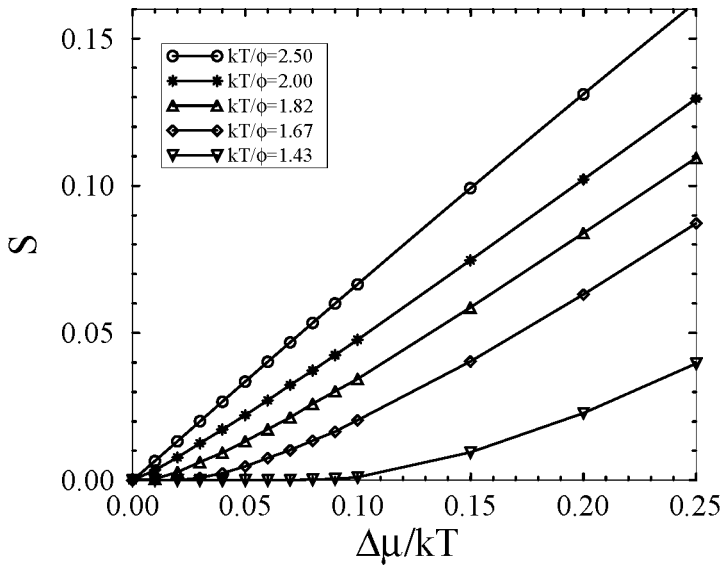

Figure 4.11: Sticking fraction S for type II surfaces as a function of the supersaturation $\Delta\mu/\mathrm{k}T$ for δ=0.6 and different temperatures ($\mathrm{k}T/\Phi$ $(c(T)^{max})$=1.90)

Still, as for type I surfaces, the sticking fraction becomes almost immediately linear when growth starts for the nearly isotropic case (δ=0.8). For the type II surface also the growth behaviour at temperatures near the maximum in the specific heat (in equilibrium) was studied. It appeared that the nucleation barrier becomes very small at temperatures above $T(c^{max})$ (figure 4.11). This is in correspondence with the step energy densities (figure 4.8) which drop to very low values at this temperature. This behaviour of the step energy as a function of temperature was found for both type I and II surfaces.

A remarkable feature of the anisotropic surfaces is that at the supersaturation at which the sticking fraction becomes more or less linear, the interface width is very small indicating that the surface is still flat. Generally, it was not possible to derive a simple nucleation model which describes the MC results for the anisotropic type I and II surfaces. Probably, these models are too simplified to capture the essential kinetics of these more complicated surfaces as compared to the (001) faces of a Kossel crystal.

4.4.3.2 Type III

The results for type III surfaces are described in detail in ref. [Grimbergen et al., 1998a]. In figure 4.12 the sticking fraction versus supersaturation is plotted for these types of surface. The temperature of kT/Φ=0.67 was chosen just below the preroughening temperature for the surface with δ=0.8 (table 4.2). It was already concluded from the connected net analysis as presented in section 4.3 that the step free energy along the [010] direction is zero for δ=1.0. This is reflected in the absence of a nucleation barrier for δ=1.0. With decreasing δ the step energy increases and thus the nucleation barrier increases.

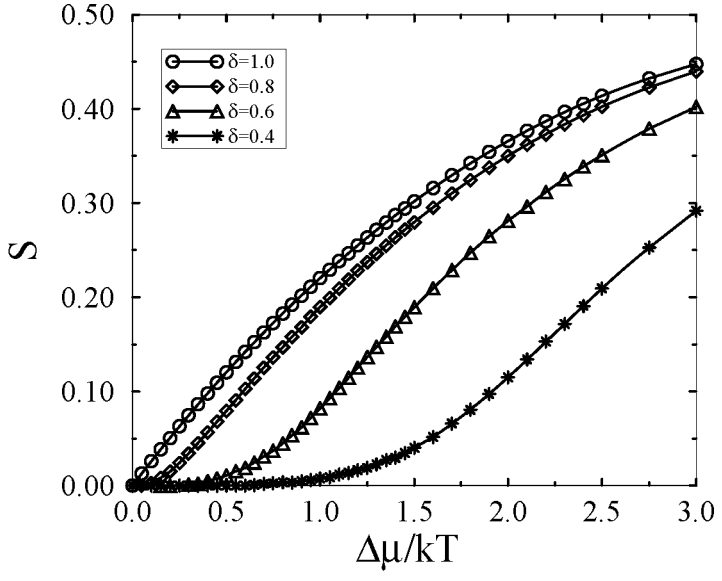

Figure 4.12: Sticking fraction versus supersaturation for type III surfaces at kT/Φ=0.67

For this type of surface the surface energy is directly related to the step energy. When δ increases the surface energy of the most favourable surface (A or B) decreases. In terms of attachment energy this implies that the growth rate will decrease for the face. This is in agreement with the MC simulation data (figure 4.12).

It can be shown that at temperatures above the preroughening temperature T^{pr} this type of face still grows layer-by-layer at low supersaturations [Grimbergen et al., 1998a]. This result was also found for type IV surfaces as explained in the next section. The general behaviour of the sticking fraction clearly deviates from that of the type I and II surfaces. Only for the very anisotropic δ=0.4 surface which corresponds to step energies Φ for steps along [010] and 0.86Φ for steps along [100], the effective anisotropy is very small in the sense that this surface behaves already like a type I isotropic surface. For this case the sticking fraction becomes indeed linear while for higher values of δ the sticking fraction saturate already at lower supersaturations to the maximum value of approximately 0.5, which is determined by the SOS condition.

4.4.3.3 Type IV

In figure 4.13 the sticking fraction versus supersaturation is plotted for a type IV surface with δ=0.6 at different temperatures. From the equilibrium simulations it was found that the preroughening temperature T^{pr} for this surface is kT^{pr}/Φ=0.67. Looking at figure 4.13 it is clear that for temperatures $T>T^{pr}$ there is still a significant nucleation barrier and the sticking fraction is clearly not linear for these temperatures. It is expected that at these temperatures the crystal face will grow as a flat face by a layer-by-layer mechanism. This is confirmed by the analysis of the average height of the surface (see eq. (4.14) as a function of time (figure 4.14). It appears that the surface grows with double layers AB (or BA) as expected from the connected net analysis.

The behaviour of the interface width for these types of surface is also remarkable. The values stick for a rather broad range of $\Delta\mu/$kT at a value of 1 and subsequently deviate slowly to higher values. The supersaturation at which the interface width starts to deviate from 1 coincides with the supersaturation at which the sticking fraction becomes linear. To our opinion the simulation data suggest that kinetic roughening may occur for this type of crystal faces, but at rather high supersaturations. This can be attributed to the strict SOS restriction that is applied which causes a decrease of available sites for attachment at the interface as the roughness increases. In contrast, the number of available sites for attachment for type I and II surfaces does not depend on the surface roughness.

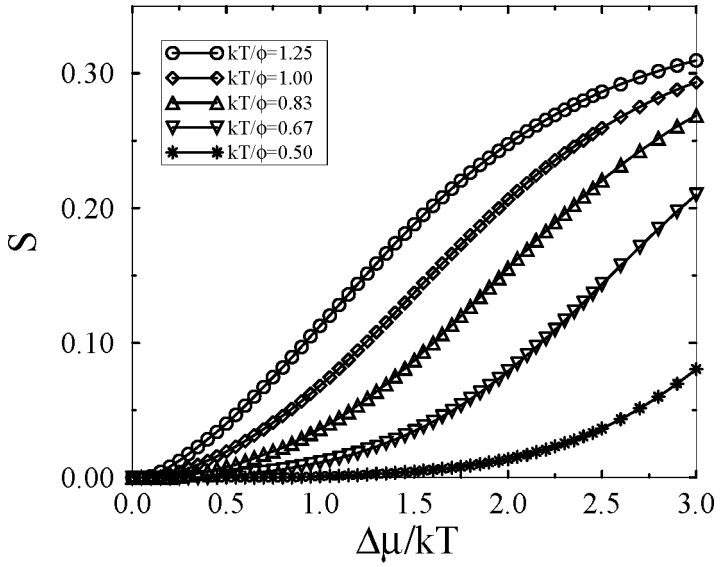

Figure 4.13: Sticking fraction versus supersaturation for a type IV surface with δ=0.6 at different temperatures (k$T(c^{max})/\Phi$=0.67)

4.5 Implications for the morphology

In this section the most widely used recipes to determine the relative growth rates of crystal faces (R_{hkl}) will be discussed and compared to the MC simulation results.

A well-known purely geometrical recipe for the relative growth rate R_{hkl} is given by

$$R_{hkl} \propto 1/d_{hkl} \ , \tag{4.15}$$

where d_{hkl} is the interplanar distance for a face (hkl) corrected for the X-ray reflection conditions given by Bravais, Friedel, Donnay and Harker (BFDH) [Donnay and Harker, 1937, Friedel, 1911]. We will refer to this method as the BFDH method. The success of this simple recipe can be attributed to the fact that for isotropic crystals faces with a large d_{hkl} have a large energy content and are, therefore, the most stable faces.

A recipe that is taking the energy of a face into account is the frequently used attachment energy method. The attachment energy is defined as the energy released when a complete growth layer attaches to the surface. The attachment energy is related to the crystal energy by $E^{cr} = E^{sl}_{hkl} + E^{att}_{hkl}$ where E^{sl}_{hkl} is the slice energy. Hartman and Bennema argued that for moderate supersaturations the relative growth rates may be obtained by [Hartman and Bennema, 1980]

$$R_{hkl} \propto E^{att}_{hkl} \ . \tag{4.16}$$

In the attachment energy method the interplanar distances are also corrected for the X-ray reflection conditions. Note that neither in the BFDH recipe nor in the attachment energy the temperature or supersaturation play a role.

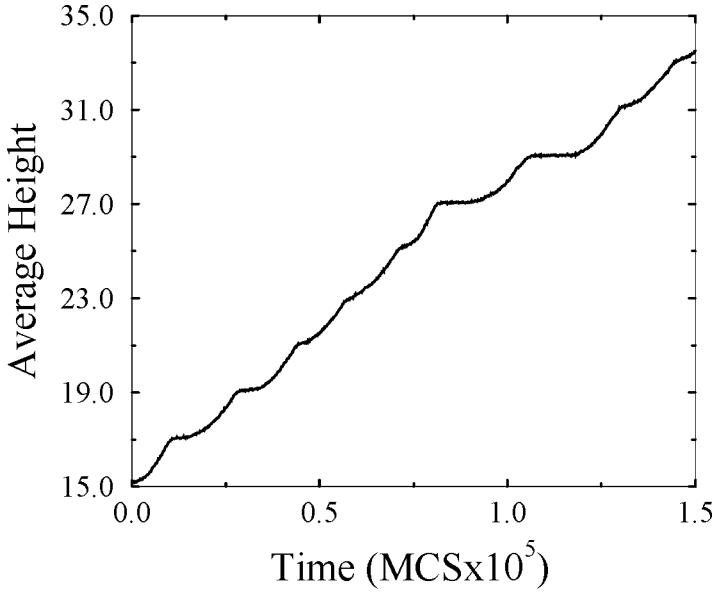

Figure 4.14: The average height of the matrix (size L=40) versus simulation time for type IV surfaces at kT/Φ=0.83 and $\Delta\mu/$kT=0.3 (kT^{pr}/Φ=0.67)

In this section the crystal graph as shown in figure 4.2 will be used to demonstrate that the above mentioned recipes may lead to a very poor prediction of the growth morphology. It is assumed that the A and B growth units are chemically equivalent, but oriented differently. The space group symmetry is supposed to be Pmm2. All connected nets were determined using the program FACELIFT [Grimbergen et al., 1997]. The connected forms found with the number of different connected nets between brackets, are {100} (1), {010} (2), {001} (2) and {011} (1). The predicted morphologies based on eq. (4.15) and eq. (4.16) are shown in figure 4.15.

Note that the bond energies used to calculate the attachment energies are defined according to relation (4.7) which guarantees a constant lattice energy for different δ. As a result the attachment energy for the {100}, {010} and {011} faces is equal to 2Φ and independent of δ. In contrast, the attachment energy for the {001} faces does depend on the anisotropy δ and is equal to $2\Phi_1$ (in case $\Phi_1<\Phi_2$) or $2\Phi_2$ (for $\Phi_1>\Phi_2$) (compare figure 4.15c and 4.15d).

Looking at figure 4.15a and 4.15b it can be observed that for this crystal graph there is already a large difference between the forms predicted using the BFDH or attachment energy recipe. This difference can be attributed to the special bond topology at the surfaces which is Kossel-like for the {110} and {100} faces and Kossel (110)-like for the {001} and {010} faces. Using the concept of symmetry roughening and pseudo symmetry roughening it is possible to modify the attachment energy prediction by removing the faces which show symmetry roughening or pseudo symmetry roughening from the morphology (see figure 4.15d).

A better way to predict the growth morphology is to derive the relative growth rates directly from the MC simulations.

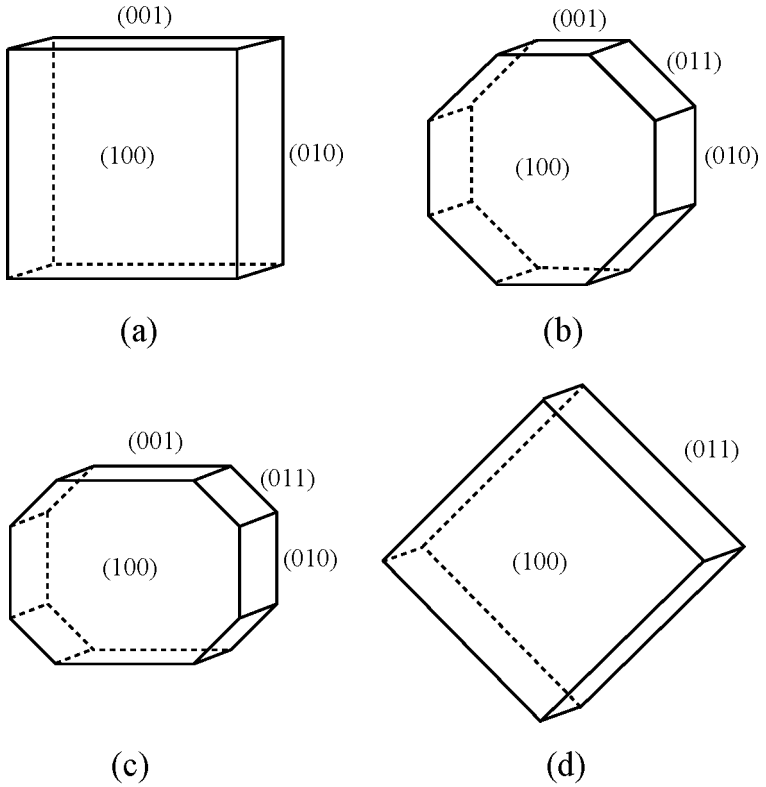

Figure 4.15: Predicted growth morphology for the model graph of figure 4.2 based on (a) $R_{hkl} \propto 1/d_{hkl}$, (b) $R_{hkl} \propto E^{att}_{hkl}$ (δ=1.0), (c) $R_{hkl} \propto E^{att}_{hkl}$ (δ=0.4) and (d) $R_{hkl} \propto E^{att}_{hkl}$ assuming that the {010} and {001} faces are symmetry roughened and have grown out.

For the simulations it was assumed that the {100} and {011} faces can be modelled by an isotropic type I (δ=1) surface, whereas the {001} and {010} faces were modelled by a type III surface with respectively δ=0.8 and δ=1. This is reasonable as an anisotropy of δ=0.8 has by far the most prominent effect on the faces {001} and {010}. The simulations were done at a temperature of kT/Φ=0.67. In figure 4.16 the growth rates are plotted as a function of supersaturation. Due to the assumption that both the {100} and {011} faces can be modelled with an isotropic type I surface, the ratio R_{100}/R_{011} is equal to the ratio of the interplanar distances d_{100}/d_{011}. The ratio R_{001}/R_{100} and R_{001}/R_{011} change as a function of supersaturation due to the difference in surface bonding topology. According to the simulation data the crystal habit will be bounded by {100} and {011} at low supersaturations ($\Delta\mu/kT$<1.25). For supersaturations $\Delta\mu/kT$>1.25 the {001} and {010} faces appear as well. Notice, however, that the {010} faces are rough due to symmetry roughening. Therefore, if these faces appear, they will be rounded-off.

Ultimately, at very high supersaturations the morphology becomes isotropic and all orientations appear. This situation is, however, reached at a supersaturation at which all faces will be kinetically rough and the morphology will be sphere-like. Moreover, in practice this situation may never be reached as at such high supersaturations growth is mainly determined by mass transport limitations which are not present in our simulation model. Therefore, the results for high supersaturations probably represent a situation which will not be encountered in practice.

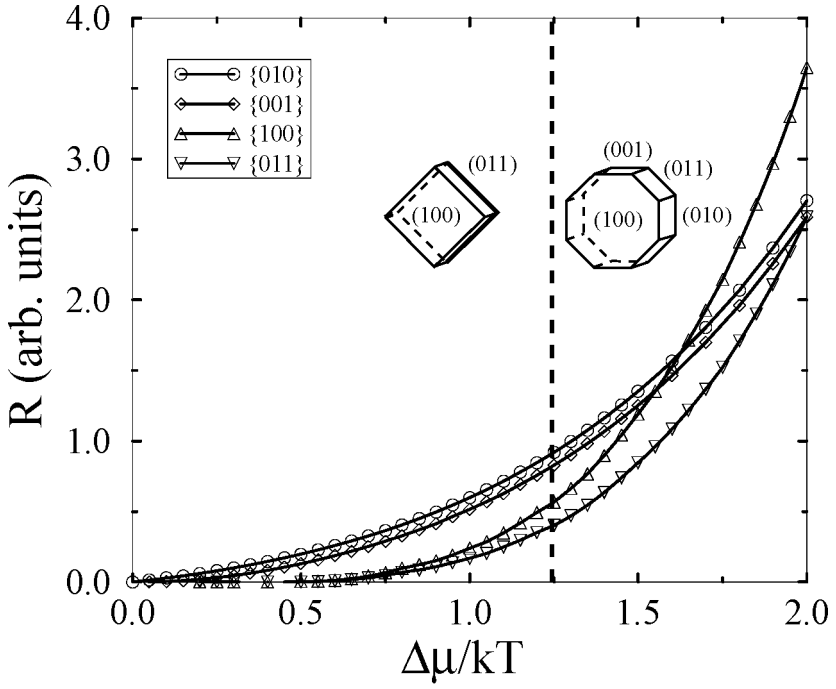

Figure 4.16: Growth rates R as a function of supersaturation for the {100}, {011}, {001} and {010} faces of the crystal graph of figure 4.2.

4.6 Discussion and Conclusion

For type I and II faces two phases could be identified, namely a flat phase and a rough phase. The effective step energy seems to be governed by the strongest connected net as presented in section 4.3. From this connected net the temperature at which the step energy becomes very small can be estimated by calculation of the 2-D Ising transition temperature T^C. The exact roughening transition temperature at equilibrium, however, is in most cases much higher than the calculated value of the strongest connected net. The 2-D Ising transition temperature based on the step energy of a complete step (001) seems to give a rather good estimate for the roughening transition temperature T^R. From the growth simulations it can be concluded that 2-D nucleation growth is mainly determined by the step energy.

For type III surfaces the step energy is determined by a difference in bond energies (Φ_p-Φ_q, figure 4.5). Therefore, the assumption that the step energy (and roughening temperature) is determined by the strongest connected net present for the orientation does not hold. Moreover, a special surface phase called a disordered flat phase was found (see ref. [Grimbergen et al., 1998a]). To our opinion the step energy becomes very small at T=T^{pr} and therefore the nucleation barrier is very small. MC growth simulations confirm this behaviour, but it is very difficult to determine the supersaturation at which kinetic roughening occurs.

Type IV faces show a maximum in the specific heat at a temperature which coincides with calculated 2-D Ising transition temperatures based on the effective step energies for the surface. At that temperature the step energies become almost zero, but the height-difference correlation function indicates that the surface is still not rough. It appears that this type of face does not show a roughening transition at finite temperatures. Similar behaviour was found for the staggered BCSOS model by Mazzeo et al. [Mazzeo et al., 1995]. Probably this is a result of the very strict SOS condition. Under growth conditions it can be shown that the nucleation barrier has not disappeared at temperatures $T>T^{pr}$. Moreover, the interface width indicates that the surface, even at rather high supersaturations, is still relatively flat. The dynamics of these types of surface need to be studied in more detail in order to understand the nucleation and growth behaviour of these types of crystal face.

The MC simulation data and the connected net analyses show that the assumption that rough faces have a high growth rate as compared to macroscopically flat growing faces is not generally valid. The growth rate does depend on both the step energy and the surface energy (or attachment energy) of a crystal face. In the case of the presence of a DOF phase, it appears that faces can have a very high growth rate and still be macroscopically flat. Experimental examples of such growth behaviour were found for the (011) face of naphthalene [Grimbergen et al., 1998c], the (110) faces of orthorhombic n-paraffins [Grimbergen et al., 1998d], the top faces of triacylglyceride (fat) crystals [Hollander et al.,] and the (110) faces of lysozyme [Grimbergen et al., 1999b].

In this paper it is shown that the BFDH and attachment energy predictions are not generally applicable as the predictive value seems to be very poor even for many practical crystal graphs, when compared with the results of a complete connected net analysis and MC simulation data. The simulation data clearly demonstrate that the morphology often depends very strongly on the temperature and supersaturation. The latter phenomenon is encountered frequently in the practice of crystal growth, although the usual methods for predicting the crystal morphology do not take it into account.

The results of the present paper indicate that it is very important to study the exact bonding topology in order to predict surface phase transitions and growth kinetics. The connected net analysis yields important information that can be used to predict the equilibrium and growth behaviour qualitatively. Moreover, for crystals with a complex bonding structure the connected net analysis offers a tool to categorize the many connected nets often present for a single orientation (hkl) into relatively simple models of surfaces of the types treated in the present paper. For the future the combination of a connected net analysis, MC simulations and statistical thermodynamical surface models appears to be the powerful tool in predicting and understanding not only the equilibrium but also the growth behaviour of crystal faces quantitatively.

Acknowledgements

R.F.P. Grimbergen would like to acknowledge the financial support of the Dutch Technology Foundation (STW).

Chapter 5

Preroughening in Organic Crystals

Preroughening in Organic Crystals

R.F.P. Grimbergen, H. Meekes and P. Bennema
H.J.F. Knops [1] and M. den Nijs [2]

Abstract

The (011) surface of the naphthalene crystal structure is described by a simple restricted solid-on-solid model which is applicable to a wide range of organic crystals. Despite the absence of next nearest neighbour bonds, the phase diagram of the model exhibits besides flat and rough phases a disordered flat phase. Monte Carlo simulations confirm this phase diagram. The presence of a DOF phase explains the sudden disappearance of the (011) facet in experimental growth shapes of naphthalene. The type of step free energy associated with surface tilt decreases rapidly, at preroughening transitions. This leads to a rapid decrease in the nucleation barrier, which results in a sudden enhanced growth rate and under certain conditions to the complete disappearance of this facet in growth shapes.

5.1 Introduction

Since the introduction of the concept of interface roughening by Burton, Cabrera and Frank [Burton et al., 1951] much effort has been put in understanding surface phase transitions. The essence of the roughening transition can be captured by a solid on solid (SOS) model. In the seventies it was realised that the generic phase transition in this model is of the Kosterlitz-Thouless (KT) type. See refs. [Weeks, 1986, van Beijeren and Nolden, 1986] for reviews.

More recently it was found that crystal surfaces may exhibit more phases when further-than-nearest-neighbour interactions are introduced in the model. Den Nijs and Rommelse introduced a phase intermediate between the rough and reconstructed phase in a simple restricted solid-on-solid (RSOS) model. This phase in which the surface is locally disordered but flat on the average was called the disordered flat (DOF) phase [Rommelse and den Nijs, 1987,den Nijs and Rommelse, 1989]. DOF phases were also predicted as a result of further neighbour interactions in SOS models that pertain to the (110) faces of noble metals [den Nijs, 1990, Mazzeo et al., 1992, Mazzeo et al., 1994] and to the (100) face of argon [Bastiaansen and Knops, 1996a, Bastiaansen and Knops, 1996b]. In a subsequent development it was observed that a layered structure in a crystal face is also capable to stabilize the DOF phase [Mazzeo et al., 1995]. Other examples of this mechanism were

[1]Institute for Theoretical Physics, University of Nijmegen, Toernooiveld 1, 6525 ED Nijmegen, The Netherlands
[2]Department of Physics, University of Washington, Seattle, Washington 98195

found for the (111) [Woodraska and Jaszczak, 1997a] and (001) [den Nijs, 1997] faces of silicon.

Disordered flat phases are well-established theoretically. They appear in many explicit models describing specific crystal surfaces, but direct evidence remains sketchy [den Nijs, 1994]. This is why it is exciting to be able to link recent anomalous experimental growth shape data for organic crystals to preroughening transitions.

In this paper we present the case of the (011) face of naphthalene as a typical example. In an in-situ vapour growth experiment this face is observed at 283 K and very low driving force ($\frac{\Delta\mu}{kT} < 0.2\%$). Increasing the driving force leads to a sudden rapid growth while the face remains flat until it disappears from the morphology [Grimbergen et al., 1998c]. This type of growth behaviour could be explained by the presence of a DOF phase at this temperature. In order to explore this possibility we formulate in this paper a SOS model based on the crystal structure of naphthalene. It turns out that the resulting model has a layered structure. It is important to notice that many organic compounds, including the interesting case of lysozyme [Grimbergen et al., 1999b] give rise to the same type of surface topology.

Table 5.1: Bonds defining the crystal graph for naphthalene and their corresponding bond energies E.

Bond		E (kcal/mol)
q	M_1-M_2[000]	4.591
p	M_1-M_1[010]	2.972
s	M_1-M_2[001]	1.392
r	M_1-M_1[001]	0.895
v	M_1-M_1[101]	0.580

This paper is organized as follows. In section 5.2 a simple restricted SOS model is derived from the (011) surface structure of naphthalene. The phase diagram for the model is presented in section 5.3 and in section 5.4 Monte Carlo simulation data that support the results are shown. Finally the results are discussed and some conclusions are drawn in section 5.5.

5.2 Description of the model

The naphthalene crystal structure has space group symmetry P 2_1/a and two molecules in the unit cell with centers M_1 at (0,0,0) and M_2 at $(\frac{1}{2}, \frac{1}{2}, 0)$. Naphthalene is a disk shaped elongated flat molecule (see figure 5.1). In the bulk the molecules M_1 and M_2 are oriented differently and are related by a two-fold screw axis along the b-axis and a glide plane a. At the surface, however, the molecules re-orient themselves as a part of surface relaxation effects. This destroys the symmetry relation. Therefore, The molecules are topologically distinct and we can treat M_1 and M_2 as if they are two distinct types of molecules. The cell parameters are a=8.213 Å, b=5.973 Å, c=8.674 Å and β=123.39° [Brock and Dunitz, 1982]. The most important interactions between naphthalene molecules in the

naphthalene crystal lattice were calculated using a force field [Grimbergen et al., 1998c]. Their strengths are shown in table 5.1.

In the Hartman-Perdok (HP) analysis [Hartman and Perdok, 1955a,Grimbergen et al., 1998b] the crystal structure is reduced to a crystal graph. A crystal graph consists of the centers of the growth units and all bonds between the growth units. The crystal graph of naphthalene is depicted in figure 5.2.

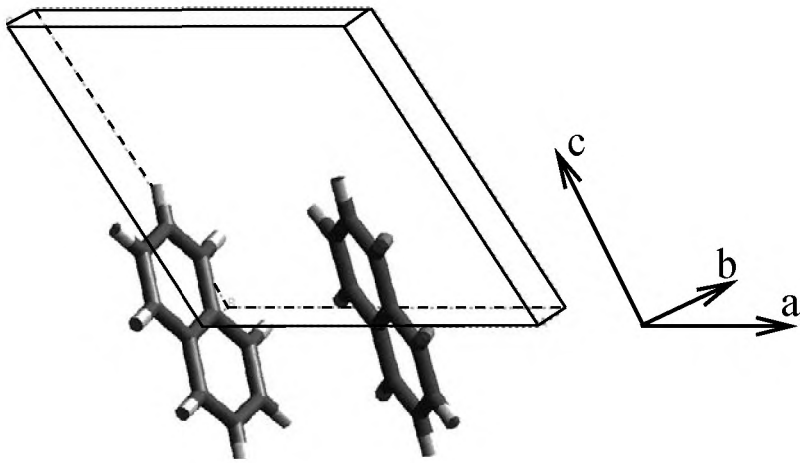

Figure 5.1: Unit cell of the naphthalene crystal structure.

The bonding structure of two flat surface configurations of the (011) face of the crystal structure is drawn in figure 5.3. For clarity only the bonds within the surface layer are shown. Note that the (011) orientation is an AB-layered structure with either M_1 or M_2 on top. The molecules M_1 or M_2 are oriented differently with respect to the face normal [Grimbergen et al., 1998c]. This difference gives rise to a difference in strength of the bonds q_1 and q_2 broken at the surface (see figure 5.3). Due to this difference only one of the two flat faces A or B is thermodynamically stable.

In the SOS limit where the bonds p, q_1 and q_2 are taken to be dominant and joined in bonds Φ_1 and Φ_2, fluctuations with respect to the flat (011) face are described by a (restricted) SOS model (see figure 5.4).

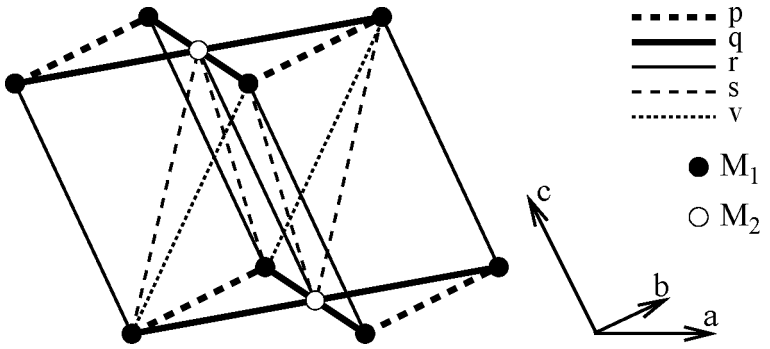

Figure 5.2: Crystal graph of naphthalene. Bonds are labeled according to ref. [Grimbergen et al., 1998c].

Height variables $h_{n,m}$ are defined on a rectangular lattice; lattice points with an even x-value (that correspond to molecules of type M_1) are at even heights; heights at odd x-values are odd. The fact that the bond q is dominant leads to the restricted SOS condition $\Delta_x h = \pm 1$. For nearest neighbours in the y-direction there is no other restriction than that heights are either even or odd, hence $\Delta_y h = 0, \pm 2, \pm 4, \ldots$. The interaction Hamiltonian that captures the essential energetics of the steps on this face is then given by

$$\frac{H}{\mathrm{k}T} = \sum_{n,m} \frac{\Phi}{2}(h_{2n,m} - 2h_{2n+1,m} + h_{2n+2,m}) + \frac{J}{2}|h_{n,m} - h_{n,m+1}| \,. \tag{5.1}$$

The first term in this expression runs over the odd sites $2n+1$ only. It represents the difference in number of broken Φ_1 and Φ_2 bonds. This can easily be seen by noting that the term between brackets gives, in view of the restriction $\Delta_x h = \pm 1$, precisely twice the difference between the number of M_1 molecules and M_2 molecules that are on top of the surface. Note that it is not the strong coupling Φ_1 or Φ_2 but the (weak) difference Φ $(= \Phi_1 - \Phi_2)$ that enters in the effective surface interaction.

The second term in the expression (5.1) runs over all sites. It represents the step energy of a step in the y-direction. Actually this energy is built from the weak (in comparison to p and q) bonds r, s and v.

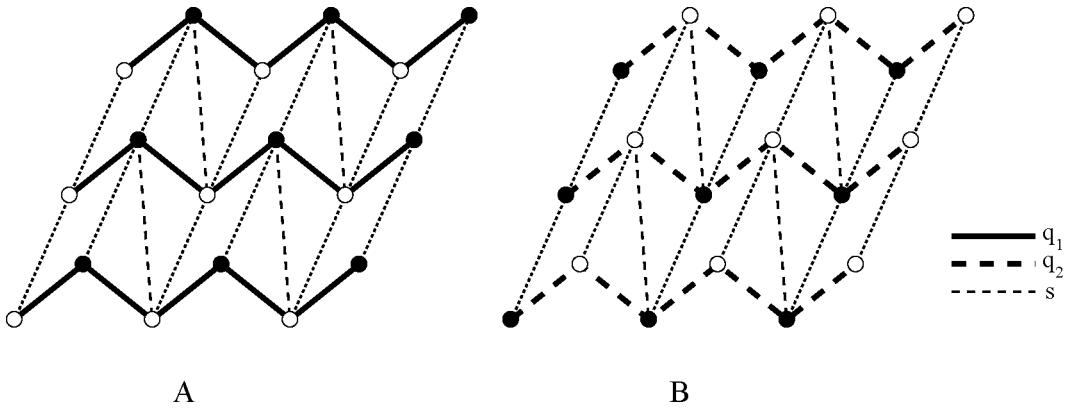

Figure 5.3: The two flat surface configurations with the lowest surface energies for the (011) orientation of the naphthalene structure. The dotted lines are added as guides to the eye.

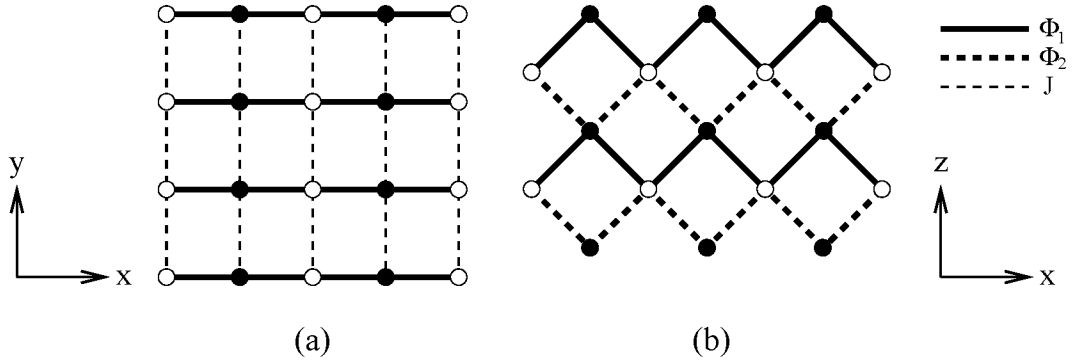

Figure 5.4: (a) Top view and (b) side view of the model. Note that x, y and z do not coincide with the cell axes a, b and c.

As we do not expect the range of interactions to be important here, we lump them together in the nearest neighbour interaction bond J. Note that Φ respectively J represent bond energies per growth unit, $h \to h+2$.

5.3 The Phase Diagram

The ground state of the SOS model with interaction (5.1) is given by $(h_{2n,m}, h_{2n+1,m})$=(0,1) i.e. a flat surface with M_2 molecules on top. A single step $\Delta_x h = \pm 1$ would bring this surface to the one with M_1 molecules on top. Since this would cost surface energy, such a step is thermodynamically not stable. The important excitations from the ground state are therefore step 2 excitations that carry the (0,1) surface to the (2,3) respectively (-2,-1) surface. A typical excitation is shown in figure 5.5. The associated step energies follow directly from the interaction (5.1). Horizontal portions of the step cost an energy J per unit length while the vertical portions have an energy Φ per unit length.

A transition of the flat phase into a new phase is expected to occur as soon as the step free energy (which is the step energy reduced by the "meander" entropy) becomes zero.

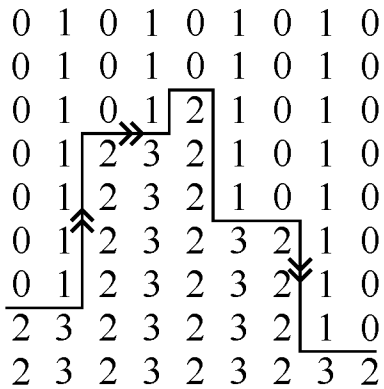

Figure 5.5: Step 2 excitation for the (0,1) phase. Arrows indicate up and down steps.

The location of these points is typically known accurately, but only numerically even for the standard SOS models. The method commonly used [Vilfan and Villain, 1988, Vilfan and Villain, 1990] to estimate the transition temperature where the steps "melt", is to calculate the step free energy of a single meandering step, ignoring the presence of other steps and also that the step might turn backwards. The step free energy that results in the present case is easy to obtain. Notice, from figure 5.5, that a step which runs in the horizontal direction can only turn upward between an odd-even site and vice versa downward between an even-odd site. The partition sum, in the SOS limit, for a step that runs over N lattice sites in the horizontal direction then becomes

$$Z_{step} = e^{-NJ}\left[\sum_{n=0}^{\infty} e^{-n\Phi}\right]^N = \left[\frac{e^{-J}}{1-e^{-\Phi}}\right]^N . \tag{5.2}$$

The transition temperature at which steps will start to proliferate over the interface is estimated from $F_{step} = -\ln Z_{step} = 0$ as

$$e^{-J} + e^{-\Phi} = 1 . \tag{5.3}$$

The Monte Carlo results, that will be presented in the next section, show that this estimate is not too far off.

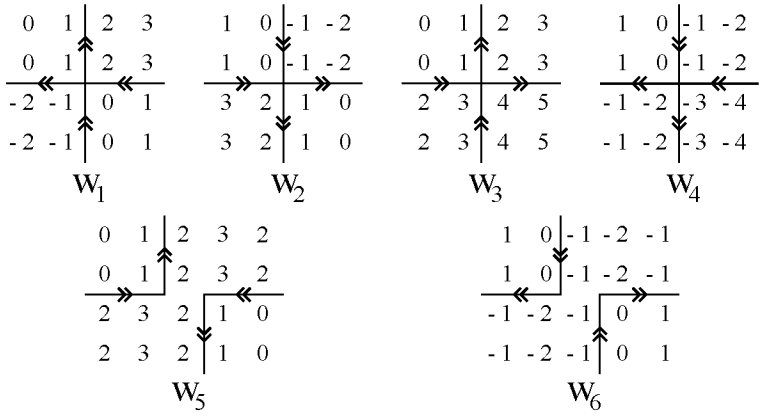

Figure 5.6: The assignment of the weights to the six possible step vertices.

Next, one has to determine the nature of the phase that is entered when the steps melt. When there is no order among the arrows associated to the steps, this phase will be a rough phase and the associated transition a KT transition. However, when the step topology or interaction is such that an up/down arrangement of arrows is preferred, a DOF phase is expected and the transition is a preroughening transition. In ref. [Rommelse and den Nijs, 1987] it was observed that the arrow distribution over a given step configuration for a restricted SOS model could be seen as a six-vertex model defined on a generalized lattice formed by the steps. As in the six-vertex model, only six possible height configurations (arrow distributions) are possible at a step vertex. In the case of ref. [Rommelse and

den Nijs, 1987] the relative weights of these vertices are determined by a next nearest neighbour interaction. In our case it is the step topology which determines the relative weights. The six possible vertices for the present model are shown in figure 5.6. It is seen from this figure that, due to the fact that vertical "up" steps run along odd/even edges while "down" steps run along even/odd edges, the vertices 1,2,3 and 4 have a structure that differs from the vertices 5 and 6. Symmetry implies that $W_1 = W_2 = W_3 = W_4$ and $W_5 = W_6$. It is the ratio $W \equiv W_1/W_5$ that determines whether the arrows order (on average) in a "flat" arrangement or remain disordered. In the case of the six vertex model the exact value of the threshold value is $W = 1/2$; the model is rough for $W > 1/2$. In ref. [den Nijs and Rommelse, 1989] it is argued that in fact the same threshold value is expected to apply for the generalized six-vertex model defined on the steps, because at this value the system can be reduced to a non-intersecting loop gas. The bare ratio $W \equiv W_1/W_5$ (that is for straight steps) is in the present case given by $W = e^{-J}$ since in vertices 1,2,3 and 4 an extra y-bond is broken as compared to vertices 5 and 6. This bare value for W predicts a preroughening transition in the phase diagram for $W < \frac{1}{2}$.

The above estimates for the roughening and preroughening transition lines assume that all steps are double in height and sharp in width. Fluctuations associated with excitations between the two favourable and unfavourable surface configurations, terraces with $2n+\frac{1}{2}$ and $2n-\frac{1}{2}$ average height, are not taken into account yet.

A terrace of the unfavourable type costs an energy of order 2Φ times its surface area and an edge energy proportional to $J/2$. Such terraces come into play in the $\Phi \to 0$ limit part of the phase diagram.

At $\Phi \simeq J$ their major impact is in excitations where double steps split-up temporarily into two steps. Such single steps are bound, because they require an energy proportional to Φ times the area between them. They renormalize the step free energy.

For $\Phi \simeq J$ we need to take this effect into account only in lowest order. Consider a straight horizontal step (in the sense of figure 5.6). A single particle can evaporate or be deposited on only one of the two adjacent sites in each column, on alternating sides of the step. These adsorptions and evaporations are independent. Therefore, the horizontal step energy renormalizes as $J' = J - \Delta$, with

$$e^{-J'} = e^{-J}[1 + e^{-2\Phi}] \tag{5.4}$$

(in lowest order). Vertical double steps (figure 5.6) do not allow for such single particle fluctuations.

The single particle fluctuations are restricted also at step meeting points, the vertices shown in figure 5.6. Consider the vertices of type 1-4. At these, the single particle fluctuations along the horizontal steps are blocked at the two sites adjacent to the vertex. We already renormalized the step energy. So we have to take back this over-correction by renormalizing the vertex energy as $W_1' = W_1 e^{2\Delta}$.

Consider the vertices 5 and 6. At these, only the sites in the middle are blocked. Therefore we need to recorrect for only one Δ. i.e. renormalize as $W_5' = W_5 e^{\Delta}$.

The net results of these excitations is that the estimate for the phase boundary of the flat phase, eq. (5.3), renormalizes into

$$e^{-J}(1 + e^{-2\Phi}) + e^{-\Phi} = 1 \tag{5.5}$$

and that the estimate of point A along this line, where the roughening transition transforms into a PR transition renormalizes from $W = \frac{1}{2}$ with $W = e^{-J}$ into

$$\frac{1}{2} = W' = \frac{e^{-J}}{(1 + e^{-2\phi})} \,. \tag{5.6}$$

The case Φ=0 is a special case because then the difference between the A and B layer disappears. Because both surfaces are thermodynamically stable roughening with a step 1 will occur due to a zero step energy independent of the value of J.

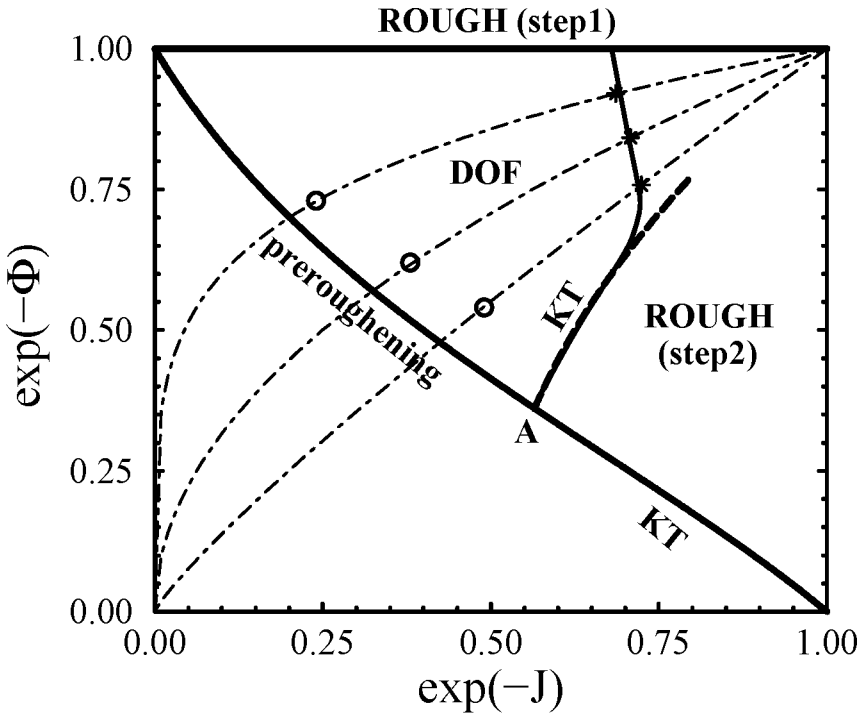

Figure 5.7: Phase diagram of the restricted SOS model with interaction (5.1). The heavy line is the preroughening and KT line that results from equation (5.5). The dashed line represents the KT transition from the DOF into the rough phase according to equation (5.6). Temperature trajectories with $\delta = \frac{\Phi}{J}$=0.22, 0.50 and 0.86 followed by the MC simulations are shown as dash-dotted lines. The dots and stars on these lines mark the preroughening and KT points respectively.

Accoring to the discussion above we expect that the region where steps proliferate is divided into two phases: a DOF phase for $W < \frac{1}{2}$ and a rough phase for $W > \frac{1}{2}$. The phase diagram that results is shown in figure 5.7. Equation (5.5) gives an estimate for the preroughening line which extends beyond point A into a (step 2) KT line. MC results to be discussed in the next section, confirm the location of the preroughening line.

The point A along this line, which marks the KT transition from the DOF phase into the rough phase, is found from the intersection with the line $W = \frac{1}{2}$. The actual shape

of the KT line, which branches from this point, is beyond the reach of the estimates that lead to equation (5.6). Excitations with $\Delta_y h \pm 4$ will tend to roughen the surface earlier and thus shift the KT transition to lower temperatures. This is confirmed by the MC results. The solid KT line for the transition from the DOF to the rough phase follows eq. 5.6 for low temperatures and is fitted to the MC data for higher temperatures.

5.4 MC simulations

5.4.1 Computational Method

The applied Metropolis MC algorithm is based on refs. [Gilmer and Bennema, 1972a, Durbin and Feher, 1991] and implemented as follows:
The rate of attachment of a molecule at a site (K^+) is proportional to the driving force $\Delta\mu$

$$K^+(\Delta\mu) = K_0^+ \exp[\Delta\mu/\mathrm{k}T] \,, \tag{5.7}$$

where k is the Boltzmann constant and T the absolute temperature. K_0^+ is the attachment rate at equilibrium given by

$$K_0^+ = P_0^+ I_0 A \,, \tag{5.8}$$

where P_0^+ is the probability that a growth unit impinging on a site is correctly positioned to attach to the crystal surface, I_0 is the equilibrium rate of impingement of growth units per unit area and A is the area of a lattice site. In our simulation we assume that P_0^+ does not depend on the type of bond which is being formed and is taken to be a constant [Gilmer and Jackson, 1977]. The rate at which a growth unit at the surface will detach depends on the underlying surface (A or B) and the number of neighbours i in the y-direction:

$$K_A^-(i, \Phi_2, J) = K_0^- \exp[-4\Phi_2 - 2iJ] \tag{5.9}$$

and

$$K_B^-(i, \Phi_1, J) = K_0^- \exp[-4\Phi_1 - 2iJ] \,, \tag{5.10}$$

where Φ_1, Φ_2 and J are the dimensionless couplings as shown in figure 5.4 and K_0^- is a constant.

At equilibrium the average detachment and attachment rates must be equal. For our layered surface structures we have assumed that the average attachment rate is equal to the average detachment rate of a growth unit with a binding energy of exactly half of the binding energy of a growth unit in the fully occupied lattice, denoted $\bar{\Phi}$ ($= 2\Phi_1 + 2\Phi_2 + 2J$):

$$K^+(\Delta\mu = 0) = K_0^- \exp[-\bar{\Phi}] \,. \tag{5.11}$$

This implies along with eq. (5.7) the relation

$$K_0^+ = K_0^- \exp[\mu_0/kT] \,, \tag{5.12}$$

where $\mu_0 = -\mathrm{k}T\bar{\Phi}$ is the average chemical potential at equilibrium. Substituting this result in (5.9) and (5.10) we find

$$K_A^-(i,\Phi,J) = K_0^+ \exp[2\Phi - 2(i-1)J] \tag{5.13}$$

and

$$K_B^-(i,\Phi,J) = K_0^+ \exp[-2\Phi - 2(i-1)J]\,. \tag{5.14}$$

Simulation results for $\Delta\mu$=0 confirm detailed balance at equilibrium. The anisotropy (δ) is defined as

$$\delta = \frac{\Phi}{J}\,. \tag{5.15}$$

The simulation model has therefore three free dimensionless parameters: J, δ and $\Delta\mu/\mathrm{k}T$. Sticking coefficients S for the surfaces were defined as

$$S = \frac{attachments - removals}{attachment\ attempts} \tag{5.16}$$

and crystal growth rates R by

$$R = Sd_{hkl}K^+\,, \tag{5.17}$$

where d_{hkl} is the interplanar distance of the face (hkl).

Simulations were done for square matrices (size LxL) for L=20, L=30 and L=40. A site on the square matrix is selected using a pseudorandom number. A second pseudo random number is used to decide whether a creation or annihilation attempt (equal probability) is made for the site. An attachment (detachment) attempt was accepted only in case the SOS condition was fulfilled. The simulation time can be expressed in Monte Carlo Sweeps (MCS). A MCS corresponds to a number of attempted moves equal to the number of matrix sites. Typical simulations of $1{\cdot}10^6$-$2{\cdot}10^6$ MCS were done after $0.5{\cdot}10^6$-$1{\cdot}10^6$ MCS equilibration.

5.4.2 Surface Transitions

As can be observed in figure 5.7 in section 5.3, it is expected that our model exhibits three different surface phases: a flat phase, a DOF phase and a rough phase. In order to confirm the results of our model several simulations at different temperatures and different anisotropies were done. In the next subsections the results of those simulations are presented.

5.4.2.1 Thermal Roughening

According to the KT theory the height-difference correlation function for a crystal surface

$$G(r) \equiv < [h(r) - h(r_0)]^2 > \tag{5.18}$$

diverges for $T \geq T^R$ as

$$\lim_{r\to\infty} G(r)/a^2 \to [K_\infty(T)/\pi] \ln(r) \, , \tag{5.19}$$

where $h(r_0)$ is the height of a reference column, r $(= |r - r_0|)$ is the lateral distance between matrix sites, a is the periodicity, $K_\infty(T)$ is a renormalised constant and $< ... >$ denotes an ensemble average. For our model the periodicity a=2 due to the AB-layered structure. The roughening transition temperature T^R can be determined from the simulation data by evaluation of $K_\infty(T)$ at different temperatures. At T=T^R, $K_\infty(T)$ takes on the universal value $K_\infty(T^R) = 2/\pi$ [Shugard et al., 1978]. Our data were obtained from simulation data of a system size of L=40 and fitted to the functional form $G(r) = [A/\pi^2] \ln r + C$ for r =6-16. In figure 5.8 the amplitude A versus kT/J is plotted for δ=0.22, δ=0.50 and δ=0.86.

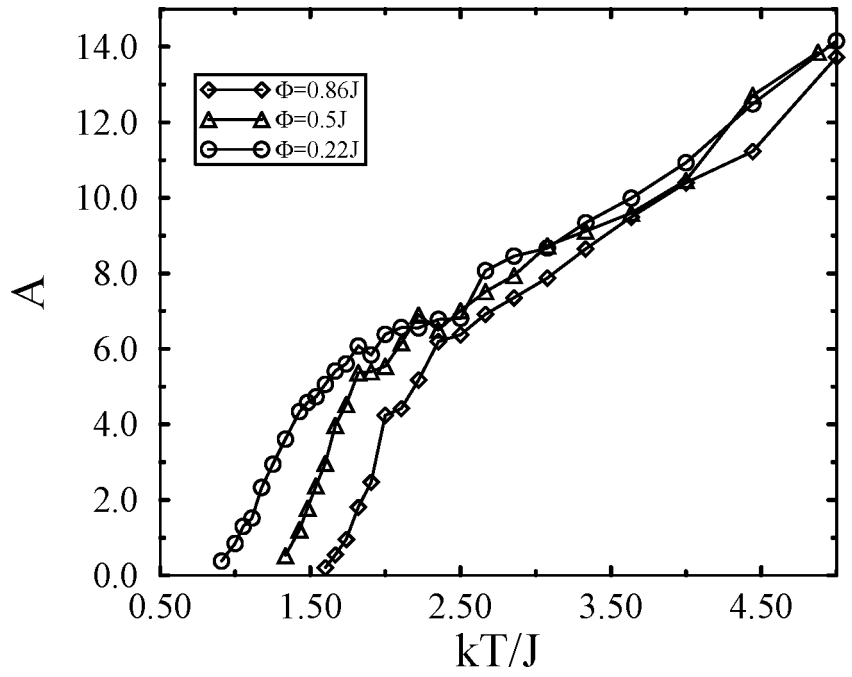

Figure 5.8: Amplitude A for the y-direction vs. kT/J for δ=0.22, δ=0.50 and δ=0.86.

From figure 5.8 it can be concluded that, independent of the the anisotropy, the amplitude A becomes 8 ($K_\infty(T^R)$=$2/\pi$) at kT/J $\approx$2.90. For all simulations it was found that the roughening transition temperature depends only very weakly on the anisotropy δ. The corresponding KT points are shown in figure 5.7.

5.4.2.2 Preroughening

Apart from the roughening transition our model shows a preroughening transition. It was shown recently for the {111} surfaces of silicon that the specific heat reaches a maximum at a temperature which coincides with a preroughening transition temperature [Woodraska and Jaszczak, 1997a]. From the MC simulations the specific heat was calculated using

$$C(T) = \frac{1}{N\mathrm{k}T^2}(< E_s^2 > - < E_s >^2) \,, \tag{5.20}$$

where N is the number of sites, k is the Boltzmann constant, T is the surface temperature and E_s is the surface energy of the complete system. Maxima were found at temperatures which are in agreement with the estimated preroughening temperature according to eq. (5.5) (see figure 5.7).

In figure 5.9 C is plotted as a function of temperature for δ=022, δ=0.50 and δ=0.86. At $T = T^{pr}$ no observable divergence of C_{max} as a function of system size was found, but the accuracy of the simulations is too small to draw definitive conclusions. For example for δ=0.5 we found for L=20: C_{max}=4.25±0.10, for L =30: C_{max}=4.33±0.19 and for L=40: C_{max}=4.44± 0.21. This is in agreement with the expected specific heat singularity at preroughening, which can be extremely weak, in particular in the vicinity of the point where the PR line merges with the roughening line [den Nijs and Rommelse, 1989].

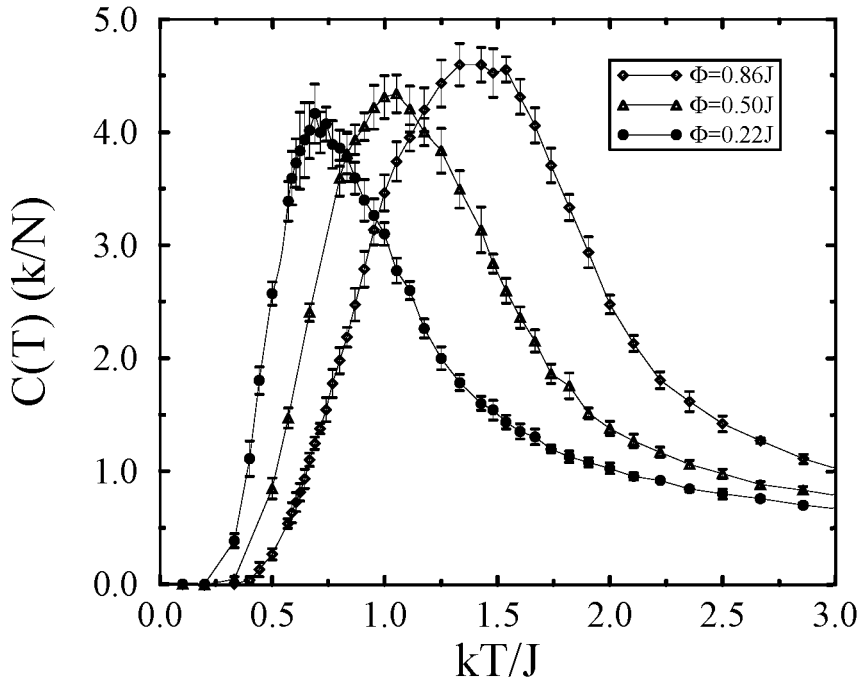

Figure 5.9: Specific heat C(T) vs kT/J for δ=0.86, δ=0.50 and δ=0.22 (L=30).

In contrast to the roughening transition temperature which depends only weakly on the anistropy, the preroughening transition temperature does depend strongly on the anisotropy δ and is in qualitative agreement with the estimate in section 5.3.

5.4.3 Dynamics

In order to compare the experimentally observed growth behaviour of the (011) face of naphthalene [Grimbergen et al., 1998c] with the growth behaviour of our restricted SOS model, MC simulations were performed with $\Delta\mu>0$. Simulations were done for δ=0.5 and different temperatures below and above T^{pr} for a perfect dislocation free surface. Therefore growth will be governed by the 2-D nucleation growth mechanism. MC moves explicitly corresponding to surface diffusion are currently not incorporated in the model. It is assumed that the effect of surface diffusion on the growth kinetics is limited for vapour growth which is considered here.

We have chosen to examine the sticking fraction S as a function of the driving force $\Delta\mu$ because this parameter shows the transition from 2-D nucleation growth nicely: the sticking fraction will increase linearly with $\Delta\mu$ in case of continuous (rough) growth for not too high driving forces. In the case of nucleation limited growth the sticking fraction is proportional to $\exp[-A/3\mathrm{k}T]$, where A is an activation barrier that depends on several factors as the step free energy and $\Delta\mu$ [van der Eerden, 1993]. The results are shown in figure 5.10.

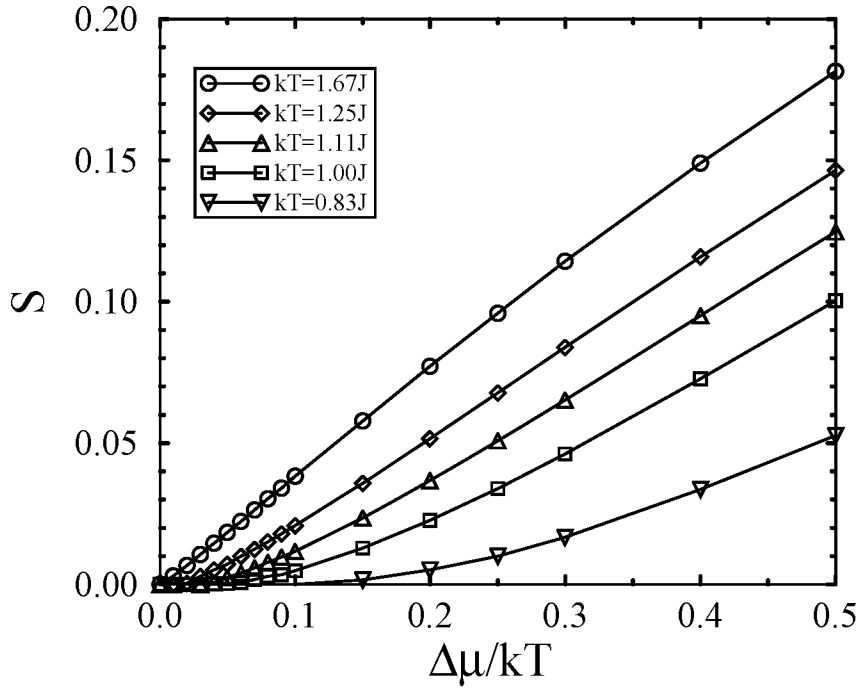

Figure 5.10: Sticking fraction S as a function of driving force at different temperatures for δ=0.50 and L=30 ($\mathrm{k}T^{pr}$=1.04J, $\mathrm{k}T^{R}$=3.17J).

It is clear that for $T < T^{pr}$ there is a nucleation barrier and the sticking fraction becomes linear at $\Delta\mu > 0$. For $T^{pr} < T < T^{R}$ the same holds, but the nucleation barrier appears to be very small. For higher temperatures (kT=1.67J) it is not possible to observe a nucleation barrier within the accuracy of our MC simulations. This might be explained by the fact that there is no nucleation barrier involved in the movement of steps that proliferate in the DOF phase.

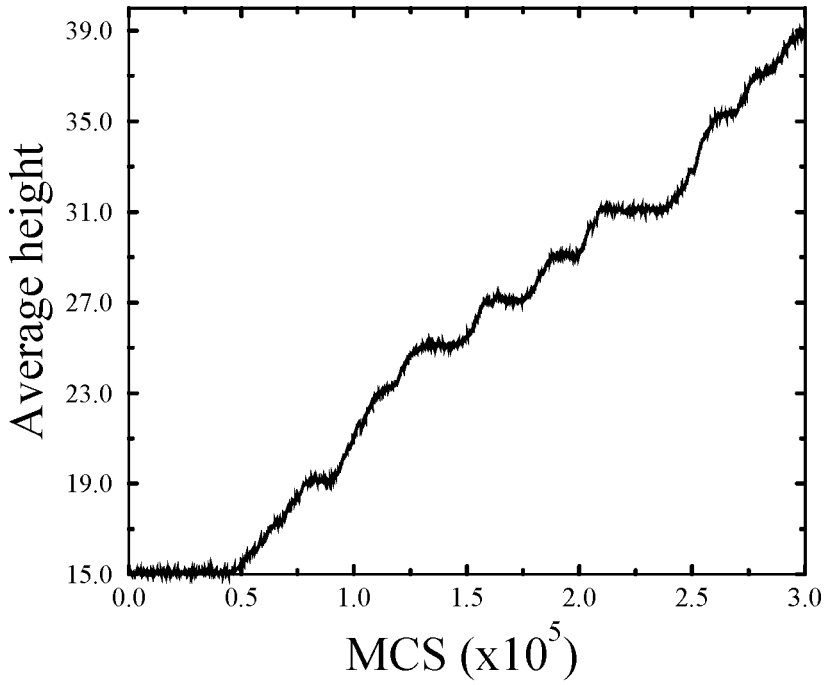

Figure 5.11: Average height $\bar{h}$ as a function of MCS for δ=0.50, L=30 and kT=1.11J. The applied driving force was $\Delta\mu$=0.05kT.

A rapid decrease in the step free energy at $T = T^{pr}$ has also been reported for silicon {111} [Woodraska and Jaszczak, 1997a]. Further evidence for growth by a layer-by-layer mechanism at $T^{pr} < T < T^{R}$ is shown in figure 5.11 where the average height $\bar{h} = 1/N \sum_i h_i$ is plotted versus the number of MCS for kT=1.11J. The figure clearly demonstrates that the crystal face grows with discrete double layers as expected for this AB-layered model. However, for simulations at higher temperatures (T^{pr}<T <T^{R}; kT>1.25J) or higher driving forces ($\Delta\mu$/kT>0.1) it was not possible to observe a layer-by-layer growth mechanism anymore suggesting that the effective step free energy has become very small and that kinetic roughening occurs.

5.5 Discussion and Conclusion

In this paper the phase diagram of a simple restricted SOS model is derived based on the {011} face of the naphthalene structure. The phase diagram exhibits flat, rough and disordered flat phases despite the absence of next nearest neighbour interactions. The DOF phase is stabilized by a difference in energy of crossing steps which is caused by a topology that depends on the orientations of the steps. Our analytical analysis in section 5.3 demonstrates the presence of the DOF phase, and the MC data, presented in section 5.4, confirm this. The specific heat maximum and the KT roughening transition are far apart as expected. At the PR transition the average height of the surface must change by half a unit, and the so-called den Nijs-Rommelse order parameter must become non-zero inside the DOF phase [den Nijs and Rommelse, 1989]. These quantities can provide a more direct confirmation of the DOF nature of the intermediate region To check these numerically will require a detailed finite size scaling analysis, which lies beyond the scope of this work, and therefore will be left for a future study.

A remarkable feature of the model is that the preroughening transition depends strongly on the anisotropy whereas the roughening temperature does depend only very weakly on the anisotropy. The latter relation was already found by Burton, Cabrera and Frank [Burton et al., 1951].

MC growth simulations ($\Delta\mu>0$) suggest that the nucleation barrier for growth drops rapidly for temperatures T just above T^{pr} ($T^{pr}<T<T^{R}$). This has two important implications for practical crystal growth.

The first implication is that at very low driving forces $\Delta\mu$ this type of crystal face has a relatively high growth rate as compared to Kossel-like faces, due to a very small nucleation barrier. Note that the difference in bond energy Φ ($=\Phi_1$-Φ_2) is the important parameter which determines the preroughening transition temperature T^{pr}. A limiting case is the situation $\Phi_1=\Phi_2$ ($\Phi = 0$) which is known as symmetry roughening where $T^{R}=0$ [Grimbergen et al., 1998b, Meekes et al., 1998]. For $\Phi\neq0$ and $T>T^{pr}$ the morphological importance of the crystal face is significantly lowered at finite driving forces. Ultimately, the face may disappear from the morphology for higher driving forces if adjacent faces have a relatively low growth rate. For the (011) faces of naphthalene this is exactly what we observed experimentally: at a temperature of 283K already at very low driving forces ($\frac{\Delta\mu}{kT}<0.2\%$) the face grows very fast as compared to the adjacent faces (110) and (111) which have a Kossel-like bonding structure at the interface and disappears as a flat growing face from the morphology. These observations strongly suggest that the (011) face of naphthalene is at 283K in the DOF phase. When the temperature was increased the (011) face was not observed anymore even at the lowest driving forces. It is known that the step free energy (the one associated with tilting the surface) decreases rapidly at preroughening transitions [Rommelse and den Nijs, 1987, den Nijs and Rommelse, 1989]. Most likely this drop is so large that the nucleation barrier for the (011) facet can not be observed experimentally because at the relevant low driving forces growth velocities are too small.

A second implication is that for $T>T^{pr}$ the barrier for kinetic roughening is very low and the crystal face will become kinetically rough already at very low driving forces. In contrast to the well-defined thermal roughening transition, it is difficult to determine

the driving force at which kinetic roughening occurs because it is not a proper phase transition. In the case of the (011) face of naphthalene, kinetic roughening was not observed experimentally, probably because the face had already disappeared from the morphology due to the high growth rate at low driving force.

This study demonstrates that equilibrium and growth behaviour of crystal surfaces can vary dramatically with the details of the bond topology of the crystal surface. Other recent studies illustrate this in different contexts, e.g. the predcition of preroughening in Si (001) type facets [den Nijs, 1997]. Generic solid-on-solid models miss-out on such details completely. One method to identify such special crystal surfaces is to perform a careful connected net analysis for a face $\{hkl\}$ as discussed in ref. [Grimbergen et al., 1998b] in combination with statistical thermodynamical models. The connected net analysis is capable to derive the most prominent faces (and their corresponding surface configurations) from the crystal structure for many types of crystal ranging from ionics to complicated organic and even macromolecular crystals like proteins. Subsequently, the resulting surfaces can be transformed into simple statistical thermodynamical surface models. We think that in this way it is possible to understand the physics of faces of complicated crystals.

Dynamics of surface models can be studied by MC simulations [Grimbergen et al., 1999a] and will be subject of future studies. Theoretical research on non-equilibrium growth phenomena has been intense in recent years (for reviews see refs. [Villain, 1991, Krug, 1995, Halpin-Healy and Zhang, 1995]). Most of these studies are numerical in nature, MC simulations of simple growth models, like the KPZ equation. The challenge is to apply and generalize the results of those (ongoing) numerical studies to actual experimental data on crystal surfaces under growth conditions.

Acknowledgements

This research is financially supported by the Dutch Technology Foundation (R.F.P. Grimbergen) , the National Science Foundation under grant number DMR 97-00430 and by the Dutch Research School of Theoretical Physics through a visitors grant (M. den Nijs).

Chapter 6

Growth behaviour of Crystal Faces containing Symmetry Related Connected Nets: a Case Study of Naphthalene and Anthracene

Growth Behaviour of Crystal Faces containing Symmetry Related Connected Nets: a Case Study of Naphthalene and Anthracene

R.F.P. Grimbergen, M.F. Reedijk, H. Meekes and P. Bennema [1]

Abstract

The morphology of naphthalene and anthracene crystals has been studied both theoretically and experimentally. A connected net analysis shows that the faces {011} and $\{2\bar{1}\bar{1}\}$ contain a pair of symmetry related connected nets giving rise to a new phenomenon called symmetry roughening. Experimentally the {011} and $\{2\bar{1}\bar{1}\}$ faces have only been observed on naphthalene crystals grown from the vapour at very low driving forces. Upon increasing the driving force the {011} faces grow out very rapidly as flat faces already at very low supersaturation. For anthracene these faces have never been observed. In this paper the relation between the connected net structure of crystal faces and the experimentally observed growth behaviour is discussed.

6.1 Introduction

It is a well-known fact that the morphology of crystals depends on growth conditions like temperature, driving force and mother phase. All these parameters influence the morphology and growth behaviour of crystal faces (hkl).

In this paper the morphology of crystals will be studied for crystals grown from the vapour and from solution as a function of driving force in order to determine both the influence of a mother phase and the driving force. The observed crystal habits will be compared with theoretically calculated morphologies. In this way the predictive value of the recently developed extension of the Hartman-Perdok theory which takes the effect of multiple connected nets for a crystal face (hkl) on the crystal morphology into account, is tested [Grimbergen et al., 1998b, Meekes et al., 1998, Grimbergen et al., 1999a].

Naphthalene and anthracene have been chosen as model compounds, because they have been studied extensively in the past [Pavlovska and Nenow, 1972, Robinson and Scott, 1967, Jetten et al., 1984, Elwenspoek et al., 1987] and crystals can be grown easily both from the vapour and solution. The reason to choose both naphthalene and anthracene is that these compounds have a similar crystal structure. The only difference is that the interactions (or bond energies) in the lattice are slightly different. Therefore, the relation between the interactions in the lattice and the macroscopic morphology can be studied directly.

[1] The work presented in this chapter has been accepted for publication in J. Phys. Chem.

The Hartman-Perdok theory [Hartman and Perdok, 1955a, Hartman and Perdok, 1955b, Hartman and Perdok, 1955c, Hartman, 1973] combined with the theory of roughening transitions in relation to connected nets [Rijpkema et al., 1982, Bennema and van der Eerden, 1987, Bennema, 1993, Grimbergen et al., 1998b] has been used to predict the crystal morphology. In order to derive a crystal habit from a crystal structure, first the most important bonds or interactions between growth units in the lattice have to be determined. The interactions between the growth units are calculated using an empirical force field. Bonds having a bond energy larger than the thermal energy kT (T is the actual growth temperature) are used in the analysis. The growth units are subsequently reduced to their corresponding centers of geometry. The centers of geometry connected by the bonds define a so-called crystal graph. From the crystal graph first all direct chains (DCs) are derived. A DC is defined as a sequence of strongly bonded growth units of which only the endpoints are identical (i.e. related by a lattice translation $[uvw]$ with $u, v, w \in Z$). A connected net (hkl) perpendicular to $\boldsymbol{k}_{hkl} = h\boldsymbol{a}^* + k\boldsymbol{b}^* + l\boldsymbol{c}^*$ is a combination of at least two non-parallel intersecting DCs $[uvw]_1$ and $[uvw]_2$ perpendicular to $\boldsymbol{k}_{hkl}$. Moreover, all equivalent growth units of a connected net differ a translation $[uvw]$ perpendicular to $\boldsymbol{k}_{hkl}$. Given the spacegroup symmetry equivalent connected nets are separated by the interplanar distance d_{hkl} according to the selection rules of Bravais, Friedel, Donnay and Harker (BFDH) [Friedel, 1911, Donnay and Harker, 1937, Grimbergen et al., 1998b]. Note that a connected net need not be stoichiometric with regard to the chemical composition of the unit cell. Therefore, only stoichiometric connected nets can be considered as the actual growth layers with which a crystal will grow.

In equilibrium a flat face or F-face (i.e. a crystal face below the roughening temperature) with normal $\boldsymbol{k}$ has the property that for all crystallographic directions $\boldsymbol{u} = u\boldsymbol{a} + v\boldsymbol{b} + w\boldsymbol{c}$ labeled by $[uvw]$ $(u, v, w \in Z)$ coplanar with the face (i.e. $\boldsymbol{u} \cdot \boldsymbol{k} = 0$) the sum of the edge free energies of a step in the $\boldsymbol{u}$ and -$\boldsymbol{u}$ direction is larger than zero [van Beijeren and Nolden, 1986], or

$$\gamma(\boldsymbol{u}) + \gamma(-\boldsymbol{u}) > 0 \quad \forall \boldsymbol{u}, \boldsymbol{u} \cdot \boldsymbol{k} = 0 \,. \tag{6.1}$$

In case equation (6.1) also holds for a single connected net of a face it can be seen that for that net the step free energy will be larger than zero for all directions $\boldsymbol{u}$ and -$\boldsymbol{u}$. It has been shown that a connected net has a 2-D Ising transition temperature T^C_{hkl} and this temperature has been used as a rough estimate for the roughening temperature T^R_{hkl} of the crystal face (hkl) [Rijpkema et al., 1982]. More specifically it has been assumed that the 2-D Ising transition temperature of the strongest connected net for a crystal face (hkl) is a (usually lower bound) estimate of the roughening temperature. Recently, it has been demonstrated that this assumption is not valid in general. Combinations of connected nets may result in a very low or even zero step energy for a face (hkl) [Grimbergen et al., 1998b].

In order to determine the growth morphology based on F-faces, Hartman and Bennema introduced the attachment energy as a habit controlling factor [Hartman and Bennema, 1980]. The attachment energy is defined as the energy released per growth unit in case a complete growth layer (i.e. stoichiometric connected net) is attached to the surface (hkl) of a crystal. The attachment energy is related to the crystallization energy by

$$E^{cr} = E^{att}_{hkl} + E^{slice}_{hkl} \,, \tag{6.2}$$

where E_{hkl}^{slice} is the interaction energy of all growth units within the stoichiometric connected net or growth layer. It was argued that it may be justified that the relative growth rates of crystal faces are proportional to the attachment energy or

$$R_{hkl} \propto E_{hkl}^{att} \; . \tag{6.3}$$

Subsequently, a Wulff plot can be used to construct the growth morphology [Wulff, 1901].

In this paper we will demonstrate that the combination of (symmetry related) connected nets, each having a very high Ising transition temperature, may result in an overall zero step energy for the crystal face (hkl) and thus a roughening temperature of zero Kelvin. Such a situation is known as symmetry roughening [Grimbergen et al., 1998b, Meekes et al., 1998]. For such faces the attachment energy is not a good parameter to determine the growth rate of the face and relation (6.3) does not hold. Moreover, even for faces that contain no symmetry related connected nets, but a pair of connected nets causing a very low step energy, the attachment energy is not a reliable measure for the growth rate [Grimbergen et al., 1998b, Grimbergen et al., 1999a]. Obviously, this has major implications for the equilibrium and growth behaviour of these specific faces. The $\{011\}$ and $\{2\bar{1}\bar{1}\}$ faces of naphthalene and anthracene are examples of such faces. Experimental observations support the theoretical results.

6.2 Theoretical morphology

The connected nets have been derived from the crystal graph using the program FACELIFT [Grimbergen et al., 1997] based on the graph-theoretical method described by Strom [Strom, 1980, Strom, 1981, Strom, 1985]. Point charges for the atoms of both naphthalene and anthracene have been calculated from the electron densities determined with GAMESS [Guest et al., 1994] using the 6-31g** basis and D_2h molecular symmetry. The electrostatic potential derived (ESPD) point charges were subsequently calculated from the electron densities using the program MOLDEN [Schaftenaar, 1992, Besler et al., 1990]. Bondenergies needed for calculation of the 2-D Ising transition temperatures and attachment energies have been calculated using the Cerius^2 software [MSI,]. The 2-D Ising transition temperatures of connected nets have been calculated using the program TCRITIC [Hoeks, 1993, Rijpkema et al., 1982]. Note that we use the term bond energy for the energy of the intermolecular interactions between the growth units.

6.2.1 Crystal Graph

Naphthalene and anthracene crystallize in space group P 2_1/a with two molecules in the unit cell with geometrical centers M_1 at (0,0,0) and M_2 at $(\frac{1}{2}, \frac{1}{2}, 0)$ [Brock and Dunitz, 1982, Brock and Dunitz, 1990]. The cell parameters are given in table 6.1. To determine the interplanar distance d_{hkl} separating physically equivalent surface structures, the selection rules $(h0l) : h = 2n$ and $(0k0) : k = 2n$ for spacegroup P 2_1/a have been applied [Tables, 1969].

Because the crystal structures of naphthalene and anthracene are very similar, a generalized crystal graph can be used to determine all connected nets for both crystals. The

Table 6.1: Cell parameters and lattice energies of naphthalene and anthracene before and after minimization. CSD indicates the cell parameters obtained from the Cambridge Structural Database.

	Naphthalene		Anthracene	
	CSD	minimized	CSD	minimized
a (Å)	8.213	8.138	8.553	8.483
b (Å)	5.973	6.043	6.016	6.045
c (Å)	8.674	8.748	11.172	11.141
β	123.39	123.71	124.60	124.40
E_{latt}(kcal/mol)	-18.36	-18.68	-26.64	-26.55

crystal graph used in this study was based on the work of Hartman who derived a general crystal graph for organic compounds having two centrosymmetric molecules in the unit cell [Hartman, 1991] and on the work of Bennema on naphthalene (see review paper [Bennema, 1993]). In the present study the p, q, r and s bond types used by Hartman (a, d, f and g bond types of Bennema) and an additional bond v have been used. The broken bond energies of these bonds are larger than kT. The t bond used by Hartman appeared to be very weak ($\approx$ 0.3 kT) and was omitted in this work. In the following the broken bond energies of these bonds will be indicated with Φ_p, Φ_q, Φ_r, Φ_s and Φ_v. Hartman applied an extra selection rule $(hkl) : h + k = 2n$ to determine the F-faces which has not been used in this work. An explanation for this choice will be given furtheron.

Table 6.2: Bonds defining the crystal graph for naphthalene and anthracene. Broken bond energies calculated for naphthalene and anthracene are given.

		Naphthalene	Anthracene
Bond		E^{bb} (kcal/mol)	E^{bb} (kcal/mol)
q	M_1-M_2[000]	4.591	7.008
p	M_1-M_1[010]	2.972	4.936
s	M_1-M_2[001]	1.392	1.626
r	M_1-M_1[001]	0.895	0.765
v	M_1-M_1[101]	0.580	0.661

Before interactions between the growth units were calculated, the crystal structure was minimized to remove bad contacts. This is a generally used method to reduce errors introduced by shortcomings in the force field parameters. During the minimization, the spacegroup symmetry was imposed and the atomic positions as well as the cell parameters a, b, c and β were optimized. The Ewald summation technique has been used to calculate non-bonded interactions in the lattice. The cell parameters of naphthalene and anthracene before and after minimization are given in table 6.1. Lattice energies have been calculated by summation of all atom-atom pair interactions between growth units of which the

geometrical center is within a cutoff radius of 30Å (table 6.1). This method has been used by Docherty et al. [Docherty et al., 1991]. It can be seen that the differences between the cell parameters before and after minimization are very small. The calculated lattice energy was -18.7 kcal/mol for naphthalene and -26.6 kcal/mol for anthracene which is in excellent agreement with the experimental values of -18.6 kcal/mol and -26.2 kcal/mol respectively [Docherty et al., 1991]. The small deviation of the cell parameters from the experimental values and the calculated lattice energies indicate that the force field used describes the crystal structures correctly. Therefore the minimized crystal structure was used to calculate all interactions between the growth units in the crystal lattices.

The calculated broken bond energies of the bonds between the growth units defining the crystal graph are listed in table 6.2. A graphical representation of the bonds in the unit cell is drawn in figure 6.1.

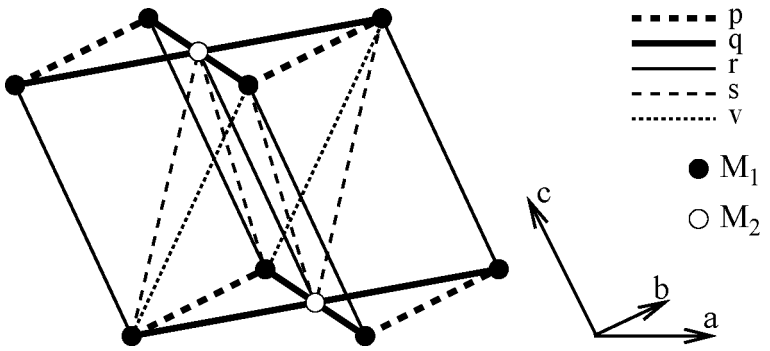

Figure 6.1: Crystal graph with the bonds defined in table 6.2.

6.2.2 Connected nets of naphthalene and anthracene

The results of the connected net analysis of naphthalene are presented in table 6.3 and of anthracene in table 6.4. The attachment energies were calculated according to the method described by Berkovitch-Yellin which has been implemented in cerius[2] [Berkovitch-Yellin, 1985, MSI,]. Note that the calculated 2-D Ising transition temperatures in table 6.3 and 6.4 are an estimate for the roughening temperature for the crystal face (hkl) in equilibrium with its vapour phase. In the discussion it will be shown that a solvent motherphase may reduce the roughening temperatures drastically.

For the $\{011\}$ and $\{2\bar{1}\bar{1}\}$ forms two connected nets were found. Because these connected nets are symmetry related, the calculated Ising transition temperature is for both connected nets the same. In the next section the physical implications of the presence of symmetry related connected nets will be discussed.

The predicted growth morphologies of naphthalene and anthracene based on E_{att} (eq.(6.3)) of table 6.3 and 6.4 are presented in figure 6.2. Both morphologies exhibit the $\{001\}$, $\{110\}$, $\{20\bar{1}\}$, $\{11\bar{1}\}$ and $\{011\}$ forms.

Table 6.3: Results of the connected net analysis for naphthalene. The form {hkl}, interplanar distance d_{hkl}, calculated attachment energy (E^{att}_{hkl}), calculated Ising temperature (T^C), number of connected nets found and indication whether the face is present in the Wulff plot (+: present; -:absent) are given.

{hkl}	d_{hkl}(Å)	E^{att}_{hkl} (kcal/mol)	T^C (K)	Nr.	Wulff plot
{001}	7.268	-11.2	1847	1	+
{110}	4.533	-22.9	965	1	+
{20$\bar{1}$}	4.104	-25.5	859	1	+
{11$\bar{1}$}	4.664	-23.5	900	1	+
{011}	4.628	-25.3	590	2	+
{200}	3.456	-28.9	498	1	-
{20$\bar{2}$}	3.704	-29.6	423	1	-
{2$\bar{1}\bar{1}$}	3.388	-29.2	370	2	-
{020}	3.002	-33.7	207	1	-

Anthracene has additionally the {20$\bar{2}$} form which is for naphthalene very close to the threshold value for appearance in the Wulff plot. The morphology of anthracene is somewhat more platy as compared to the naphthalene morphology. This can be explained by the p and q bonds which are much stronger for anthracene than for naphthalene, because of the larger anisotropy of the molecules.

Table 6.4: Results of the connected net analysis for anthracene. The form {hkl}, interplanar distance d_{hkl}, calculated attachment energy (E^{att}_{hkl}), calculated Ising temperature (T^C), number of connected nets found and indication whether the face is present in the Wulff plot (+: present; -:absent) are given.

{hkl}	d_{hkl}(Å)	E^{att}_{hkl} (kcal/mol)	T^C (K)	Nr.	Wulff plot
{001}	9.197	-12.2	2881	1	+
{110}	4.574	-33.4	1246	1	+
{20$\bar{1}$}	4.172	-36.3	1187	1	+
{11$\bar{1}$}	4.874	-33.6	1222	1	+
{011}	5.034	-35.6	829	2	+
{200}	3.520	-40.9	648	1	-
{20$\bar{2}$}	4.158	-41.1	617	1	+
{2$\bar{1}\bar{1}$}	3.428	-41.9	450	2	-
{020}	3.008	-49.2	203	1	-

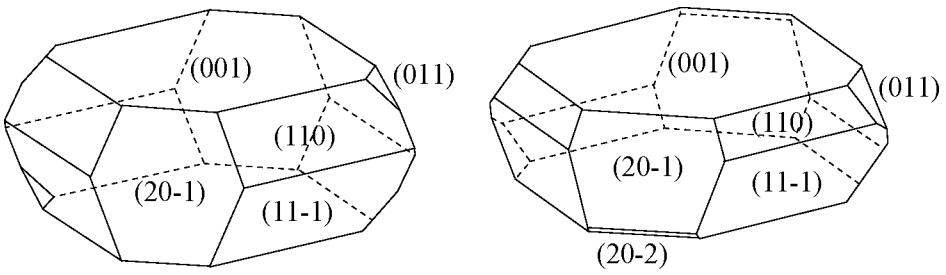

Figure 6.2: Calculated theoretical morphologies based on attachment energies for naphthalene (left) and anthracene (right).

6.2.3 Multiple connected nets

For the crystal faces $\{011\}$ and $\{2\bar{1}\bar{1}\}$ more than one connected net is found. These can be considered as possible growth layers. The usual procedure is to determine the connected net with the highest slice energy and consequently the lowest attachment energy. This connected net is then considered to be the actual growth layer determining the growth and equilibrium behaviour of the crystal face.

However, for the $\{011\}$ and $\{2\bar{1}\bar{1}\}$ faces a special situation occurs already mentioned by Hartman [Hartman, 1991]. He found that for naphthalene type of crystals having two centrosymmetric molecules in the monoclinic unit cell at special positions ((0,0,0) and $(\frac{1}{2},\frac{1}{2},0)$), the situation occurs that for all faces (hkl) with $h+k=2n+1$ exactly the same surface energy is found at distances $\frac{1}{2}d_{hkl}$ instead of d_{hkl}. For this reason Hartman introduced for these types of structure the extra selection rule $(hkl) : h+k=2n$. In another paper Hartman demonstrates that these faces grow relatively fast because of nucleation at a partial step with height $\frac{1}{2}d_{hkl}$ [Hartman and Heijnen, 1983].

In our opinion the $\{011\}$ and $\{2\bar{1}\bar{1}\}$ faces grow very fast because of a zero step free energy in a direction $[uvw]$ as a result of a pair of connected nets which are related to each other by a center of symmetry.

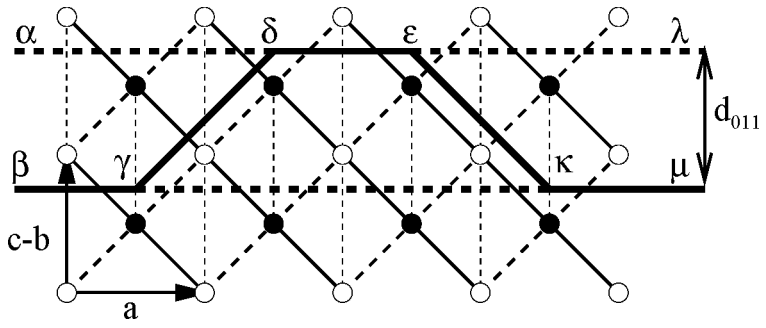

Figure 6.3: $[0\bar{1}1]$ Projection of a schematic drawing of the bonding structure for the (011) face. The open circles represent molecules 1 (M_1) and the filled circles molecules 2 (M_2). The diagonal dashed bonds represent q bonds, the vertical dashed bonds represent superimposed p and r bonds and the solid bonds represent superimposed q and s bonds. The v bonds are not drawn.

Due to their symmetry relation the connected nets have exacly the same slice and attachment energies. This can be seen in figure 6.3 for the (011) face. Note that the v bonds are not drawn for clarity sake. These bonds do not contribute to the step energy.

Looking at figure 6.3 it can be seen that for the crystallographic direction $\boldsymbol{u} = [100]$ relation (6.1) does not hold. The broken bond step energy for [100] is equal to the difference in broken bond surface energy of the surfaces bounded by $\beta\gamma\delta\epsilon\lambda$ and $\beta\gamma\kappa\mu$. The broken bond step energy is equal to $(8\Phi_r+8\Phi_p+8\Phi_q+5\Phi_s)-(8\Phi_r+8\Phi_p+8\Phi_q+4\Phi_s) = \Phi_s$. For the step in the $[\bar{1}00]$ direction, the corresponding surfaces are bounded by $\alpha\delta\epsilon\kappa\mu$ and $\beta\gamma\kappa\mu$. The broken bond energy for this step is $(8\Phi_r + 8\Phi_p + 8\Phi_q + 3\Phi_s) - (8\Phi_r + 8\Phi_p + 8\Phi_q + 4\Phi_s) = -\Phi_s$. Note that for the individual steps the contribution of the bonds p, q, r and also v (not drawn) to the step energy is zero. The summation of the step energies for the directions $\boldsymbol{u}$ and -$\boldsymbol{u}$ is zero. This is a special case of the condition of eq. (6.1). Usually a face becomes rough when the step free energy becomes zero for steps in both the $\boldsymbol{u}$ and -$\boldsymbol{u}$ directions. A zero step free energy implies that there is no effective preference for a growth unit to be incorporated in a kink site or any other lattice site on the crystal surface. In this special case the step free energies of the individual step directions are non-zero but have an opposite sign. Consequently, based on broken bond step energies, the roughening temperature should be zero Kelvin (see eq. (6.1)) and the crystal face should grow in a rough mode and consequently very fast.

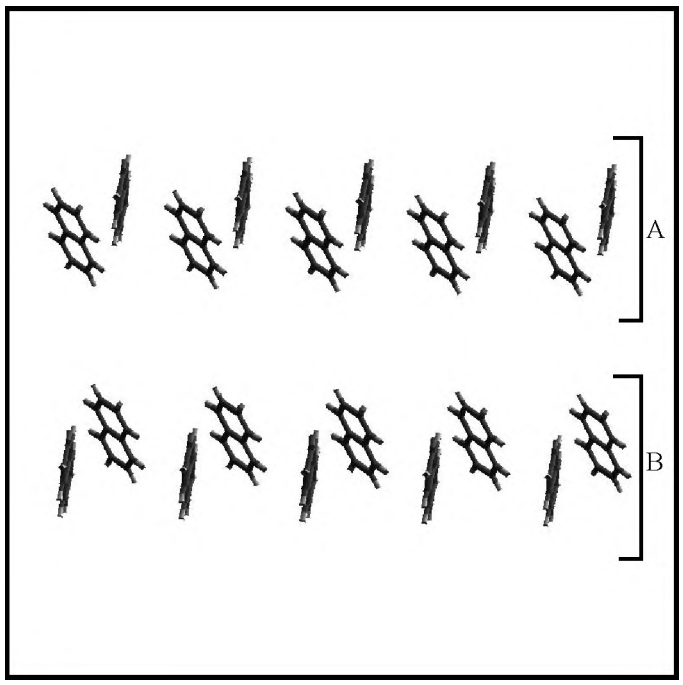

Figure 6.4: $[0\bar{1}1]$ Projection of the two surface configurations of the (011) face of naphthalene.

This phenomenon was described in recent papers and called symmetry roughening [Meekes et al., 1998]. For the $\{2\bar{1}\bar{1}\}$ faces the same situation occurs.

In figure 6.4 it can be seen that the two connected nets represent different surface configurations. The molecules at the crystal - motherphase interface of the two surfaces indicated with A and B have different orientations with respect to the surface. For this reason the surface *free* energy of the two surface configurations will be different because of a difference in molecular entropy or due to surface relaxation. In the bonding structure of the (011) face the surface free energy and step free energy cannot be treated independently. Consequently, the step free energy will be larger than zero in case the entropy term for the surface free energy is taken into account and the face will have a roughening temperature larger than zero Kelvin. For this reason it is expected that the $\{011\}$ and $\{2\bar{1}\bar{1}\}$ faces might occur on the morphology of naphthalene type of crystals at equilibium conditions. Because of the low step free energy, the faces will grow very rapidly when a driving force is applied and disappear from the morphology [Grimbergen et al., 1999a].

Note that the 2-D Ising transition temperatures of connected nets are not a good approximation for the roughening temperature of these types of face, where a pair of connected nets causes a very low step energy.

6.3 Experimental

6.3.1 Vapour growth

The crystal growth experiments were carried out in a specially designed vapour growth cell as shown schematically in figure 6.5. A fotograph of the complete and dismantled vapour growth cell is presented in figure 6.6. The cell consists of two main parts, a cold finger and a copper wall. Crystals sublime at the cell wall and crystals grow on the cold finger. The temperature difference between these two parts can be controlled using thermostated baths. The temperature is measured with three thermocouples (copper/constantan) type T, one in the cold finger and two in the cell wall. The crystals can be observed in-situ with a microscope via the glass window. To prevent the crystals from nucleating on the window a screen heater has been attached to the window. The pressure in the cell can be measured by a vacuum gauge.

After evacuating the cell for one night at 70° C to remove air and water, naphthalene or anthracene p.a. quality is put into the cell and the cell is evacuated again. The cell is connected to two separate thermostated baths to control the temperature of the cell wall and the cold finger independently. The temperature of the cold finger was kept at a constant temperature (T_0) of 283.2K for naphthalene and 326.5K for anthracene. The supersaturation was imposed by increasing the temperature of the copper outer wall (T) of the vapour growth cell.

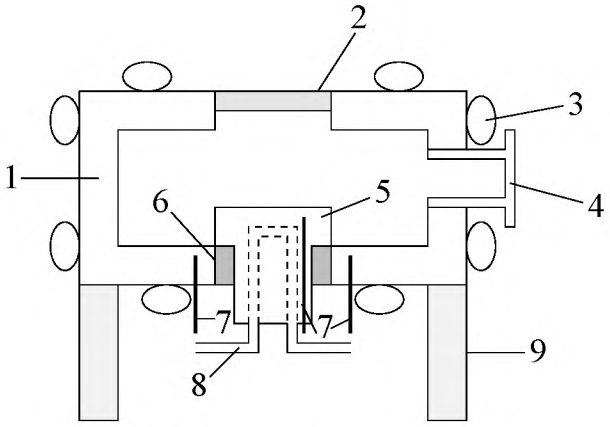

Figure 6.5: Schematic side view of the vapour growth cell. (1) copper cell wall, (2) glass window, (3) heating flow tubes, (4) vacuum flange, (5) cold finger, (6) thermally insulating ring, (7) thermocouple, (8) heating tubes, (9) support.

The supersaturation in the vapour growth cell has been calculated assuming ideal gas behavior using [van Leeuwen, 1979]

$$\frac{\Delta\mu}{\mathrm{kT}_0} = \ln\frac{T}{T_0} \tag{6.4}$$

The crystals were nucleated at a high supersaturation ($\frac{\Delta\mu}{\mathrm{kT}} \approx 0.052$) and after nucleation the crystals were allowed to grow for some days at very low supersaturation ($\frac{\Delta\mu}{\mathrm{kT}} < 0.002$). Then the supersaturation was increased by a fixed rate per minute while the crystals were observed with an optical microscope.

6.3.2 Solution growth

The experimental setup for solution growth is somewhat different from the vapour growth experiments. A small glass growth vessel containing the crystals is cooled in a larger vessel. This vessel is kept at constant temperature (±0.02K) using a thermostated bath. The entire growth unit is placed on a microscope stage of a microscope equiped with a video or photo camera [Vogels et al., 1990].

Naphthalene crystals have been grown from ethanol and cyclo-hexane solution using the following procedure. First a saturated solution is prepared and poured out into the small crystallisation vessel. An air bubble is left in the vessel to compensate for differences in volume due to thermal expansion. The glass cell is sealed off and put into the larger thermostated vessel and the temperature is lowered until crystals nucleate. Then the temperature is increased until a single crystal is left and the equilibrium temperature is determined. Subsequently, the remaining crystal was used for the observations.

It was not possible to determine a reliable solubility enthalpy for ethanol, because no reproducable solubility data could be measured. Elwenspoek et al. found the same irreproducable solubility behaviour for methanol [Elwenspoek et al., 1987]. Therefore, the driving force in the solution growth experiments will be expressed as the temperature difference between the equilibium temperature and the actual growth temperature ($\Delta T = T - T_{eq}$).

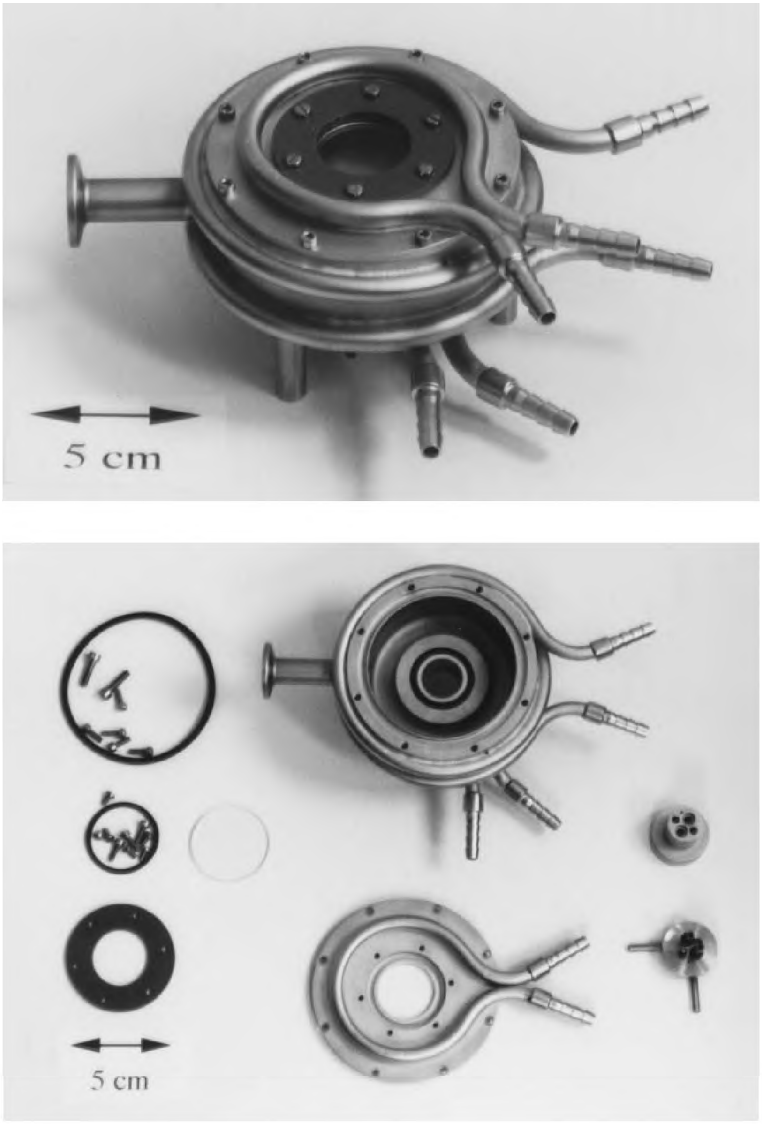

Figure 6.6: Photograph of the vapour growth cell: complete (top) and dismantled (bottom).

6.3.3 Results

6.3.3.1 Vapour growth

In table 6.5 the results of the vapour growth experiments of naphthalene and anthracene are presented. The observed morphologies are drawn in figure 6.8.

After nucleation at a supersaturation of $\frac{\Delta\mu}{kT} \approx 5.2\%$, the naphthalene crystals showed the $\{001\}$, $\{110\}$ and $\{20\bar{1}\}$ forms. Most of the crystals nucleated on one of the $\{001\}$ faces. The crystals were left at a very low supersaturation of approximately $\frac{\Delta\mu}{kT} = 0.07\%$ ($\Delta T = 0.2$K) for several days. Then, the $\{20\bar{2}\}$, $\{1\bar{1}\bar{2}\}$, $\{2\bar{1}\bar{1}\}$ and the $\{011\}$ forms developed, but these facets were not found on all crystals in the growth cell. A crystal was chosen showing $\{011\}$ faces and observed by an optical microscope while the temperature of the outer wall of the growth cell was increased by 0.002K/min. At a supersaturation

Table 6.5: Results of the vapour growth experiments of naphthalene and anthracene. + indicates that the face was always present; +/- indicates that the face has been found sometimes; - indicates that the face has never been observed

	Naphtalene			Anthracene		
Form	Low $\frac{\Delta\mu}{kT}$	High $\frac{\Delta\mu}{kT}$	$(\frac{\Delta\mu}{kT})^{cr}(\%)$	Low $\frac{\Delta\mu}{kT}$	High $\frac{\Delta\mu}{kT}$	$(\frac{\Delta\mu}{kT})^{cr}(\%)$
$\{001\}$	+	+	-	+	+	-
$\{110\}$	+	+	-	+	+	-
$\{20\bar{1}\}$	+	+	-	+	+	-
$\{11\bar{1}\}$	+	-	3.8	+	-	1.8
$\{011\}$	+/-	-	0.2	-	-	-
$\{20\bar{2}\}$	+/-	-	0.2-3.8	-	-	-
$\{2\bar{1}\bar{1}\}$	+/-	-	0.2-3.8	-	-	-
$\{1\bar{1}\bar{2}\}$	+/-	-	0.2-3.8	-	-	-

of 0.2%, the (011) face disappeared rapidly from the morphology because of a sudden increase of its relative growth rate (see figure 6.7).

Optically the face remained very flat during the increase in growth rate. The process was reversible. Upon decreasing the supersaturation, the (011) face reappeared on the crystal. The same phenomenon was observed for the $(11\bar{1})$ faces. These faces disappeared very quickly from the crystal morphology at a supersaturation of 3.8% and also stayed flat during the increase of the growth rate. No accurate critical supersaturations for the $\{1\bar{1}\bar{2}\}$, $\{2\bar{1}\bar{1}\}$ and $\{20\bar{2}\}$ faces have been measured. The $\{1\bar{1}\bar{2}\}$ and $\{2\bar{1}\bar{1}\}$ faces were in many cases rounded off at the edges indicating thermal or kinetic roughening. The order of disappearance at increasing supersaturation of the above mentioned forms is $\{011\}$, $\{2\bar{1}\bar{1}\}$,$\{1\bar{1}\bar{2}\}$, $\{20\bar{2}\}$ and $\{11\bar{1}\}$.

The anthracene crystals had to be grown at a higher temperature (326.5K) as compared to naphthalene (283.2K), because the vapour pressure is much lower and consequently the crystals did not grow at low temperatures. Generally, the anthracene crystals grew much slower than the naphthalene crystals. At low supersaturation, the $\{001\}$, $\{110\}$, $\{20\bar{1}\}$ and $\{11\bar{1}\}$ forms were observed, whereas at increasing supersaturation the $\{11\bar{1}\}$ faces disappeared from the morphology. The critical supersaturation at which the $\{11\bar{1}\}$ faces suddenly started to grow very rapidly is 1.8%. A SEM photo of an anthracene crystal grown from the vapour at a supersaturation higher than 1.8% is shown in figure 6.9.

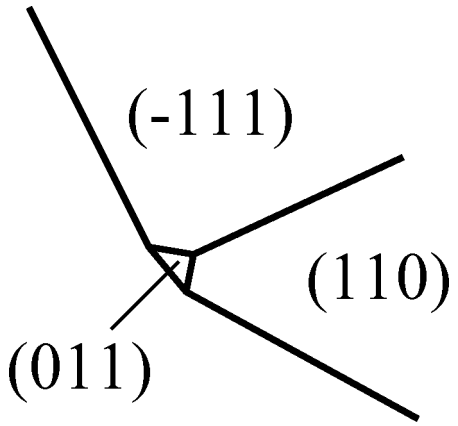

Figure 6.7: In-situ observation of the disappearance of one of the {011} faces of a naphthalene crystal growing from the vapour at 283K. The temperature difference ΔT at t=0 was 0.4K and was increased with 0.002K/min.The pictures were taken at t=68 (A), t=106 (B) and t=125 min (C).

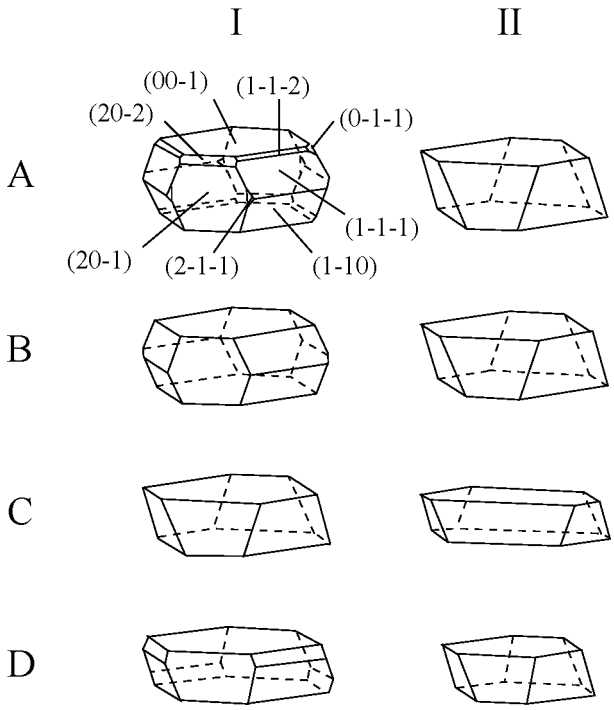

Figure 6.8: Experimental morphologies for naphthalene and anthracene. I: Low driving force; II: High driving force; A: Naphthalene vapour; B: Naphthalene ethanol; C: Naphthalene cyclohexane; D: Anthracene vapour.

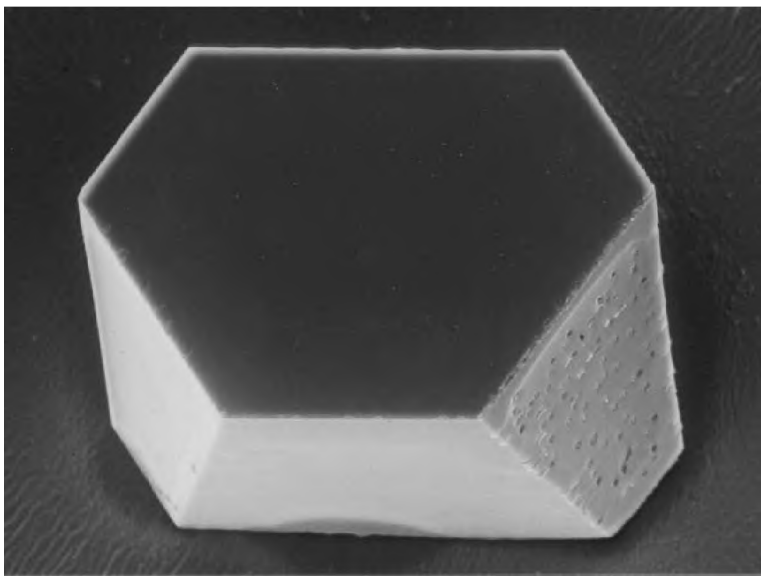

Figure 6.9: SEM picture of anthracene crystal grown from the vapour at high driving force (magnification 450x).

Table 6.6: Results of the solution growth experiments of naphthalene in ethanol and cyclo-hexane. + indicates that the face was present; - indicates that the face was not observed

	Ethanol		Cyclo hexane	
Form	Low $\frac{\Delta\mu}{kT}$	High $\frac{\Delta\mu}{kT}$	Low $\frac{\Delta\mu}{kT}$	High $\frac{\Delta\mu}{kT}$
$\{001\}$	+	+	+	+
$\{20\bar{1}\}$	+	-	+	+
$\{110\}$	+	+	+	+
$\{11\bar{1}\}$	+	-	-	-

6.3.3.2 Solution growth

The results of the solution growth experiments are summarized in table 6.6. Drawings of the observed morphologies are presented in figure 6.8. At low driving forces the naphthalene crystals grown from ethanol show the $\{001\}$, $\{20\bar{1}\}$, $\{110\}$ and $\{11\bar{1}\}$ forms. At higher supersaturations (ΔT>0.4K), the $\{11\bar{1}\}$ faces disappear and at very high supersaturations (ΔT>2.0K) the $\{20\bar{1}\}$ form disappears. The undercoolings at which the $\{11\bar{1}\}$ disappeared from the morphology are listed in table 6.7. For the $\{20\bar{1}\}$ form no quantitative measurements were done, because the results could not be reproduced. The morphological importance of the $\{20\bar{1}\}$ faces appeared to depend on the driving force at which crystals were nucleated. When the crystals were nucleated at high driving forces (ΔT>10K), the $\{20\bar{1}\}$ was hardly observed whereas at lower driving forces (ΔT=0.2-2K) the $\{20\bar{1}\}$ became more important. This may be attributed to dislocation formation at high driving forces.

Table 6.7: Critical undercooling for the $\{11\bar{1}\}$ faces of naphthalene grown from ethanol

T_{eq} (K)	ΔT (K)
291.3	0.4
289.4	1.0
284.2	2.0

When naphthalene crystals were grown from cyclo hexane solution, only the $\{001\}$, $\{110\}$ and $\{20\bar{1}\}$ faces were observed. At low driving force (ΔT=0.05-0.1K, T_{eq}=290K) the crystals had a hexagon like shape. At higher supersaturations (ΔT=0.6K, T_{eq}=290K), the $\{20\bar{1}\}$ became very important and the crystals became needle shaped. The same morphology has been reported for naphthalene crystals grown from n-hexane solution [Elwenspoek et al., 1987].

6.4 Discussion

The theoretical morphologies based on the attachment energies (eq. (6.3)) of naphthalene and anthracene are in good agreement with the experimentally observed crystal habits. The predicted faces based on attachment energies are both for naphthalene and anthracene $\{001\}$, $\{20\bar{1}\}$, $\{110\}$, $\{11\bar{1}\}$ and $\{011\}$. All these faces have been observed on naphthalene crystals grown from the vapour at low supersaturation and, except for $\{011\}$, also on anthracene crystals.

The $\{020\}$ faces have been observed neither for naphthalene nor for anthracene. This is in agreement with the theory, because these faces have a roughening temperature of 207 K and 202 K for naphthalene and anthracene respectively, which is lower than the temperature at which the crystals were grown (283 K and 326 K respectively).

Another form that occurred neither on naphthalene nor on anthracene crystals was $\{200\}$. The attachment energy of this form is very close to the threshold value for appearance in the Wulff plot and the Ising temperature is higher than the actual growth temperature. Therefore it is expected that this form may be observed on crystals at equilibrium conditions. For naphthalene the $\{200\}$ form was also not found by Pavlovska and Nenow [Pavlovska and Nenow, 1972]. Robinson and Scott reported the $\{200\}$ form for anthracene crystals grown from the vapour [Robinson and Scott, 1967].

For the naphthalene crystals grown from the vapour, the $\{1\bar{1}\bar{2}\}$ form has been found on some crystals at very low supersaturations and equilibrium conditions. According to the connected net analysis this form is not an F-form, because no connected net $(1\bar{1}\bar{2})$ has been found. However, addition of a very weak bond u (M_1[000]-M_1[111], E^{bb}=0.142 kcal/mol $\approx$ 0.25 kT) to the crystal graph will make the $\{1\bar{1}\bar{2}\}$ form an F-form. The single connected net thus found consists of the very strong q bond and the added weak bond u. The 2-D Ising temperature of the $\{1\bar{1}\bar{2}\}$ connected nets is 379K. The attachment energy for the $\{1\bar{1}\bar{2}\}$ faces is -27.4 kcal/mol. With this attachment energy the form is not present on the theoretical growth form. This example clearly demonstrates that it is very important to include even weak bonds in the crystal graph in order to find all possible F-faces having a roughening temperature larger than the actual growth temperature. In general, crystal faces containing a connected net consisting of a very strong DC $[uvw]_1$ and a very weak intersecting non-parallel DC $[uvw]_2$ still have a rather high 2-D Ising transition temperature as long as the anisotropy is not too large [Burton et al., 1951, Grimbergen et al., 1999a]. These type of faces may occur on crystals at equilibrium conditions as flat faces.

The most striking result of this work is the observation and growth behaviour of the $\{011\}$ faces on naphthalene crystals. To our knowledge these faces have only been observed by Pavlovska and Nenow for naphthalene crystals grown from the vapour at room temperature and left under equilibrium conditions for one month [Pavlovska and Nenow, 1972]. In section 2.3 it has been shown that, because of the presence of two symmetry related connected nets corresponding to slightly different surfaces, the $\{011\}$ faces have a very low effective step free energy according to eq. (6.1). Consequently, the faces will have a low roughening temperature and a high growth rate due to a low 2-D nucleation barrier. The fact that the growth rate of the $\{011\}$ faces drastically increased beyond a threshold supersaturation of 0.2% can be explained by this low nucleation barrier. The growth

behaviour of crystal faces containing multiple connected nets as compared to faces with a single connected net is subject of a forthcoming paper [Grimbergen et al., 1999a]. When the {011} faces started to grow no indication of a roughening effect was observed. The crystal face grew very fast as a flat face and disappeared from the morphology because of the high growth rate compared to the adjacent faces. It can be concluded that the {011} faces have a roughening temperature larger than the growth temperature of 283.2K. At higher growth temperatures (T>285K) the {011} form has not been observed probably because this temperature is higher than the actual roughening temperature for {011} form or due to a very small barrier for kinetic roughening.

In case of anthracene the {011} form is not found, probably because the crystals are grown at higher temperatures due to the larger lattice energy. Therefore, the step free energy (γ) will be relatively low resulting in a high growth rate already at very low supersaturation. Alternatively, the face could already be rough at the actual experimental growth temperature. This form was also not observed by Robinson et al. on anthracene crystals grown from the vapour [Robinson and Scott, 1967]. They observed the {001}, {20$\bar{1}$}, {110}, {11$\bar{1}$}, {011}, {20$\bar{2}$}, {11$\bar{2}$} and {200} forms which are all valid F-forms (see table 6.4).

The {2$\bar{1}\bar{1}$} faces have the same topology as the {011} faces and also contain two symmetry related connected nets. They have been observed as very tiny rounded-off faces on some naphthalene crystals and never on anthracene crystals. This is in agreement with the very low step free energy giving rise to a very low roughening temperature and a high growth rate. For both the {011} and {2$\bar{1}\bar{1}$} forms, the calculated 2-D Ising transition temperature is not a good estimate for the actual roughening temperature of the crystal face, because of the presence of multiple connected nets.

The {11$\bar{1}$} form contains a single connected net. However, at higher driving forces the face disappears from the morphology due to an increased growth rate. This behaviour has been found for naphthalene crystals grown from the vapour and from ethanol and for anthracene crystals grown from the vapour. It is not possible to explain these observations from the connected net structure. Comparison of the {110} and {11$\bar{1}$} connected nets shows that these orientations have the same type of connected net and almost the same attachment energy and Ising transition temperature (see table 6.3 and 6.4). It is expected that these faces have similar growth behaviour at moderate supersaturations. It has been shown that very high supersaturations tend to produce more extreme crystal habits [Hartman and Bennema, 1980]. It is expected that the faces having the lowest attachment energy and the largest d_{hkl} will become dominant. For {11$\bar{1}$} and {110}: $d_{11\bar{1}} > d_{110}$ and $E^{att}_{11\bar{1}} > E^{att}_{110}$. The {11$\bar{1}$} form will become less important at higher supersaturations which is confirmed by the experimental results. However, we are not able to explain the large increase in growth rate for the {11$\bar{1}$} faces as compared to the {110} faces at such a low driving force completely.

Note that looking at the order of disappearance of the crystal faces at increasing supersaturation, the faces containing multiple connected nets disappeared from the morphology at the lowest driving forces.

Comparing the observed morphologies of naphthalene grown from solution or from vapour, it can be concluded that in solution less faces occur. This can be attributed to a lowering of the effective bond energies. The bond energies used in this paper to calculate

the 2-D Ising transition temperatures T^C_{hkl} are bond energies Φ_i calculated in the bulk structure. Addition of all these bonds yields the sublimation enthalpy:

$$\sum_i \Phi_i = \Delta H_{subl} \ . \tag{6.5}$$

The bondenergies for a crystal grown from solution are:

$$\sum_i \Phi_i = \Delta H_{diss} \ . \tag{6.6}$$

The 2-D Ising transition temperatures in solution can be roughly estimated by [Bennema, 1993]

$$T^C_{solution} = \frac{\Delta H_{diss}}{\Delta H_{subl}} \, T^C_{calc} \ . \tag{6.7}$$

In general, dissolution enthalpies are lower than the sublimation enthalpies. This implies that the Ising transition temperatures will be lower in solution. A lowering of the transition temperature also implies that the step free energy will be lower resulting in a low barrier for kinetic roughening. Consequently, less faces will occur on crystals grown from solution as compared to crystals grown from the vapour. Using the dissolution enthaply of naphthalene in n-hexane is ΔH^{n-hex}_{diss}=7.9 kcal/mol [Elwenspoek et al., 1987] and the sublimation enthalpy of naphthalene ΔH_{subl}=17.4 kcal/mol the roughening temperatures in table 6.3 have to be multiplied with a factor 0.45 according to eq. (6.7). The corrected 2-D Ising transition temperatures of the faces in table 6.3 are $\{001\}$ ($T^C_{n-hex} = 831K$), $\{110\}$ ($T^C_{n-hex} = 434K$), $\{20\bar{1}\}$ ($T^C_{n-hex} = 386K$), $\{11\bar{1}\}$ ($T^C_{n-hex} = 405K$), $\{011\}$ ($T^C_{n-hex} = 266K$), $\{200\}$ ($T^C_{n-hex} = 224K$), $\{20\bar{2}\}$ ($T^C_{n-hex} = 190K$), $\{2\bar{1}\bar{1}\}$ ($T^C_{n-hex} = 167K$) and $\{020\}$ ($T^C_{n-hex} = 93K$). The Ising temperatures of the last 5 faces are lower than the actual experimental growth temperature. Therefore these facets are not expected to occur on the morphology of naphthalene crystals grown from n-hexane solution. This theoretical result is confirmed by Elwenspoek et al. [Elwenspoek et al., 1987]. The result of n-hexane may be comparable to our results for cyclo-hexane. The experimental results for cyclo-hexane show that none of the above mentioned faces having a very low Ising temperature occur on the morphology. Anomalies can be expected in case a solvent has a special interaction with a specific crystal face (hkl) as then eq. (6.7) does not hold [Elwenspoek et al., 1987, Shekunov and Latham, 1996].

6.5 Conclusions

In this paper we have shown that the morphology of naphthalene and anthracene crystals depends strongly on the applied driving force, temperature and mother phase. The connected net analysis combined with Ising transition temperature and attachment energy calculations predicts the most important faces observed on experimentally grown crystals. However, the attachment energy prediction of the growth morphology does not take the influence of a mother phase, driving force and symmetry related pairs of connected nets into account. For specific orientations having multiple connected nets the attachment energy is not a good parameter for the relative growth rate.

We have found experimental evidence that the {011} and {$2\bar{1}\bar{1}$} faces have a very low step free energy which is attributed to a pair of connected nets giving rise to a zero step energy (symmetry roughening) in the broken bond approximation. However, because of the different molecular structure at the interfaces corresponding to the two connected nets the step free energy will be larger than zero, but very low. Experimentally the {011} faces have been observed on naphthalene crystals at very low supersaturation and disappear from the morphology rapidly beyond a threshold supersaturation due to an increase in relative growth rate. This is attributed to the presence of a symmetry related pair of connected nets causing a low 2-D nucleation barrier. In our opinion this example demonstrates the importance to determine all connected nets of a crystal structure in order to understand the growth behaviour. Moreover, it has been shown that the standard attachment energy method to determine the morphological importance of a crystal face (hkl) fails for faces containing a pair of connected nets that gives rise to a very low step free energy in spite of a low attachment energy.

The connected net structure of the {$11\bar{1}$} faces is almost equal to that of the {110} faces. Nevertheless, the {$11\bar{1}$} faces show an increased growth rate as compared to the {110} faces at higher supersaturations. This cannot be explained by the connected net analysis. However, this is another example that the attachment energy description of relative growth rates of crystal faces does not hold in general.

Observation of the {$1\bar{1}\bar{2}$} faces demonstrates that it is important to include even very weak bonds in the connected net analysis in order to determine all faces with a roughening temperature above the actual growth temperature.

Finally, the morphologies of naphthalene crystals grown from solution exhibit less faces as compared to vapour grown crystals. This can be attributed to a lowering of the effective bond energies at the crystal-mother phase interface resulting in a lower roughening temperature and thus a higher growth rate.

Acknowledgements

R.F.P. Grimbergen would like to acknowledge the financial support of the Dutch Technology Foundation (STW).

Chapter 7

Morphology of Orthorhombic n-Paraffin Crystals I: the Influence of Multiple Connected Nets

Morphology of Orthorhombic n-Paraffin Crystals I: the Influence of Multiple Connected Nets

R.F.P. Grimbergen, P.J.C.M. van Hoof, H. Meekes and P. Bennema [1]

Abstract

The morphology of orthorhombic paraffin crystals is predicted on the basis of a complete connected net analysis. Many facet orientations (hkl) contain multiple connected nets. The connected nets found are categorized in terms of symmetry relations and the physical implications of the presence of multiple connected nets are discussed. From the analysis of step energies it can be concluded that at low supersaturation the growth morphology is bounded by {001}, {100}, {111} and {010} faces, whereas at higher supersaturations the {001}, {111}, {110} and {010} faces are present. The predicted morphologies differ from the conventional prediction based on the attachment energy.

7.1 Introduction

In the past extensive research has been carried out on crystallization of n-alkanes because of the practical relevance. Paraffins are present in many products derived from crude oil. At low temperature conditions the paraffins crystallize and cause problems as the platy crystals form a gel which blocks filters of for instance diesel engines.

n-Paraffins crystallize in four modifications: triclinic, monoclinic, orthorhombic and hexagonal depending on the number of carbon atoms in the paraffin chain, the temperature and the presence of impurities. The growth mechanism of even numbered n-paraffins has been studied extensively by Boistelle , Simon and others [Simon et al., 1974a, Simon et al., 1974b, Boistelle and Doussoulin, 1976, Boistelle and Madsen, 1978, Madsen and Boistelle, 1979, Boistelle et al., 1976, Simon and Boistelle, 1981].

The crystal morphology of orthorhombic n-paraffin crystals [Bennema et al., 1992, Bennema, 1993], triclinic [Liu and Bennema, 1994] and monoclinic n-paraffin crystals [Liu and Bennema, 1993b] has been studied in the past using the well-established Hartman-Perdok theory integrated with the theory of roughening transitions. Especially the roughening transition of the {110} faces of orthorhombic odd numbered n-paraffin crystals has been studied in detail [Liu et al., 1992, Liu et al., 1993, Liu and Bennema, 1993a].

In this paper both the equilibrium and growth morphology of orthorhombic odd numbered n-paraffin crystals will be derived from the crystal structure applying the principles of a recently developed extension to the Hartman-Perdok theory [Grimbergen et al., 1998b, Meekes et al., 1998, Grimbergen et al., 1999a]. The paraffin structure is an example of a crystal structure that contains multiple connected nets for a single orientation

[1] The work presented in this chapter has been accepted for publication in J. Cryst. Growth

(hkl), something which occurs for many other crystal structures. Some of those connected nets are symmetry related and can cause symmetry roughening [Grimbergen et al., 1998b, Meekes et al., 1998]. Also the {110} faces of odd-numbered n-paraffins which have a low threshold for kinetic roughening contain multiple connected nets. In contrast to what has been done upto now, we take all connected nets found for an orientation (hkl) into account. Apart from the physical implications of the presence of multiple connected nets for a single facet orientation (hkl), the influence of a large anisotropy in step free energies will be discussed.

In section 7.2 a short theoretical introduction to the recently developed extension of the Hartman-Perdok theory is presented. Section 7.3 describes the general crystal graph of the orthorhombic paraffin structure. Following a preliminary paper concerning the problem to determine all connected nets of the crystal graph of orthorhombic paraffin [Strom and Bennema, 1998], in section 7.4 a topological analysis will be carried out concerning the structure of the 71 different connected nets which were derived from the crystal graph on basis of the graph theoretical method, developed by Strom [Strom, 1980, Strom, 1981, Strom, 1985]. All symmetry relations between the connected nets for a single orientation (hkl) will be analyzed. It will be shown that specific combinations of symmetry related connected nets cause symmetry roughening [Meekes et al., 1998]. The theoretically derived equilibrium and growth morphology will be presented and discussed in section 7.5. Finally some conclusions will be drawn.

In a forthcoming paper the theoretical results obtained will be confronted with a rich variety of morphological and crystal growth data of orthorhombic paraffin crystals grown from the vapour, melt and different solvents at various supersaturations [van Hoof et al., 1998a].

7.2 Connected net analysis and roughening

Already in 1955 Hartman and Perdok found that the morphology of crystals could be derived from the crystal structure [Hartman and Perdok, 1955a, Hartman and Perdok, 1955b, Hartman and Perdok, 1955c]. This can be achieved by determination of all Periodic Bond Chains (PBCs) which are chains of strongly bonded growth units in the crystal lattice. It is supposed that along the PBC directions the crystal grows relatively fast. Hartman and Perdok stated that facet orientations (hkl) which are coplanar with at least two non-parallel intersecting PBCs will occur as flat faces (F-faces) on the crystal morphology. Around 1980 the Hartman-Perdok theory was integrated with the theory of surface roughening and the concept of connected net was introduced. See for a survey ref. [Bennema, 1993]. A connected net is a set of growth units connected by bonds constituting a network. Equivalent connected nets are separated by the interplanar distance d_{hkl}, corrected for the selection rules of the space group of the crystal according to the law of Bravais, Friedel, Donnay and Harker (BFDH). Connected nets can be derived from a so-called crystal graph. A crystal graph is defined as an infinite set of points corresponding to the centres of the growth units with strong bonds between these points.

7.2.1 Thermal roughening

In general it can be shown [van Beijeren and Nolden, 1986] that a flat face (hkl) (i.e. a crystal facet below the roughening temperature T^R) with normal $\boldsymbol{k}$ has the property that for all crystallographic directions $\boldsymbol{u} = u\boldsymbol{a} + v\boldsymbol{b} + w\boldsymbol{c}$ labeled by $[uvw]$ $(u, v, w \in Z)$ coplanar with the face (i.e. $\boldsymbol{u} \cdot \boldsymbol{k} = 0$) the sum of the step free energy γ of a step in the $\boldsymbol{u}$ and $-\boldsymbol{u}$ direction is larger than zero, or

$$\gamma(\boldsymbol{u}) + \gamma(-\boldsymbol{u}) > 0 \quad \forall\, \boldsymbol{u}, \boldsymbol{u} \cdot \boldsymbol{k} = 0\,. \tag{7.1}$$

In case eq. (7.1) is satisfied, the facet orientation (hkl) may appear on the equilibrium morphology as a flat face. In the past the roughening transition temperature T^R_{hkl} was estimated qualitatively by the 2-D Ising transition temperature T^C_{hkl} of the strongest connected net [Rijpkema et al., 1982].

In order to find all possible flat facet orientations (hkl) at a certain temperature for each orientation the step free energy in all directions $\boldsymbol{u}$ has to be determined. To our knowledge there is no general method available to calculate these step free energies. However, the analysis of all connected nets for an orientation (hkl) can be used to determine the faces with the highest step free energies and lowest surface energies which determine the equilibrium and growth morphology.

Recently, it has been shown that for specific orientations (hkl) parallel to more than one (symmetry related) connected net, application of eq. (7.1) results in a zero step energy. This phenomenon was called macroscopic symmetry roughening [Grimbergen et al., 1998b, Meekes et al., 1998]. Macroscopic symmetry roughening can even occur for orientations for which the attachment energy is very small and thus the slice energy is large. Obviously, the assumption that the 2-D Ising temperature T^C_{hkl} of the strongest connected net is a good measure for the roughening temperature T^R_{hkl} does not hold for these types of crystal facet.

Another case of symmetry roughening is microscopic symmetry roughening. In such a case eq. (7.1) is satisfied but the energy of a domain wall between two symmetry related connected nets or surface configurations is zero. Microscopic roughening was also found in statistical thermodynamical Solid-On-Solid models and introduced as a DisOrdered Flat (DOF) phase [Rommelse and den Nijs, 1987, den Nijs and Rommelse, 1989]. Note that microscopically rough facets may occur on the crystal morphology as flat faces because the overall step free energy for the orientation (hkl) is larger than zero, although the microscopic surface structure is rough.

It can be concluded that an orientation (hkl) will have a roughening temperature larger than zero kelvin in case the combination of all connected nets present assures that eq. (7.1) is satisfied.

7.2.2 Kinetic roughening

Facets with a roughening temperature larger than the actual growth temperature may also become rough because of kinetic roughening. In that case the crystal facet becomes rough at a supersaturation at which the free energy of formation of a 2-D nucleus has vanished. 2-D nucleation will proceed everywhere on the surface and the facet becomes rough. It

has been demonstrated by Monte Carlo simulations for a rectangular lattice with step energies γ_x and γ_y in the x-direction and y-direction respectively (γ_x+γ_y=constant) that a larger anisotropy in the step energy causes a lower nucleation barrier [van der Eerden et al., 1977]. Therefore, faces with a high anisotropy will grow faster and become rough at lower supersaturations as compared to isotropic faces. In general, faces that have a low roughening temperature will also become rough kinetically at low supersaturation. Alternatively, facets containing combinations of connected nets resulting in a very low step energy in a certain direction may also have a very low nucleation barrier and become kinetically rough at very low supersaturations [Grimbergen et al., 1999a]. Thus, even pairs of connected nets that are not symmetry related (and do not cause symmetry roughening) can become kinetically rough at very low supersaturations due to a very low effective step free energy. This can be regarded as pseudo symmetry roughening.

7.2.3 Construction of the morphology

The equilibrium morphology (based on the lowest surface free energies) may be approximated by [Kern, 1987]

$$D_{hkl} \propto d_{hkl} E^{att}_{hkl} , \tag{7.2}$$

where D_{hkl} is the center-to-face distance in the Wulff plot [Wulff, 1901], d_{hkl} is the interplanar distance and E^{att}_{hkl} is the attachment energy for the crystal face (hkl). The attachment energy of a face is defined as the energy released when a complete growth layer (connected net) is attached to the surface {hkl}. The attachment energy is related to the crystal energy E_{cryst} by $E_{cryst} = E^{att}_{hkl}+E^{slice}_{hkl}$. The equilibrium morphology obtained by eq. (7.2) has to be corrected for cases of symmetry roughening. Macroscopically, symmetry roughened orientations will not occur as well-defined flat faces on the equilibrium morphology as for these cases the step free energy is zero. The same holds for faces above their roughening temperature T^R.

Hartman and Bennema [Hartman and Bennema, 1980] showed that the relative growth rate R_{hkl} of a crystal face (hkl) increases as the attachment energy E^{att}_{hkl} increases. An approximate growth morphology can be constructed using a Wulff plot assuming that the relative growth rate R_{hkl} is proportional to the attachment energy:

$$R_{hkl} \propto E^{att}_{hkl} . \tag{7.3}$$

Note that the predicted morphology based on the attachment energy is independent of the supersaturation. Obviously this cannot be true because it is known from many experiments that the relative growth rate R depends on many parameters among which the supersaturation. However, the attachment energy tends to give a reasonable estimate of the growth morphology over a rather long range of supersaturation. To our opinion the predictive value of the morphology obtained by eq. (7.3) can be enhanced when it is corrected for cases of mutiple connected nets giving rise to symmetry roughening or a very low step free energy resulting in an unexpected low nucleation barrier and a relatively high growth rate already at low supersaturations [Grimbergen et al., 1999a].

7.3 Crystal graph of orthorhombic paraffin

The orthorhombic paraffin crystal structure has space group symmetry Pbcm and the generalized cell parameters for paraffins with chain length n are a=4.970 Å , b=7.478 Å and $c = nc_0 + c'_0$, where c_0=2.546 Å and c'_0=3.750 Å [Smith, 1953]. There are four symmetry equivalent molecules M_1, M_2, M_3 and M_4 in the unit cell with their corresponding centers at $(\frac{1}{4}, 0, \frac{1}{4})$, $(\frac{3}{4}, 0, \frac{3}{4})$, $(\frac{3}{4}, \frac{1}{2}, \frac{1}{4})$ and $(\frac{1}{4}, \frac{1}{2}, \frac{3}{4})$ respectively. The paraffin chains are parallel to the c-axis. The BFDH selection rules for the spacegroup Pbcm are $\{0kl\} : k = 2n$, $\{h0l\} : l = 2n$, $\{0k0\} : k = 2n$ and $\{00l\} : l = 2n$. Note that in the following a distinction will be made between the orientation $\{hkl\}$ with h, k and l mutually prime and the connected nets which will be indicated with indices $\{hkl\}$ corrected for the BFDH selection rules or the stoichiometry. In most cases only the generating connected nets will be given. All symmetry related connected nets can be found by application of the spacegroup symmetry elements.

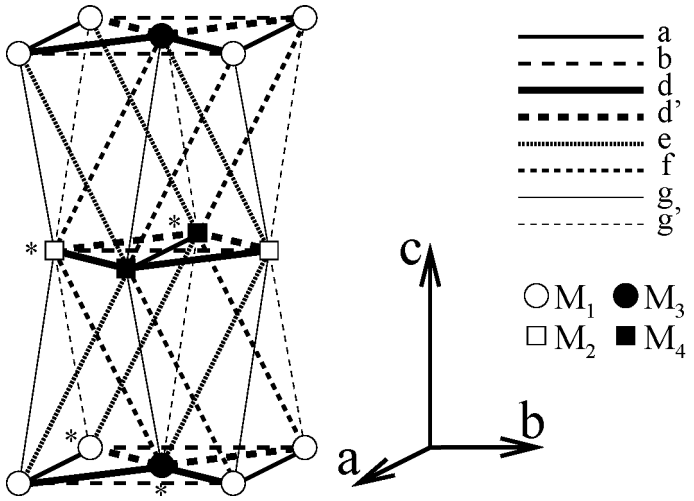

Figure 7.1: Crystal graph of orthorhombic paraffin. The c-axis is shortened for matter of clarity. Marked geometrical centers are positioned in the unit cell [000]. Bond labels were taken from ref. [Bennema et al., 1992].

In figure 7.1 the unit cell of the crystal graph of orthorhombic paraffin is presented. Exactly the same crystal graph was used before to explain the morphology of paraffin crystals [Bennema et al., 1992, Bennema, 1993]. Note that the c-axis is shortened for clarity sake. Three strong first nearest neighbour lateral body-body bonds d, d' and a can be recognized and a much weaker next nearest neighbour lateral body-body bond b. Furthermore, three weak head tail bonds e, g and g' and an even weaker next nearest neighbour bond f can be seen. Apart from the f bond all bonds have an energy equal or larger than kT (T at room temperature, k is Boltmann's constant). In this study all bond energies have been calculated for $C_{23}H_{48}$ because in a forthcoming paper [van Hoof et al., 1998a] experimental results for paraffins having this chainlength will be presented. The bond energies have been calculated from the crystal structure using the following procedure. First electrostatic potential derived (ESPD) MNDO atomic point charges were

Table 7.1: Bonds defining the crystal graph of orthorhombic paraffin. The bond energies Φ are calculated for $C_{23}H_{48}$. Note that in the broken bond convention $\Phi^{bb} = -\frac{1}{2}\Phi$. All bonds are defined with respect to $M_1[000]$.

Lateral bonds		
Label	Bond	Φ (kcal/mol)
a	M_1-$M_1[100]$	-8.910
b	M_1-$M_1[010]$	-1.587
d	M_1-$M_3[\bar{1}00]$	-14.885
d'	M_1-$M_3[000]$	-14.642
Head-tail bonds		
Label	Bond	Φ (kcal/mol)
e	M_1-$M_4[000]$	-0.566
f	M_1-$M_4[0\bar{1}0]$	-0.286
g	M_1-$M_2[\bar{1}00]$	-0.568
g'	M_1-$M_2[000]$	-0.644

calculated with MOPAC. The Dreiding force field parameters were used for calculation of intra- and inter molecular interactions. The energy of the crystal structure was minimized while symmetry was imposed and the cell parameters a, b and c were allowed to change. For calculation of long range non-bonded interactions the Ewald summation technique was applied. After minimization of the crystal structure the cell parameters were a=5.026 Å , b=7.284 Å and c=62.784 Å. The calculated lattice energy after minimization was -47.0 kcal/mol per paraffin molecule. This lattice energy may be compared to a calculated experimental lattice enthalpy (V_{exp}) given by [Hagler et al., 1976]

$$V_{exp} = -\Delta H_{subl} - 2RT \ , \tag{7.4}$$

where ΔH_{subl} is the sublimation enthalpy and $2RT$ represents a correction for the difference between the gas phase enthalpy and the vibrational contribution to the lattice enthalpy. Experimental sublimation enthalpy data are given in ref. [Bennema et al., 1992]. For $C_{23}H_{48}$ the sublimation enthalpy is 46.3 kcal/mol per growth unit and the experimental lattice energy according to eq. (7.4) is -47.5 kcal/mol per growth unit(T=298K). The calculated lattice energy of -47.0 kcal/mol is in good agreement with this 'experimental' lattice energy. The bond energies of the bonds defined in the crystal graph were calculated in the minimized crystal structure and are given in table 7.1. The calculated bond energies are comparable to those presented in ref. [Bennema et al., 1992] (parameter set 1b). The crystal energy calculated from the bonds constituting the crystal graph is -42.1 kcal/mol per growth unit($\approx$90% of the total lattice energy). In the following all attachment and slice energies will be calculated from the calculated bonds of the crystal graph and will be expressed in kcal/mol per unit cell content (i.e. per four paraffin molecules).

7.4 Connected nets and symmetry relations

The connected net analysis was done applying the program FACELIFT [Grimbergen et al., 1997]. In Table 7.2 all connected nets derived from the paraffin graph presented in Fig. 7.1 are summarized. The connected nets are classified according to symmetry relations. A singlet is defined as a single connected net (hkl) which is not related by symmetry to any other connected net of the same orientation (hkl). A doublet (quartet) is defined as two (four) symmetry related connected nets for an orientation (hkl). In two cases connected nets which are connected subnets having a periodicity twice as small as the corresponding nets (hkl) are also given (compare (004) with (002) and (200) with (100)). The reason that connected subnets are also taken into consideration will be discussed below. Note that all together 71 different connected nets can be identified in the crystal graph of paraffin according to table 7.2. The 2-D Ising temperature of the connected nets was calculated, if possible, using the program TCRITIC [Hoeks, 1993]. In case the Ising temperature could not be calculated exactly, the transition temperature was estimated on the basis of a simplified connected net [Rijpkema et al., 1982].

In the following subsections we will analyze the structure of all different connected nets and analyze what the implications are for the growth kinetics and morphology of different connected nets for a single orientation (hkl). The applicability of the Ising transition temperature as given in table 7.2 will be discussed.

7.4.1 The {001} form

The most prominent orientation both experimentally and theoretically is the (001) orientation. Because of the two-fold screw axis along the c-axis and the c-glide the interplanar distance is d_{002}. Physically identical surface configurations are separated by d_{002} and the crystal will grow with layers d_{002}. For this orientation six connected nets have been found (see figure 7.2). The most important one is clearly the planar singlet $S_1\{002\}$ consisting of the strong lateral bonds a, b, d and d'. Additionally, two doublets were found $D_1\{002\}$, $D_2\{002\}$ which consist of half of the content of two singlets $S_1\{002\}$ separated by the interplanar distance d_{002}. The doublet $D_1\{004\}$ is equivalent to the singlet $S_1\{002\}$ but contains half of the growth units. The connected nets $D_1\{002\}$, $D_2\{002\}$ and $D_1\{004\}$ do not contain the very strong d and d' bonds which explains the low slice energies and Ising temperatures as compared to $S_1\{002\}$.

The doublets $D_1\{002\}$, $D_2\{002\}$ and $D_1\{004\}$ are examples of pairs of connected nets related by a glide mirror b $\parallel \mathbf{k}$ with the glide $\perp \mathbf{k}$ ($\mathbf{k}$ is the face normal) which could give rise to microscopic symmetry roughening in case there would be no other connected net present. However, for the same orientation the strong singlet $S_1\{002\}$ exists. This singlet contains the strong d and d' bonds that actually have the bond energy that is released on realizing a domain wall for the doublets. Therefore, the growth kinetics and morphology of the $\{001\}$ orientation will be dominated by the $S_1\{002\}$ connected net.

Table 7.2: Inventory of all generating connected nets of the crystal graph in fig. 7.1 ordered by decreasing d_{hkl}. In the first column the symmetry related connected nets are labeled with S for singlet, D for doublet and Q for quartet. The subscript indicates the reference number of the n-plet and the face orientation is indicated with $\{hkl\}$. In the second column the the symmetry operations of the space group P 2/b 2_1/c 2_1/m generating all members of the doublet or quartet are given and in the third column the slice energy is shown. In the last column the conventionally calculated 2-D Ising temperatures of the strongest connected nets are given. For some connected nets the Ising temperatures were estimated because exact calculation was not possible.

Net	Symmetry	E_{hkl}^{slice} (kcal/mol)	T^C (K)	Net	Symmetry	E_{hkl}^{slice} (kcal/mol)	T^C (K)
$S_1\{002\}$		-160.1	5834	$D_1\{112\}$	$\bar{1}$	-46.5	840
$D_1\{002\}$	b	-44.4	≈ 2460	$D_2\{112\}$	$\bar{1}$	-46.1	821
$D_2\{002\}$	b	-43.7	≈ 2460				
$D_1\{004\}$	b	-42.0	1230	$S_1\{020\}$		-40.5	1123
				$S_2\{020\}$		-37.9	882
$S_1\{100\}$		-71.5	> 2200	$S_3\{020\}$		-36.8	739
$S_2\{100\}$		-70.8	> 2200				
$Q_1\{100\}$	2_1^y,2_1^z,b,c,$\bar{1}$	-69.5	≈ 2200	$S_1\{021\}$		-39.2	991
$D_1\{100\}$	2_1^y,b,$\bar{1}$	-67.2	≈ 2200	$S_2\{021\}$		-38.6	897
$D_2\{100\}$	2_1^y,b,$\bar{1}$	-66.0	≈ 2200				
$D_3\{100\}$	2_1^z,c	-38.7	≈ 2200	$S_1\{022\}$		-37.3	805
$D_4\{100\}$	2_1^z,c	-37.9	≈ 2200				
				$S_1\{120\}$		-32.3	≈ 70
$S_1\{102\}$		-67.2	1305	$S_2\{120\}$		-31.5	≈ 70
$S_2\{102\}$		-66.0	1257				
				$S_1\{121\}$		-32.8	77
$S_1\{110\}$		-63.7	1563	$S_2\{121\}$		-32.3	79
$S_2\{110\}$		-62.6	1448	$S_3\{121\}$		-32.3	77
$D_1\{110\}$	2_1^z,$\bar{1}$	-48.4	≈ 1280	$S_4\{121\}$		-31.7	77
$D_2\{110\}$	2_1^z,$\bar{1}$	-48.4	≈ 1280				
$D_3\{110\}$	2_1^z,$\bar{1}$	-46.8	≈ 1280	$S_1\{200\}$		-9.7	336
$D_4\{110\}$	2_1^z,$\bar{1}$	-46.4	≈ 1280	$S_2\{200\}$		-8.9	300
$D_5\{110\}$	2_1^z,$\bar{1}$	-46.3	≈ 1280	$S_3\{200\}$		-8.6	285
$D_6\{110\}$	2_1^z,$\bar{1}$	-45.9	≈ 1280				
				$S_1\{202\}$		-8.8	292
$S_1\{111\}$		-63.1	1504				
$D_1\{111\}$	$\bar{1}$	-47.6	≈ 835	$D_1\{210\}$	2_1^z,$\bar{1}$	-31.2	≈ 70
$D_2\{111\}$	$\bar{1}$	-47.4	≈ 835				
$D_3\{111\}$	$\bar{1}$	-47.3	≈ 835	$D_1\{211\}$	$\bar{1}$	-32.1	75
$D_4\{111\}$	$\bar{1}$	-47.1	≈ 835	$D_2\{211\}$	$\bar{1}$	-31.9	75

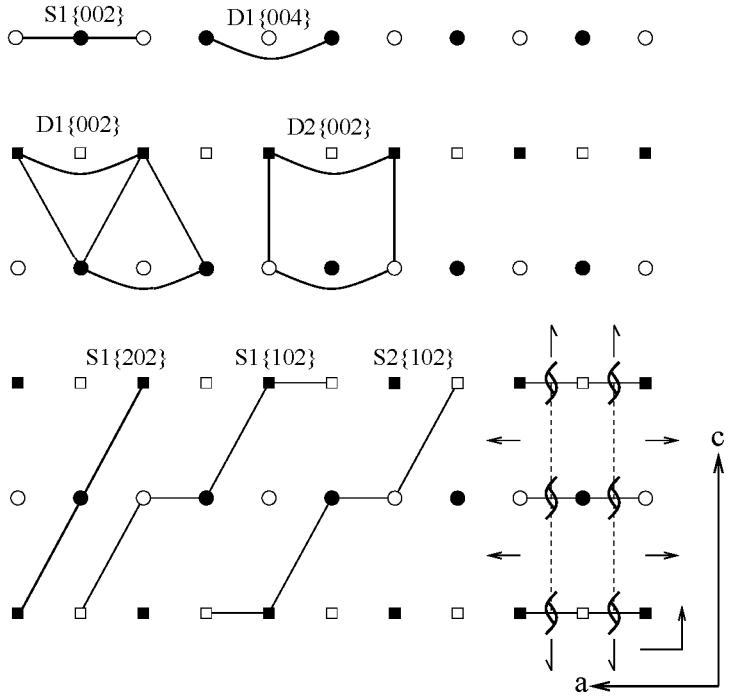

Figure 7.2: Generating connected nets for the orientations {001}, {101} and {102} projected along $[0\bar{1}0]$. The growth units are represented as in figure 7.1.

7.4.2 The {100} form

The (100) orientation contains 17 different connected nets divided in 2 singlets, 1 quartet and 4 doublets for the {100} and 3 singlets for the {200} connected nets (see table 7.2). Starting from the two singlets $S_1\{100\}$ and $S_2\{100\}$ it is possible to derive all other connected nets $Q_1\{100\}$, $D_1\{100\}$, $D_2\{100\}$, $D_3\{100\}$ and $D_4\{100\}$ by translating constituting growth units of the two singlets along the a direction. In this way all 14 connected nets {100} can be derived (figure 7.3).

The {200} connected nets $S_1\{200\}$, $S_2\{200\}$ and $S_3\{200\}$ are connected subnets of the {100} singlets.

For the {100} orientation five singlets occur $S_1\{100\}$, $S_2\{100\}$ $S_1\{200\}$, $S_2\{200\}$ and $S_3\{200\}$. The doublets $D_1\{100\}$, $D_2\{100\}$, $D_3\{100\}$ and $D_4\{100\}$ and the quartet $Q_1\{100\}$ would cause microscopic symmetry roughening if there were no singlet present. Therefore, the growth kinetics and morphology will be determined by the singlets.

As already mentioned, the {100} connected nets containing all four growth units can be built from the {200} connected subnets which contain half of the growth units. Analysis of the two most important singlets $S_1\{100\}$ and $S_2\{100\}$ shows that these nets consist of two $S_1\{200\}$ connected nets separated by d_{200} (see figure 7.3). For the $S_1\{100\}$ the two $S_1\{200\}$ singlets are connected to each other by g and d bonds while for $S_2\{100\}$ the g' and d' bonds connect the two subnets. This results in a very small difference in surface energy between the surface bounded by $S_1\{100\}$ and the surface bounded by $S_2\{100\}$. This difference is 0.33 kcal/mol per mesh area in terms of broken bonds.

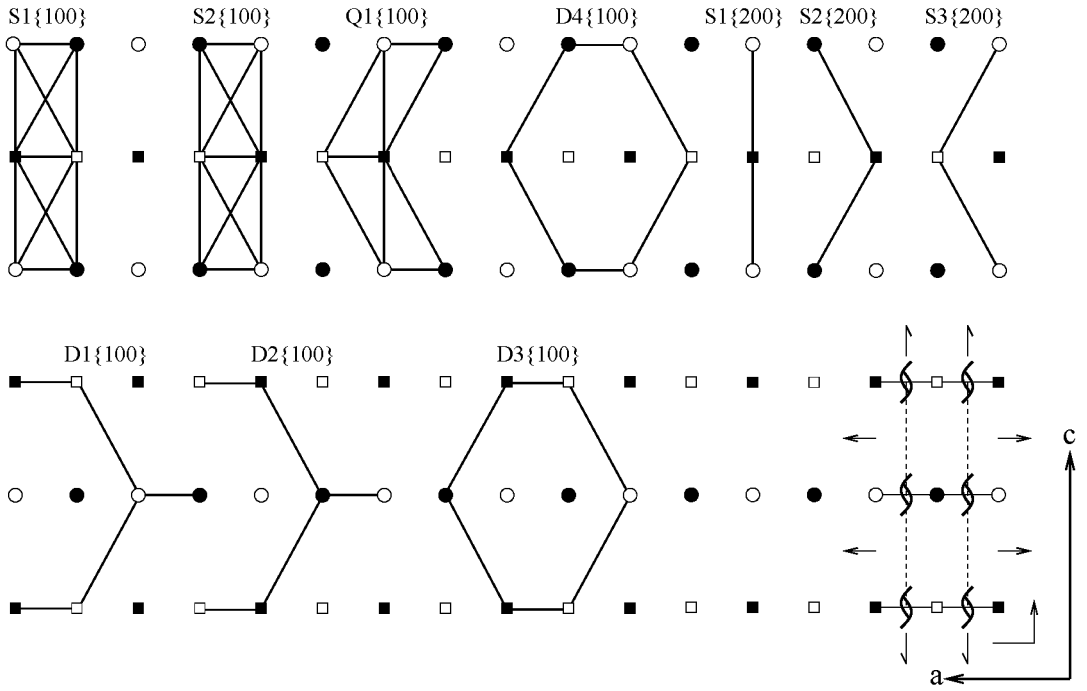

Figure 7.3: Generating connected nets for the orientation {100} projected along $[0\bar{1}0]$. The growth units are represented as in figure 7.1.

Therefore, it is expected that at very low supersaturations the growth for the orientation will be determined by the $S_1\{100\}$ connected net and at a higher supersaturation the difference in surface energy between the $S_1\{100\}$ and $S_2\{100\}$ will be compensated and the face will grow with half layers according to the connected net $S_1\{200\}$ [Grimbergen et al., 1999a].

7.4.3 The {110} form

The (110) orientation contains 14 connected nets. There are two singlets $S_1\{110\}$ and $S_2\{110\}$ and six doublets $D_1\{110\}$, $D_2\{110\}$, $D_3\{110\}$, $D_4\{110\}$, $D_5\{110\}$ and $D_6\{110\}$ present (table 7.2). The [001] projection of all connected nets is drawn in figure 7.4.

The singlets $S_1\{110\}$ and $S_2\{110\}$ have a roof-like structure while the doublets $D_1\{110\}$ and $D_2\{110\}$ consist of chains of connected tetrahedrons in the [001] direction consisting of d', e, f and g' bonds ($D_1\{110\}$) or d, e, f and g bonds ($D_2\{110\}$) which are interconnected by bonds d ($D_1\{110\}$) or d' ($D_2\{110\}$).

The orientation {110} contains two important singlets $S_1\{110\}$ and $S_2\{110\}$. The $S_1\{110\}$ connected net represents the most favorable surface configuration of the two singlets.

All doublets show microscopic symmetry roughening and boundary swapping due to the two-fold screw axis (2_1^z) and the inversion. Symmetry roughening is, however, supressed by the horizontal bonds present in the singlets.

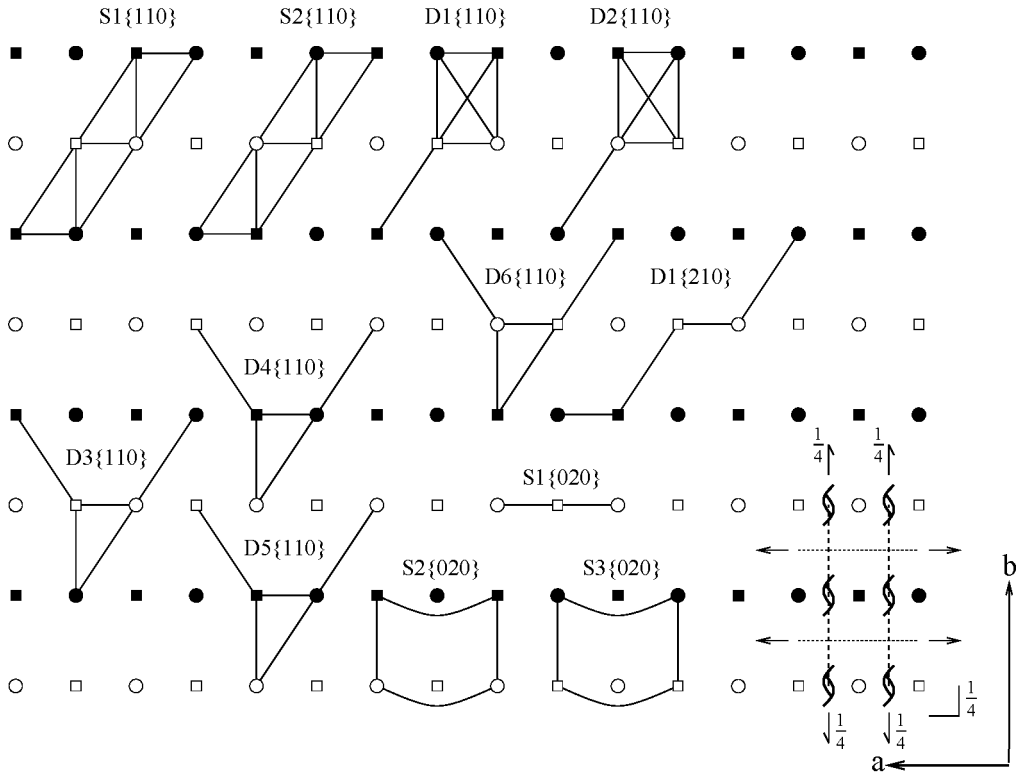

Figure 7.4: Generating connected nets for the orientations {110}, {010} and {210} projected along [001]. The growth units are represented as in figure 7.1.

Thus, the growth kinetics and morphology are determined by the two singlets $S_1\{110\}$ and $S_2\{110\}$ which provide the step free energy. In figure 7.5 the $[01\bar{1}]$ projection is drawn for these two connected nets. It can be seen that the broken bond energy corresponding to a step along $[1\bar{1}0]$ per growth unit in the step is equal to the difference in broken bond surface energy of the surfaces bounded by $\alpha\beta\gamma\delta$ and $\alpha\beta\epsilon\phi\gamma\delta$. Thus, the step energy is equal to the difference in bond energy of bonds e and f. In terms of broken bond energies this is 0.14 kcal/mol per growth unit. This effective step energy along $[01\bar{1}]$ for the

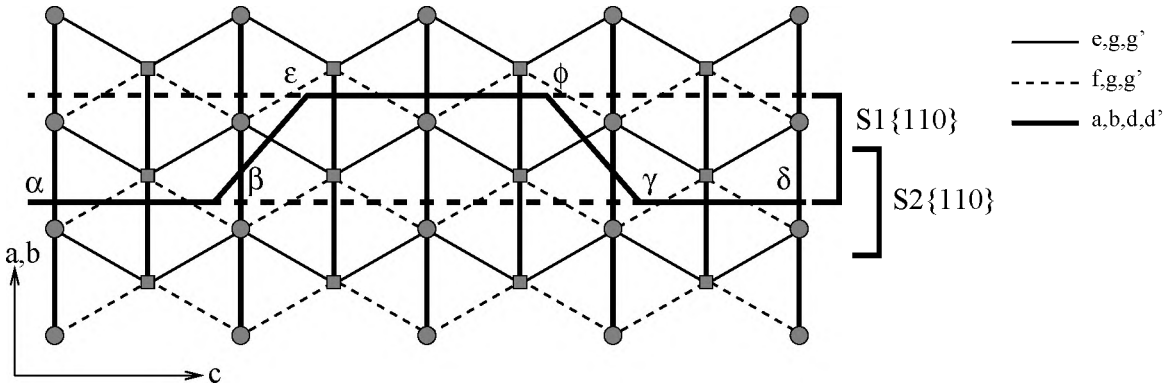

Figure 7.5: Structure projection along $[01\bar{1}]$. The connected nets $S_1\{110\}$ and $S_2\{110\}$ are indicated and a complete step d_{110} is drawn. The grey squares indicate growth units 2 and 4 and the grey circles indicate growth units 1 and 3.

orientation {110} is very small as compared to the slice energy of $S_1\{110\}$ and $S_2\{110\}$. It is known from Monte Carlo growth simulations that a decrease in step energy along a direction $[uvw]$ decreases the nucleation barrier [Grimbergen et al., 1999a]. Therefore it is expected that the {110} orientation will grow relatively fast already at a very low supersaturation.

7.4.4 The {111} form

For the {111} orientation nine connected nets were found one singlet and four doublets (table 7.2). A $[01\bar{1}]$ projection of the connected nets is shown in figure 7.6. The most prominent connected net with the lowest attachment energy for the orientation {111} is $S_1\{111\}$. The other doublets can be derived topologically from this singlet by translation of a growth out of the plain of the singlet. This can be done in 8 unique ways giving rise to the 4 doublets.

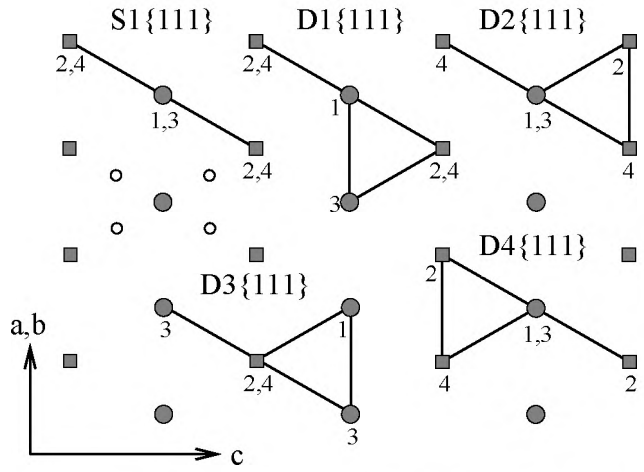

Figure 7.6: Generating connected nets for {111} projected along $[01\bar{1}]$. The grey squares indicate growth units 2 and 4 and the grey circles indicate growth units 1 and 3. The small circles indicate the centers of symmetry. The numbers indicate which growth units are part of the connected net.

All four doublets give rise to microscopic symmetry roughening and boundary swapping due to the center of symmetry (table 7.2). Nevertheless, the singlet $S_1\{111\}$ contains bonds which are formed on creation of a domain wall for the doublets. Therefore, the growth kinetics and morphology for the orientation {111} will be governed by the singlet $S_1\{111\}$.

7.4.5 The {010} form

Due to the 2-fold screw axis along the *b*-axis and the b-glide physically equivalent surfaces are separated by d_{020}. Therefore, the connected nets are {020} connected nets. For the {010} orientation three singlets are found $S_1\{020\}$, $S_2\{020\}$ and $S_3\{020\}$ In figure 7.4 all connected nets {020} are drawn. The $S_1\{020\}$ connected net is a planar net and the

$S_2\{020\}$ and $S_3\{020\}$ singlets containing half of the growth units can be regarded as a combination of two $S_1\{020\}$ singlets separated by d_{020}. The singlets $S_2\{020\}$ and $S_3\{020\}$ would cause pseudo symmetry roughening in case the singlet $S_1\{020\}$ was not present. This singlet contains bonds that are formed on creation of a domain wall between domains of $S_2\{020\}$ and $S_3\{020\}$. In section 4.7 more examples of pseudo symmetry roughening will be treated. The growth behaviour of the {010} orientation will be determined by the $S_1\{020\}$ singlet which represents the most favorable growth layer.

7.4.6 The {112}, {211} and {210} form

The forms {112}, {211} and {210} have in common that there are solely doublets which have a comparable topology present. In figure 7.4 the doublet $D_1\{210\}$ is drawn as an example. The doublets are macroscopically symmetry roughened because the effective broken bond step energy is zero. Therefore, these orientations will grow in a rough mode and very fast. Because of the center of symmetry that relates the two connected nets constituting a doublet, there is boundary swapping and therefore the effective step free energy will be non-zero. However, in practice the step free energy will be very low and therefore the threshold for kinetic roughening will be very small [Grimbergen et al., 1999a].

7.4.7 The {102}, {021}, {120} and {121} form

In figure 7.2 the two singlets $S_1\{102\}$ and $S_2\{102\}$ are shown as an example for all connected nets of the forms {102}, {021}, {120} and {121} which contain only even numbers of singlets. For all these orientations the effective step energy is very low because of the presence of two singlets which form a pseudo doublet. The situation is comparable to that of the connected nets $S_1\{110\}$ and $S_2\{110\}$ as discussed in section 4.3. Due to the bonding structure the effective step energy is determined by a difference in broken bond energies instead of a full broken bond energy. For this reason the roughening temperature of these types of face will be larger than zero kelvin but can become very low. Moreover, the nucleation barrier will be very low, resulting in a high growth rate at low supersaturations. Therefore, these faces will not appear on the growth morphology, except for very low supersaturation.

7.4.8 The {011} and {101} form

The {011} and {101} form are the only forms that contain a single connected net, respectively $S_1\{022\}$ and $S_1\{202\}$. The singlet $S_1\{202\}$ is drawn in figure 7.2. For orientations containing a single connected net it is expected that the conventional theories should be applicable. For that reason the calculated 2-D Ising transition temperatures T^C_{hkl} should be a good estimate for the roughening temperature T^R_{hkl} of the orientation (hkl). Both forms can occur on the equilibrium morphology as flat faces at temperatures below their corresponding roughening temperatures. In the growth morphology the faces will not occur because of the rather high relative attachment energies.

7.4.9 Anisotropy and roughening temperatures T^R_{hkl}

In the above it has been shown that the presence of multiple connected nets for an orientation may result in a lowering of the effective step energy. Often, the step energy along a specific direction $[uvw]$ coplanar with (hkl) is decreased significantly as has been shown for (110). For this reason the roughening temperature T^R_{hkl} may be lower than the 2-D Ising transition temperature T^C_{hkl} of the strongest connected net of the orientation (hkl). In order to estimate the actual roughening temperature for an orientation (hkl), it is possible to construct a single substitute flat connected net. From the substitute connected net the effective Ising transition temperature and the anisotropy δ_{hkl} can be determined. We define the anistropy of an orientation (hkl) δ_{hkl} as

$$\delta_{hkl} = \frac{\gamma_{uvw_1}}{\gamma_{uvw_2}} \tag{7.5}$$

where $[uvw]_1$ and $[uvw]_2$ are two directions along which the lowest step energies γ_{uvw_1} and γ_{uvw_2} per growth unit for the orientation (hkl) are realised. Note that in eq. (7.5) δ is defined for $\gamma_{uvw_1} \leq \gamma_{uvw_2}$.

In figure 7.7 the procedure is shown for the (110) orientation (see also figure 7.5). The two strong singlets $S_1\{110\}$ and $S_2\{110\}$ reduce to the substitute connected net $S_{sub}\{110\}$ consisting of the d, d' and substitute s bond. The latter actually represents a bond with bondstrength $\Phi_s = (\Phi_e - \Phi_f)$.

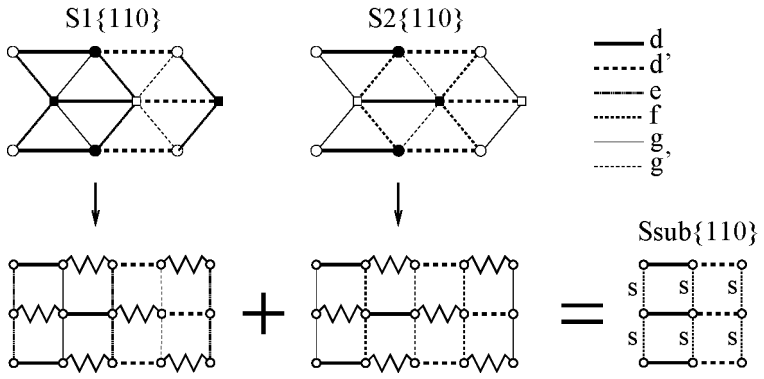

Figure 7.7: Projection on top of the two singlets $S_1\{110\}$ and $S_2\{110\}$. The substitute connected net Ssub{110} for calculation of an estimate of the roughening transition temperature is drawn. The wiggled bonds have an infinite bondstrength and the substitute s bonds with bondstrength $\Phi_s = (\Phi_e - \Phi_f)$ are indicated in the substitute connected net.

This procedure has been applied to the (110), (102), (021), (120) and (121) orientations which all contain pairs of singlets giving rise to a lowering of the step energy. In table 7.3 all orientations are listed with the effective Ising transition temperature T^C_{hkl} and the anisotropy δ_{hkl}. The orientations which contain solely a symmetry related pair of connected nets giving rise to macroscopic symmetry roughening have a roughening temperature of zero kelvin because the effective step energy along at least one direction $[uvw]$ is zero.

Table 7.3: The broken bond attachment energy of the strongest connected net, the effective Ising transition temperature taking multiple connected nets and anisotropy into account for all orientations $\{hkl\}$. The marked transition temperatures could not be calculated exactly, because the (substitute) connected net was not planar or the calculation did not converge.

Form	$E^{att,str}_{hkl,bb}$ (kcal/mol)	T^{C}_{hkl}(K) (K)	δ_{hkl}
{001}	-8.2	5834	1.000
{100}	-96.8	$\approx$ 672 *	0.423
{102}	-101.1	$\approx$ 246 *	0.023
{110}	-104.6	1073	0.019
{111}	-105.2	1504	0.059
{112}	-121.8	0	0.000
{010}	-127.8	1123	0.128
{021}	-129.1	747	0.029
{011}	-131.0	805	0.033
{120}	-136.0	<70 *	1.000
{121}	-135.6	<77 *	1.000
{101}	-159.5	292	0.182
{210}	-137.1	0	0.000
{211}	-136.2	0	0.000

7.5 Predicted morphology

Using the information of all connected nets as descibed in the previous sections it is possible to predict the morphology as a function of supersaturation. In order to compare the results of this complete connected analysis with the results of the traditional attachment energy prediction, first the results of the latter prediction will be presented.

In figure 7.8 the calculated morphologies based on eq. (7.3) are presented. The morphology based on the broken bond energies does not show the {111} faces, but these are very close to the threshold value for appearance. When for the attachment energy calculation all interactions between the growth units within a cutoff radius of 40Å are taken into account the morphology changes slightly and tiny {111} facets are present. The morphology did not change when the cutoff radius was increased. Notice that in these conventionally predicted morphologies are independent of supersaturation.

In case the results of the complete connected net analysis are taken into account it is possible to estimate the effect of supersaturation on the morphology. In figure 7.9 the influence of the driving force on the morphology is shown. At equilibrium conditions ($\Delta\mu = 0$) the morphology can be constructed using eq. (7.2) (figure 7.9a). Note that the equilibrium morphology still depends on the temperature.

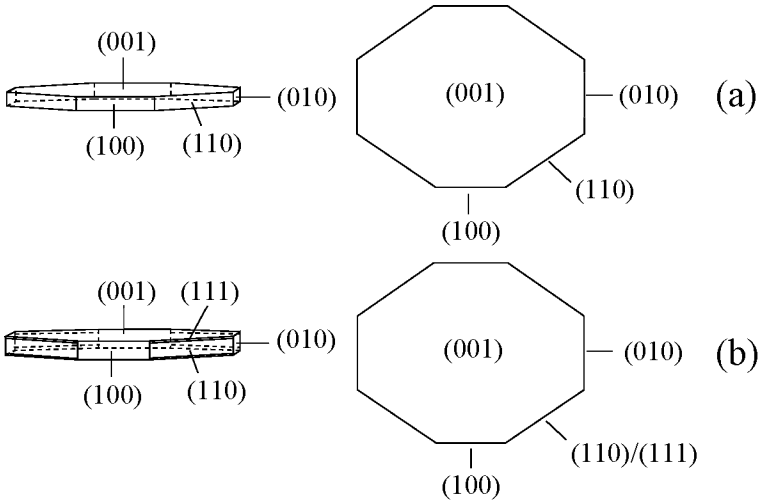

Figure 7.8: The growth morphology of $C_{23}H_{48}$ based on E^{att}_{hkl}. (a) Conventional morphology based on the broken bond attachment energies. (b) Conventional morphology based on an attachment energy calculations using an interaction summation cutoff of 40Å.

Facets having an effective roughening transition temperature which is lower than the actual temperature of the crystal will not appear as well-defined flat faces on the equilibrium morphology, but appear as rounded-off faces. The effective roughening temperatures of all orientations are given in table 7.3. Symmetry roughened faces will, in principle, never appear as flat faces on the morphology.

For the growth morphologies the result of the traditional attachment energy prediction based on the summation radius cutoff (figure 7.8b) was used as a start and the morphological importance of the faces was modified according to the results of the complete connected net analysis. This complete analysis does not only involve surface and attachment energies but also step energies and anisotropies which are crucial parameters in the crystal growth process. Obviously, a low effective step energy results in a low nucleation barrier. It was shown in literature that also a large anisotropy lowers the nucleation barrier [van der Eerden et al., 1977]. Looking at table 7.3 it is expected that orientations with a low 2-D Ising transition temperature T^C_{hkl} and/or a high anisotropy ($\delta \ll 1$) will start to grow rapidly already at low driving forces because of a low nucleation barrier. Therefore, many of the faces present in the equilibrium morphology are not present in the growth morphology. Moreover, most of the faces have a relatively high attachment energy. Faces that can appear in the Wulff plot because of a low attachment energy are {001}, {100}, {111}, {110} and {010}. For the growth morphology only these faces were considered.

Looking at table 7.3 it is clear that the (100) face has the lowest roughening temperature. It was pointed out in section 4.2 that this face can grow with half layers $S_1\{200\}$ at higher supersaturations. In figure 7.9 the morphological importance of the {100} faces at low driving force was taken proportional to the conventional attachment energy of $S_1\{100\}$ whereas at intermediate supersaturation the attachment energy of $S_1\{200\}$ was used because of the assumption that the growth proceeds with half layers $S_1\{200\}$.

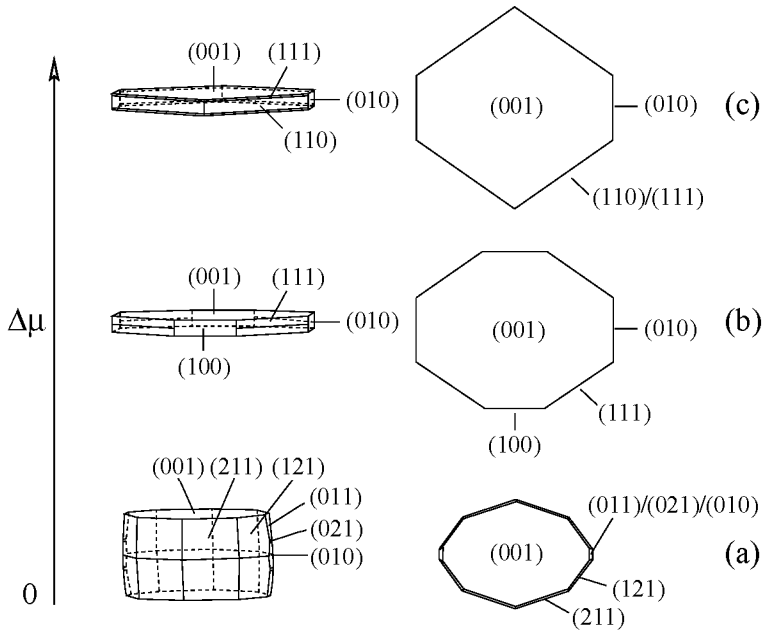

Figure 7.9: The morphology of $C_{23}H_{48}$ as a function of supersaturation based on the complete connected net analysis. (a)Equilibrium morphology, (b) growth morphology at low supersaturation, (c) growth morphology at intermediate supersaturation.

Concerning the {110} and {111} faces it was assumed that at low driving forces the {111} faces have a higher nucleation barrier as compared to the {110} faces because of a lower anisotropy (see table 7.3). At low supersaturation the {110} faces were left out while at higher supersaturations when the nucleation barrier has vanished for both the {111} and {110} the conventional attachment energy was used for the Wulff plot.

7.6 Discussion

The morphology of orthorhombic n-paraffin crystals is obviously dominated by the {001} form because of the presence of the isotropic S_1{002} connected net consisting of the strong lateral d, d', a and b bonds. The strongest PBCs for this orientation are along [100], [010], [110] and [1$\bar{1}$0] all containing d and/or d' bonds. Note that these PBCs are the strongest PBCs of the orthorhombic n-paraffin crystal structure. In general, it is expected that the most prominent F-faces will contain at least one of these strong PBCs, because such a strong PBC guarantees a high step free energy for all directions $[uvw]$ non-parallel with the PBC direction and coplanar with the facet orientation (hkl). This is directly reflected in the growth morphology which is bounded by faces in the zones $< 100 >$, $< 010 >$ and $< 1\bar{1}0 >$. The remaining F-faces {120}, {121}, {210} and {211} are in the zones $< 210 >$ and $< 120 >$ which do not contain one of the strong PBCs with d and (or) d' bonds. These side faces have a very low roughening temperature T^R because

the step free energy is small along at least two non-parallel directions $[uvw]$ (table 7.3). Therefore these facets will not occur on the growth morphology.

In the following we will focus on the side faces. For the zones $< 100 >$, $< 010 >$ and $< 1\bar{1}0 >$ more than one F-face (hkl) was found.

In the $< 010 >$ zone F-faces for the orientations (100), (102) and (101) were found. The (100) orientation is clearly the most favorable orientation because of the low attachment energy and the rather high estimated roughening temperature. Note that despite the presence of a PBC along [010] consisting of d bonds the roughening temperature is rather low. In a sense this situation can be compared to that of the (110) orientation (see figure 7.5) for which the step energy is determined by a difference in bond energies instead of individual bond energies. In the case of (100) the d and d' bond have to be substracted from each other as the e and f for the (110) orientation. Therefore, the step free energy along [001] is mainly determined by the b, e and f bonds which are cut on creating a step. Further analysis shows that the (100) face may grow with half layers (200) (connected net $S_1\{200\}$). This was already found by Bennema et al. [Bennema et al., 1992]. It is expected that at low supersaturations growth of the (100) orientation will be determined by growth layers $S_1\{100\}$ whereas at higher supersaturations the face will grow with half layers $S_1\{200\}$. This can be considered as a sort of pseudo BFDH law effective for higher supersaturations [Grimbergen et al., 1999a]. The implication for the growth morphology is that at low driving forces the (100) face will occur on the morphology and at increasing supersaturation the face will grow out because growth proceeds by half layers. Because of the high attachment energy the (101) orientation will not appear on the growth morphology. The (102) face might show up on the morphology as a flat face in case the growth temperature is below the roughening temperature of this face which is rather low, again due to a high anisotropy because of pseudo symmetry roughening ($T^R_{102} \approx 246$K).

In the $< 100 >$ zone the (010), (021) and (011) F-faces are found. The attachment energy, roughening temperature and anisotropy of (010) are the most favorable. Thus, the (020) face will appear on the growth morphology whereas the (021) and (011) faces will grow faster because of a higher anisotropy, a lower roughening temperature and a higher attachment energy.

The $< 1\bar{1}0 >$ zone contains the most prominent faces on the growth morphology apart from (001). The (112) face is symmetry roughened based on the broken bond step energy. However, this face will formally have a roughening temperature higher than zero kelvin as the actual step free energy will be larger than zero. In practice the step free energy will be very small and the face will become rough at very low temperatures or at a very small supersaturation. Therefore this face will not occur as a flat face on the equilibrium morphology at higher temperatures and will not appear on the growth morphology. The difference between the (110) and (111) faces is that for (111) one important singlet was found while for the (110) orientation two important singlets were found. The attachment energy is almost the same and the Ising transition temperatures indicate that the (110) face will become rough at lower temperatures as compared to the (111) face because of the presence of two singlets causing a low step free energy along the $[1\bar{1}0]$ direction. Actually, there is evidence that the roughening temperature of (110) based on the substitute connected net is a measure for the temperature at which the (110) face enters a DisOr-

dered Flat (DOF) phase. A disordered flat crystal facet will grow fast because of a low 2-D nucleation barrier, but will not become macroscopically rough due to an overall step free energy larger than zero. At higher temperatures the facet will become rough. Such a situation has been found for the (011) face of the naphthalene structure [Grimbergen et al., 1998c]. Based on the anisotropy and the roughening transition temperatures it is expected that at low supersaturation the (111) face will be the slowest growing face because of a relatively high nucleation barrier. At higher supersaturations, the growth rate of the (110) and (111) faces will be comparable.

7.7 Conclusion

The complete connected net analysis of the orthorhombic n-paraffin structure shows a wide variety of (symmetry related) connected nets. Multiple connected nets for a single orientation (hkl) can result in symmetry roughening ({112}, {210} and {211}) or in a much smaller effective step free energy than expected on the basis of analysis of the individual connected nets due to the presence of two singlets ({102}, {120}, {121}, {021} and {110}). This has major implications for the morphological importance of these types of face. In practice these faces will grow faster at low supersaturations than expected on the basis of the conventional attachment energies.

The growth morphology at low supersaturations will be bounded by the {001}, {100}, {111} and {010} faces whereas at higher supersaturations the {001}, {110}, {111} and {010} faces will be present. Note that in solutions the roughening temperatures (and step free energies) may become much lower because of interactions between the solvent and the crystal surface. Therefore, the roughening transition temperatures and 2-D nucleation barrier can become very small.

To our opinion many studies in the past on the side faces of paraffin crystals have to be reconsidered because the conclusions were based on the assumption that the {110} faces were the side faces. In this study it is shown that the {111} faces have to be considered as important side faces as well. Moreover, the side face morphology turns out to depend strongly on the supersaturation. Experimental evidence for these conclusions will be reported in the near future [van Hoof et al., 1998a]. The findings of this study are relevant for many crystal structures with faces containing multiple connected nets.

Acknowledgements

R.F.P. Grimbergen would like to acknowledge the financial support of the Technology Foundation (STW) and P.J.C.M. van Hoof acknowledges the financial support of Shell Netherlands B.V..

Chapter 8

Morphology of Orthorhombic n-Paraffin Crystals II: a Comparison between Theory and Experiments

Morphology of Orthorhombic n-Paraffin Crystals II: a Comparison between Theory and Experiments

P.J.C.M. van Hoof, R.F.P. Grimbergen, H. Meekes,
W.J.P. van Enckevort and P. Bennema [1]

Abstract

n-Paraffin crystals have been grown from the vapour, solution and the melt. The morphology of these crystals is compared with the predicted morphology on the basis of a recent, thorough connected net analysis. The morphology of the crystals grown from the vapour phase is in very good agreement with the predicted morphology and for the first time faceted {111}, {010} and {100} faces have been observed. The morphology depends on the supersaturation in accordance with the connected net analysis. The crystals grown from solutions have very large aspect ratios, which can be understood in terms of the dependence of the growth rate of the different faces on the step free energies of those faces.

8.1 Introduction

Crystal growth and morphology of n-paraffin crystals have been studied in great detail during the past years; an overview is given by Turner [Turner, 1971] and Boistelle [Boistelle, 1980]. Crystal growth kinetics of {001} and {110} faces of n-$C_{28}H_{58}$ and n-$C_{36}H_{74}$ crystals have been studied by Simon et al. [Simon et al., 1974a, Simon et al., 1974b], Boistelle, Doussoulin and Lundager Madsen [Boistelle and Doussoulin, 1976, Madsen and Boistelle, 1979, Boistelle and Aquilano, 1977]. The morphology of monoclinic, triclinic and orthorhombic structures of n-paraffin crystals was analysed by Bennema et al. [Bennema et al., 1992, Bennema, 1993], Liu and Bennema [Liu and Bennema, 1994, Liu and Bennema, 1993b] and Strom and Bennema [Strom and Bennema, 1998]. Roughening transitions of {110} faces of orthorhombic n-paraffin crystals have been studied by Liu et al. [Liu et al., 1992, Liu et al., 1994b, Liu et al., 1993].

There are several reasons for studying the morphology of orthorhombic n-paraffin crystals. First of all, n-paraffins are good model compounds to study the fundamentals of the Hartman-Perdok theory for crystal morphology prediction [Hartman and Perdok, 1955a, Hartman and Perdok, 1955b, Hartman and Perdok, 1955c] and especially the recent extensions to that theory [Grimbergen et al., 1998b, Meekes et al., 1998, Grimbergen et al., 1999a]. These recent extensions, which will also be a subject of this paper, comprise a new kind of roughening effect, namely symmetry roughening and the lowering of the

[1] The work presented in this chapter has been accepted for publication in J. Cryst. Growth

effective step energy due to the presence of multiple connected nets. Furthermore, n-paraffin crystallisation is very important for the petroleum industry because crude oil and many of its products contain long chain n-paraffins which cause severe problems upon crystallisation. For this reason a good understanding of the morphology is of practical use as it is a help to find ways to influence or even prevent the crystallisation.

In this paper we shall study the morphology of orthorhombic n-paraffin crystals from an experimental point of view and make a comparison with the results of a recent PBC analysis by Grimbergen et al. [Grimbergen et al., 1998d]. Although morphology studies on these compounds have been presented before [Bennema et al., 1992,Bennema, 1993,Strom and Bennema, 1998], Grimbergen et al. reported a complete list of all possible F-faces with a physical interpretation. In particular, the recent extensions to the Hartman-Perdok theory were used in that interpretation. To be able to compare the calculated morphologies of the orthorhombic n-$C_{23}H_{48}$ crystals with experimental morphologies we performed several types of experiments, namely crystal growth from the vapour, solution and melt. In case of the calculations no interactions between molecules in the solid phase and solute molecules (solvent molecules or vapour molecules) have been taken into account. Therefore it is expected that the calculated morphology will be in best agreement with the morphologies of crystals grown from the vapour phase, as it is assumed that in these systems the solid-vapour and vapour-vapour interactions can be neglected and only interactions between solid particles have to be considered. We performed vapour phase growth experiments at different temperatures and supersaturations. Also crystals from n-hexane and toluene solutions at different temperatures and at different supersaturations have been grown. Some morphology experiments on orthorhombic n-paraffin crystals grown from solutions have been carried out before [Bennema et al., 1992,Bennema, 1993, Liu et al., 1993] and are in agreement with the results of this study. Finally, melt growth experiments have been performed on n-$C_{23}H_{48}$ crystals.

8.2 Predicted morphology

8.2.1 Introduction

The predicted (calculated) morphology of orthorhombic n-paraffins and in particular n-$C_{23}H_{48}$ have been presented by Grimbergen et al. [Grimbergen et al., 1998d]. Here, only some highlights of that paper and of some recent extensions to the Hartman-Perdok theory that are used are summarised. In general, a Hartman-Perdok analysis starts with reducing the crystal structure to its crystal graph, in which molecules are represented by points, mutually connected by the relevant bonds. Then, Periodic Bond Chains (PBCs), being the chains of strongly bonded molecules, are determined. Orientations (hkl) which are coplanar with at least two interconnected non-parallel PBCs can in principle occur on the crystal morphology as flat faces and can be determined from the combination of PBCs. In later extensions of the Hartman-Perdok theory such a combination of PBCs is called a connected net which is defined as a set of growth units connected by bonds constituting a network. Furthermore, connected nets are restricted to some crystallographic rules. One of these rules is determined by the Bravais, Friedel, Donnay, Harker (BFDH) law, which imposes restrictions on the miller indices (hkl) just as in x-ray crystallography.

In this paper we use indices (hkl) which are mutually prime when faces or orientations are indicated. Connected nets or growth layers, however, can have non-prime indices according to the BFDH law.

Since $d_{hkl}E_{hkl}$ is equal to the specific surface energy [Kern, 1987] the equilibrium morphology can be constructed by applying

$$D_{hkl} \propto d_{hkl}E^{att}_{hkl} \ , \tag{8.1}$$

where D_{hkl} is the distance from the centre of the crystal to the face (hkl) and E^{att}_{hkl} is the attachment energy of a face (hkl), which is defined as the energy per unit cell content that is released when a complete growth layer is attached to the surface (hkl). Hartman and Bennema [Hartman and Bennema, 1980] stated that E^{att}_{hkl} is a measure for the relative growth rate of a face and thus for its occurrence on the growth morphology:

$$R \propto E^{att}_{hkl} \ . \tag{8.2}$$

Often many connected nets can be found for one orientation (hkl) and usually the connected net with the lowest attachment energy is taken as the stable surface configuration and will thus determine the morphological importance of that orientation. Recently, however, it has been stressed that the different connected nets of one orientation can lower the effective step energy in such a way that the orientation becomes less important or even disappears from the equilibrium or growth morphology [Grimbergen et al., 1998b, Meekes et al., 1998, Grimbergen et al., 1999a]. Here, three special cases will be distinguished that are important for the morphology prediction of the orthorhombic n-paraffin crystals.

So-called macroscopic symmetry roughening of an orientation (hkl) occurs when two or more connected nets of that orientation are symmetry related in such a way that the resulting step energy is zero. This can even occur for faces that according to the attachment energy criterion are very important, because E^{att}_{hkl} is very low. It will result in a roughening temperature of zero Kelvin or, if the symmetry element implies the presence of so-called boundary swapping between two connected nets, in a very low step free energy.

Secondly, microscopic symmetry roughening, which is related to a DisOrdered Flat phase or DOF phase, may occur when the energy of a domain wall between the two surfaces which are bounded by symmetry related connected nets is zero. Although the step energy for the orientation is still larger than zero there will occur disorder within the surface layer. This causes an increase in the growth rate and the face can disappear from the growth morphology [Grimbergen et al., 1999a].

In some cases, if multiple connected nets for an orientation (hkl) do not show macroscopic or microscopic symmetry roughening it may be possible to construct a substitute connected net with a lower effective step energy. Such pseudo-symmetry related connected nets can have a very low threshold for kinetic roughening. In such situations one can speak of pseudo-symmetry roughened connected nets. In the case of orthorhombic n-paraffins for 5 orientations two connected nets can be substituted with a simple net for which the bonds in two directions are equal to the lowest step energies of the combination of nets [Grimbergen et al., 1998d]. It may be clear that this can decrease the step energy and thus the roughening temperature drastically and thus will increase the growth rate of such a face.

Table 8.1: The attachment energy based on broken bonds of the strongest connected net, the effective Ising transition temperature and anisotropy (see text) for all orientations (hkl) containing possible F-faces for orthorhombic n-$C_{23}H_{48}$ [Grimbergen et al., 1998d]. The marked transition temperatures could not be calculated exactly, because the (substitute) connected net was not planar or the calculation did not converge.

Connected net Form	$E^{att,str}_{hkl,bb}$ (kcal/mol)	T^{C}_{hkl}(K) (K)	δ_{hkl}
{002}	-8.2	5834	1.000
{100}	-96.8	$\approx$ 672 *	0.423
{102}	-101.1	$\approx$ 246 *	0.023
{110}	-104.6	1073	0.019
{111}	-105.2	1504	0.059
{112}	-121.8	0	0.000
{020}	-127.8	1123	0.128
{021}	-129.1	747	0.029
{022}	-131.0	805	0.033
{120}	-136.0	<70 *	1.000
{121}	-135.6	<77 *	1.000
{101}	-159.5	292	0.182
{210}	-137.1	0	0.000
{211}	-136.2	0	0.000

8.2.2 Growth morphology

The complete connected net analysis [Grimbergen et al., 1998d] yielded 71 connected nets. Table 8.1 lists all orientations that may occur on the morphology. The anisotropy of the {112}, {210} and {211} forms equals zero due to symmetry roughening. The Ising transition temperature T^{c}_{hkl} [Rijpkema et al., 1982] is used as an estimation for the roughening temperature T^{R}_{hkl} of the orientation (hkl). The values for T^{c}_{hkl} have been determined using a substitute connected net for the cases of pseudo-symmetry roughened connected nets. The anisotropy δ_{hkl}, defined as the ratio of energies of the weakest and the second weakest step energy in two different directions along the face is also given in table 8.1. The growth morphology on the basis of the attachment energies calculated over all attachment bonds with a cutoff radius of 40 Å and equation (8.2) is given in figure 8.1 for two special cases. In figure 8.1a the morphology at low supersaturation is given, that is the faces {110} are left out and in figure 8.1b the morphology at high supersaturation is given, for which the faces {100} do not appear anymore. Here we will shortly explain the two cases, more details have been given in the paper of Grimbergen et al. [Grimbergen et al., 1998d].

At low supersaturation it is expected that the (111) orientation instead of the (110) orientation will be the dominant side face on the the growth form, despite its slightly

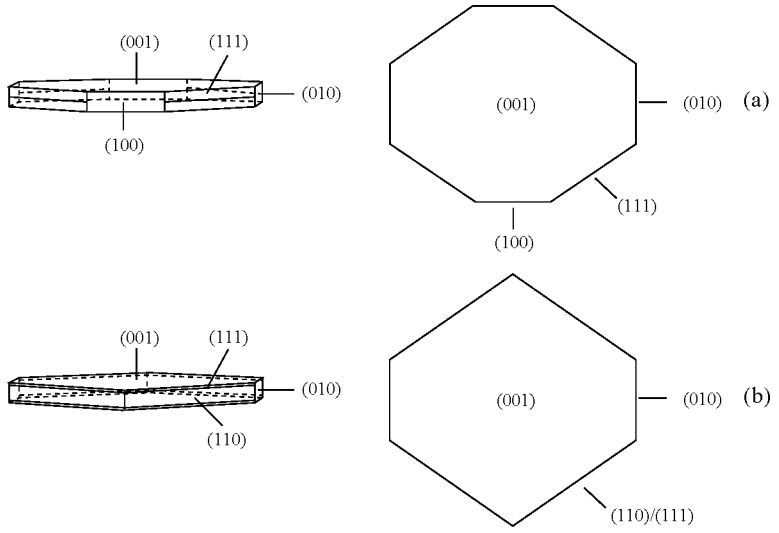

Figure 8.1: The growth morphology of n-$C_{23}H_{48}$ based on attachment energy calculations using summation cutoff of 40 Å. a) Morphology at low supersaturations (the forms {110} are left out) and b) morphology at high supersaturations (the forms {100} do not appear any more).

higher attachment energy. The reason for this is that the (110) orientation has a very low effective step energy and a high anisotropy in comparison with the (111) orientation, due to the combination of two connected nets of (110). At high supersaturation the growth rate will be more determined by the attachment energy than by the step energy and the relative growth rate of the (110) faces will be low as compared to the (111) faces.

Furthermore it is expected that at low supersaturations the orientation (100) will grow with complete layers. If the supersaturation is in the same order as the difference in surface energy the two layers (200) of this orientation will grow with half layers [Grimbergen et al., 1999a]. The growth rate of the half layers will be relatively high and the orientation will not be present on the morphology at high supersaturations.

To study the morphology in more detail we introduce the aspect ratios R_1 and R_2. Where R_1 is defined as

$$R_1 = \frac{D_{110/111}}{D_{001}} \tag{8.3}$$

and R_2 is defined as

$$R_2 = \frac{D_{010}}{D_{110/111}}\ , \tag{8.4}$$

where D_{hkl} is the measured distance from the centre of the crystal to the face (hkl). In case of the calculated morphologies (figure 8.1) an R_1 of 5.3 and an R_2 of 1.1 is found.

8.3 Experimental setup

8.3.1 Vapour growth

The growth experiments from the vapour phase have been carried out in a vapour phase growth cell (figure 8.2). This cell consists of a closed compartment with a flange on which

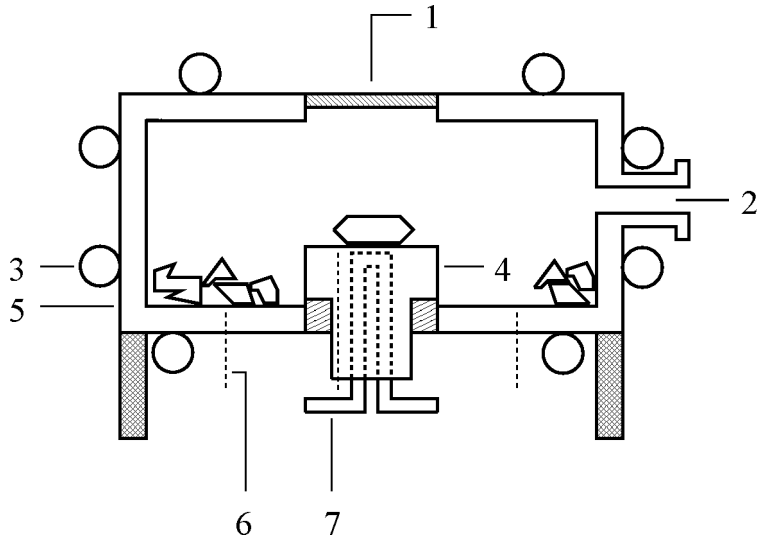

Figure 8.2: A schematic drawing of the vapour growth cell used in our experiments. 1) Glass window, 2) vacuum flange, 3) heating tube, 4) cold finger with crystal, 5) thermostated wall with bulk material, 6) thermo couple and 7) cold finger water inlet.

a vacuum pump can be mounted. During the experiments a pressure of about 10^{-9} bar is maintained. The bulk n-$C_{23}H_{48}$ material is placed inside the cell and can be heated by the outer wall using the water thermostated heating tubes. The n-$C_{23}H_{48}$ molecules in the vapour state crystallise on a cold finger, of which the temperature can be controlled independently from the outer wall by a cold water flow. The temperature is measured using copper-constantan thermocouples which are mounted on the outer wall and in the cold finger. The crystals on top of the cold finger are observed trough a glass window using an optical, polarisation reflection microscope.

Normally the driving force for crystallisation is defined as the difference between the chemical potential of the molecules in the solid phase and in the vapour phase divided by kT: $\Delta\mu/\mathrm{k}T$. For ideal gases this implies that $\Delta\mu = \mathrm{k}T\ln(P/P_0)$, where P is the pressure of the bulk vapour, P_0 the equilibrium pressure at the crystallisation temperature T and k the Boltzmann constant. However, to be able to grow crystals it was necessary to let the vacuum pump work continuously during the experiments. Therefore the exact bulk vapour pressure at the cold finger was not known. This makes it impossible to calculate the driving force in the above described terms for our vapour experiments and therefore we will simply use the temperature difference $\Delta T = (T_0 - T)$, with T_0 the temperature of the bulk material and T the temperature of the cold finger, as a measure for the driving

force.

We have performed experiments at 287 K, 303 K and at 312 K at supersaturations (ΔT) ranging from 2 K to 8 K. At 287 K experiments have been done at supersaturations of 2, 4, 6 and 8 K and at 303 K and 312 K only at a supersaturation of 2 K. For every experiment we examined as many crystals as possible by optical (polarisation) microscopy, scanning electron microscopy (SEM) and a selection of the crystals by atomic force microscopy (AFM). We have determined the morphology of the crystals by measuring the angles between the faces and measuring the size of the different faces. Besides the macroscopic morphology, also the growth mechanisms, such as homogeneous and heterogeneous two dimensional nucleation and spiral growth relevant for the different faces, have been determined. As source material we used n-$C_{23}H_{48}$ from Alfa with a purity of $> 99\%$.

8.3.2 Solution growth

To be able to examine the morphology of crystals grown from solutions we used a thermostated growth cell [Vogels et al., 1990]. This method implies in-situ observation by optical transmission microscopy of crystals in a closed cell with a fixed amount of compound and solvents. An in-situ thickness measurement device [Madsen, 1976, van Hoof et al., 1998b] was used to determine the thickness of the observed crystals. The saturation temperature T_s and thus the crystallisation temperature at a given supersaturation could be changed from cell to cell by changing the amount of n-$C_{23}H_{48}$ in the cell, whereas the super (under) saturation was changed by lowering or raising the temperature T of the system below or above the saturation temperature T_s. The supersaturation will then be defined as

$$\sigma = \frac{\Delta\mu}{\mathrm{k}T} \approx \frac{\Delta H_{diss}}{\mathrm{R}T_s T}\Delta T \ , \tag{8.5}$$

where ΔH_{diss} is the enthalpy of dissolution, R the gas constant and $\Delta T = T_s - T$.

We have performed experiments on n-$C_{23}H_{48}$/n-hexane, n-$C_{23}H_{48}$/toluene and on n-$C_{23}H_{48}$/50% n-hexane/50% toluene systems at several temperatures ranging from 275 K to 296 K. For every system the crystal morphology, including the aspect ratio of the top and side faces, and the roughening temperatures of the side faces have been studied. As source material we used n-$C_{23}H_{48}$ from Alfa with a purity of $> 99\%$, n-hexane and toluene both from Merck, ultra pure.

8.3.3 Melt growth

Two experimental setups were used to study the crystal morphology from the melt. The first is the thermostated cell that was used for the solution growth experiments. In case of crystal growth from the melt the glass cell contained only pure ($> 99\%$) n-$C_{23}H_{48}$ material and the crystallisation temperature T was slightly lower than the melting temperature T_m of n-$C_{23}H_{48}$. Here the supersaturation was defined by

$$\sigma = \frac{\Delta\mu}{\mathrm{k}T} \approx \frac{\Delta H_m}{\mathrm{R}T_m T}\Delta T \ , \tag{8.6}$$

where ΔH_m is the enthalpy of melting and $\Delta T = T_m - T$.

A second setup was used to examine solid state phase transitions at several degrees below the melting point. In this setup crystals were grown between two glass plates only a few hundred microns apart. This made it possible to obtain single crystals from the melt which were not "overgrown" by others even at several degrees below T_m. The solid state phase transitions of these crystals could then be studied as a function of temperature, using a transmission polarisation microscope. As source material we used n-$C_{23}H_{48}$ from Alfa with a purity of $> 99\%$.

8.4 Experimental results

8.4.1 Vapour growth

Figure 8.3 shows a scanning electron micrograph of some crystals grown at 287 K at a supersaturation of approximately 6 K and at 303 K at a supersaturation of 2 K, whereas figure 8.4 schematically shows two morphologies, obtained at temperatures of 287 K and 303 K both at a supersaturation of 2 K. At 287 K the faces {001}, {111} or {110} and {010} were prominent and about 10% of the crystals showed {100} faces, whereas at 303 K only the faces {001}, {111}, {110} and {010} were observed.

Because the crystals were very small and because of the small angle (7°) between the faces {111} and {110} it was very difficult to distinguish whether the side faces consisted of one of them or both. Also SEM measurements were very difficult, because most of the side faces were slightly rounded. This is probably due to the relatively high temperature and the low pressure during the gold sputtering prior to SEM observation in combination with the low melting temperature of the crystals. However, some SEM measurements and many optical microscopy measurements showed that the side face orientations {110}/{111} of the crystals grown at 303 K consisted of two faces and sometimes of one face. It was not possible to measure the angle between the two faces. Figure 8.3b shows a SEM photograph which demonstrates the presence of two faces. Because it was difficult to distinguish between the {110} and the {111} faces in the subsequent part of this paper they will be noted as {110}/{111} faces.

At a temperature of 287 K and a supersaturation of 2 K the aspect ratio R_1 varies between 10 and 30 and $R_2 \approx 1.1$. Table 8.2 shows the morphology of the crystals at this temperature for increasing supersaturations. At a supersaturation of 6 K most of the faces {010} and {100} were rough, i.e. not flat, and at a supersaturation of 8 K in addition most of the {110}/{111} faces were rough. At these supersaturations both rough and faceted faces were found, however because the rough faces did not occur at lower supersaturations we will mark the former supersaturations as the critical supersaturations for kinetic roughening. We note that for (100) only a few faces were present, so that the critical supersaturation for this face contains a large error.

AFM and optical microscopy studies of the {001} faces [Plomp et al.,] of crystals grown at different supersaturations showed that they were covered with steps oriented in one direction. The origin of the steps was located near the point where the crystals were attached to the cold finger, which is likely to act as a heterogeneous step source. At some distance from this source the steps bunched resulting in steps of approximately 5 mono

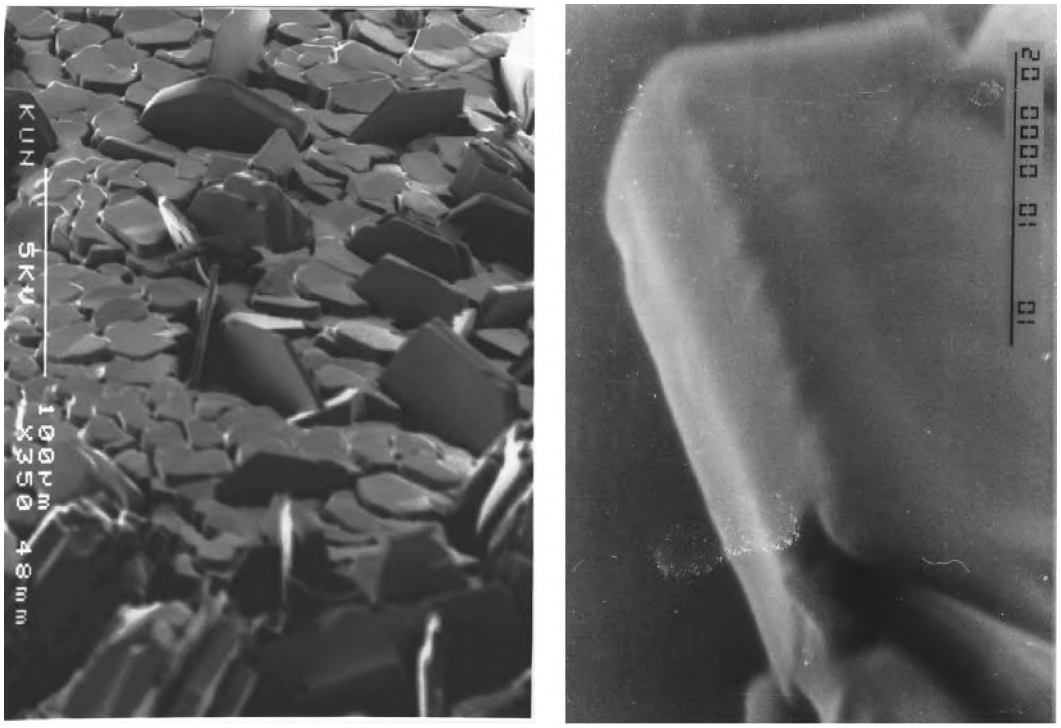

(a) (b)

Figure 8.3: Electron micrographs of vapour grown crystals. a) Crystals grown at 287 K and approximately 6 K supersaturation. The scale bar indicates 100μm. b) Crystal grown at 303 K and 2 K supersaturation; the side faces are {111} faces. The scale bar indicates 10μm.

steps high. Due to their limited width, on the other faces, that is {111}/{110}, {100} and {010}, no surface topographic investigations with AFM were performed.

Measurements at different temperatures and at the lowest possible supersaturation, $\Delta T = 2$ K, have been used as an estimation for the roughening temperature. The faces {001}, {110}/{111} and {010} were faceted at the temperatures of 287 K and 303 K. At a

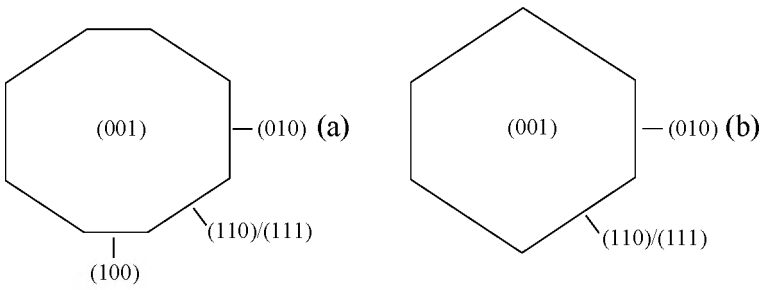

Figure 8.4: The morphology of n-$C_{23}H_{48}$ crystals grown from the vapour phase at a supersaturation of 2 K, a) at 287 K and b) at 312 K.

Table 8.2: Morphology of n-$C_{23}H_{48}$ crystals grown from the vapour phase at 287 K. '+' denotes that the orientation was found and '−' denotes that the according orientation was found, however in a rough mode.

ΔT (K)	2	4	6	8
{001}	+	+	+	+
{110}/{111}	+	+	+	−/+
{010}	+	+	−/+	−/+
{100}	+	+	−/+	−/+

temperature of 312 K only the faces {001} were faceted and all of the faces {110}/{111} and {010} were rough. The faces {100} were only observed (and were faceted) at the lowest temperature of 287 K. These observations suggest that 287 K $< T^R_{100} <$ 303 K, 303 K $< T^R_{110}$, T^R_{111}, $T^R_{010} <$ 312 K and 312 K $< T^R_{001}$.

8.4.2 Solution growth

The morphologies of n-$C_{23}H_{48}$ crystals grown from n-hexane solutions, toluene solutions and a mixture of 50% n-hexane and 50% toluene were examined. All the morphologies of the n-$C_{23}H_{48}$ crystals grown from these systems were about the same. Figure 8.5 shows

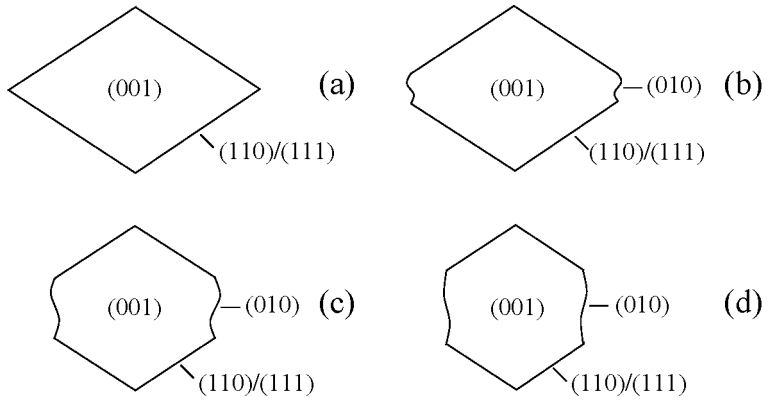

Figure 8.5: Schematic drawing of the morphology of n-$C_{23}H_{48}$ crystals occurring for all solutions at different temperatures T below the roughening temperature T_R of the {110}/{111} faces. a) $T^R - T = 8$ K, b) $T^R - T = 5$ K, c) $T^R - T = 1$ K and d) $T^R - T = 0.1$ K. For all cases $\Delta T \approx 0.01$ K.

that very flat, lozenge shaped crystals were found with large {001} faces and narrow {110} or {111} faces and depending on the temperature, rough {010} orientations. Because the crystals were very thin (≥ 1 μm) we were not able to distinguish between the {110} and {111} faces.

The occurrence of the rough {010} orientation depended on the temperature and was different for every system. However if the temperature of each experiment was scaled according to the roughening temperature of the {110}/{111} faces, i.e. $(T_R - T)$, it turned out that the occurrence of the {010} orientation was the same in every system (figure 8.5). The roughening temperatures of the {110}/{111} faces of crystals grown from pure n-hexane, pure toluene and a mixture of 50% n-hexane and 50% toluene were determined and turned out to be respectively 284 K, 290 K and 288 K. The aspect ratio R_1 for n-$C_{23}H_{48}$ crystals grown at 278 K and 282 K at low supersaturations from n-hexane solutions varied from 250 to 1000. The aspect ratio R_2 of n-$C_{23}H_{48}$ crystals grown from a variety of solutions at a variety of temperatures depended on the temperature and ranged from 1 (for $T_R - T = 0.1$ K) to 1.6 (for $T_R - T = 5$ K). We note that the crystals were always grown on the bottom of the glass cell and therefore only one surface {001} was able to grow, which resulted in crystals two times too thin. Therefore, to compare the morphology of the grown crystals with the calculated morphologies, R_1 should be divided by two, which leads to a value between 125 and 500.

8.4.3 Melt growth

Figure 8.6 shows a photograph of an n-$C_{23}H_{48}$ crystal grown from the melt at about 0.01 K below its melting point of 320.7 K. The crystals exhibit only large, flat {001}

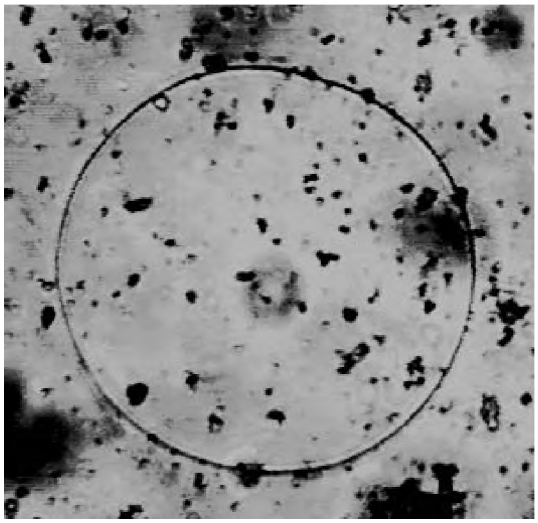

Figure 8.6: Photograph of one circular n-$C_{23}H_{48}$ crystal grown from the melt, 0.01 K below the melting point.

faces. The aspect ratio R_1 is in the order of that of the vapour grown crystals and varies between 30 and 50. Figure 8.6 clearly shows that all orientations other than {001} were not faceted and thus that these faces grew above their roughening temperatures or critical supersaturations.

8.5 Discussion

8.5.1 Morphology of vapour grown crystals

The morphology of the crystals grown from the vapour phase is in good agreement with the morphology predicted by the connected net analysis [Grimbergen et al., 1998d] as shown in figure 8.1. All the predicted faces {001}, {110}, {111}, {010} and {100} have been observed experimentally. Note that this is to our knowledge for the first time that faceted {111}, {010} and {100} faces have been observed. The {001} face was faceted at every temperature and supersaturation, which can be understood because it has a very high roughening temperature of about 6000 K. It was difficult to distinguish between the {110} and {111} faces, because of the small angle of 7° between them. However, SEM and optical microscopy of crystals grown at 303 K at a low supersaturation ($\Delta T = 2$ K) revealed either {111} faces or -sometimes- {110} faces. For crystals grown at other temperatures and supersaturations it was not possible to distinguish between the two faces. Note that faces similar to the {111} faces have been observed by Bennema et al. [Bennema et al., 1992] in case of the crystallisation of n-paraffins in the presence of 100 ppm additive. These observed faces are in fact tapered {111} faces.

Grimbergen et al. [Grimbergen et al., 1998d] explained that for the orientation {110} a combination of the two strongest connected nets leads to a very low effective step energy and that therefore at low supersaturation the {111} faces will be dominant. That might exactly be the case here. The reason that crystals have been observed both with {111} and with {110} faces is probably due to inhomogeneity in the supersaturation, as a result of thermal gradients over the crystals and/or cold finger.

The {010} faces are more stable than the {100} faces, because they were present at almost every crystal at every temperature, whereas the {100} faces were present at 10% of the crystals only at a temperature of 287 K. Although the {100} faces have a lower attachment energy and a higher δ than the {010} faces (table 8.1), they have a much lower threshold for kinetic roughening because they can grow with half layers beyond a certain supersaturation [Grimbergen et al., 1998d].

The aspect ratio R_2 is exactly the same for the predicted and the observed vapour phase morphologies, whereas the aspect ratio R_1 differs somewhat. R_1 is 5.3 for the predicted morphology and varies between 10 and 30 for the vapour phase morphology. This larger value of the observed R_1 is explained by the fact that the bonds in the faces {110}, {111}, {010} and {100} are much more anisotropic than in the {001} faces. This results in higher growth rates for these faces than predicted on the basis of E^{att}_{hkl} as given in equation (8.2) [van der Eerden et al., 1977, Liu and Bennema, 1993a, Grimbergen et al., 1999a], which is applicable only to isotropic crystals, and thus results in thinner crystals. Moreover, we expect that R_1 will be even higher for ideal vapour grown crystals, that is without the presence of a step source. The {001} faces were covered with steps which originated from the cold finger. Due to this heterogeneous step source the growth rate of this face is higher and thus R_1 is lower than expected. This implies that if a large difference in anisotropy of the different faces is involved, i.e. in our case $\delta = 1.0$ for the {001} faces and $\delta < 0.13$ for all the relevant side faces, E^{att} is not a good measure for the growth rate and thus for the growth morphology. The effect of the anisotropy on the

growth rate have been studied by van der Eerden et al. [van der Eerden et al., 1977] and is subject of a forthcoming paper [Grimbergen et al., 1999a].

All the faces {110}, {111} and {010} were faceted at a temperature of 303 K and at a supersaturation of 2 K and rough at a temperature of 312 K and a supersaturation of 2 K. This can be due to two reasons. First, the roughening temperatures of all the faces {110}, {111} and {010} can be between 303 K and 312 K. This is, however, very unlikely because the calculated Ising temperatures are much higher and show much larger mutual differences (about 400 K). It is also possible that the crystals at 312 K have not been grown in the orthorhombic phase but in the pseudo-hexagonal phase. The temperature of crystallisation (312 K) is 1.7 K below the temperature of a well-known bulk phase transition from the orthorhombic phase to the pseudo hexagonal phase at 313.7 K [Broadhurst, 1962]. However, due to homologous impurities the temperature of this phase transition can be lower [Pechhold et al., 1966] and can thus result in rough faces. If this is the case then the roughening temperatures of the faces {110}, {111} and {010} of crystals in the orthorhombic phase can be higher than 312 K.

8.5.2 Morphology of solution grown crystals

One of the most remarkable results is that the aspect ratio R_1 for the morphology of solution grown crystals is much higher (125 to 500) than the predicted value (5.3). Furthermore, only the {001} and {110}/{111} faces were found to be faceted. The latter can easily be explained by the fact that for crystals grown from solutions as compared with those grown from vapour the effective bond energies [Bennema, 1993] are lower, which results in lower roughening temperatures or lower critical supersaturations. Apparently the effective bond energies have been lowered to such an extent that the roughening temperatures or critical supersaturations of the faces {010} and {100} are lower than the temperature or supersaturation of the experiments and that the roughening temperatures or critical supersaturations of the {001} and {110}/{111} faces are still higher than the temperature or the supersaturation of the experiments. It was impossible to distinguish between the faces {110} and {111}.

In figure 8.5 the morphology of crystals grown from different kinds of solution have been grouped according to their difference in crystallisation temperature and the roughening temperature of the {110}/{111} faces, which can be different for each kind of solution. The similar behaviour for the different solutions suggests that the roughening temperatures of the {010} and {110}/{111} faces are lowered to a comparable extent in solutions compared to each other and to the calculated values. Furthermore, it turns out that, at temperatures close to $T^R_{110/111}$, the rough {010} faces have about the same growth rate as the {110}/{111} faces. This indicates that the growth rate of rough orientations can be in the same range as that of faceted faces.

The ratio R_1 of the morphology of crystals grown from solutions is between 125 and 500, whereas that of the morphology of crystals grown from the vapour and of the predicted morphology is respectively 10-30 and 5.3. An explanation in terms of adsorbed n-paraffin molecules lying flat on the surface of the crystals was given by Liu and Bennema [Liu et al., 1994a].

Here we like to mention a second possibility. The growth morphology of a crystal

will be determined by the relative growth rate of the different faces. The growth rate will be determined by, among others, the growth mechanism of a face (hkl) and the step free energy. If the growth mechanism of a face (hkl) is known, i.e. spiral growth or 2D nucleation growth, the step free energy can be used [Burton et al., 1951] to determine the relative growth rate of that face. However, practical analytical expressions for this always involve constants which are not easily determined. Furthermore the side faces have in common that the anisotropy in step energy is much larger than for the {001} faces, which results in much higher growth rates of the side faces and thus in thinner crystals than predicted on basis of equation (8.2). Finally, it is to be expected that this effect depends on strongly on the supersaturation [Grimbergen et al., 1999a].

8.5.3 Morphology of melt grown crystals

From literature [Broadhurst, 1962, Doucet et al., 1981] it is known that n-$C_{23}H_{48}$ crystals have three different phases, an orthorhombic phase (below 313.7 K), a rotator phase I (between 313.7 K and 318.6 K) and a rotator phase II (between 318.6 K and 320.7 K). Rotator phase I exhibits a pseudo hexagonal symmetry and thus optical birefringence along the c-axis, whereas rotator phase II exhibits an hexagonal symmetry and no birefringence along the c-axis. Crossed polarisers showed that the grown crystals exhibited a birefringence along the c-axis and upon cooling only one phase transition was found. From this it follows that during cooling the crystals directly entered the rotator phase I, omitting rotator phase II. Therefore a comparison of the morphology of these crystals with the calculated morphology of the orthorhombic phase can not be made.

8.6 Conclusions

The morphology of the crystals grown from the vapour phase is in very good agreement with the predicted morphology based on the extended connected net analysis of Grimbergen et al [Grimbergen et al., 1998d]. All the predicted faces {001}, {110}, {111}, {010} and {100} are observed. Note that, to our knowledge, this is the first time that the faces {111}, {010} and {100} have been observed. The sequence in roughening temperatures and critical supersaturations is as predicted and understood in terms of attachment energies and anisotropy in step free energies. The aspect ratio R_1 is somewhat larger than predicted which can be due to the larger anisotropy in step free energy of the faces {110}, {111}, {010} and {100} in comparison with the faces {001}. The roughening temperatures of the faces {001}, {110}, {111} and {010} of crystals grown from the vapour are probably higher than 312 K and that of the {100} face is in between 287 K and 303 K.

The faces of the crystals grown from solutions have lower roughening temperatures, because the bond energies of those crystals are much lower than for crystals grown from the vapour. Both faceted {001} and {110}/{111} faces are observed. It was impossible to distinguish between the {110} and {111} faces of crystals grown from the solution. At temperatures close to $T^R_{110/111}$ rough {010} orientations were observed, which shows that rough faces can have similar growth rates as faceted faces. The sequence of roughening temperatures is still as predicted. The aspect ratio R_1 is much larger than that of crystals

grown from the vapour and the predicted value. This can be due to adsorbed molecules which lay flat on the crystalline surfaces or due to the dependence of the growth rate of the different faces on the step free energy. The latter explanation will be the subject of future research.

Acknowledgements

P.J.C.M. van Hoof would like to acknowledge the financial support of Shell International Oil Products B.V. and R.F.P. Grimbergen acknowledges the financial support of the Dutch Technology Foundation (STW).

Chapter 9

Theoretical Morphology of ϵ-Caprolactam: Monomer versus Dimer Analysis

Theoretical Morphology of ϵ-Caprolactam: Monomer versus Dimer Analysis

R.F.P. Grimbergen and E.P.G. van den Berg

Abstract

The morphology of ϵ-caprolactam is derived theoretically from the crystal structure by a rigorous connected net analysis. The analysis is done by taking either monomers or hydrogen-bonded dimers as growth units. The monomer analysis yields the $\{100\}$, $\{11\bar{1}\}$, $\{110\}$ and $\{31\bar{1}\}$ faces as most important F-faces whereas the dimer analysis yields the $\{100\}$, $\{11\bar{1}\}$, $\{110\}$ and $\{20\bar{1}\}$ forms. For the $\{110\}$ faces growth may proceed via growth layers $\{220\}$ having a thickness of $\frac{1}{2}d_{110}$ depending on the growth conditions. In the latter case the $\{110\}$ form will become morphologically less important or may even disappear from the morphology.

9.1 Introduction

ϵ-Caprolactam ($C_6H_{11}NO$, CAP) is a commercially very important compound because it is a direct precursor for nylon-6. For this reason quite some experimental work has been done for this compound in order to study its growth behaviour in industrial crystallizers. More fundamental work has been done by van der Heijden [van der Heijden, 1992], Geertman [Geertman, 1993, Geertman and van der Heijden, 1992] and van den Berg [van den Berg, 1997]. Geertman and van den Berg already derived the theoretical morphology based on single CAP molecules and compared it to the case of dimerized molecules. The results were compared with the experimental morphology for a number of solvents. However, their connected net analyses were incomplete and contained some errors.

It is the aim of this study to derive all connected nets of ϵ-caprolactam from the crystal structure starting from either monomers or dimers as growth units and construct the theoretical growth morphology. The connected nets for both cases were derived using the graph-theoretic method described by Strom [Strom, 1980, Strom, 1981, Strom, 1985]. The results of the monomer and dimer analysis are compared. Moreover, the implications of multiple connected nets for a single orientation (hkl) will be discussed. The theoretical results are compared with experimental data from literature [Geertman, 1993, Geertman and van der Heijden, 1992, van den Berg, 1997].

9.2 Connected net analysis

In 1955 Hartman and Perdok presented a theory for prediction of crystal morphology from the crystal structure [Hartman and Perdok, 1955a, Hartman and Perdok, 1955b, Hartman

and Perdok, 1955c, Hartman, 1973]. They stated that crystal faces that appear on the crystal morphology must be F-faces consisting of at least two intersecting non-parallel Periodic Bond Chains (PBCs). Later Bennema introduced the concept of connected nets which made it possible to apply the theory of surface roughening transitions and estimate oder-disorder transition temperatures [Rijpkema et al., 1982]. Recently, some extensions were added to the existing theory which demonstrate that there is a strong relation between the exact bonding topology at the surface $\{hkl\}$ and the equilibrium and growth behaviour of that face $\{hkl\}$. It was shown that specific combinations of connected nets can give rise to very small effective step free energies resulting in a lowering of the roughening temperature T^R and a high relative growth rate. For some special cases where connected nets are symmetry related, the step free energy is zero. This situation is known as symmetry roughening [Grimbergen et al., 1998b, Meekes et al., 1998, Grimbergen et al., 1999a].

The complete procedure to derive all connected nets is described below. First the most important bonds or interactions between growth units in the lattice have to be determined. The interactions between the growth units are calculated using an empirical force field. Bonds having a bond energy larger than the thermal energy kT (T is the actual growth temperature) are used in the analysis. The growth units are subsequently reduced to their corresponding centers of geometry. The centers of geometry connected by the bonds define a so-called crystal graph. From the crystal graph first all direct chains (DCs) are derived. A DC is defined as a sequence of strongly bonded growth units of which only the endpoints are identical (i.e. related by a lattice translation $[uvw]$ with $u, v, w \in Z$). Connected nets (hkl) perpendicular to $\boldsymbol{k}_{hkl} = h\boldsymbol{a}^* + k\boldsymbol{b}^* + l\boldsymbol{c}^*$ can be constructed by combining at least two non-parallel intersecting DCs $[uvw]_1$ and $[uvw]_2$ perpendicular to $\boldsymbol{k}_{hkl}$. Equivalent growth units of a connected net differ a translation $[uvw]$ perpendicular to $\boldsymbol{k}_{hkl}$. Given the spacegroup symmetry equivalent connected nets are separated by the interplanar distance d_{hkl} according to the selection rules of Bravais, Friedel, Donnay and Harker (BFDH) [Friedel, 1911, Donnay and Harker, 1937, Grimbergen et al., 1998b]. Note that a connected net need not be stoichiometric with regard to the chemical composition of the unit cell. Therefore, only stoichiometric connected nets can be considered as the actual growth layers with which a crystal will grow. In this paper only stoichiometric connected nets are considered.

In order to determine the growth morphology based on F-faces, Hartman and Bennema introduced the attachment energy as a habit controlling factor [Hartman and Bennema, 1980]. The attachment energy is defined as the energy released per growth unit in case a complete growth layer (i.e. stoichiometric connected net) is attached to the surface (hkl) of a crystal. The attachment energy is related to the crystallization energy by

$$E^{cr} = E^{att}_{hkl} + E^{slice}_{hkl} \ , \tag{9.1}$$

where E^{slice}_{hkl} is the interaction energy of all growth units within the stoichiometric connected net or growth layer. It was argued that it may be justified that the relative growth rates of crystal faces are proportional to the attachment energy or

$$R_{hkl} \propto E^{att}_{hkl} \ . \tag{9.2}$$

Subsequently, a Wulff plot can be used to construct the growth morphology [Wulff, 1901].

9.3 Crystal graph

9.3.1 Crystal structure

Caprolactam crystallizes in the monoclinic spacegroup C2/c with unit cell dimensions a=19.28 Å, b=7.78 Å, c=9.57 Å and β=112.39° [Winkler and Dunitz, 1975]. There are 8 molecules in the unit cell (Z=8). In the crystal structure all CAP-molecules are pairwise hydrogen-bonded via a double hydrogen bridge between the carbonyl and the amine group. Because these hydrogen bonds are very strong both monomers (single CAP molecules) and dimers (hydrogen bonded CAP molecules) will be considered as growth unit for crystal growth. The unit cell for monomers and dimers is depicted in figure 9.2.

atom	charge	atom	charge
N1	-0.6148	H3	0.0222
O1	-0.6276	H4	0.0429
C1	0.6752	H5	0.0349
C2	-0.1397	H6	0.0211
C3	-0.0082	H7	0.0072
C4	-0.0681	H8	0.0346
C5	0.0064	H9	0.0571
C6	-0.0006	H10	0.0822
H1	0.0643	H11	0.3530
H2	0.0579		

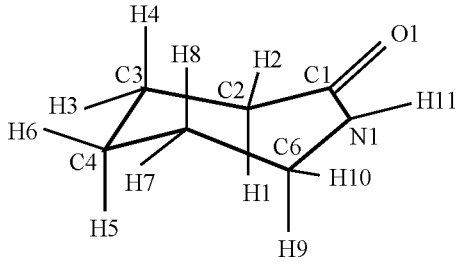

Figure 9.1: Atomic point charges of ϵ-caprolactam

9.3.2 Calculation of the bonds

In order to determine the crystal graph of a crystal structure first the growth units have to be determined. As mentioned before, in this study both monomers and dimers of CAP-molecules will be considered as growth units. The next step is to determine all strong interactions between the growth units in the crystal lattice. For that purpose the Dreiding force field [MSI,] was used with atomic point charges calculated using the following procedure. First the electrondensities of a single CAP-molecule were calculated with GAMESS using the 6-31g** basis [Guest et al., 1994]. Second, electrostatic potential derived (ESPD) point charges were subsequently calculated from the electrondensities using the program MOLDEN [Schaftenaar, 1992,Besler et al., 1990]. The resulting atomic charges are listed in the table in figure 9.1. These charges were used for all calculations of both monomers and dimers.

Before interactions between the growth units were calculated, the experimental crystal structure was minimized to remove bad contacts. During the minimization, the space-group symmetry was imposed and the cell parameters were optimized. The Ewald summation technique was used to calculate non-bonded interactions in the lattice. The cell parameters after minimization were (difference with experimental values between brackets)

a=20.876 Å (+8%), b=7.529 Å (-3%), c=9.645 Å (+1%) and β=115.65° (+3%). Apart from the a-axis all cell parameters do not differ very much from the experimental values. Comparing the minimized and experimental crystal structure it can be seen that the CAP-molecules have an identical orientation in the unit cell and the molecular conformation was not changed. All molecules are somewhat shifted along the a axis which explains the elongation of this axis. All subsequent calculations in this paper were done using the minimized crystal structure.

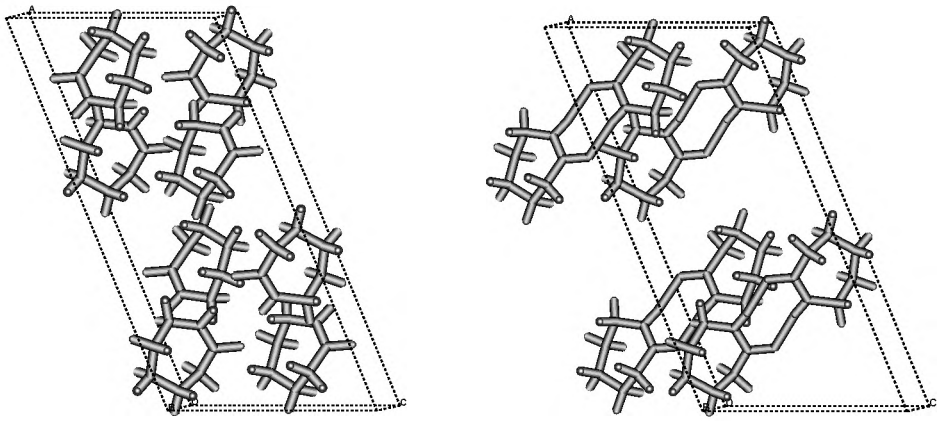

Figure 9.2: The unit cell of caprolactam based on monomer (left) and dimer (right) growth units.

After the minimization procedure the lattice energy was calculated by summation of all atom-atom pair interactions between growth units of which the geometrical center is within a cutoff radius of 50Å of the central molecule according to

$$E_{latt} = \frac{1}{2} \sum_{k=1}^{N} \sum_{i=1}^{n} \sum_{j=1}^{n'} V_{kij} \ , \tag{9.3}$$

where N is the number of surrounding molecules within the cutoff radius, n the number of atoms of the central molecule, n' the number of atoms of the surrounding molecule and V_{kij} the interaction between the atoms. Within the cutoff radius of 50Å the lattice energy converged to a value of -21.1 kcal/mol. To check the consistancy of the force field, the calculated lattice energy can be compared with an "experimental lattice energy" V_{exp} which can be obtained from the experimentally determined sublimation enthaply ΔH_{subl} via

$$V_{exp} = -\Delta H_{subl} - 2RT \ , \tag{9.4}$$

where $2RT$ represents a correction for the difference between the gas phase enthalpy and the vibrational contribution to the lattice enthalpy [Hagler et al., 1976]. The sublimation enthalpy of 19.9 kcal/mol is obtained from ref. [Aihara, 1960]. Using a temperature of 298K, we obtain V_{exp}= -20.5 kcal/mol. The calculated lattice energy of -21.1 kcal/mol is in very good agreement with this "experimental lattice energy".

The minimized crystal structure was used to calculate the bonds between the growth units (figure 9.2). All bonds having an energy of less than kT ($\approx$0.6 kcal/mol for room temperature) were not included.

In the case of dimers also the minimized crystal lattice was used to calculate all bonds. Therefore, the hydrogen bonds were replaced with covalent bonds in such a way that the entire lattice was build from these covalently bonded "dimer molecules" (see figure 9.2). Subsequently, the interactions between the dimers were calculated. The calculated lattice energy based on "dimer molecules" was -26.5 kcal/mol.

9.3.3 The monomer graph

The bonds of the crystal graph for monomer growth units was determined using the method described in the previous section. In a crystal graph the growth units are reduced to their corresponding geometrical center M_n ($n = 1 - 8$). The interactions between the growth units are indicated as bonds between the corresponding geometrical centers. The results for the monomers are given in table 9.1. The crystal energy based on the bonds of the crystal graph is 92% of the calculated lattice energy. All attachment energies were calculated from the bonds defined in the crystal graph.

Table 9.1: Bonds defining the monomer crystal graph of caprolactam. In column 2-4 of the table the fractional coordinates of the geometrical centers M_n of the monomers are given. In column 5 and 6 all bonds and bond energies are listed. The crystal energy based on the defined bonds is -19.3 kcal/mol.

M_n	X	Y	Z	Bond	E (kcal/mol)
M_1	0.865	0.232	0.879	$M_1 - M_7[000]$	-16.60
M_2	0.135	0.232	0.621	$M_1 - M_4[001]$	-2.82
M_3	0.135	0.768	0.121	$M_1 - M_6[0\bar{1}0]$	-2.41
M_4	0.865	0.768	0.379	$M_1 - M_4[0\bar{1}0]$	-2.31
M_5	0.365	0.732	0.879	$M_1 - M_2[100]$	-1.71
M_6	0.635	0.732	0.621	$M_1 - M_3[101]$	-1.60
M_7	0.635	0.268	0.121	$M_1 - M_3[1\bar{1}1]$	-1.53
M_8	0.365	0.268	0.379	$M_1 - M_7[001]$	-1.13
				$M_1 - M_2[101]$	-1.03

9.3.4 The dimer graph

For the dimer graph it is assumed that the growth units are hydrogen-bonded CAP dimers. Therefore, the number of growth units is halved with respect to the monomer analysis and for the same reason the number of bonds is also reduced. The geometrical centers and bonds of the dimer crystal graph are listed in table 9.2. The crystal energy based on the bonds of the dimer crystal graph is 88% of the calculated lattice energy.

Table 9.2: Bonds defining the dimer crystal graph of caprolactam. In column 2-4 of the table the fractional coordinates of the geometrical centers M_n of the dimers are given. In column 5 and 6 all bonds and bond energies are listed. The crystal energy based on the defined bonds is -23.5 kcal/mol.

M_n	X	Y	Z	Bond	E (kcal/mol)
M_1	0.25	0.75	0.50	$M_1 - M_4[000]$	-7.74
M_2	0.75	0.75	0.00	$M_1 - M_2[001]$	-1.96
M_3	0.75	0.25	0.50	$M_1 - M_1[001]$	-1.83
M_4	0.25	0.25	0.00	$M_1 - M_3[\bar{1}0\bar{1}]$	-1.67
				$M_1 - M_6[\bar{1}1\bar{1}]$	-1.65
				$M_1 - M_1[010]$	-0.86

9.4 Results

For the monomer and dimer analysis the BFDH selection rules were applied to determine the growth layer thickness d_{hkl}. The selection rules for the space group C2/c are (hkl) : $h+k = 2n; (h0l) : l = 2n, h = 2n; (0k0) : k = 2n$ [Tables, 1969]. A special situation occurs for the dimer analysis because the "dimer molecules" are situated at special positions. As a result the attachment energy for faces (hkl) with $k+l \neq 2n$ and $h+l \neq 2n$ is repeated exactly at $\frac{1}{2}d_{hkl}$. A comparable situation was found for the (011) faces of the naphthalene structure [Hartman, 1991, Grimbergen et al., 1998c].

The connected nets were determined from the crystal graphs using the program FACELIFT [Grimbergen et al., 1997]. The results are shown in table 9.3.

From the attachment energies in table 9.3 the growth morphology for the monomer and dimer case were constructed using eq. (9.2). The morphologies are drawn in figure 9.3.

9.5 Comparison with previous PBC analyses

In this section the connected net analysis results of the present study are compared with previous analyses as reported by Geertman [Geertman and van der Heijden, 1992] and van den Berg [van den Berg, 1997].

As compared to the results of Geertman and van der Heijden, for the monomer analysis much more connected nets are found. This can be attributed to the difference in method used to determine the connected nets and the fact that in this study an additional bond is included. In contrast, the dimer analysis yielded less F-faces as compared to ref. [Geertman and van der Heijden, 1992]. There are, however, some errors in the results of Geerman and ven der Heijden which cannot be attributed to the difference in search method or number of included bonds. In the monomer analysis of ref. [Geertman and van der Heijden, 1992] the $\{21\bar{2}\}$ form is reported which does not fulfill the mentioned BFDH selection rules (see section 9.4). The same holds for the dimer results which contain the $\{20\bar{1}\}$ form.

Table 9.3: Results of the connected net analysis for monomers and dimers. The form {hkl}, interplanar distance d_{hkl}, calculated attachment energy for the most stable connected net ($E_{hkl}^{att,st}$), and the number of stoichiometric connected nets found (Nr.) are given. Note that the attachment energies are expressed in kcal/mol unit cell content, i.e. for monomers per 8 CAP molecules and for dimers per 4 CAP dimers. The marked forms correspond to subslices.

		Monomer		Dimer	
{hkl}	d_{hkl}(Å)	$E_{hkl}^{att,st}$ (kcal/mol)	Nr.	$E_{hkl}^{att,low}$ (kcal/mol)	Nr.
{200}	8.913	-23.5	6	-21.1	1
{110}	7.130	-41.9	16	-45.0	2
$\{1\bar{1}\bar{1}\}$	6.018	-45.0	14	-48.4	1
{111}	5.180	-87.2	9		
$\{31\bar{1}\}$	4.815	-47.8	9	-56.2	1
$\{20\bar{2}\}$	4.748	-122.9	1	-82.5	1
{310}	4.722	-84.0	12		
{400}*	4.457	-113.7	1	-83.0	1
{002}	4.424	-128.6	2		
$\{1\bar{1}\bar{2}\}$	4.046	-125.1	4		
$\{40\bar{2}\}$	3.990	-75.8	2	-77.1	1
{020}	3.890	-72.8	1	-78.7	1
$\{3\bar{1}\bar{2}\}$	3.865	-94.4	4		
{311}	3.724	-125.2	4		
{220}*	3.565	-77.4	2	-79.8	2
$\{1\bar{1}2\}$	3.526	-131.4	4		
{021}	3.561	-97.9	4		
$\{2\bar{2}\bar{1}\}$	3.497	-67.7	4		
$\{51\bar{1}\}$	3.454	-95.7	4		
$\{5\bar{1}\bar{2}\}$	3.195	-104.1	4		
{221}	3.145	-104.9	4		
$\{4\bar{2}\bar{1}\}$	3.017	-104.9	4		
$\{31\bar{3}\}$	2.932	-129.6	4		
$\{13\bar{1}\}$	2.502	-102.2	4		

Furthermore, in their dimer analysis the $\{02\bar{2}\}$, {131} and {313} faces are found as proper F-faces which are not found in the current analysis.

In ref. [van den Berg, 1997] it is argued that because of the special positions of the dimer growth units the special BFDH selection rule (hkl):$k+l = 2n$ must be applied. Faces that do not fulfill this rule ({110}) were left out. This is not correct since the selection rule only indicates that the attachment energy is repeated by a period $\frac{1}{2}d_{hkl}$ instead of d_{hkl} (see section 9.4). The surface configurations, however, are different and will cause a different surface free energy for the two surfaces. In the discussion the situation for the {110} faces will be explained in more detail.

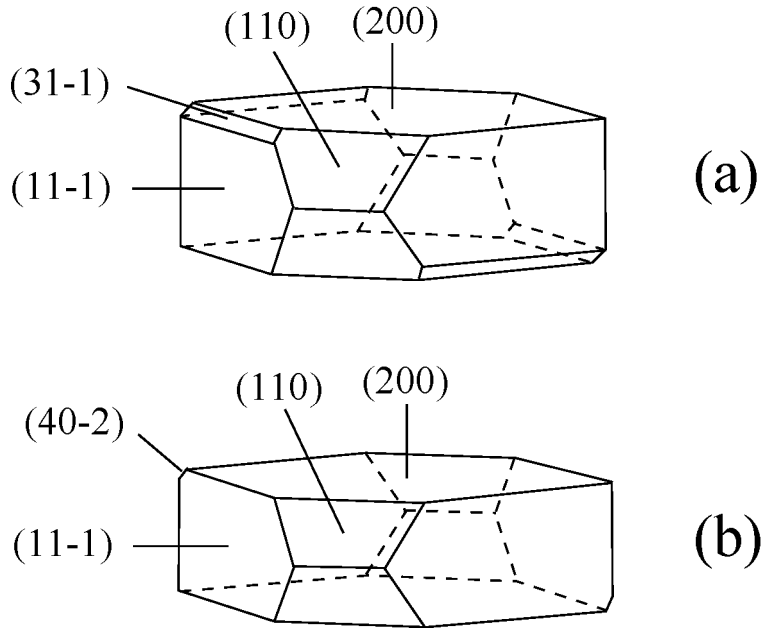

Figure 9.3: The morphology of ϵ-caprolactam based on the attachment energy (eq. (9.2)) for (a) monomer and (b) dimer analysis.

9.6 Discussion

Experimentally the {200}, {110}, {11$\bar{1}$} and {31$\bar{1}$} forms are frequently observed on crystals grown from different solvents and the melt [Geertman and van der Heijden, 1992, van den Berg, 1997]. Looking at table 9.3 it is obvious that both the monomer and dimer analysis yield these forms as most important F-faces. The attachment energies of these faces are clearly most favourable as compared to the other faces. The molecular composition of the strongest connected nets for the (200), (110), (11$\bar{1}$) and (31$\bar{1}$) orientations of the monomer analysis turns out to be equivalent to that of the dimer analysis. This can be explained by the presence of the strong hydrogen bonds which, in case of the monomer analysis, contribute to the slice energy. In the dimer analysis the hydrogen bonds are by definition in the slice as they are part of the dimer growth units.

Another important feature of the strongest connected nets found for the (200), (110), (11$\bar{1}$) and (31$\bar{1}$) orientation is that these nets are strong planar connected nets. Therefore, the presence of other connected nets for these facets will not affect the effective step free energy [Grimbergen et al., 1998d]. This was found for both the connected nets of the monomer and the dimer analysis.

In the monomer analysis often multiple connected nets were found for the higher index faces. In many cases pairs of connected nets were symmetry related and symmetry roughening occurs. Also pairs of connected nets causing a very low step free energy were found. In the present study these connected nets are not considered explicitly as they are of no relevance to the growth morphology. The attachment energy of these faces is much too high for appearance on the growth morphology. In case the effect of a lower step free energy or symmetry roughening would be taken into account, the morphological

importance would decrease even more. For the equilibrium morphology these types of F-face should be carefully analyzed as they may occur on the Wulff plot.

For the (110) orientation a special situation occurs. The two connected nets with the lowest attachment energy have an AB-layered structure as depicted in figure 9.4. The attachment energy is exactly equivalent for the two surface configurations. However, the molecular configuration at the crystal-motherphase interface differs significantly and therefore the surface free energy for the two surfaces will be rather different.

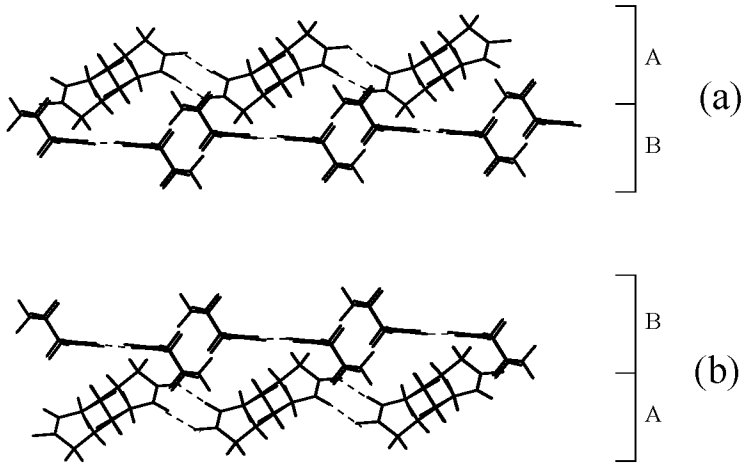

Figure 9.4: [$\bar{1}$10] Projection of the molecular structure of the two most favourable surface configurations of the (110) face of CAP. The two configurations have exactly the same surface and attachment energy (based on the bond energies of the crystal graph). The structure can be regarded as a built up from A and B layers which are both proper connected nets (see table 9.3).

As already mentioned in the previous section a similar situation was found for the (011) faces of the naphthalene structure. The difference between the (011) faces of naphthalene and the (110) faces of CAP is that in the naphthalene structure no connected nets (022) are present whereas in the CAP-structure (220) connected nets are found. For the (011) faces of naphthalene it was found both theoretically and experimentally that the effective step free energy was very small. In case of the (110) faces of CAP the step free energy will still be finite because of the presence of the (220) connected nets. These connected nets guarantee a step free energy larger than zero for the (110) orientation. The calculated attachment energy of the two (220) connected nets is only slightly different (-79.80 kcal/mol vs. -79.86 kcal/mol). In figure 9.4 these connected nets are indicated with A and B. It is to be expected that under growth conditions the (110) facets of CAP can grow alternately with layer $(220)_1$ and $(220)_2$ beyond a certain supersaturation depending on the difference in surface free energy. The difference in surface free energy of the two surface configurations will depend on the specific interaction of the surface with the mother phase. In case the (110) orientation grows with half layers (220), the morphological importance will decrease. Based on the attachment energy of the (220) connected nets (see table 9.3) the (110) facet would not be present on the growth morphology. Moreover, no other faces will appear in case the (110) face is not included in the Wulff plot, because

the attachment energy of all remaining faces is higher than the threshold value for appearance in the Wulff plot. These theoretical results are in agreement with experimental results: the (110) faces are observed on crystals grown from water, acetone, acetonitrile, alcohols, aromatic compounds and ethylacetate and are not observed on crystals grown from acetic acid, alkanes, cyclo-hexane and tetrahydrofuran [Geertman and van der Heijden, 1992, van den Berg, 1997]. However, more experiments are needed in order to study the growth behaviour of the faces of CAP as a function of supersaturation in more detail.

9.7 Conclusions

In this paper for the first time the complete set of stoichiometric connected nets of CAP is presented assuming either single CAP molecules or hydrogen-bridged CAP dimers as growth units. The most important F-faces of ϵ-caprolactam, $\{200\}$, $\{110\}$, $\{11\bar{1}\}$ and $\{31\bar{1}\}$, which are observed experimentally, are found in both the monomer and dimer analysis. The fact that the most important surface configurations (connected nets) found by the monomer and dimer analysis are equivalent can be explained by the presence of very strong hydrogen bonds in the crystal lattice. Connected nets which contain hydrogen-bonded CAP molecules have a high slice energy and consequently a low attachment energy. Therefore, these connected nets determine the growth morphology. The (110) face may grow alternately with half layers $(220)_1$ and $(220)_2$ causing an increase in relative growth rate. The influence of the nature of different solvents on the morphology must be attributed to a difference of relative stabilization of the different surfaces.

Acknowledgements

R.F.P. Grimbergen would like to acknowledge the financial support of the Dutch Technology Foundation (STW).

Chapter 10

Explanation for the Supersaturation Dependence of the Morphology of Lysozyme Crystals

Explanation for the Supersaturation Dependence of the Morphology of Lysozyme Crystals

R.F.P. Grimbergen, E. Boek [1], H. Meekes and P. Bennema

Abstract

In this paper the experimentally observed dependence of the growth morphology on the supersaturation of crystals of the protein lysozyme is explained by the presence of multiple connected nets or surface configurations. The F-forms found by the connected net analysis are {110}, {101} and {111}. From the connected nets the step free energies are estimated. It is shown that the {110} faces will be dominant at low supersaturation, whereas at high supersaturation the {110} and {101} faces have about equal morphological importance as predicted by the attachment energy criterion. The results of the morphological analysis are compared with earlier published Monte Carlo simulation data. Depending on the relative bond strengths flat, rough or disordered flat (DOF) surface phases will occur which have major implications for the growth behaviour of the crystal faces.

10.1 Introduction

Crystallization of hen egg white lysozyme has already been studied for some years since it is an ideal model system for crystallization of proteins in general. The growth behaviour of lysozyme depends on many parameters like the pH, salt concentration, temperature and supersaturation [Nadarajah et al., 1995]. Lysozyme crystals show {110} and {101} faces. Growth of these faces may proceed by dislocations (spiral growth) or 2-D nucleation depending on the supersaturation [Vekilov and Rosenberger, 1996, Durbin and Feher, 1993]. The exact nature of the growth units during the process of crystal growth has been discussed for some time. There is evidence for the presence of dimer, tetramer, octamer and even larger aggregates in solution especially at very high supersaturations [Pusey, 1991, Nadarajah et al., 1995, Li et al., 1995]. The influence of these aggregates cannot be discarded because the effective supersaturation will be affected by these aggregates [Nadarajah et al., 1995].

Recently, the theoretical morphology based on both monomer and tetramer growth units was treated in a graph-theoretic analysis by Strom and Bennema [Strom and Bennema, 1997a]. However, the influence of the supersaturation was not considered.

In this paper the attention is focused on the influence of the supersaturation on the relative growth rates of the {110}, {101} and {111} faces of tetragonal lysozyme. For the connected net analysis monomers are considered to be the growth units, but it will be shown that this does not necessarily imply that the results of the analysis apply to growth by monomers only. For the derivation of the relative growth rates of the crystal faces it is assumed that crystal growth proceeds by 2-D nucleation.

[1]Present address: Schlumberger Cambridge Research, High Cross, Madingley Road, Cambridge CB3 OEL, England

Durbin and Feher have put a lot of effort in studying the growth morphology of lysozyme as a function of supersaturation [Durbin and Feher, 1986]. They measured growth rates for the {110} and {101} faces and found a cross-over in relative growth rates of these faces resulting in a drastic change in the growth morphology as a function of supersaturation which is indicated in figure 10.1.

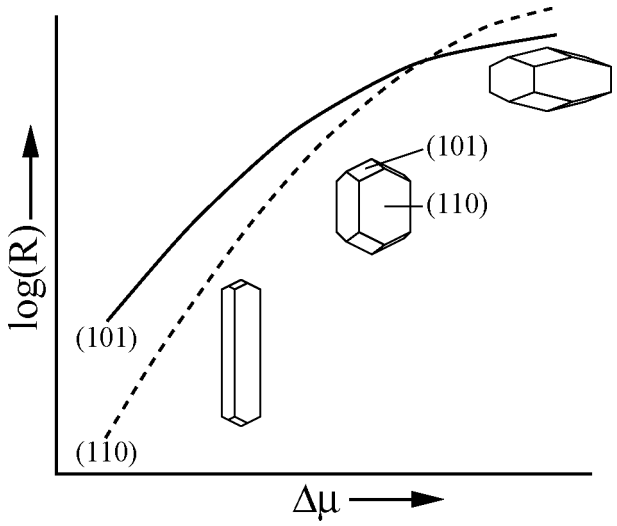

Figure 10.1: Growth rates for the {110} and {101} faces of tetragonal lysozyme at 24°C, pH=4.6 and [NaCl] = 5% w/v. Reprinted from S.D. Durbin and G. Feher *J. Crystal Growth* **110** (1991) p.41 with kind permission of Elsevier Science-NL, Sara Burgerhartstraat 25, 1055 KV Amsterdam.

Moreover, Monte Carlo (MC) simulations were performed using a simple bonding model containing three different types of bond X, Y and Z [Durbin and Feher, 1991]. It was shown that, depending on the relative bond strengths of the X, Y and Z bond and assuming a 2-D nucleation growth mechanism, MC simulations are able to reproduce the experimentally observed cross-over behaviour. Moreover, the MC data reproduced the shape of experimentally observed 2-D nuclei.

It is the aim of this paper to confront the observed and simulated growth behaviour with the results of a morphology prediction based on a modern connected net analysis [Grimbergen et al., 1998b]. The growth behaviour can be explained by the presence of multiple connected nets which may cause pseudo symmetry roughening [Grimbergen et al., 1998b, Meekes et al., 1998, Grimbergen et al., 1999a]. Multiple connected nets can cause a very low effective step free energy along specific crystallographic directions which results in a very small nucleation barrier [Grimbergen et al., 1999a]. Moreover, statistical thermodynamical surface models predict that a special surface phase called a disordered flat (DOF) phase [Rommelse and den Nijs, 1987, den Nijs and Rommelse, 1989] might occur for specific surface bonding topologies. It has already been shown that these surface phases can occur for organic crystals like naphthalene [Grimbergen et al., 1998c, Grimbergen et al., 1998a]. DOF phases give rise to a small nucleation barrier and relatively fast (flat) growth. It will be shown that the crystal faces of lysozyme might exhibit a DOF phase.

In section 10.2 first all connected nets will be derived assuming that the X, Y and Z interactions [Durbin and Feher, 1991] are the most important interactions in the crystal lattice. The effective step energies in terms of X, Y and Z bonds are derived in section 10.3 and in section 10.4 the presence of a DOF phase is explained. In section 10.5 the results will be compared with data from literature. Finally, in section 10.6 some conclusions will be drawn.

10.2 Connected net analysis

The hen egg white protein lysozyme crystallizes at low temperatures in a tetragonal spacegroup and at high temperatures in a orthorhombic spacegroup due to a thermally induced conformational change of the lysozyme molecules [Jollès and Berthou, 1972, Berthou and Jollès, 1974]. The present study is based on the tetragonal structure with spacegroup $P4_32_12$ having eight molecules in the unit cell. The cell parameters are a=79.1Å and c=37.9Å. The asymmetric unit is a single lysozyme molecule [Bernstein, 1977]. The general reflection conditions for this spacegroup are $(00l) : l = 4n$ and $(h00) : h = 2n$ [Tables, 1969]. In table 10.1 the fractional coordinates of the molecules in the unit cell are given. The interactions between the protein molecules in the crystal lattice are very difficult to

Table 10.1: Fractional coordinates of the centers of molecules M_n (n=1-8) in the unit cell.

n	x	y	z
1	0.0158	0.2845	0.4749
2	0.9842	0.7155	0.9749
3	0.2845	0.0158	0.5251
4	0.7155	0.9842	0.0251
5	0.5158	0.2155	0.7751
6	0.4842	0.7845	0.2751
7	0.7845	0.4842	0.7249
8	0.2155	0.5158	0.2249

calculate. Following ref. [Durbin and Feher, 1991] we use three important bonds defined as X, Y and Z to describe the major interactions between the molecules in the lattice. The crystal graph of the lysozyme structure, which consists of the centers of the molecules in the unit cell and all bonds of these molecules in the lattice, is drawn in figure 10.2. All molecules have a fourfold bonding coordination in the lattice (see figure 10.2). The bonds with respect to M_1 are X: $M_1 - M_4[\bar{1}\bar{1}0]$, Y: $M_1 - M_3[000]$, Z: $M_1 - M_8[000]$ and Z: $M_1 - M_7[\bar{1}00]$. These bonds result in a crystal energy of $4X$+$4Y$+$8Z$ per unit cell content (i.e. per 8 molecules).

Using the program FACELIFT [Grimbergen et al., 1997] all connected nets were derived from the crystal graph on the basis of direct chains of bonds (DCs) [Strom, 1980]. Only connected nets containing all eight molecules (M_1-M_8) were allowed in order to retain a stoichiometric composition with respect to the unit cell content. In correspondence with ref. [Strom and Bennema, 1997b] connected nets were found for only three

orientations {110}, {101} and {111}. However, the number of stoichiometric connected nets found differs significantly from the numbers reported by Strom [Strom and Bennema, 1997b]. Using FACELIFT 26 connected nets were found for {110} and {101} and 49 connected nets for {111}, whereas Strom reported 14, 18 and 3 connected nets respectively. For {110} and {101} Strom claims to give all possible connected nets. For {111} only the most important ones were reported.

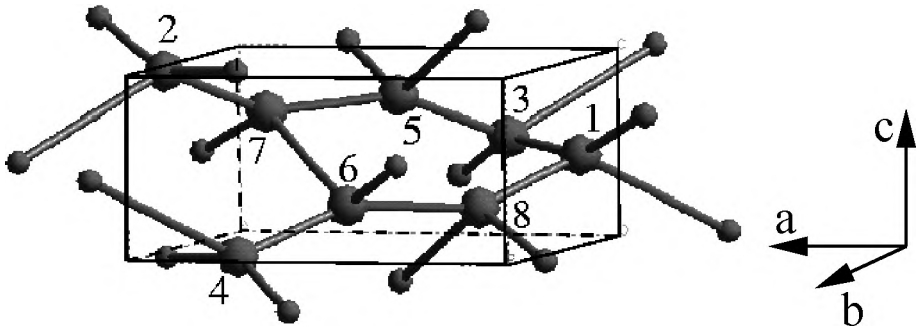

Figure 10.2: Crystal graph of the tetragonal lysozyme structure. The large numbered spheres indicate the centers of molecules of the unit cell and the small spheres are centers of molecules in neighbouring cells.

The reason for this discrepancy is not clear, but inspection of the connected nets found by FACELIFT ensures that these are all valid connected nets. Note that many of the connected nets contain dangling growth units. The various ways in which such dangling growth units can be attached to the connected nets explains the large number of connected nets found. Especially for the {111} faces many of such connected nets occur.

Table 10.2: Slice and attachment energies of the two most favourable singlets of each face (hkl). The connected nets are indicated as $(hkl)_n$. The crystal energy is $4X{+}4Y{+}8Z$. In the last column the step energy is given assuming for each connected net $(hkl)_n$ or surface configuration (see section 10.3).

(hkl)	$E^{slice}_{(hkl)_n}$	$E^{att}_{(hkl)_n}$	$E^{step}_{(hkl)_n}$
$(110)_1$	$2X{+}2Y{+}8Z$	$2X{+}2Y$	$2Z$-X-Y
$(110)_2$	$4X{+}4Y{+}4Z$	$4Z$	$X{+}Y$-$2Z$
$(101)_1$	$2X{+}4Y{+}6Z$	$2X{+}2Z$	Y-X
$(101)_2$	$4X{+}2Y{+}6Z$	$2Y{+}2Z$	X-Y
$(111)_1$	$3X{+}3Y{+}6Z$	$X{+}Y{+}2Z$	X-Y
$(111)_2$	$3Y{+}6Z$	$4X{+}Y{+}2Z$	Y-X

Inspection of all connected nets shows that for all orientations many symmetry related pairs of connected nets (i.e. doublets) exist as well as singlets which are transformed into itself by the symmetry operations of the spacegroup that leave the orientation invariant. The symmetry related doublets would cause symmetry roughening in case the singlets would not be present [Grimbergen et al., 1998b,Meekes et al., 1998]. Note that symmetry roughening for pairs of connected nets does not depend on the relative bond strengths of the X, Y and Z bonds. Therefore, in order to determine the step (free) energy, the attention is focused on the singlets. The slice and attachment energies of the two most favourable singlets for each orientation are given in table 10.2. In the next section the effective step energies will be derived. Note that the slice and attachment energy are related to the crystal energy by $E^{cr}=E^{att}_{hkl}+E^{slice}_{hkl}$; all energies are defined per unit cell content.

10.3 Step energy analysis

The connected nets found by the connected analysis can be used to determine the broken bond step energy based on the bonds defined in the crystal graph. In this section the directions having the lowest step energy will be presented for all F-faces {110}, {101} and {111}. It is assumed that $(110)_1$, $(101)_1$ and $(111)_1$ (table 10.2) represent the most favourable surface configuration, unless mentioned otherwise. This is always the case when it is assumed that $|X|\leq|Y|\leq|Z|$. In figure 10.3 the $[1\bar{1}0]$ projection of the lysozyme graph of figure 10.2 is shown. The two singlets of table 10.2 are indicated and two complete steps up and down are shown for the lowest energy surface $(110)_1$. As shown in ref. [Grimbergen et al., 1998b] the step energy in terms of bonds of the crystal graph can be calculated by the difference in surface energy of the surface bounded by $\alpha\beta\gamma\delta$ and $\alpha\beta\epsilon\kappa\gamma\delta$ which is equal to $4Z$-$2X$-$2Y$.

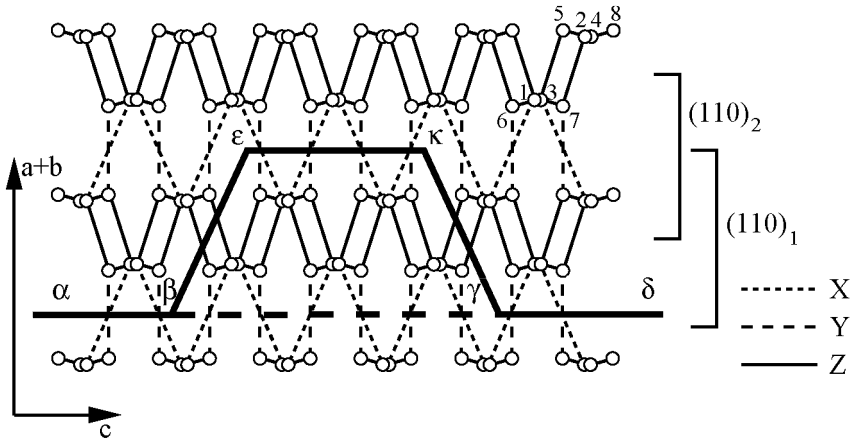

Figure 10.3: Projection of the lysozyme structure along $[1\bar{1}0]$. The two connected nets $(110)_1$ and $(110)_2$ are indicated. Starting from the surface with the lowest surface energy, two complete steps (up and down) are drawn. The clusters of molecules indicated with the numbers of the molecules in the unit cell correspond to zig-zagging DCs seen end on. These DCs consist of the bond sequence X-Z-Y-Z-X... etc.

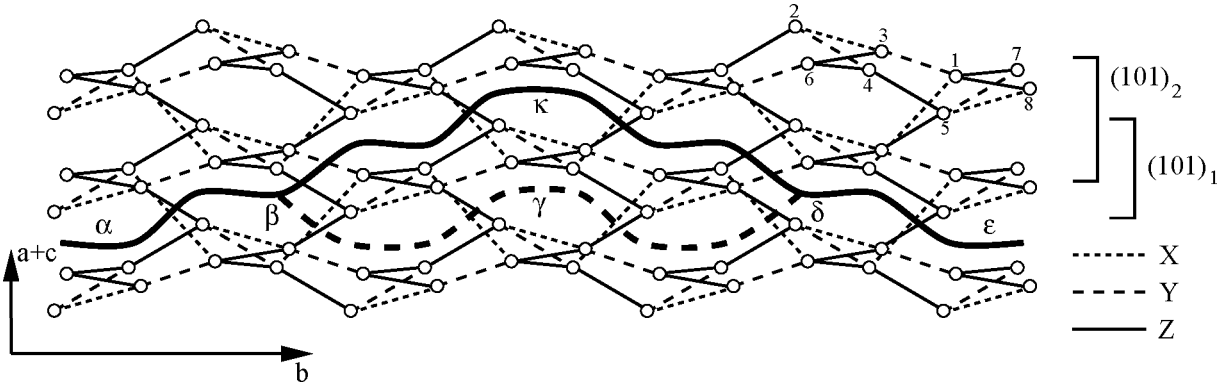

Figure 10.4: Projection of the lysozyme structure along $[\bar{1}01]$. The two connected nets $(101)_1$ and $(101)_2$ are indicated. Starting from the surface with the lowest surface energy, two complete steps (up and down) are drawn. The clusters of molecules indicated with the numbers of the molecules in the unit cell correspond to zig-zagging DCs seen end on. These DCs consist of the bond sequence *X-Y-Z-Z-X...* etc.

The step energy per unit cell for a single step along $[1\bar{1}0]$ equals exactly half of this energy (see table 10.2). Note that the step energy of two complete steps (up and down) for this face is equal to the difference in attachment energy of the two singlets $(110)_2$ and $(110)_1$. This is caused by the special bonding topology of the surface where the step and surface energy are directly related as they have bonds in common. Steps along [001] always involve a step energy equal to the sum of the bond energies of two bonds X, Y or Z for a single step.

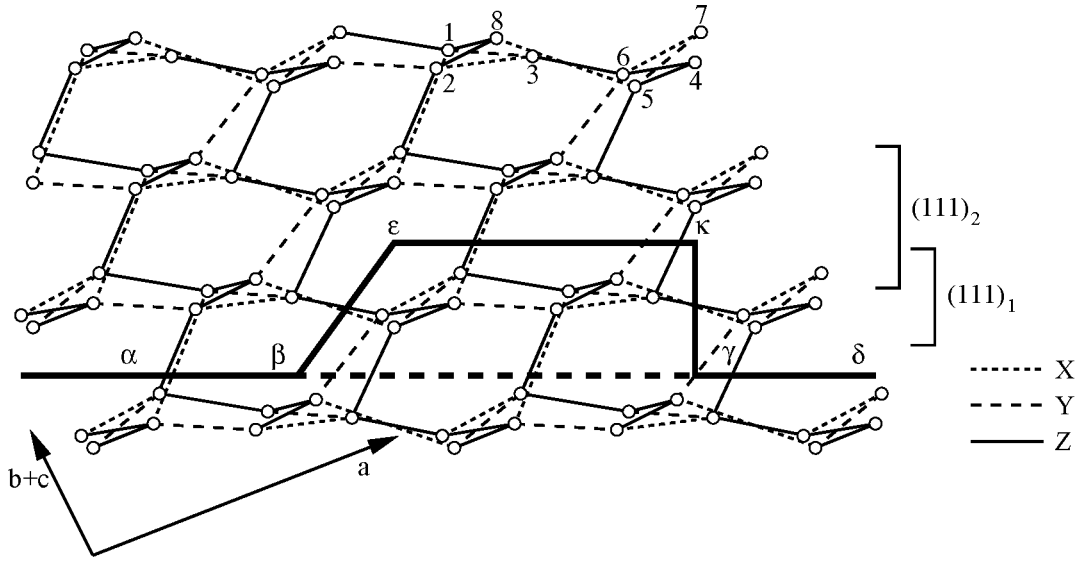

Figure 10.5: Projection of the lysozyme structure along $[01\bar{1}]$. The two connected nets $(111)_1$ and $(111)_2$ are indicated. Starting from the surface with the lowest surface energy, two complete steps are drawn. The clusters of molecules indicated with the numbers of the molecules in the unit cell correspond to zig-zagging DCs seen end on. These DCs consist of the bond sequence *X-Y-Z-Z-X...* etc.

A comparable situation is found for the (101) face. Figure 10.4 shows a $[\bar{1}01]$ projection of the lysozyme crystal structure. The two connected nets $(101)_1$ and $(101)_2$ are indicated and again two complete steps up and down along $[\bar{1}01]$ are drawn. In this case the connected nets $(101)_1$ and $(101)_2$ both represent an undulating surface configuration. Like for the (110) face, the step energy can be derived from the difference in surface energy of the surface with and without steps. The difference in surface energy of the surface $\alpha\beta\gamma\delta\epsilon$ and $\alpha\beta\kappa\delta\epsilon$ is equal to $2Y$-$2X$, which again equals the difference in attachment energy for $(101)_2$ and $(101)_1$ due to the special bonding topology. Despite the fact that for this surface the step up (left hand side) and step down (right hand side) are topologically not equivalent, the step energy of these steps is the same and equals Y-X per unit cell. Steps along [010], again, have a step energy equal to the sum of the energies of two bonds X, Y or Z.

In contrast to the (110) and (101) face the step energy of the (111) face cannot be derived directly from the attachment energies of the singlets $(111)_1$ and $(111)_2$. This can be attributed to the bonding topology that differs from the special bonding topology of the (110) and (101) surface. Comparing figure 10.5 with figure 10.4 and figure 10.3 it can be seen that for the (111) face the step energy is not equal for an up (left hand side) and down (right hand side) step. The step energy of the step up is equal to X-Y and for the step down X+Z.

10.4 Disordered flat phases

A disordered flat (DOF) phase is a surface phase in between the flat and rough phase. On a small scale the surface is disordered while on a larger scale an ordering of steps up and down exists [Rommelse and den Nijs, 1987, den Nijs and Rommelse, 1989]. Recently, it was shown that specific crystal faces of organic molecules can exhibit a DOF phase. Theoretical [Grimbergen et al., 1998a] and experimental [Grimbergen et al., 1998c] evidence for the presence of a DOF phase was found for the {011} faces of naphthalene.

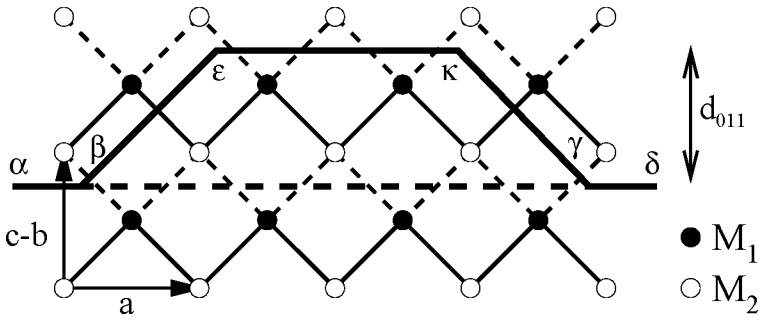

Figure 10.6: $[0\bar{1}1]$ Projection of a simplified naphthalene structure according to ref. [Grimbergen et al., 1998a]. Strong PBCs are located on top of the molecule centers and are seen end on. A complete step up and down is indicated for the (011) face.

The complete phase diagram for these types of crystal face shows that on increasing the temperature a preroughening (PR) transition is observed at $T{=}T^{PR}$ which is a phase transition from a flat into a DOF phase. When the temperature is increased even more a phase transition is found where the DOF phase transforms into a rough phase at $T{=}T^{R}$. This is a conventional Kosterlitz-Thouless (KT) transition type [Grimbergen et al., 1998a]. The growth behaviour of a DOF phase has not been studied in detail yet, but it is clear that at PR the step energy drops drastically. Therefore, the 2-D nucleation barrier for crystal faces at $T{>}T^{PR}$ is very small [Grimbergen et al., 1998a].

When the surface bonding topology of the {110} and {101} faces of the tetragonal lysozyme structure is compared with the bonding topology of the (011) face of the naphthalene structure it becomes clear that they are comparable. In figure 10.6 it is shown that along the $[0\bar{1}1]$ direction there are very strong DCs which cause a large step energy. In contrast, the step energy along the [100] direction, as indicated in the figure, is determined by the difference in bond energy of the dashed and solid bonds.

In figure 10.3 and figure 10.4 an equivalent topology is found for the {110} and {101} faces of lysozyme. In those cases the indicated step energies are also determined by a difference in bond energy and in the direction perpendicular to these steps strong (zigzagging) DCs determine the step energy. To our opinion the {110} and {101} faces of tetragonal lysozyme can be compared directly to the generic model of the (011) face of naphthalene as presented in ref. [Grimbergen et al., 1998a]. Therefore, the phase diagram of this model will also apply to the {110} and {101} faces of lysozyme which implies that DOF surface phases may occur depending on the temperature. This generic model was also treated in a broader perspective of different generic models by Grimbergen et al. [Grimbergen et al., 1999a].

10.5 Discussion

Using the results of the connected net and step energy analysis, it is possible to explain the relation between the growth morphology and the supersaturation as presented in figure 10.1. The results of the connected net analysis are compared with the MC simulation data of Durbin and Feher [Durbin and Feher, 1991] for different ratios of bond energies $X{:}Y{:}Z$. Apart from the relative growth rates, the observed surface structure will be derived. Sometimes the results for different bond energy ratios will be compared. It is then assumed that the values for the growth rate found by Durbin and Feher have not been corrected for the differences in crystallization energy. The relative attachment and step energies for all connected nets of table 10.2 are given for the different bond energy ratios in table 10.3.

10.5.1 Growth rates

The most important result of the MC simulations was that the experimental growth curves for (110) and (101) could be reproduced using a bond ratio of X:Y:Z=2:4:5. However, other ratios of bonds were also simulated as shown in figure 10.7.

For a bond energy ratio of X:Y:Z=1:1:1 the attachment energies for all connected nets except $(111)_2$ are equivalent (see table 10.3). As a result the step energies of the {110} and {101} faces are zero and for the {111} faces the energy of a step up is zero (see figure 10.5). Therefore, the roughening temperature of the {110} and {101} faces will be zero kelvin. Due to the fact that the step energy has become zero along a single direction $[uvw]$, the nucleation barrier for 2-D nucleation vanishes and the faces will grow relatively fast already at low supersaturations. The MC results for this ratio (figure 10.7) show that the growth rate of the (101) face is lower than the growth rate of the (110) face. This can be attributed to the SOS restriction used in the MC simulations. For rough surfaces, the SOS condition which was applied for the {101} faces results in a smaller sticking fraction [Durbin and Feher, 1991, Grimbergen et al., 1999a].

According to the present connected net analysis it can be concluded that a lysozyme crystal would be bounded by {111} faces assuming a bond ratio of X:Y:Z=1:1:1 due to the finite step energy (X + Z) for a step down.

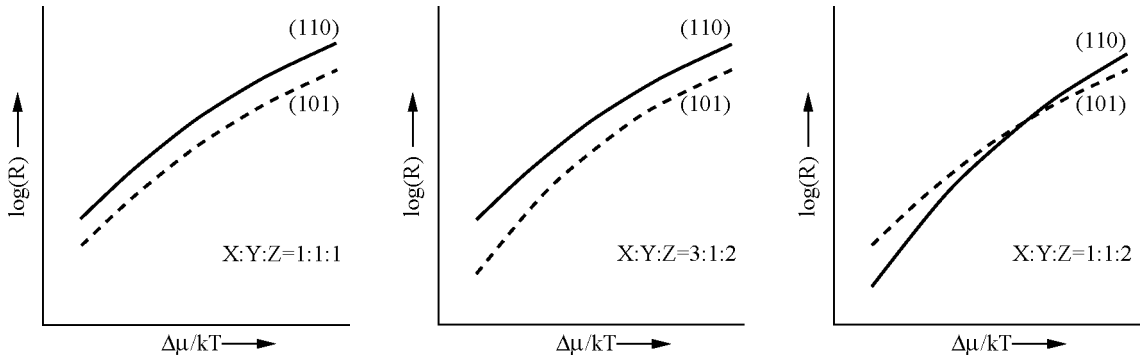

Figure 10.7: Growth rates versus supersaturation of the {110} and {101} faces for different X:Y:Z bond energy ratios obtained from MC simulations. A bond energy Φ/kT=8 was used. Reprinted from S.D. Durbin and G. Feher *J. Crystal Growth* **110** (1991) p.45 with kind permission of Elsevier Science-NL, Sara Burgerhartstraat 25, 1055 KV Amsterdam.

A bond ratio of X:Y:Z=3:1:2 gives rise to an interesting situation. The ratio of attachment energies of the most favourable connected nets for each orientation are: $E^{att}_{110_1}$=$E^{att}_{110_2}$:$E^{att}_{101_2}$:$E^{att}_{111_1}$=4:3:4. The step energy of the most favourable (101) connected net is larger than zero, whereas the step energy of the (110) face is zero. For the (111) face both the step up (see figure 10.5 left side) and down (figure 10.5 right side) are larger than zero for this bond ratio. The zero step energy for the (110) face results in (pseudo) symmetry roughening and the 2-D nucleation barrier vanishes. However, the (111) and (101) face may grow by a layer-by-layer mechanism at low supersaturations. Because of the comparable attachment energy of the (111) face with respect to the (101) face, this face would occur on the growth morphology. The MC results in figure 10.7 show that at

low supersaturation the growth rate of the (101) face is somewhat lower as compared to the simulation with X:Y:Z=1:1:1 due to the nucleation barrier whereas the (110) face shows no nucleation depression. This is in correspondence with the step energies.

For a bond ratio of X:Y:Z=3:1:2 the morphology of the lysozyme crystal based on the attachment energies would be determined mainly by {101} faces (see figure 10.1, high supersaturation) as the {111} faces were not considered in the MC experiments. Note that reversing the ratio for X and Y (X:Y:Z=1:3:2) does not affect the step energies of the {110} and {101} faces and also not the attachment energies (see table 10.2) due the symmetry of the bonds. The only difference would be that the attachment energy of $(101)_1$ and $(101)_2$ is reversed making $(101)_2$ the preferred surface configuration instead of $(101)_1$. This symmetry was also found in the MC simulation data [Durbin and Feher, 1991]. A special situation occurs for the (111) face. The step energy for a step down (figure 10.5 right side) is larger than zero, but the step energy for a step up (figure 10.5 left side) is smaller than zero. For the creation of a 2-D nucleus both steps are formed and the overall step energy (step up +step down) is larger than zero. Therefore, there is still a nucleation barrier. Thus, the mentioned symmetric behaviour for the (110) and (101) face is not found for the (111) face.

Table 10.3: Relative attachment energies of the two most favourable singlets of each face (hkl) for different bond ratios X:Y:Z. The connected nets are indicated as $(hkl)_n$. The resulting step energies for each connected net or surface configuration $(hkl)_n$ are also given. Note, that the crystallization energies for the different bond energy ratios differ.

face	X:Y:Z=1:1:1		X:Y:Z=3:1:2		X:Y:Z=1:1:2		X:Y:Z=2:4:5	
(hkl)	$E^{att}_{(hkl)_n}$	$E^{step}_{(hkl)_n}$	$E^{att}_{(hkl)_n}$	$E^{step}_{(hkl)_n}$	$E^{att}_{(hkl)_n}$	$E^{step}_{(hkl)_n}$	$E^{att}_{(hkl)_n}$	$E^{step}_{(hkl)_n}$
$(110)_1$	4	0	8	0	4	2	12	4
$(110)_2$	4	0	8	0	8	-2	20	-4
$(101)_1$	4	0	10	-2	6	0	14	2
$(101)_2$	4	0	6	2	6	0	18	-2
$(111)_1$	4	0	8	2	6	0	16	-2
$(111)_2$	7	0	17	-2	9	0	22	2

In case a bond ratio of X:Y:Z=1:1:2 is chosen, the ratio of attachment energies equals $E^{att}_{110_1}$:$E^{att}_{101_1}$($=E^{att}_{101_2}$):$E^{att}_{111_1}$=2:3:3. The step energy of the (101) face is zero (pseudo symmetry roughening) and the step energy of a step up for the (111) face is zero. In contrast, the step energy of the (110) face is rather high resulting in a nucleation barrier. This is reflected in the MC data as shown in figure 10.7. At low supersaturations the growth rate of the (110) face is smaller than that of the (101) face due to the nucleation barrier. When the supersaturation is increased, the nucleation barrier vanishes eventually and a cross-over in growth rates takes place. At high supersaturation both the (110) and (101) face do not have a nucleation barrier anymore. Although the attachment energy of the (110) face is equal in the case of a bond energy ratio X:Y:Z=1:1:1, the relative growth rate of this face at high supersaturations is relatively small for the present bond ratio (see figure 10.7). Thus, even at high supersaturations the finite step energy for the present sit-

uation seems to reduce the growth rate as compared to the case X:Y:Z=1:1:1, for which the step energy equals zero. Comparing the attachment energies (and step energies) for $(110)_1$ and (101) one would expect that the latter has the highest growth rate. On the other hand, at high supersaturations the distinction between the attachment energy of the $(hkl)_1$ and the $(hkl)_2$ face will be less relevant as all bonds that make up these energies play a role in the growth process. In other words, once the nucleation barrier, if present, has been overcome both attachment energies will become as important, especially at the highest supersaturations. The average attachment energy of $(110)_1$ and $(110)_2$ is equal to that of (101). Therefore, the growth rates of both faces would become equal at high supersaturations. The cross-over of the growth curves must be attributed to the applied SOS conditions for the {110} and {101} faces [Durbin and Feher, 1991].

Durbin and Feher have shown that a bond ratio of X:Y:Z=2:4:5 reproduced the experimental data. This ratio is reflected in the bonding distances (distance between the centers of the molecules which are mutually bonded), which is 37.67Å for the X-bond, 30.12Å for the Y-bond and 25.96Å for the Z-bond. In the light of the attachment energies and step energies the choice of bonds which resulted in an optimal fit of the MC data with the experimental results can be understood. The above mentioned bond ratio results in a ratio of the attachment energies of $E^{att}_{110_1}$:$E^{att}_{101_1}$:$E^{att}_{111_1}$=6:7:8 and a ratio of step energies of E^{step}_{110}:E^{step}_{101}=2:1. The step energies for (111) are -2 for a step up and 7 for a step down. The overall step energies for all orientations are larger than zero and therefore symmetry roughening does not occur. Considering the {110} and {101} faces, the {110} faces have the largest nucleation barrier resulting in the smallest relative growth rate at low supersaturation. At higher supersaturations the nucleation barrier vanishes and cross-over behaviour is observed as shown in figure 10.1. As in the case X:Y:Z=1:1:2 the average attachment energies of the (110) and the (101) face are equal. Therefore, one would expect comparable growth rates at high supersaturations. Once again, the cross-over behaviour must be attributed to the difference in SOS condition applied for the {110} and {101} faces.

Regarding the possible presence of oligomeric growth units the following has to be noted. For oligomeric growth units the crystal graph will be a sub-graph of the one used in the present paper. Nevertheless, the essentials of the connected net analysis will not be affected as the connected nets in figures 10.3, 10.4 and 10.5 all contain strong DCs parallel to the crystallographic directions of the low energy steps, that is along the projection directions in those figures. These DCs contain four molecules. Oligomeric growth units can be integrated into these DCs during the growth process. Such an integration does not alter the step energies as derived in the monomeric connected net analysis. Therefore, the conclusions drawn from the present analysis will also apply to the oligomeric case. Of course the absolute growth rates of the faces could change as the kinetics of incorporation of oligomers is expected to be more complicated. The situation is expected to change when the aggregates become very large (typically $>$ 8 molecules) in which case a connected net analysis will not be very meaningful.

10.5.2 Surface structure

The surface structure of the {110} and {101} faces of lysozyme has been studied by electron micrographs [Durbin and Feher, 1990] and AFM [Durbin and Carlson, 1992, Durbin and Feher, 1993]. It was found that the {110} faces show 2-D nuclei which are clearly elongated along the $[\bar{1}10]$ direction ($v_{\bar{1}10}^{step} > v_{001}^{step}$). This can be explained by the step energies of steps in the [001] and $[\bar{1}10]$ direction. From the connected net analysis it was found that steps along the $[\bar{1}10]$ direction (the corresponding step velocity is v_{001}^{step}) have a small step energy as compared with steps along [001] ($v_{\bar{1}10}^{step}$) as can be observed in figure 10.3. Therefore, the growth rate of a step in the [001] direction will be relatively high as compared with the growth rate of steps in the $[\bar{1}10]$ direction resulting in ellipsoidal 2-D nuclei as observed in experiments. Also ellipsoidal spirals were observed which have the same elongated shape.

For the (101) direction the same behaviour is reported, although the pictures of 2-D nuclei on this surface are less regular as compared to the (110) face. In the previous section it was shown that for a bond ratio of X:Y:Z=2:4:5 the step energy ratio equals E_{110}^{step}:E_{101}^{step}=2:1. Due to the smaller step energy the (101) face will enter the DOF phase at lower temperatures than the (110) face. The experimental fact that the 2-D nuclei are irregularly shaped may be attributed to the presence of a DOF phase for the (101) face whereas the (110) face will still be in the flat phase.

The small step energy of steps on the (110) face along the $[1\bar{1}0]$ direction give rise to a relatively small nucleation barrier which explains the observed 2-D nucleation growth for these faces at relatively low supersaturation [Durbin and Feher, 1993].

10.6 Conclusions

In this paper it is shown that the growth and surface morphology of tetragonal lysozyme crystals can be explained by a connected net analysis based on three different bond types X, Y and Z. Depending on the ratio of bond strenghts of these bonds flat or rough growth occurs. Previously published experimental and MC results can be explained in detail taking the attachment and step energies into account. The remarkable supersaturation dependence of the relative growth rates of the {110} and {101} faces, which is observed experimentally, follows directly from the analysis. It is shown that a DOF surface phase may occur depending on the relative bond strengths and temperature. In the future in-situ X-ray diffraction measurements on lysozyme crystal surfaces as a function of temperature might provide direct evidence for the presence of a DOF surface phase.

Acknowledgements

R.F.P. Grimbergen acknowledges the financial support of the Dutch Technology Foundation (STW).

Chapter 11

The Growth Morphology of Cesium Halide Crystals Evidence for Surface Phase Transitions

The Growth Morphology of Cesium Halide Crystals Evidence for Surface Phase Transitions

R.F.P. Grimbergen, G. Bögels and H. Meekes

Abstract

The theoretical growth morphology for bcc cesium halides (CsCl, CsBr and CsI) is derived from the crystal structure taking multiple connected nets into account. Connected nets were found for the {001}, {110} and {111} orientations. Apart from a normal flat surface phase, also c2x2 reconstructed, disordered flat (DOF) and rough phase may occur for these types of crystal face. Experimental results for cesium halide crystals grown from the vapour phase show a transition from a cubic to a dodecahedral habit on increasing the supersaturation or decreasing the ionic character of the halide. The growth temperature appears to be a very critical parameter and determines whether this transition is observed. The morphological change is attributed to the growth behaviour of the {001} faces and is explained by a transition from the c2x2 reconstructed phase into a DOF or rough phase.

11.1 Introduction

A well-known theory for the prediction of crystal morphology starting from the crystal structure is the Hartman-Perdok theory. Recently, some extensions were added to this theory which made it possible to understand the growth behaviour of crystal faces for which more than one surface configuration or connected net exist [Grimbergen et al., 1998b, Meekes et al., 1998, Grimbergen et al., 1999a]. It was found that the presence of multiple connected nets for a single orientation can lead to an unexpectedly small or even zero step free energy. This results in high growth rates for such a face even at low supersaturations and in a low roughening temperature T^R. Experimental evidence for this behaviour was found for the {110} faces of orthorhombic n-paraffin crystals [Grimbergen et al., 1998d], the {011} faces of naphthalene [Grimbergen et al., 1998c], the {101} faces of the protein lysozyme [Grimbergen et al., 1999b] and many faces in triacylglyceride (fat) crystals [Hollander et al.,]. For the {011} faces of naphthalene the presence of a so-called disordered flat (DOF) phase was identified [Grimbergen et al., 1998a].

The Disordered flat phase was first described by Rommelse and den Nijs [Rommelse and den Nijs, 1987, den Nijs and Rommelse, 1989] for a simple restricted SOS model and can be regarded as a surface phase which is locally disordered but ordered (flat) on a macroscopic scale. The growth characteristics of DOF surfaces have not been studied in great detail yet, but there are indications that these faces can grow relatively fast while staying flat on a macroscopic scale and that the step free energy drops dramatically at the transition from a flat into a DOF phase [Grimbergen et al., 1998c, Grimbergen et al., 1999a].

A generalized statistical thermodynamical surface model of the {001} faces of the CsCl structure has been studied in detail by Mazzeo et al. [Mazzeo et al., 1995]. They derived the phase diagram for these types of face based on the so-called staggered BCSOS model. Three surface phases were identified, a flat, a DOF and a c2x2 reconstructed phase depending on the temperature and anisotropy of the cation-cation and anion-anion interaction. More recently, Davidson et al. [Davidson and den Nijs, 1997] showed that for these types of crystal face also a deconstructed rough phase can be identified.

In the present paper the influence of these surface phases on the growth morphology of cesium halides (CsCl, CsBr and CsI) is studied. A connected net analysis is performed and the results are interpreted using the statistical thermodynamical results of the BCSOS model. This series of crystals was chosen because of the simplicity of the structure and the presence of orientations containing multiple connected nets. The anisotropy between the anion-anion and cation-cation interactions, which is an important parameter in the BCSOS models, increases in the series going from CsCl to CsI. Moreover, the crystals can be grown from the vapour phase which excludes any effects of a solvent or melt on the crystal morphology.

This paper is organized as follows. The results of the connected net analysis of section 11.2 lead to a predicted growth morphology (subsection 11.2.5). These predictions are confronted with Monte Carlo growth simulations (section 11.3) and results of vapour growth experiments in section 11.4. Experimental and theoretical results are compared and discussed in section 11.6 and in section 11.7 some conclusions are drawn.

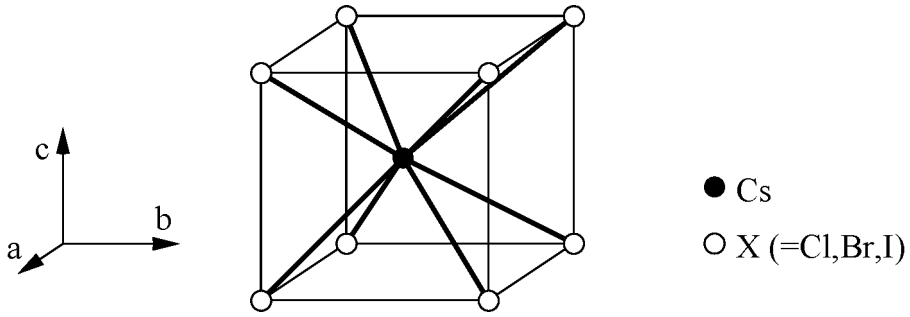

Figure 11.1: The crystal graph for the bcc cesium halides.

11.2 Connected net analysis

In this section all connected nets for CsCl, CsBr and CsI are derived from the crystal structure. See ref. [Grimbergen et al., 1998b] for a general review of the connected net analysis. Note that the results of this analysis are generally applicable to CsCl-type structures. The connected nets were derived from the crystal graph using the program FACELIFT [Grimbergen et al., 1997].

Cesium halides crystallize in either a body-centered (bcc) cesium chloride or face-centered (fcc) rock-salt structure. For instance, CsF crystallizes in a fcc lattice whereas

CsCl has either a fcc T>479°C or bcc T<479°C lattice [Rao and Rao, 1978]. For CsBr and CsI only the bcc structure is found. In the present study the attention is focused on the bcc structure. The spacegroup for the bcc structures is Pm3m and the lattice constants are 4.112Å (CsCl), 4.287Å (CsBr) and 4.560Å (CsI) [han, 1994]. For the spacegroup Pm3m there are no selection rules for the Miller indices (hkl) [Tables, 1969]. Apart from the lattice constants, the crystal lattices are identical and therefore a single generalized crystal graph was defined as shown in figure 11.1. In the crystal graph the cesium and halide atoms are represented as spheres and the interactions between the atoms as bonds between the spheres. In the connected net analysis only first nearest neighbour bonds were taken into account. The nearest neighbour interaction energy is defined as Φ.

In table 11.1 the results of the connected net analysis based on the crystal graph of figure 11.1 are presented. Due to the limited number of growth units in the unit cell and limited number of bonds used in the connected net analysis, only five connected nets exist.

Table 11.1: The connected nets of the crystal graph in figure 11.1. The interplanar distance d_{hkl} in terms of the lattice constant a, the number of connected nets found and the symmetry relation between the connected nets are given.

{hkl}	d_{hkl}	Nr.	Symmetry
{001}	a	2	$\bar{1}$
{110}	$\frac{1}{2}\sqrt{2}\ a$	1	-
{111}	$\frac{1}{3}\sqrt{3}\ a$	2	$\bar{1}$

11.2.1 The (001) orientation

For the (001) orientation two symmetry related nets were found which are depicted in figure 11.2. Since the center of symmetry is located exactly in the center of the atoms, the two connected nets can be transformed into each other by these centers. According to ref. [Meekes et al., 1998] such a symmetry relation gives rise to symmetry roughening and thus a zero step free energy. This can be understood rather easily by calculating the surface energy per mesh area of the (001) surface bounded by $\alpha\beta\gamma\delta$ and the surface bounded by $\alpha\beta\epsilon\phi\gamma\delta$ [Grimbergen et al., 1998b]. Obviously, the number of bonds cut is equivalent. Therefore, the step energy in terms of broken bonds is zero. However, there is a difference between the two connected nets. For the $(001)_1$ connected net the Cs atoms are on top, whereas for the $(001)_2$ connected net the halide atoms are at the surface; both cases result in a polar surface. The two surface configurations are related by a center of symmetry and therefore the polarity of the two connected nets is reversed. This is known as boundary swapping [Meekes et al., 1998]. Moreover, there will be effectively a surface free energy difference between the surface bounded by the cesium atoms and the surface bounded by the halide atoms.

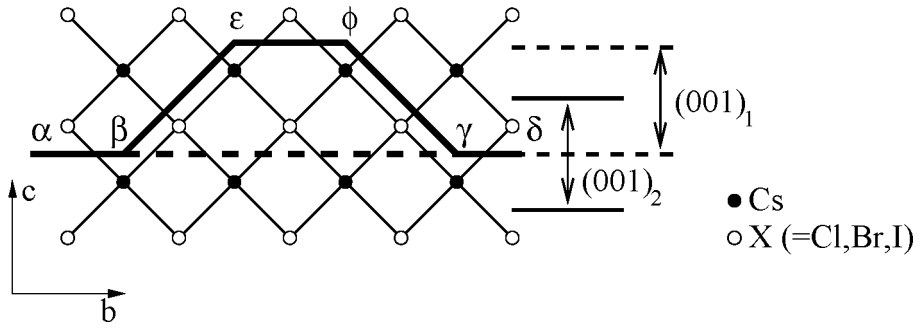

Figure 11.2: Projection along [100] of the crystal graph of figure 11.1. The two connected nets for the (001) orientation are indicated with $(001)_1$ and $(001)_2$. A complete step on the (001) face is shown.

Due to the direct relation between the surface free energy and step free energy for this type of surfaces, the effective step free energy will be non-zero. However, in practice the step free energy can be rather small.

Taking also the repulsive anion-anion and cation-cation interactions into account, it is clear that the {001} surfaces will have a relatively high surface free energy.

11.2.2 The (110) orientation

In contrast to the {001} and {111} faces for the {110} faces a single connected net is found. This is a perfectly flat apolar connected net with both cations and anions in the slice. A projection of the connected net is shown in figure 11.3. The broken bond step energy per unit cell for a step along [001] or $[1\bar{1}0]$ on the (110) face equals Φ.

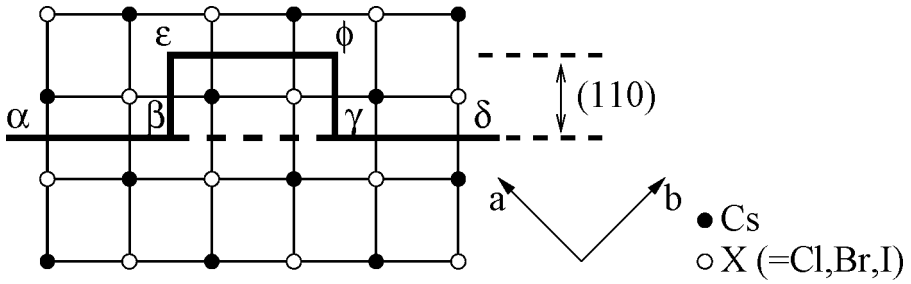

Figure 11.3: Projection along [001] of the crystal graph of figure 11.1. The connected net for the (110) orientation is indicated. A step on the (110) face is shown.

11.2.3 The (111) orientation

The (111) orientation contains, like the (001) orientation, two symmetry related connected nets. The two connected nets are shown in figure 11.4. Calculating the broken bonds of the surfaces bounded by $\alpha\beta\gamma\delta$ and $\alpha\beta\epsilon\gamma\delta$ yields equal broken bond surface energies.

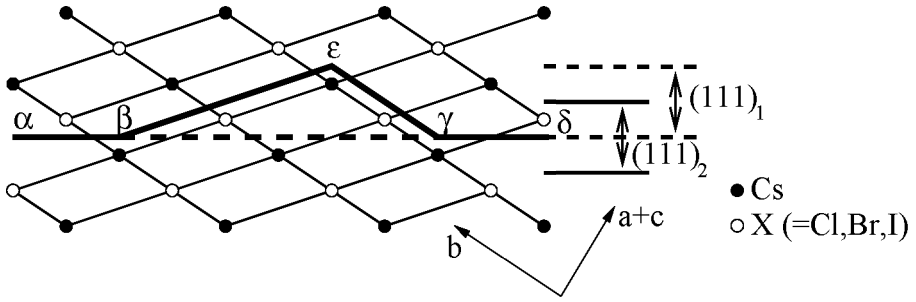

Figure 11.4: Projection along $[10\bar{1}]$ of the crystal graph of figure 11.1. The two connected nets for the (111) orientation are indicated with $(111)_1$ and $(111)_2$. A complete step on the (111) face is shown.

Therefore, the broken bond step energy is zero for the (111) orientation and symmetry roughening occurs. The situation at the interface is comparable to that of the (001) face. The $(111)_1$ connected net results in Cs atoms at the interface whereas the $(111)_2$ connected net results in halide atoms at the interface. Consequently, the surface free energy of $(111)_1$ will differ from that of $(111)_2$ and the effective step free energy will be larger than zero. Like the (001) surface, the (111) surface is polar and the polarity of the two connected nets is opposite due to boundary swapping.

Note that the ions on the {111} faces have a threefold coordination of bonds in contrast to the ions on the {001} faces which have a fourfold bonding coordination. The anion-anion and cation-cation distances for the {111} faces are larger ($\sqrt{2}a$) than for the {001} faces (a).

11.2.4 Surface reconstruction

When we go beyond the standard connected net analysis and take also the repulsive next nearest neighbour interactions into account, it becomes clear that especially the polar faces {001} and {111} become less stable. Due to the repulsive interactions between equally charged ions, it is possible that the surface reconstructs in order to reduce the repulsive interactions at the surface. For the {001} faces this reconstruction is the well-known c2x2 reconstruction as depicted in figure 11.5 [Mazzeo et al., 1995]. Note that reconstructions cannot be found by a standard connected net analysis due to the usually applied so-called flatness criterion [Grimbergen et al., 1998b].

In figure 11.5 the reconstruction is shown with the halide atoms at the surface. Note that the surface may be terminated by Cs-atoms or halide atoms. Both of these surface configurations are two-fold degenerate because an equivalent reconstructed surface is obtained by a lattice translation. An equivalent surface configuration as the one shown in figure 11.5 can for instance be found by a translation along [100] or [010].

A reconstruction of the {111} faces is less favourable as compared to the {001} faces due to the larger cation-cation and anion-anion distances. Therefore, it is expected that the {111} surfaces will not be reconstructed as easily.

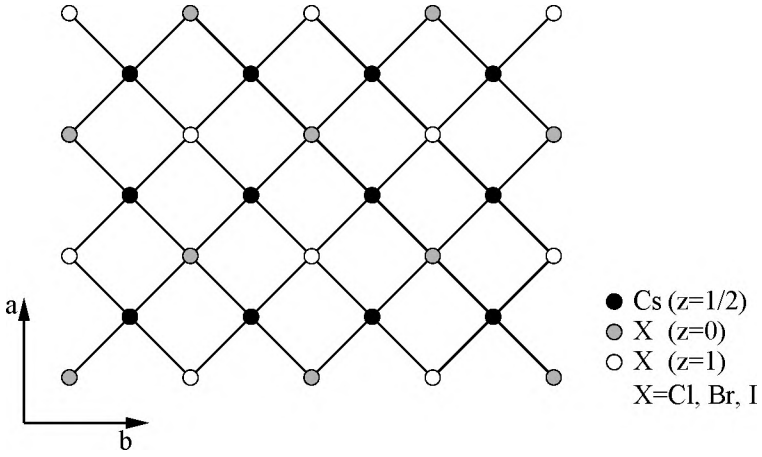

Figure 11.5: Top view on a c2x2 reconstructed (001) surface.

Surface reconstructions influence the equilibrium and growth behaviour of the crystals. As has been shown in previous papers [Grimbergen et al., 1999a,Grimbergen et al., 1998a], the transition from a flat into a DOF phase results in a dramatic decrease in the step free energy. This results in a very small nucleation barrier and relatively fast growth already at small supersaturations. Experimental evidence for this behaviour was found for the {011} faces of naphthalene [Grimbergen et al., 1998c]. The transition from a reconstructed into a DOF phase which can be expected for the {001} faces of the CsCl structure according to refs. [Mazzeo et al., 1995, Davidson and den Nijs, 1997] is also expected to have a dramatic influence on the growth behaviour of such faces. Therefore, we performed MC simulations for the {001} faces taking, apart from first nearest neighbour interactions, also next nearest neighbour repulsive interactions into account. Both equilibrium and growth simulations were done. The results are presented in section 11.3.

11.2.5 Theoretical growth morphology

The growth morphology of CsX can be derived using the classical Bravais-Friedel-Donnay-Harker law for the growth rate $R_{hkl} \propto 1/d_{hkl}$ or the relation $R_{hkl} \propto E^{att}_{hkl}$ [Hartman and Bennema, 1980] where d_{hkl} is the interplanar distance of a face and E^{att}_{hkl} is the attachment energy E^{att}_{hkl} of a face (hkl). The attachment energy is defined as the energy released per mole unit cell content when a complete growth layer attaches to the surface. Using the relation $R_{hkl} \propto 1/d_{hkl}$ results in a cubic morphology bounded by the {001} faces (figure 11.6a).

Assuming only first nearest neighbour bonds, the attachment energy is for the {001} and {110} faces 2Φ and for the {111} faces 2.5Φ. This gives rise to a cubo-dodecahedral morphology as shown in figure 11.6b. When also the low step free energies for the {001} and {111} faces are considered as deduced above, the only flat faces at moderate supersaturations will be the {110} faces resulting in a dodecahedron (figure 11.6c). This is indeed the morphology which is frequently observed.

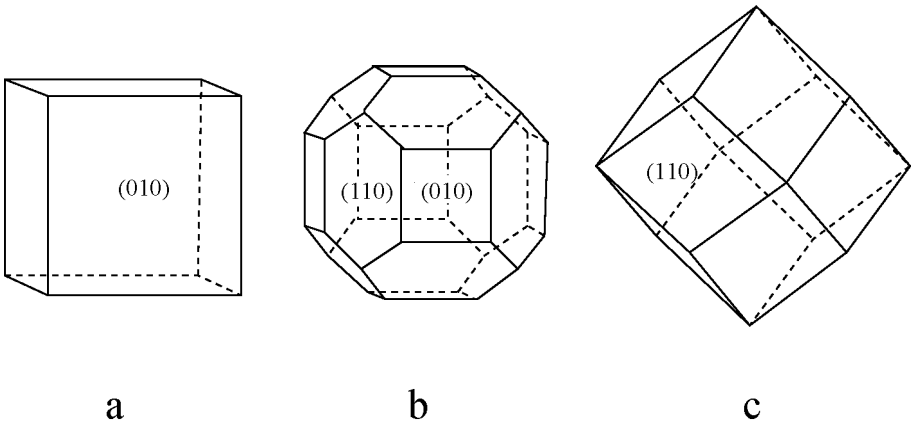

Figure 11.6: Theoretical morphologies of CsX based on (a) $R_{hkl} \propto 1/d_{hkl}$, (b) $R_{hkl} \propto E^{att}_{hkl}$ and (c) same as (b), but modified taking the step energies into account.

11.3 Monte Carlo simulations

11.3.1 Setup

In order to study the equilibrium and growth behaviour of the {100} and {110} faces of CsX a standard Monte Carlo (MC) simulation algorithm was implemented similar to the one described in ref. [Grimbergen et al., 1999a]. A simple cubic Kossel (100) model was used to model the {110} faces of CsX [Gilmer and Bennema, 1972a]. For this orientation only attractive nearest neighbour bonds were taken into account. In the simulations the bond energy per growth unit is defined as the dimensionless ratio $\Phi/\mathrm{k}T$. The rate of attachment was chosen to be proportional to the driving force $\Delta\mu$

$$K^+(\Delta\mu) = K_0^+ \exp[\Delta\mu/\mathrm{k}T], \tag{11.1}$$

where k is the Boltzmann constant, T the absolute temperature and K_0^+ is the attachment rate at equilibrium [Gilmer and Bennema, 1972a]. The rate of detachment is strongly site dependent and is given by

$$K^-(i,\Phi) = K_0^- \exp[-2\Phi/\mathrm{k}T - 2i\Phi/\mathrm{k}T], \tag{11.2}$$

where K_0^- is a constant and i is the number of nearest neighbours. The simulation of the (110) face has two free parameters: $\Phi/\mathrm{k}T$ and $\Delta\mu/\mathrm{k}T$.

The CsX (001) face is modelled by a cubic body-centered SOS (BCSOS) model with next nearest neighbour repulsive interactions in order to introduce a c2x2 reconstruction (see figure 11.7) Anisotropy is introduced in order to model the differences between the halides. The anisotropy is reflected in the next nearest neighbour repulsive interactions by defining different detachment rates for an A (Cs on top) or B (X on top) layer. This is done by implementing separate detachment rates for these layers:

$$K_A^-(i,\Phi,\Phi_1) = K_0^- \exp[-4\Phi/\mathrm{k}T - 2i\Phi_1/\mathrm{k}T] \tag{11.3}$$

and

$$K_B^-(i,\Phi,\Phi_2) = K_0^- \exp[-4\Phi/\mathrm{k}T - 2i\Phi_2/\mathrm{k}T], \tag{11.4}$$

where K_0^- is a constant, Φ is the nearest neighbour attractive bond, Φ_1 and Φ_2 are repulsive next nearest neighbour bonds for layer A and B respectively and i is the number of next nearest neighbours of a specific site.

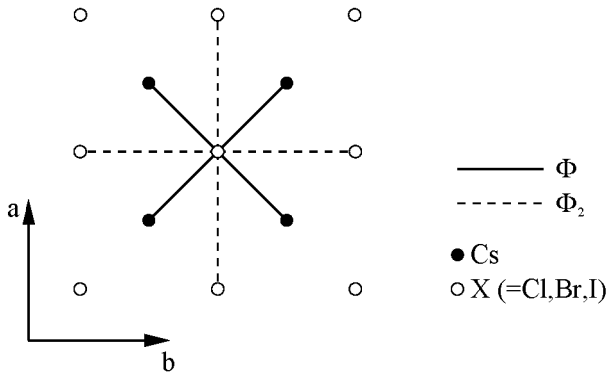

Figure 11.7: Top view on the (001) surface with X on top. The attractive bond Φ and repulsive Φ_2 bond used in the MC simulations are indicated. For Cs on top Φ_2 is replaced by Φ_1.

The relation between Φ, Φ_1 and Φ_2 was chosen as

$$\frac{1}{2}\sqrt{3}\,\Phi = -\frac{\Phi_1 + \Phi_2}{2}, \tag{11.5}$$

where the factor $\frac{1}{2}\sqrt{3}$ represents the difference in bonding distance of the repulsive next nearest neighbour bonds and the attractive nearest neighbour bonds. The anistropy δ is introduced by

$$\delta = \frac{\Phi_1}{\Phi_2}. \tag{11.6}$$

Note that the simulation for the (001) face has three independent parameters δ, $\Phi/\mathrm{k}T$ and $\Delta\mu/\mathrm{k}T$.

Sticking coefficients S for the surfaces were defined as

$$S = \frac{attachments - removals}{attachment\ attempts} \tag{11.7}$$

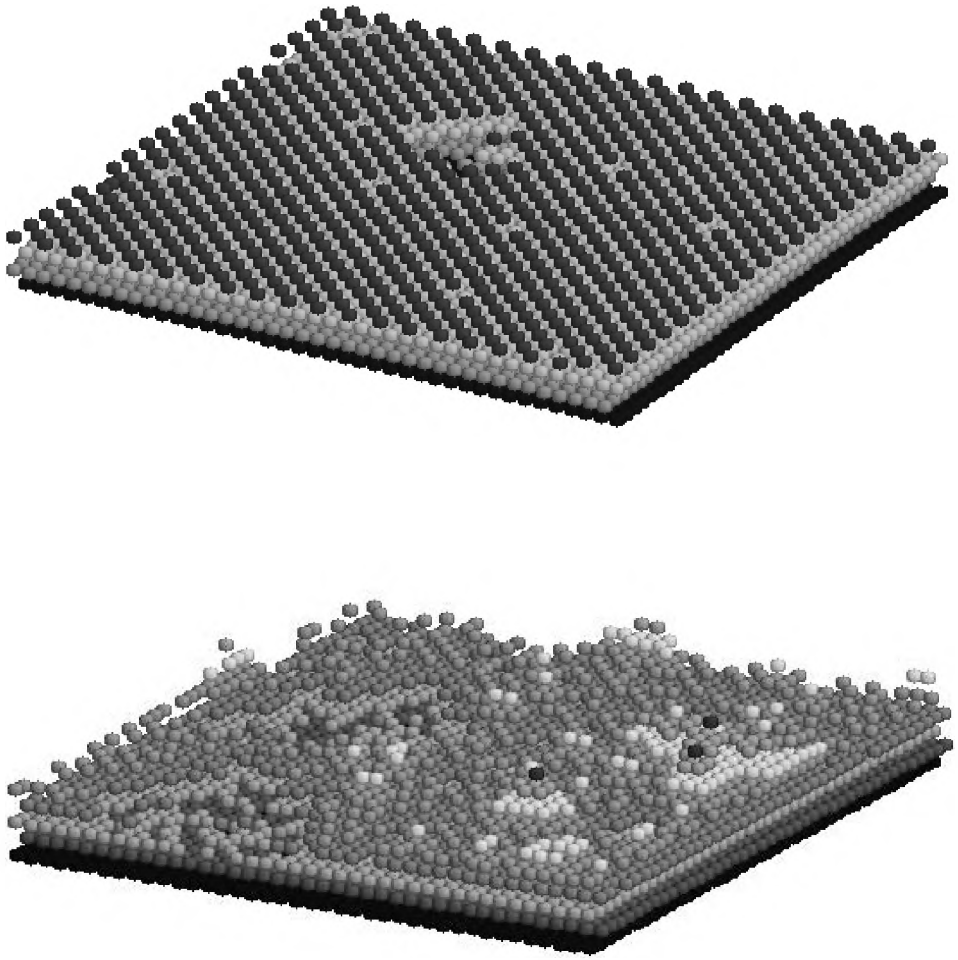

Figure 11.8: Two snapshots of the MC simulations of the (001) surface with δ=0.6. Top: c2x2 reconstructed surface at kT/Φ=0.80. Bottom: the (001) surface at a temperature of kT/Φ=1.18.

During the simulations several quantities were calculated as probe for surface phase transitions, namely the specific heat $c(T)$, the height correlation function $G(r)$ and the interface width $\sqrt{< \delta h^2 >}$ [Grimbergen et al., 1999a].

Simulations were done for square matrices (size LxL) for L=30 and L=40. For the (110) face a standard sc Kossel SOS condition was applied, whereas for the (001) face a BCSOS condition was used. The simulation time can be expressed in Monte Carlo Sweeps (MCS). A MCS corresponds to a number of attempted moves equal to the number of matrix sites. Typically simulations of $1{\cdot}10^6$-$2{\cdot}10^6$ MCS were performed after $0.5{\cdot}10^6$-$1{\cdot}10^6$ MCS equilibration.

11.3.2 Equilibrium

Equilibrium simulations were done for the (110) face and the (001) face. For the simple cubic Kossel model of the (110) face the roughening transition is known and is found at a temperature of kT^R/Φ=1.28 [Leamy and Gilmer, 1974]. For these types of surface only a flat and a rough phase exist. Our MC simulation data confirm this.

As already mentioned the situation is more complicated for the (001) face. In order to study the dependence of the phase transition temperature on the anisotropy δ, MC simulations of (001) were performed for different anisotropies. For the symmetric surface with δ=1 the surface is already rough at zero kelvin, but for δ<1 the c2x2 reconstructed surface is the most stable configuration at low temperatures [Mazzeo et al., 1995,Davidson and den Nijs, 1997]. This is indeed confirmed by the MC simulations. When the temperature was increased, the surface became more and more disordered and a surface phase transition could be identified. Two snapshots of the surface during the MC simulations at a temperature below and above the phase transition are shown in figure 11.7.

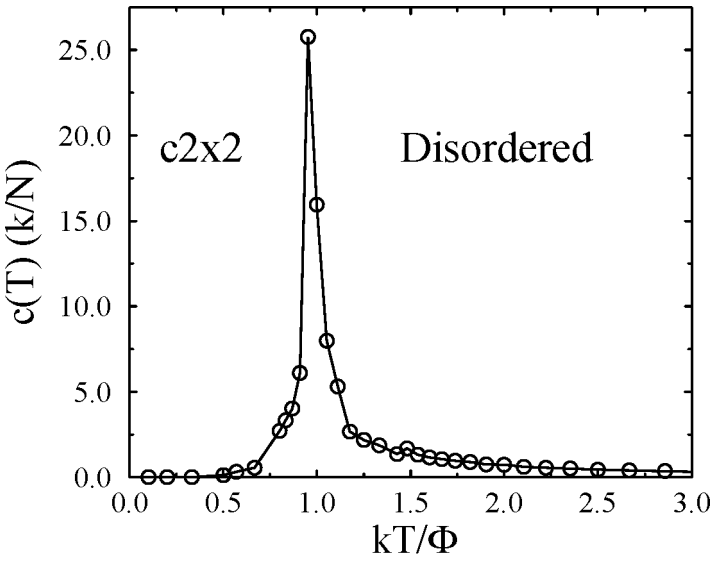

Figure 11.9: Specific heat c(T) versus the temperature kT/Φ for the (001) face with an anisotropy of δ=0.6.

In figure 11.9 the specific heat $c(T)$is plotted against the temperature kT/Φ for δ=0.6. The sharp peak indicates the phase transition. Maxima in the specific heat were found for δ=0.4 (kT/Φ=1.11), δ=0.6 (kT/Φ=0.95), δ=0.8 (kT/Φ=0.72) and δ=0.9 (kT/Φ=0.62). The phase transition temperatures increase with decreasing δ and the temperatures agree very well with the Ising transition line as reported in refs. [Mazzeo et al., 1995, Davidson and den Nijs, 1997]. According to these phase diagrams the phase transition will be either from a c2x2 reconstructed into a rough phase or a transition from a c2x2 reconstructed into a DOF phase. It is beyond the scope of this paper to study these transitions in detail.

11.3.3 Dynamics

In our experiments the CsX crystals are grown at a certain temperature and supersaturation $\Delta\mu$. Therefore influence of the supersaturation was modelled by MC simulations with $\Delta\mu/\mathrm{k}T>0$. First a series of simulations was done to determine the influence of the temperature on the sticking fraction S of both the {110} and {001} faces. For that purpose simulations were performed keeping the supersaturation at a fixed value while increasing the temperature. An example is given in figure 11.10 for the (110) face and the (001) face (δ=0.9).

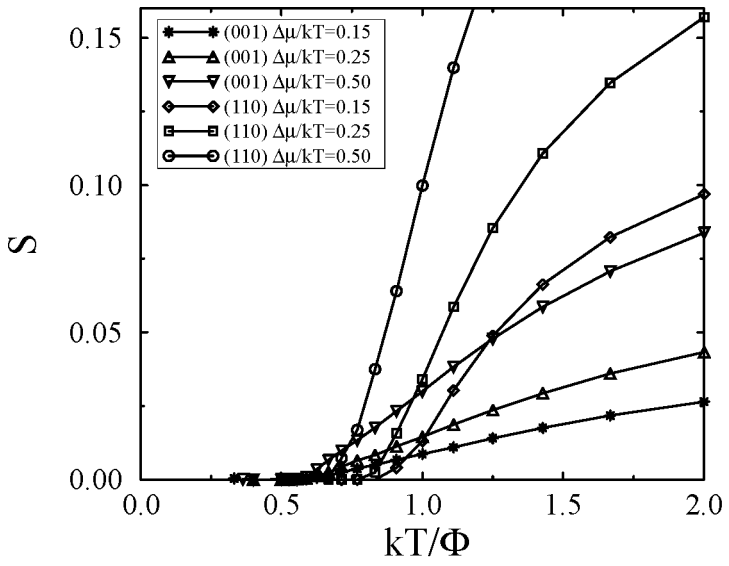

Figure 11.10: Sticking fraction S versus temperature $\mathrm{k}T/\Phi$ for the (110) and the (001) face (δ=0.9) of CsX at different supersaturations.

An interesting result is that the temperature at which the growth rate (or S) for the (001) face starts to increase rapidly coincides with the temperature at which a maximum in $c(T)$ was found in the equilibrium simulations. Another important result is the crossing of the growth rate curves of the {110} and {001} faces that results in a change of morphology. At low temperatures a dodecahedron ({110}) is found whereas at higher temperatures a cubic morphology ({001}) is observed. Figure 11.10 also shows that the temperature at which the crossing appears decreases when the supersaturation is increased.

In order to study the influence of the anisotropy δ on the growth rates, a series of simulations was performed keeping the supersaturation fixed while increasing the temperature for various δ for the (001) face. The results for the (110) which are independent of the anisotropy and (001) face using $\Delta\mu/\mathrm{k}T$=0.25 are plotted in figure 11.11. Decreasing δ (i.e. higher anisotropy (eq. 11.6)) results in a shift of the temperature at which growth commences to higher temperatures. This is caused by a stabilization of the c2x2 reconstructed phase for higher anisotropy as a result of the constraint given by eq. (11.5).

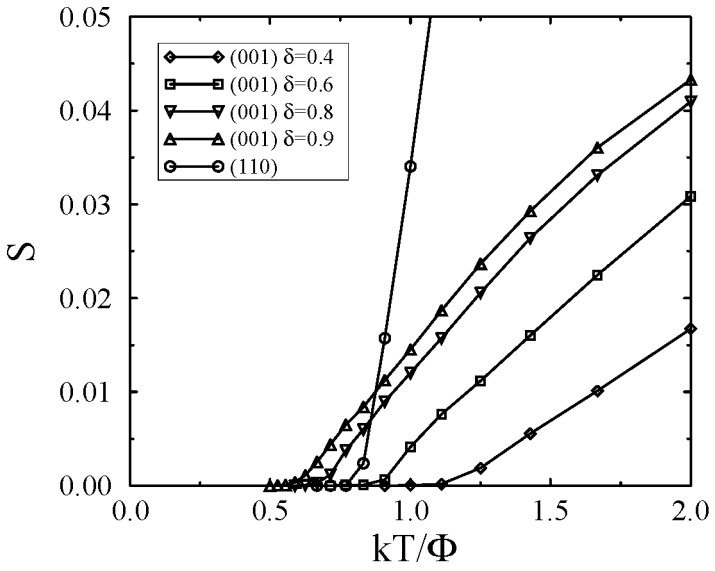

Figure 11.11: Sticking fraction S versus temperature kT/Φ for the (110) face and (001) face as a function of anisotropy δ at a fixed supersaturation of $\Delta\mu/kT$=0.25.

The result of the shift is that the crossing of growth rate curves of the {110)} and {001} faces does no longer occur for higher anisotropy. Therefore, within our model for δ=0.4 and δ=0.6 and a supersaturation $\Delta\mu/kT$=0.25 only cubic ({001}) crystals are found. For the more isotropic {001} faces (δ=0.8 and δ=0.9) dodecahedrons are observed at low temperatures and cubes at higher temperatures. For the case of δ=0.9 the morphological change is shown in figure 11.12. Due to the geometry of the lattice, the transition from {110} to {001} occurs when $R_{110} \geq \sqrt{2} R_{001}$.

As can be observed in figure 11.12, the sticking fraction of the (110) face increases very rapidly with the supersaturation when it crosses the sticking fraction curve of the {001} faces. Therefore, it is expected that the morphological transition from dodecahedrons to cubes will be observed in a very small range of temperature.

11.4 Experimental

Cesium halide crystals were grown in an evacuated quartz tube containing about 200 mg of pure CsX at temperatures of 120 degrees below the melting point T_{melt} of CsX. For matter of completeness the halides F, Cl, Br and I were studied. The background pressure just outside the tube was 10^{-6} mbar. The growth experiments were performed for a period of 10 hours. The crystals were grown on copper and quartz substrates. The temperature of the copper substrate had a gradient: a high temperature in the center of the furnace and a lower temperature to the outside. Due to this gradient different types of morphology appeared on different parts of the substrate. The temperature of the furnace and the copper substrate was measured to make it possible to determine the range of temperature differences (ΔT) for which the different morphologies were formed.

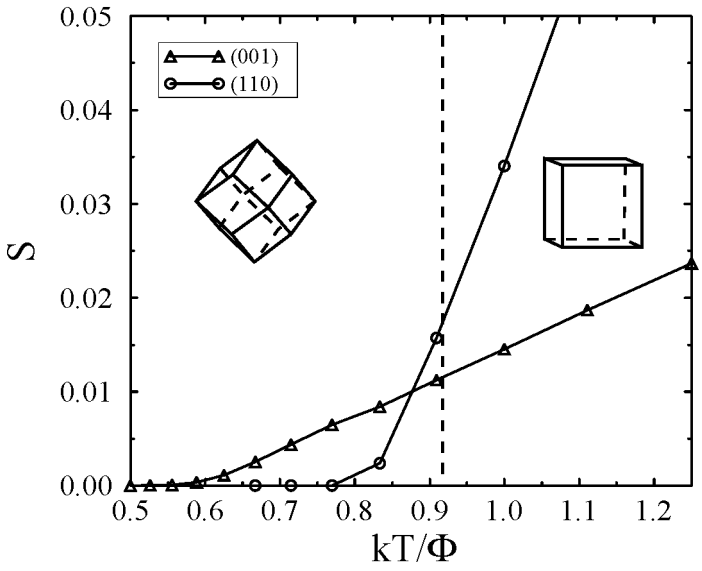

Figure 11.12: Sticking fraction S versus temperature kT/Φ for the (110) face and (001) face (δ=0.9) at a fixed supersaturation of $\Delta\mu/\mathrm{k}T$=0.25. The dashed line indicates the temperature at which the morphological change appears.

On the copper substrate a layer of at least 2 μm of badly developed morphologies appeared. On this layer single cesium halide crystals were observed. The copper substrate was placed about 25 cm in the furnace and 20 cm outside the furnace (room temperature) to obtain the temperature gradient (see figure 11.13). The temperature of the substrate was measured using six copper-constantan (type T) thermocouples using constantan wires welded in the substrate with a mutual separation of six centimeter. Four couples were placed inside the furnace and the other two outside.

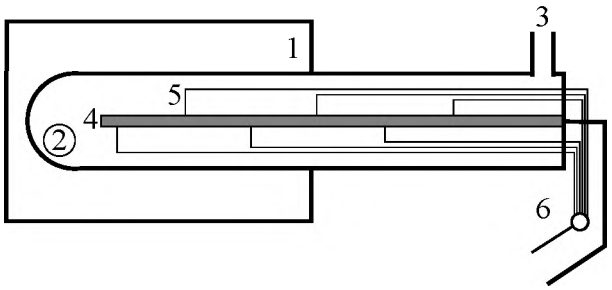

Figure 11.13: The vapour phase growth setup; (1) Furnace, (2) CsX (X=F,Cl,Br,I), (3) Vacuum pump, (4) Copper substrate, (5) Thermocouple and (6) Constantan wires.

The temperature gradient over the quartz substrate was much smaller due to the relatively small thermal conductivity of quartz as compared to copper. For quartz only the actual furnace temperatures were measured. On the quartz substrate only single crystals appeared. The single crystals grown on the copper substrate had a size between 4 and

100 μm, on the quartz substrate it was between 0.5 and 5 μm. After the growth experiments the substrate was cut in parts and prepared for examination by scanning electron microscopy (SEM). With the SEM the precise position of the different morphologies could be determined. The vacuum-pump was a Balzers TCP 1231 and the SEM used was a JEOL JSM-T300.

11.5 Experimental results

The observed morphology depended on the driving force for crystallization, that is the temperature difference between the furnace and the substrate (ΔT) and the furnace temperature. In section 11.5.1 the influence of ΔT on the morphology will be described. In section 11.5.2 the furnace temperature will be varied to study the relation between the applied furnace temperature and the morphology. The ΔT for the quartz substrate was estimated to be only a few degrees whereas for copper a minimum around one hundred degrees was found.

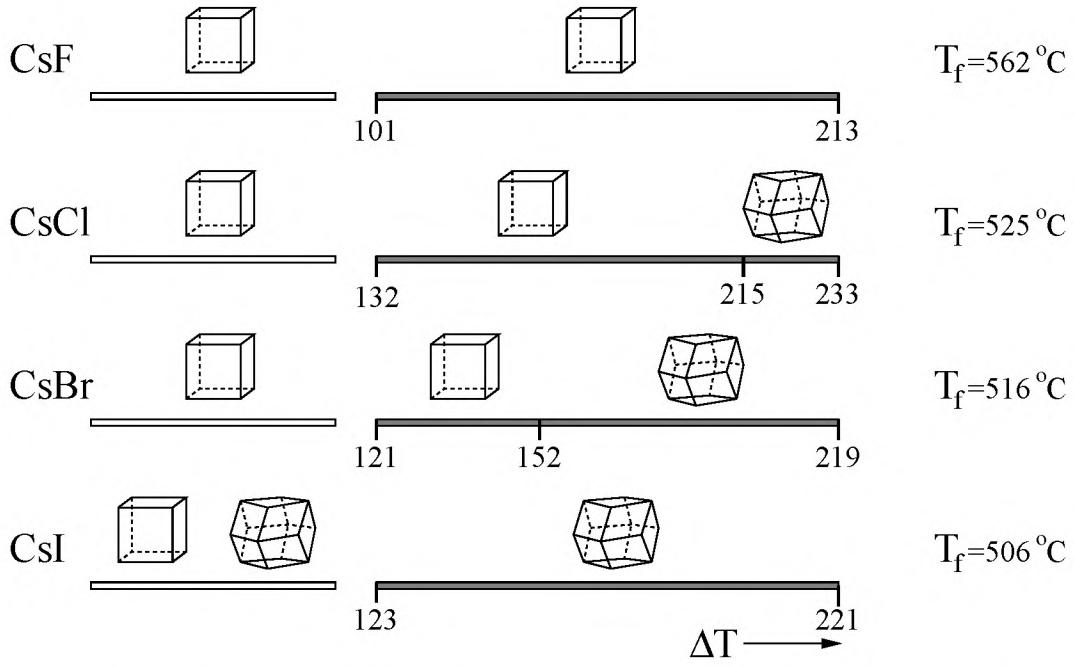

Figure 11.14: Experimental results of the vapour growth experiments. The driving force is indicated with the temperature difference ΔT. The white bar indicates the results for growth on a quartz substrate and the grey bar indicates results for growth on a copper substrate. The applied furnace temperatures T_f are indicated and were for all experiments 120°C below T_{melt} of CsX.

11.5.1 Morphology as a function of driving force

Cesium fluoride vapour-grown crystals gave a single morphology. On the quartz substrate cubic crystals were observed on the entire substrate. On the copper substrate also only cubic crystals were observed for ΔT=101°C till ΔT=213°C. This experimental result was expected due to the rocksalt fcc structure of CsF. For this type of structure the cubic faces are the most stable faces and can be compared with the {110} faces of the cesium chloride bcc structure.

Two different morphologies for cesium chloride were observed. On the quartz substrate cubic crystals were observed. The temperature on the quartz substrate was estimated to be a few degrees below the furnace temperature (525°C) and therefore higher than 479°C, the phase transition temperature of cesium chloride [Rao and Rao, 1978]. For this reason, the crystals grown on the quartz substrate were fcc-type as the CsF crystals.

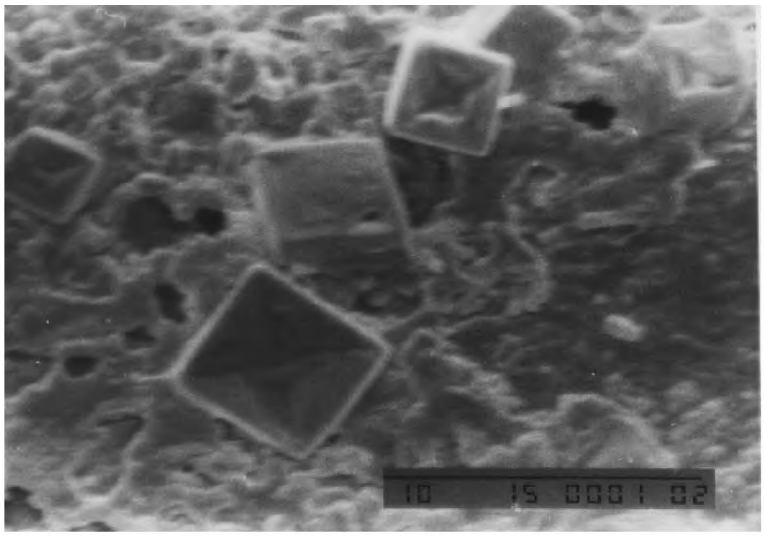

Figure 11.15: Cubic CsCl crystals grown from the vapour on a copper substrate. The scale bar represents 10μm.

On the copper substrate the highest temperature is 393°C, which is below the phase transition temperature of cesium chloride. So all crystals observed on the copper substrate have a bcc structure. From ΔT=132°C till ΔT=215°C cubic morphologies were observed on the copper substrate (see figure 11.15) whereas from ΔT=215°C till ΔT=233°C dodecahedral crystals were formed.

For cesium bromide crystals also two different morphologies were found. On the quartz substrate exclusively cubic crystals were observed. On the copper substrate cubic crystals were grown for ΔT=121°C till ΔT=152°C and dodecahedral crystals from ΔT=152°C till ΔT=219°C. An example of dodecahedral crystals is shown in figure 11.16. The furnace temperature applied for both experiments was 516°C.

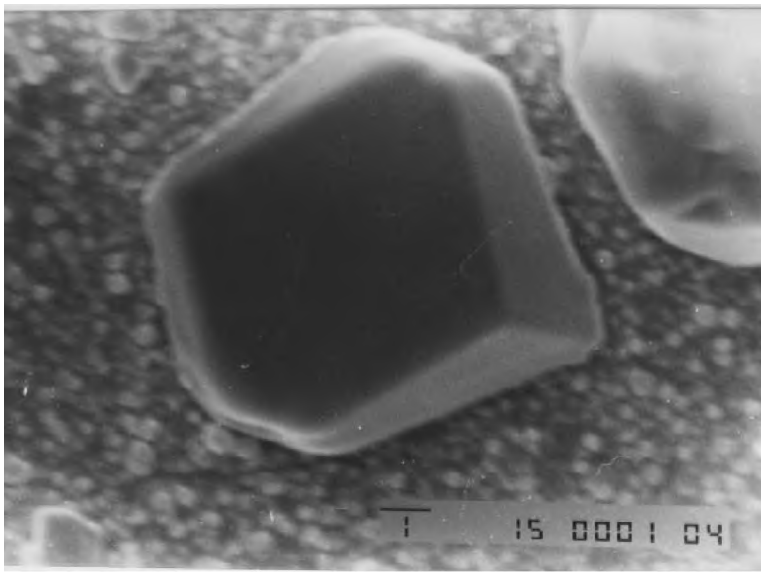

Figure 11.16: Dodecadral CsBr crystals grown from the vapour on a copper substrate. The scale bar represents 1μm.

For cesium Iodide also two distinct morphologies were observed. On the quartz substrate cubic and dodecahedral crystals were found. At relatively low ΔT on the quartz substrate cubic crystals were observed while at relatively higher ΔT dodecahedral crystals were found. On the copper substrate only dodecahedral crystals were observed from ΔT=123°C till ΔT=221°C. The furnace temperature applied for both experiments was 506°C.

11.5.2 Morphology as a function of the furnace temperature

In the previous section it was shown that for cesium chloride cubic and dodecahedral crystals were found on the copper substrate at a furnace temperature of 525°C. Increasing the funace temperature, with only 7 degrees, led to solely dodecahedral crystals over the entire length of the copper substrate. Lowering the furnace temperature with 5 degrees led to only cubic crystals on the copper substrate. The same temperature dependence was found for cesium bromide. This implies that the morphology of the cesium halide crystals is not only dependent on the ΔT but also on the furnace temperature. In fact the temperature has a much more pronounced effect as compared to the driving force ΔT.

This behaviour differs from the vapour growth of for example AgX (X=Cl, Br) [Bögels et al., 1998]. For AgX also two different morphologies appear. At relatively low ΔT cubic crystals were found whereas at higher ΔT the {111} faces became more pronounced. For AgX the furnace temperature does not influence (within the range of the measurement) the morphology of the AgX crystals.

For cesium iodide the situation is different as compared to cesium chloride and bromide. Changing the furnace temperature has no influence on the morphology. At higher temperatures only dodecahedral crystals are visible, as aspected. At lower temperatures (till 15 degrees below the furnace temperature of 506°C) also dodecahedral crystals were found on the entire lenght of the copper substrate. Lowering the furnace temperature

even more led to smaller crystals from which the morphology could not be determined even at longer growth times. This is in agreement with the observation that for cesium iodide the dodecahedral faces are stable over a wide range of ΔT as compared to cesium chloride and cesium bromide.

11.6 Discussion

The most striking result of this work is the remarkable dependence of the crystal morphology of bcc CsX crystals on the temperature of the substrate. At high substrate temperatures cubic crystals are observed, whereas at a lower substrate temperatures dodecahedrons were found independent of the halide. Both morphologies were predicted by the standard connected net analysis (figure 11.6), but the temperature dependence cannot be derived directly from such an analysis. However, this experimental result can be explained by the MC simulation data of figure 11.12. The simulation data show that the {001} faces start to grow at a temperature that coincides with the phase transition temperature (see section 11.3.2). At this temperature the c2x2 reconstructed phase turns into a DOF phase or a rough phase depending on the parameter δ. As a result, the step free energy decreases rapidly and the crystal face already grows at small driving forces which is observed in the simulations. The phase transition temperature is rather low as compared to the temperature at which the {110} faces start to grow. Due to the difference in bonding topology, the {001} faces grow relatively slow as compared to the {110} faces at higher temperatures. Therefore, a crossing in growth rates is found as shown in figure 11.12. This crossing gives rise to a morphological change from dodecahedrons ({110}) to cubes ({001}).

Moreover, the MC data demonstrate that this change may occur in a very narrow range of the temperature. This is exactly what is observed experimentally. The region in which cubo-dodecahedrons were observed was exteremly small.

The influence of the furnace temperature is very pronounced. At lower furnace temperatures cubic crystals were observed and at higher temperatures dodecahedrons. This experimental result cannot be explained by the MC simulation results.

The experiments also show that a decrease of the ionic strength of the substance (going from CsCl to CsI) leads to higher stability of the {110} faces. For the MC simulations the decrease of the ionic strength corresponds to a decrease of δ. Using the MC results presented in section 11.3 it is not possible to explain this phenomenon directly. However, when the lattice energy as a function of ionic strength is taken into account, it is clear that the bondstrength Φ used in the MC simulations has to decrease as the ionic strength decreases due to the decrease in lattice energy. Therefore, the temperature (see figure 11.11) at which the morphological transition occurs will increase going from CsCl to CsI. This is in agreement with the experimental observations (figure 11.14).

11.7 Conclusion

In this paper the experimentally observed temperature dependence of the growth morphology of CsX crystals is explained by a combination of a modern connected net analysis and MC simulations. Due the difference bonding topology of the (001) and (110) face, the (001) face starts growing at a rather low temperature or at a relatively small driving force as compared to the (110) face. However, at higher temperatures (or driving forces) the (001) face grows relatively slow but in a flat mode. This can be explained by a surface phase transtion from a c2x2 reconstructed into a DOF phase which is confirmed by MC simulations.

Acknowledgements

The authors would like to thank E. Vlieg for valuable discussions. R.F.P. Grimbergen acknowledges the financial support of the Dutch Technology Foundation (STW).

References

[han, 1994] (1994). *CRC Handbook of Chemistry and Physics (75^{th} edition)*. CRC Press Inc.

[Aihara, 1960] Aihara, A. (1960). *Bull. Chem. Soc. Jpn.*, 33:1188.

[Bastiaansen and Knops, 1996a] Bastiaansen, P. and Knops, H. (1996a). *Phys. Rev. B*, 53:126.

[Bastiaansen and Knops, 1996b] Bastiaansen, P. and Knops, H. (1996b). *J. Chem. Phys.*, 104:3822.

[Bennema, 1993] Bennema, P. (1993). *Handbook of Crystal Growth*, volume 1, chapter 7. Ed. D.T.J. Hurle (Elsevier Amsterdam).

[Bennema, 1996] Bennema, P. (1996). On the crystallographic and statistical mechanical foundations of the forty-year old hartman-perdok theory. *J. Crystal Growth*, 166:17–28.

[Bennema et al., 1992] Bennema, P., Liu, X., Lewtas, K., Tack, R., Rijpkema, J., and Roberts, K. (1992). *J. Crystal Growth*, 121:679–696.

[Bennema and van der Eerden, 1987] Bennema, P. and van der Eerden, J. (1987). *Morphology of crystals*, pages 1–75. Terra Scientific Publishing company (TERRAPUB).

[Berkovitch-Yellin, 1985] Berkovitch-Yellin, Z. (1985). *J. Am. Chem. Soc.*, 107:8239–8253.

[Bernstein, 1977] Bernstein, F. (1977). *J. Mol. Biol.*, 112:535–542.

[Berthou and Jollès, 1974] Berthou, J. and Jollès, P. (1974). *Biochem. Biophys. Acta*, 336:222.

[Besler et al., 1990] Besler, B., Merz, K., and Kollman, P. (1990). *J. Comp. Chem.*, 11:431–439.

[Bögels et al., 1998] Bögels, G., Meekes, H., Bennema, P., and Bollen, D. (1998). submitted for publication.

[Boistelle, 1980] Boistelle, R. (1980). *Current topics in material science*, volume 4, page 413. North Holland Publishing Company.

[Boistelle and Aquilano, 1977] Boistelle, R. and Aquilano, D. (1977). Interaction energy and growth mechanisms on twinned and polytypic crystals of long-chain even n-alkanes. i. interaction-energy calculations. *Acta Cryst. A*, 33:642.

[Boistelle and Doussoulin, 1976] Boistelle, R. and Doussoulin, A. (1976). Spiral growth mechanisms of the (110) faces of octacosane crystals in solution. *J. Crystal Growth*, 33:335.

[Boistelle and Madsen, 1978] Boistelle, R. and Madsen, H. L. (1978). *J. Crystal Growth*, 43:141.

[Boistelle et al., 1976] Boistelle, R., Simon, B., and Pepe, G. (1976). *Acta Cryst. B*, 32:1240.

[Bravais, 1849] Bravais, A. (1849). *Études cristallographiques, Part I: Du Cristal considéré comme un assemblage de points.* Paris.

[Broadhurst, 1962] Broadhurst, M. (1962). An analysis of the solid phase behavior of the normal paraffins. *J. Research A*, 66a(3):241.

[Brock and Dunitz, 1982] Brock, C. and Dunitz, J. (1982). *Acta Cryst. B*, 38:2218.

[Brock and Dunitz, 1990] Brock, C. and Dunitz, J. (1990). *Acta Cryst. B*, 46:795.

[Buerger, 1947] Buerger, M. (1947). The relative importance of the several faces of a crystal. *Am. Mineral.*, 32:593–606.

[Burton et al., 1951] Burton, W., Cabrera, N., and Frank, F. (1951). The growth of crystals and the equilibrium structure of their surfaces. *Philos. Trans. R. Soc. London, Ser. A*, 243:299–358.

[Curie, 1885] Curie, P. (1885). On the formation of crystals and on the capillary constants of their different faces. *Bull. Soc. Fr. Mineral.*, 8:145.

[Davidson and den Nijs, 1997] Davidson, D. and den Nijs, M. (1997). *Phys. Rev. E*, 55:1331.

[den Nijs, 1990] den Nijs, M. (1990). *Phase transitions in Surface Films*, pages 247–267. Plenum, New York.

[den Nijs, 1994] den Nijs, M. (1994). *The Chemical Physics of Solid Surfaces and Heterogeneous Catalysis*, volume 7, chapter 4. Elsevier, Amsterdam.

[den Nijs, 1997] den Nijs, M. (1997). *J. of Phys. A*, 30:397–404.

[den Nijs and Rommelse, 1989] den Nijs, M. and Rommelse, K. (1989). *Phys. Rev. B*, 40:4709–4734.

[Docherty et al., 1991] Docherty, R., Clydesdale, G., Roberts, K., and Bennema, P. (1991). *J. of Phys. D: Applied Physics*, 24:89.

[Donnay and Donnay, 1961] Donnay, J. and Donnay, G. (1961). *C.R. Acad. Sci. Paris*, 252:908–909.

[Donnay and Harker, 1937] Donnay, J. and Harker, D. (1937). A new law of crystal morphology extending the law of bravais. *Am. Mineral.*, 22:446–467.

[Doucet et al., 1981] Doucet, J., Denicolo, I., and Craievich, A. (1981). Evidence of a phase transition in the rotator phase of the odd-numbered paraffins $c_{23}h_{48}$ and $c_{25}h_{52}$. *J. Chem. Phys.*, 75(10):5125.

[Durbin and Carlson, 1992] Durbin, S. and Carlson, W. (1992). *J. Crystal Growth*, 122:71–79.

[Durbin and Feher, 1986] Durbin, S. and Feher, G. (1986). Crystal growth studies of lysozyme as a model for protein crystallization. *J. Crystal Growth*, 76:583–592.

[Durbin and Feher, 1990] Durbin, S. and Feher, G. (1990). *J. Mol. Biol.*, 212:763–774.

[Durbin and Feher, 1991] Durbin, S. and Feher, G. (1991). Simulation of lysozyme crystal growth by the monte carlo method. *J. Crystal Growth*, 110:41–51.

[Durbin and Feher, 1993] Durbin, S. and Feher, G. (1993). In situ studies of protein crystal growth by atomic force microscopy. *J. of Phys. D: Applied Physics*, 26:B128–B132.

[Elwenspoek et al., 1987] Elwenspoek, M., Bennema, P., and van der Eerden, J. (1987). *J. Crystal Growth*, 83:297.

[Elwenspoek and van der Eerden, 1987] Elwenspoek, M. and van der Eerden, J. (1987). *J. of Phys. A*, 20:669–678.

[Friedel, 1911] Friedel, G. (1911). *Leçon de Cristallographie.* Paris,Hermann.

[Geertman, 1993] Geertman, R. (1993). PhD thesis, University of Nijmegen.

[Geertman and van der Heijden, 1992] Geertman, R. and van der Heijden, A. (1992). *J. Crystal Growth*, 125:363.

[Gilmer, 1976] Gilmer, G. (1976). Growth on imperfect crystal faces. i. monte-carlo growth rates. *J. Crystal Growth*, 35:15–28.

[Gilmer and Bennema, 1972a] Gilmer, G. and Bennema, P. (1972a). Computer simulation of crystal surface structure and growth kinetics. *J. Crystal Growth*, 13/14:148–153.

[Gilmer and Bennema, 1972b] Gilmer, G. and Bennema, P. (1972b). Simulation of crystal growth with surface diffusion. *Journ. of Applied Physics*, 43:1347–1360.

[Gilmer and Jackson, 1977] Gilmer, G. and Jackson, K. (1977). *1976 Crystal Growth and Materials.* Eds. E. Kaldis and H.J. Scheel (North Holland, Amsterdam).

[Goldschmidt, 1923] Goldschmidt, V. (1913-1923). *Atlas der Kristallformen.*

[Grimbergen et al., 1999a] Grimbergen, R., Bennema, P., and Meekes, H. (1999a). On the prediction of crystal morphology. III. equilibrium and growth behaviour of crystal faces containing multiple connected nets. *Acta Cryst. A*, 55:84–94.

[Grimbergen et al., 1999b] Grimbergen, R., Boek, E., Meekes, H., and Bennema, P. (1999b). in the press.

[Grimbergen et al., 1998a] Grimbergen, R., Meekes, H., Bennema, P., Knops, H., and den Nijs, M. (1998a). Preroughening in organic crystals. *Phys. Rev. B*, 58:5258–5265.

[Grimbergen et al., 1998b] Grimbergen, R., Meekes, H., Bennema, P., Strom, C., and Vogels, L. (1998b). On the prediction of crystal morphology. I. the hartman-perdok theory revisited. *Acta Cryst. A*, 54:491–500.

[Grimbergen et al., 1997] Grimbergen, R., Meekes, H., and Boerrigter, S. (1997). C-program FACELIFT for connected net analysis, Dept. of Solid State Chemistry, University of Nijmegen.

[Grimbergen et al., 1998c] Grimbergen, R., Reedijk, M., Meekes, H., and Bennema, P. (1998c). Growth behaviour of crystal faces containing symmetry-related connected nets: A case study of naphthalene and anthracene. *J. Phys. Chem.*, B102:2646–2653.

[Grimbergen et al., 1998d] Grimbergen, R., van Hoof, P., Meekes, H., and Bennema, P. (1998d). Morphology of orthorhombic n-paraffin crystals: the influence of multiple connected nets. *J. Crystal Growth*, 191:846–860.

[Groth, 1906] Groth, P. (1906). *Chemische Kristallographie.*

[Guest et al., 1994] Guest, M., Kendrick, J., van Lenthe, J., van Schoeffel, K., and Sherwood, P. (1994). *GAMESS-UK Users Guide and Reference Manual.* Computing for Science (CFS) Ltd., Daresbury Laboratory.

[Hagler et al., 1976] Hagler, A., Huler, E., and Lifson, S. (1976). *J. Am. Chem. Soc.*, 96:5319.

[Halpin-Healy and Zhang, 1995] Halpin-Healy, T. and Zhang, Y. (1995). *Phys. Rep.*, 254:215.

[Hartman, 1973] Hartman, P. (1973). *Crystal Growth, an Introduction*, pages 367–402. North Holland Publishing Company.

[Hartman, 1978] Hartman, P. (1978). *Can. Mineral.*, 16:387–391.

[Hartman, 1987] Hartman, P. (1987). *Morphology of Crystals*, volume A, pages 269–319. Terra Scientific Publishing company (TERRAPUB).

[Hartman, 1989] Hartman, P. (1989). *J. Crystal Growth*, 96:667–672.

[Hartman, 1991] Hartman, P. (1991). Structural morphology of organic compounds having two centrosymmetric molecules in a monoclinic unit cell. *J. Crystal Growth*, 110:559.

[Hartman and Bennema, 1980] Hartman, P. and Bennema, P. (1980). The attachment energy as a habit controlling factor: I theoretical considerations. *J. Crystal Growth*, 49:145–156.

[Hartman and Heijnen, 1983] Hartman, P. and Heijnen, W. (1983). Growth mechanisms of a crystal face for which more than one surface structure is possible. *J. Crystal Growth*, 63:261–264.

[Hartman and Perdok, 1955a] Hartman, P. and Perdok, W. (1955a). *Acta Cryst.*, 8:49.

[Hartman and Perdok, 1955b] Hartman, P. and Perdok, W. (1955b). *Acta Cryst.*, 8:521.

[Hartman and Perdok, 1955c] Hartman, P. and Perdok, W. (1955c). *Acta Cryst.*, 8:525.

[Haüy, 1792] Haüy, R. (1792). *J. Phys.*, 19:366.

[Herring, 1953] Herring, C. (1953). *in Structure and properties of solid surfaces*, pages 5–81. Chicago Press.

[Hoeks, 1993] Hoeks, B. (1993). C-program TCRITIC, program for calculating Ising transition temperatures, Dept. of Solid State Chemistry, University of Nijmegen.

[Hollander et al.,] Hollander, F., Boerrigter, S., van de Streek, C., Grimbergen, R., Meekes, H., and Bennema, P. The implication of the topology of connected nets on the morphology of β-monoacid triacylglycerol crystals.

[Jetten et al., 1984] Jetten, L., Human, H., Bennema, P., and van der Eerden, J. (1984). On the observation of the roughening transition of organic crystals, growing from solution. *J. Crystal Growth*, 68:503–516.

[Jollès and Berthou, 1972] Jollès, P. and Berthou, J. (1972). *FEBS Lett.*, 23:21.

[Kaischew and Stranski, 1934] Kaischew, R. and Stranski, I. (1934). über den mechanismus des gleichgewichts kleiner kriställchen ii. *Z. Phys. Chem.*, B26:114–116.

[Kern, 1987] Kern, R. (1987). *Morphology of crystals*, pages 77–206. Terra Scientific Publishing company (TERRAPUB).

[Kossel, 1927] Kossel, W. (1927). Zur theorie des kristallwachstums. *Nachr. Ges. Wiss. Göttingen*, pages 135–143.

[Kosterlitz and Thouless, 1973] Kosterlitz, J. and Thouless, D. (1973). *J. of Phys. C: Condensed Matter*, 6:1181–1203.

[Kosterlitz and Thouless, 1974] Kosterlitz, J. and Thouless, D. (1974). *J. of Phys. C: Condensed Matter*, 7:1046.

[Krug, 1995] Krug, J. (1995). *Scale Invariance, Interfaces, and Non-Equilibrium Dynamics.* Plenum Press.

[Leamy and Gilmer, 1974] Leamy, H. and Gilmer, G. (1974). *J. Crystal Growth*, 24/25:499–502.

[Li et al., 1995] Li, M., Nadarajah, A., and Pusey, M. (1995). *J. Crystal Growth*, 156:121.

[Liu and Bennema, 1993a] Liu, X. and Bennema, P. (1993a). Kinetic roughening in relation to the roughening transition in odd-numbered alkane crystals. *J. Crystal Growth*, 128:69.

[Liu and Bennema, 1993b] Liu, X. and Bennema, P. (1993b). On the morphology of normal alkane crystals with monoclinic structures: theory and observations. *Journal of Applied Crystallography*, 26:229.

[Liu and Bennema, 1994] Liu, X. and Bennema, P. (1994). On the morphology of crystals of triclinic even normal alkanes: theory and observation. *J. Crystal Growth*, 135:209.

[Liu et al., 1994a] Liu, X., Bennema, P., Meijer, L., and Couto, M. (1994a). Ordering of paraffin-like molecules at the solid-fluid interface. *Chem. Phys. Letters*, 220:53–58.

[Liu et al., 1992] Liu, X., Bennema, P., and van der Eerden, J. (1992). Rough-flat-rough transition of crystal surfaces. *Nature*, 356:778–780.

[Liu et al., 1995a] Liu, X., Boek, E., Briels, W., and Bennema, P. (1995a). *Nature*, 374:342–345.

[Liu et al., 1995b] Liu, X., Boek, E., Briels, W., and Bennema, P. (1995b). *J. Chem. Phys.*, 103:3747–3754.

[Liu et al., 1994b] Liu, X., Knops, H., Bennema, P., van Hoof, P., and Faber, J. (1994b). Roughening transition in n-paraffin crystals and the coupled ising-solid-on-solid model. *Philos. Magazine Letters*, 70(1):15–21.

[Liu et al., 1993] Liu, X., van Hoof, P., and Bennema, P. (1993). Surface roughening of normal alkane crystals: solvent dependent critical behavior. *Phys. Rev. Letters*, 71(1):109.

[Madsen, 1976] Madsen, H. L. (1976). Rapid measurement of very low growth rates of birefringent crystals. *J. Crystal Growth*, 32:84–88.

[Madsen and Boistelle, 1979] Madsen, H. L. and Boistelle, R. (1979). Growth kinetics of the (001) faces of hexatriacontane ($c_{36}h_{74}$ in solution. *J. Crystal Growth*, 46:681.

[Mazzeo et al., 1995] Mazzeo, G., Carlon, E., and van Beijeren, H. (1995). Phase diagram of the two component body-centered solid-on-solid model. *Phys. Rev. Letters*, 74:1391–1395.

[Mazzeo et al., 1992] Mazzeo, G., Jug, G., Levi, A., and Tosatti, E. (1992). *Surface Science*, 273:237.

[Mazzeo et al., 1994] Mazzeo, G., Jug, G., Levi, A., and Tosatti, E. (1994). *Phys. Rev. B*, 49:7625.

[Meekes et al., 1998] Meekes, H., Bennema, P., and Grimbergen, R. (1998). On the prediction of crystal morphology. II. symmetry rougheni ng of pairs of connected nets. *Acta Cryst. A*, 54:501–510.

[MSI,] MSI. Molecular Simulations Inc., San Diego CA, Cerius^2 software (1997) version 3.0.

[Müller-Krumbhaar, 1978] Müller-Krumbhaar, H. (1978). *Current Topics in Material Science*, pages 1–46. North Holland.

[Nadarajah et al., 1995] Nadarajah, A., Forsythe, E., and Pusey, M. (1995). *J. Crystal Growth*, 151:163–172.

[Niggli, 1920] Niggli, P. (1920). The relation between the growth forms and the structure of crystals. *Z. Anorg. Chem.*, pages 55–81.

[Nolden and van Beijeren, 1994] Nolden, I. and van Beijeren, H. (1994). *Phys. Rev. B*, 49:17224.

[Onsager, 1944] Onsager, L. (1944). Two-dimensional model with an order-disorder transition. *Phys. Rev.*, 65:117–149.

[Pavlovska and Nenow, 1972] Pavlovska, A. and Nenow, D. (1972). *J. Crystal Growth*, 12:9–12.

[Pechhold et al., 1966] Pechhold, W., Dollhopf, W., and Engel, A. (1966). *Acustica*, 17:61.

[Plomp et al.,] Plomp, M., van Hoof, P., and van Enckevort, W. to be published.

[Prestipino et al., 1995] Prestipino, S., Santoro, G., and Tosatti, E. (1995). *Phys. Rev. Letters*, 75:4468–4471.

[Pusey, 1991] Pusey, M. (1991). Estimation of the initial equilibrium constants in the formation of tetragonal nuclei. *J. Crystal Growth*, 110:60–65.

[Rao and Rao, 1978] Rao, C. and Rao, K. (1978). *Phase transitions in solids (an approch to the study of the chemistry and physics of solids)*, page 21. McGraw-Hill, New York.

[Rijpkema et al., 1982] Rijpkema, J., Knops, H., Bennema, P., and van der Eerden, J. (1982). Determination of the ising critical temperature of f-slices with an application to garnet. *J. Crystal Growth*, 61:295–306.

[Robinson and Scott, 1967] Robinson, P. and Scott, H. (1967). *J. Crystal Growth*, 1:187–194.

[Rommelse and den Nijs, 1987] Rommelse, K. and den Nijs, M. (1987). *Phys. Rev. Letters*, 59:2578–2581.

[Schaftenaar, 1992] Schaftenaar, G. (1992). MOLDEN: A portable electron density program. *QCPE Bulletin*, 12:3.

[Shekunov and Latham, 1996] Shekunov, B. and Latham, R. (1996). Growth anisotropy of n-methylurea crystals in methanol. *J. Phys. Chem.*, 100:5464.

[Shugard et al., 1978] Shugard, W., Weeks, J., and Gilmer, G. (1978). *Phys. Rev. Letters*, 41:1399–1402.

[Simon and Boistelle, 1981] Simon, B. and Boistelle, R. (1981). Crystal growth from low temperature solutions. *J. Crystal Growth*, 52:779.

[Simon et al., 1974a] Simon, B., Grassi, A., and Boistelle, R. (1974a). Cinétique de croissance de la face (110) de la paraffine $c_{36}h_{74}$ en solution ii. croissance en présence d'un inhibiteur la dioctadécylamine $(c_{18}h_{37})_2nh$. *J. Crystal Growth*, 26:90.

[Simon et al., 1974b] Simon, B., Grassi, A., and Boistelle, R. (1974b). Cinétique de croissance de la face (110) de la paraffine $c_{36}h_{74}$ en solution i. croissance en mileu pur. *J. Crystal Growth*, 26:77.

[Smith, 1953] Smith, A. (1953). The structure of the normal paraffin hydrocarbons. *J. Chem. Phys.*, 21:2229.

[Stranski, 1928] Stranski, I. (1928). Zur theorie des kristallswachstums. *Z. Phys. Chem.*, A136:259–278.

[Stranski and Kaischew, 1934] Stranski, I. and Kaischew, R. (1934). über den mechanismus des gleichgewichts kleiner kriställchen i. *Z. Phys. Chem.*, B26:100–113.

[Strom, 1980] Strom, C. (1980). Graph-theoretic construction of periodic bond chains i. general case. *Z. Kristallogr.*, 153:99–113.

[Strom, 1981] Strom, C. (1981). Graph-theoretic construction of periodic bond chains ii. ionic case. *Z. Kristallogr.*, 154:31–43.

[Strom, 1985] Strom, C. (1985). Finding f faces by direct chain generation. *Z. Kristallogr.*, 172:11–24.

[Strom and Bennema, 1997a] Strom, C. and Bennema, P. (1997a). Combinatorial compatability as habit-controlling factor in lysozyme crystallization. ii. morphological evidence for tetrameric growth units. *J. Crystal Growth*, 173:159–166.

[Strom and Bennema, 1997b] Strom, C. and Bennema, P. (1997b). Combinatorial compatability as habit-controlling factor in lysozyme crystallization. i. monomeric and tetrameric f faces derived graph-theoretically. *J. Crystal Growth*, 173:150–158.

[Strom and Bennema, 1998] Strom, C. and Bennema, P. (1998). to be published.

[Strom and Hartman, 1989] Strom, C. and Hartman, P. (1989). Comparison between gaussian and exponential charge distributions in ewald surface potentials and fields: Nacl, aragonite and, phlogopite. *Acta Cryst. A*, 45:371–380.

[Strom and Heijnen, 1981] Strom, C. and Heijnen, W. (1981). *J. Crystal Growth*, 51:534–540.

[Sun et al., 1990] Sun, B., Hartman, P., Woensdregt, C., and Schmidt, H. (1990). *J. Crystal Growth*, 100:605–614.

[Sunagawa, 1977] Sunagawa, I. (1977). Natural crystallization. *J. Crystal Growth*, 42:214–223.

[Swendsen, 1977] Swendsen, R. (1977). *Phys. Rev. B*, 15:5421–5431.

[Swendsen, 1978] Swendsen, R. (1978). Correlation functions in xy model and step free energy in roughening models. *Phys. Rev. B*, 17:3710–3713.

[Tables, 1969] Tables (1969). *International Tables for X-Ray Crystallography*, volume 1. The Kynoch Press, Birmingham, England.

[Turner, 1971] Turner, W. (1971). Normal alkanes. *Ind. Eng. Chem. Prod. Res. Develop.*, 10(3):238.

[van Beijeren, 1977] van Beijeren, H. (1977). Exactly solvable model for the roughening transition of a crystal surface. *Phys. Rev. Letters*, 38:993–996.

[van Beijeren and Nolden, 1986] van Beijeren, H. and Nolden, I. (1986). *Topics in current physics, structure and Dynamics of Surfaces II*, volume 43, pages 259–300. Springer Verlag.

[van den Berg, 1997] van den Berg, E. (1997). PhD thesis, University of Nijmegen.

[van der Eerden, 1976] van der Eerden, J. (1976). Roughening transition in mean-field and pair approximation of ising models. *Phys. Rev. B*, 13:4942–4948.

[van der Eerden, 1993] van der Eerden, J. (1993). *Handbook of Crystal Growth*, volume 1, pages 307–475. North Holland Publishing Company.

[van der Eerden et al., 1977] van der Eerden, J., van Leeuwen, C., Bennema, P., van der Kruk, W., and Veltman, B. T. (1977). *Journ. of Applied Physics*, 48:2124.

[van der Heijden, 1992] van der Heijden, A. (1992). PhD thesis, University of Nijmegen.

[van der Voort, 1991a] van der Voort, E. (1991a). *J. Crystal Growth*, 110:662–668.

[van der Voort, 1991b] van der Voort, E. (1991b). *J. Crystal Growth*, 110:653–661.

[van Enckevort and Bennema, 1998] van Enckevort, W. and Bennema, P. (1998). to be published.

[van Hoof et al., 1998a] van Hoof, P., Grimbergen, R., van Enckevort, W., Meekes, H., and Bennema, P. (1998a). Morphology of orthorhombic n-paraffin crystals: a comparison between theory and experiment. *J. Crystal Growth*, 191:861–872.

[van Hoof et al., 1998b] van Hoof, P., van Enckevort, W., Schoutsen, M., Bennema, P., and Liu, X. (1998b). Change of morphology and growth mechanism of thin n-paraffin crystals induced by homologous impurities. *J. Crystal Growth.* accepted for publication.

[van Leeuwen, 1979] van Leeuwen, C. (1979). *J. Crystal Growth*, 46:91.

[van Veenendaal et al., 1998] van Veenendaal, E., van Hoof, P., van Suchtelen, J., van Enckevort, W., and Bennema, P. (1998). to be published.

[Vekilov and Rosenberger, 1996] Vekilov, P. and Rosenberger, F. (1996). *J. Crystal Growth*, 158:540–551.

[Vilfan and Villain, 1988] Vilfan, I. and Villain, J. (1988). *Surface Science*, 199:2165.

[Vilfan and Villain, 1990] Vilfan, I. and Villain, J. (1990). *Phys. Rev. Letters*, 65:1830.

[Villain, 1991] Villain, J. (1991). *J. Phys. Fr. I*, 1:19.

[Voets et al., 1998] Voets, J., Gerritsen, J., Grimbergen, R., and van Kempen, H. (1998). *Surface Science.* accepted for publication.

[Vogels et al., 1990] Vogels, L., Marsman, H., and Verheijen, M. (1990). *J. Crystal Growth*, 100:439.

[Volmer and Weber, 1926] Volmer, M. and Weber, A. (1926). Keimbildung in übersättigen gebilden. *Z. Phys. Chem.*, 119:277–301.

[Weeks, 1986] Weeks, J. (1986). *Ordering in strongly fluctuating condensed matter systems*, page 293. Ed. T. Riste, Plenum Press N.Y.

[Wells, 1946] Wells, A. (1946). Crystal habit and internal structure. *Phil. Mag.*, 37:184.

[Winkler and Dunitz, 1975] Winkler, F. and Dunitz, J. (1975). *Acta Cryst. B*, 31:268.

[Woensdregt, 1990] Woensdregt, C. (1990). PhD thesis, University of Utrecht.

[Woodraska and Jaszczak, 1997a] Woodraska, D. and Jaszczak, J. (1997a). *Phys. Rev. Letters*, 78:258–261.

[Woodraska and Jaszczak, 1997b] Woodraska, D. and Jaszczak, J. (1997b). *Surface Science*, 374:319–332.

[Wulff, 1901] Wulff, G. (1901). *Z. Kristallogr. Miner.*, 34:449–531.

Summary

The work in this thesis can be divided into two parts:

- Theory: chapter 2-5
- Experiments and interpretation: chapter 6-11

In chapter 2 the Hartman-Perdok theory is reconsidered and an F-face is redefined as a crystal face having a roughening transition temperature larger than zero Kelvin(T^R_{hkl}>0). It is demonstrated that a crystallographic orientation (hkl) which contains more than one connected net (i.e. surface configuration) may have a zero step free energy. When a pair of symmetry related connected nets gives rise to a zero step energy this is called *symmetry roughening*. The results of a connected net analysis are linked to the results of simple statistical thermodynamical surface models as described in literature. Finally, it is shown that the presence of multiple connected nets can have important implications for the prediction of the theoretical equilibrium and growth morphology.

In chapter 3 all symmetry relations between connected nets are categorized and their implications regarding symmetry roughening are discussed. It is shown that the cases of symmetry roughening are in a sense complementary to the classical BFDH law. Moreover, a distinction is made between microscopic and macroscopic symmetry roughening. Microscopic roughening is, like macroscopic roughening, caused by a symmetry related pair of connected nets, but does not give rise to a macroscopic roughening of the face.

The growth and equilibrium behaviour of crystal faces containing (symmetry) related multiple connected nets is studied in chapter 4. The results of a connected net analysis are compared with the results of Monte Carlo (MC) simulations. Apart from the well-known flat and rough surface phases also disordered flat (DOF) were identified for specific surface bonding structures. These surface phases may influence the growth behaviour of a crystal face dramatically. This is illustrated by calculation of the relative growth rates R_{hkl} of crystal faces (hkl) as a function of supersaturation by MC simulations. Specific crystal faces containing multiple connected nets can show anomalous growth behaviour due to (pseudo) symmetry roughening. Moreover, it is demonstrated that the classical recipes $R_{hkl} \propto 1/d_{hkl}$ and $R_{hkl} \propto E^{att}_{hkl}$ fail completely for these types of face. Using the relative growth rates obtained from MC simulations it is possible to predict the growth morphology as a function of supersaturation.

In chapter 5 the phase diagram for the {011} faces of naphthalene is derived from a simplified restricted SOS model. The phase diagram consists of a flat, DOF and rough region. The DOF phase is separated from the flat phase by a preroughening transition line. MC simulations confirm the result of the statistical thermodynamical surface model and

show a maximum in the specific heat $c(T)$ at $T{=}T^{pr}$. At the preroughening temperature the effective step energy decreases drastically which causes a significant lowering of the nucleation barrier. Therefore, the growth rate of a face in the DOF phase will be relatively high at low supersaturation. However, MC simulations indicate that such a face still grows by a layer-by-layer growth mechanism.

Experimental evidence for the presence of a preroughening transition is presented in chapter 6. Vapour growth experiments of naphthalene and anthracene were done and anomalous growth behaviour was found for the {011} faces of naphthalene. These faces could be observed at very low supersaturations at 283 K. On increasing the supersaturation, the faces disappeared very rapidly already at very low supersaturation due to a sudden increase in growth rate. This behaviour is explained by the presence of a DOF phase.

Chapter 7 describes the results of a rigorous connected net analysis for orthorhombic n-paraffins. The complete set of connected nets is treated and all symmetry relations are analyzed. As a result it is found that the side face structure of n-paraffin crystals may, apart from the {110} faces, also show {100}, {010} and {111} faces.

The experimentally observed morphology of orthorhombic n-paraffin crystals grown from solution, melt and the vapour are compared with the theoretical prediction in chapter 8. For the first time flat {010}, {100} and {111} faces were observed on crystals grown from the vapour. The large aspect ratio of crystals grown from solution is explained in terms of the step free energy of those faces.

In chapter 9 the theoretical morphology of the industrially very important compound ϵ-caprolactam (a precursor for nylon-6) is derived. Due to the presence of hydrogen-bonded pairs of molecules in the crystal lattice the connected net analysis was done assuming both monomers and hydrogen-bonded dimers as growth units. The results of the two analyses are very similar. It is argued that, due to the presence of two stacked connected nets, the {110} faces may grow with half layers with a thickness d_{220} dependent on the growth conditions. Experimental data from literature show that the presence of these faces depends on the solvent from which the ϵ-caprolactam crystals are grown.

The experimentally observed dependence of the supersaturation of the morphology of the protein lysozyme is explained in chapter 10. The crystals are bounded by {110} and {101} faces. At low supersaturations needles (along the c-axis) are observed, whereas at higher supersaturations block-like crystals are found which is in agreement with the attachment energy prediction. A detailed connected net analysis based on the crystal graph which contains only three bonds X, Y and Z predicts that pseudo symmetry roughening may occur for a certain bond ratios $X{:}Y{:}Z$. Based on the step energies of the three F-faces {110}, {101} and {111} it is possible to understand the dependence of the morphology on the supersaturation. The results are in agreement with previously published MC simulation data. Moreover, the experimentally observed surface structure of the {110} and {101} faces can be explained from the results of the analysis. There are strong indications that, depending on the temperature, DOF surface phases might occur for the faces of lysozyme.

Chapter 11 treats the growth morphology of a series of cesium halides (CsF, CsCl, CsBr and CsI). Vapour growth experiments show a very distinct transition from a cubic ({001}, at high temperature) to a dodecahedral ({110}, at low temperature) morphology

as a function of temperature and supersaturation. It appears that the temperature is the critical parameter which determines whether the transition is observed. Moreover, the transition temperature depends on the halide. A connected net analysis yields the {001}, {110} and {111} faces as F-forms when only first nearest neighbour bonds are taken into account. In principle the connected nets found for {001} and {111} faces would cause symmetry roughening. However, when (repulsive) next nearest neighbour bonds are considered, it becomes clear that the {001} faces are stabilized by a c2x2 reconstruction. The relative growth rates of the {001} and {110} faces as a function of temperature were determined by MC simulations at a fixed supersaturation. The simulation results confirm the experimentally observed transition from a cubic into a dodecahedral morphology when the temperature is increased. Moreover, our MC results are in agreement with the Ising transition temperatures as given by the phase diagram of the statistical thermodynamical staggered BCSOS model. It is concluded that the observed dependence of the temperature might be related to a phase transition of the {001} faces from a reconstructed c2x2 into a deconstructed rough or DOF phase dependent on the anisotropy.

Samenvatting

Het in dit proefschrift beschreven onderzoek kan worden verdeeld in twee delen

- Theorie: hoofdstuk 2-5
- Experimenten and interpretatie: hoofdstuk 6-11

In hoofdstuk 2 wordt de Hartman-Perdok theorie beschouwd en een F-vlak gedefinieerd als een kristalvlak met een verruwingstemperatuur hoger dan nul graden Kelvin (T^R_{hkl}>0). Er wordt aangetoond dat een kristallografische richting (hkl) die meer dan één connected net (oppervlakte configuratie) bevat, een stap energie kan hebben van nul. Wanneer een paar van connected netten een stap energie van nul veroorzaakt, wordt dat aangeduid met de term *symmetrieverruwing*. De resultaten van een connected analyse worden gecombineerd met de resultaten van eenvoudige statistisch thermodynamische oppervlaktemodellen zoals beschreven in de literatuur. Tenslotte wordt aangetoond dat de aanwezigheid van meerdere connected netten verstrekkende gevolgen kan hebben met betrekking tot het voorspellen van de theoretische evenwichts- en groeimorfologie.

In hoofdstuk 3 worden alle symmetrierelaties tussen connected netten gecategorizeerd en de implicaties met betrekking tot symmetrieverruwing bediscussieerd. Er wordt aangetoond dat gevallen van symmetrieverruwing complementair zijn met de klassieke BFDH wet. Verder wordt een onderscheid gemaakt tussen microscopische en macroscopische symmetrieverruwing. Microscopische verruwing wordt, net zoals macroscopische verruwing, veroorzaakt door een symmetrie gerelateerd paar van connected netten, maar leidt niet tot macroscopische verruwing van een kristalvlak.

Het evenwichts- en groeigedrag van kristalvlakken die (symmetrie gerelateerde) connected netten bevatten wordt onderzocht in hoofdstuk 4. De resultaten van een connected net analyse worden vergeleken met de resultaten van Monte Carlo (MC) simulaties. Afgezien van de bekende vlakke en ruwe oppervlakte fasen zijn ook wanordelijk vlakke (DOF) fasen aangetoond voor specifieke oppervlaktebindingsstructuren. Deze oppervlakte fasen kunnen het groeigedrag van een kristalvlak enorm beïnvloeden. Dat wordt geïllustreerd aan de hand van de berekening van relatieve groeisnelheden R_{hkl} van kristalvlakken (hkl) als funktie van de oververzadiging met behulp van MC simulaties. Specifieke kristalvlakken die meerdere connected netten bevatten kunnen een afwijkend groeigedrag vertonen als gevolg van (pseudo) symmetrieverruwing. Verder wordt aangetoond dat de klassieke recepten $R_{hkl} \propto 1/d_{hkl}$ en $R_{hkl} \propto E^{att}_{hkl}$ compleet falen voor dit type kristalvlak. Wanneer de relatieve groeisnelheden van de MC simulaties worden gebruikt is het mogelijk om de groeimorfologie te voorspellen als funktie van de oververzadiging.

In hoofdstuk 5 wordt het fasediagram van de {011} vlakken van naftaleen afgeleid uit een vereenvoudigd SOS model. Het fasediagram bestaat uit een vlakke, DOF en ruwe fase. De DOF fase is gescheiden van de vlakke fase door een pre-verruwingsovergangslijn. MC simulaties bevestigen het resultaat dat verkregen is met het statistisch thermodynamische oppervlaktemodel en laten een maximum in de specifieke warmte $c(T)$ zien bij $T{=}T^{pr}$. Op de pre-verruwingstemperatuur neemt de effectieve stap energie drastisch af wat resulteert in een behoorlijke verlaging van de nucleatiebarrière. Daardoor zal de groeisnelheid van een vlak in de DOF fase relatief hoog zijn bij lage oververzadiging. MC simulaties laten echter zien dat een dergelijk vlak nog steeds groeit via een laag-voor-laag mechanisme.

Experimenteel bewijs voor de aanwezigheid van een pre-verruwingsovergang wordt gepresenteerd in hoofdstuk 6. Groeiexperimenten van naftaleen en antraceen vanuit de gasfase zijn uitgevoerd waarbij een afwijkend groeigedrag werd gevonden voor de {011} vlakken van naftaleen. Deze vlakken zijn alleen bij hele lage oververzadigingen en een temperatuur van 283 K waargenomen. Wanneer de oververzadiging werd opgevoerd, verdwenen de vlakken zeer snel reeds bij een lage oververzadiging als gevolg van een hoge relatieve groeisnelheid. Dit gedrag kan worden verklaard met de aanwezigheid van een DOF fase.

Hoofdstuk 7 bevat de resultaten van een rigoreuze connected net analyse van orthorombische n-paraffines. De complete set van connected netten wordt behandeld en geanalyseerd. Uit de resultaten van de analyse blijkt dat als zijvlakken op paraffine kristallen, afgezien van {110} vlakken, tevens {100}, {010} en {111} vlakken te verwachten zijn.

De experimenteel waargenomen morfologie van orthorombische n-paraffine kristallen die zijn gegroeid uit een oplossing, smelt en damp wordt vergeleken met de theoretische voorspelling in hoofdstuk 8. Voor het eerst zijn {010}, {100} en {111} vlakken waargenomen op kristallen die zijn gegroeid uit de gasfase. De geringe dikte van de kristallen die uit een oplossing zijn gegroeid wordt verklaard in termen van stap vrije energieën van de vlakken.

In hoofdstuk 9 wordt de theoretische morfologie van het industrieel belangrijke ϵ-caprolactam (een precursor voor nylon-6) voorspeld. Door de aanwezigheid van waterstofbrug gebonden moleculen in het kristal, is de connected net analyse gedaan met de aanname dat zowel monomeren als dimeren als groeieenheid kunnen fungeren. Het resultaat van deze twee analyses is vergelijkbaar. Verder wordt aangetoond dat de {110} vlakken kunnen groeien met halve lagen, vanwege de aanwezigheid van twee halve lagen met een dikte van d_{220}, afhankelijk van de groeicondities. Experimentele gegevens uit de literatuur laten zien dat de aanwezigheid van de {110} vlakken afhangt van het oplosmiddel waaruit de ϵ-caprolactam kristallen zijn gegroeid.

De experimenteel waargenomen relatie tussen de oververzadiging en de waargenomen morfologie van het eiwit lysozyme wordt verklaard in hoofdstuk 10. De morfologie van de lysozyme kristallen bestaat uit {110} en {101} vlakken. Bij lage oververzadiging worden naalden (in de richting van de c-as) waargenomen, terwijl bij hogere oververzadiging blok-vormige kristallen worden gevonden die overeenkomen met de theoretische attachment energie voorspelling van de morfologie. Een gedetailleerde connected net analyse gebaseerd op een kristal-graph met drie bindingstypen X, Y en Z, voorspelt dat pseudo-symmetrieverruwing kan optreden voor bepaalde bindingsverhoudingen $X{:}Y{:}Z$. Het experimentele feit dat de morfologie sterk afhangt van de oververzadiging kan worden be-

grepen door een analyse van de stap energieën van de {110}, {101} en {111} vlakken. De resultaten zijn in overeenstemming met eerder gepubliceerde MC simulatie data. Verder is het mogelijk om de experimenteel waargenomen oppervlaktestructuur van de {110} en {101} vlakken te verklaren met de resultaten van de analyse. Er zijn sterke aanwijzingen dat, afhankelijk van de temperatuur, DOF oppervlaktefasen kunnen voorkomen bij de vlakken van lysozyme.

Hoofdstuk 11 behandelt de groeimorfologie van een serie cesium halide verbindingen (CsF, CsCl, CsBr en CsI). Gasfase groeiexperimenten laten een scherpe overgang zien van een kubische morfologie ({001}) bij hoge temperatuur naar een dodecaëder morfologie ({110}) bij lage temperatuur. Het blijkt dat de temperatuur een kritische parameter is die bepaalt of de overgang wordt waargenomen. Verder hangt de overgangstemperatuur af van het halide. Een standaard connected net analyse geeft de {001}, {110} en {111} vlakken als F-vlakken wanneer alleen eerste-buurinteracties worden meegenomen. In principe zouden de connected netten voor {001} en {111} symmetrieverruwing veroorzaken. Wanneer echter de (repulsieve) tweede-buurinteracties worden meegenomen wordt het duidelijk dat de {001} vlakken worden gestabiliseerd door een c2x2 oppervlaktereconstructie. De relatieve groeisnelheden van de {001} en {110} vlakken als funktie van de temperatuur (bij constante oververzadiging) zijn berekend met MC simulaties. De simulatieresultaten bevestigen de experimenteel waargenomen overgang van een kubische naar een dodecaëder morfologie wanneer de temperatuur wordt verhoogd. De MC simulatieresultaten zijn verder in overeenstemming met de Ising overgangstemperaturen zoals die worden beschreven in de literatuur voor het statistisch thermodynamische BCSOS model. Er zijn aanwijzingen dat de waargenomen temperatuurafhankelijkheid gerelateerd kan worden aan een fase overgang van de {001} vlakken van een c2x2 reconstructed fase naar een gedeconstrueerde ruwe of DOF fase afhankelijk van de anisotropie.

List of Publications

- R.J.W. Schuurman, R.F.P. Grimbergen, H.W. Scheeren and R.J.M. Nolte, *Receptors functionalized with chiral aza-crown ether rings. Attempted enantioselective catalysis of a Michael addition reaction*, Recl. Trav. Chim. Pays-Bas **115** (1996), 357-362

- R.J.W. Schuurman, A. v.d. Linden, R.F.P. Grimbergen, R.J.M. Nolte and H.W. Scheeren, *Effect of Branching in Alkylgroups of Tertiary Amines on Their Performance as Catalysts in the High Pressure Promoted Baylis-Hillman Reaction*, Tetrahedron **52** (1996), 8307-8314

- C.S. Strom, R.F.P. Grimbergen, I.D.K. Hiralal, B.G. Koenders and P. Bennema, *Growth layers I. Derivation of F-slices illustrated by sodium oxalate*, J. Cryst. Growth **149** (1995), 96-106

- C.S. Strom, R.F.P. Grimbergen, I.D.K. Hiralal, B.G. Koenders and P. Bennema, *Growth layers II. Comparison of the theoretical and experimental morphology of sodium oxalate*, **149** (1995), 107-112

- L.P.J. Vogels, R.F.P. Grimbergen, C.S. Strom, P. Bennema, S.A. Roberts and R.F. Blanks, *On the theoretical and experimental morphology of paraxylene*, Chem. Phys. **203** (1996), 69-80

- R.F.P Grimbergen and P. Bennema, *An Automated Method for PBC Analyses applied to Benzoic Acid. A Comparison between the Monomer and Dimer Analysis*, Proceedings of the Third International Workshop on Crystal Growth of Organic Materials (CGOM III), august 27-31 (1995), Washington DC

- R.F.P. Grimbergen, H. Meekes and P. Bennema, *Prediction of Crystal Morphology in relation to Temperature and Supersaturation*, Proceedings of the Fourth International Workshop on Crystal Growth of Organic Materials (CGOM IV), september 17-19 (1997), Bremen

- P.J.C.M. van Hoof, L.J.P. Vogels and R.F.P. Grimbergen, *On the roughening transition of anisotropic (pseudo) hexagonal lattices*, accepted for publication in J. Cryst. Growth

- J. Voets, J.W. Gerritsen, R.F.P. Grimbergen and H. van Kempen, *Chain Length Dependent Structure of Alkanethiols Forming Dimers on Au (111)*, accepted for publication in Surface Science

- R.F.P. Grimbergen, H. Meekes, P. Bennema, C.S. Strom and L.J.P. Vogels, *On the Prediction of Crystal Morphology I: the Hartman-Perdok Theory revisited* (Chapter 2), accepted for publication in Acta Cryst. A.

- H. Meekes, P. Bennema and R.F.P. Grimbergen, *On the Prediction of Crystal Morphology II: Symmetry Roughening of Pairs of Connected Nets* (Chapter 3), accepted for publication in Acta Cryst. A.

- R.F.P. Grimbergen, P. Bennema and H. Meekes *On the Prediction of Crystal Morphology III: Growth and Equilibrium Behaviour of Crystal Faces containing Multiple Connected Nets* (Chapter 4), submitted for publication to Acta Cryst. A.

- R.F.P. Grimbergen, H. Meekes, P. Bennema, H.J.F. Knops and M. den Nijs, *Preroughening in Organic Crystals* (Chapter 5), submitted for publication to Phys. Rev. B.

- R.F.P. Grimbergen, M.F. Reedijk, H. Meekes and P. Bennema, *Growth Behaviour of Crystal Faces containing Symmetry Related Connected Nets: a Case Study of Naphthalene and Anthracene* (Chapter 6), accepted for publication in J. Phys. Chem.

- R.F.P. Grimbergen, P.J.C.M. van Hoof, H. Meekes and P. Bennema, *Morphology of Orthorhombic n-Paraffin Crystals I: the Influence of Multiple Connected Nets* (Chapter 7), accepted for publication in J. Cryst. Growth

- P.J.C.M. van Hoof, R.F.P. Grimbergen, H. Meekes, W.J.P. van Enckevort and P. Bennema, *Morphology of Orthorhombic n-Paraffin Crystals II: a Comparison between Theory and Experiments* (Chapter 8), accepted for publication in J. Cryst. Growth

- R.F.P. Grimbergen and E.P.G. van den Berg, *Theoretical Morphology of ϵ-Caprolactam: Monomer versus Dimer Analysis* (chapter 9), submitted for publication to J. Cryst. Growth

- R.F.P. Grimbergen, E.S. Boek and H. Meekes, *Explanation for the Supersaturation Dependence of the Morphology of Lysozyme Crystals* (chapter 10), to be submitted for publication

- R.F.P. Grimbergen, G. Bögels and H. Meekes, *The Growth Morphology of Cesium Halide Crystals: Evidence for Surface Phase Transitions* (chapter 11), to be submitted for publication

Curriculum Vitae

Naam: Reinier Grimbergen
Geboren: 8 december 1969 te Nijmegen

Opleiding:

1982 - 1988: Stedelijk Gymnasium, Nijmegen; ongedeeld VWO
1988 - 1993: Studie Scheikunde aan de Katholieke Universiteit Nijmegen
Hoofdrichting: Fysisch Organische Chemie (Prof. dr. R. Nolte)
Stage-onderwerp: Synthese en karakterisatie van chirale katalysatoren (synzymen) en het testen van de katalytische activiteit
Nevenrichting: Computational Chemistry (Dr. Noordik)
Stage-onderwerp: Modelleren van binding substraten in chirale holte-moleculen
1994 - 1998: Promotie onderzoek bij de vakgroep Vaste Stof Chemie
in dienst van de Stichting voor de Technische Wetenschappen (STW/NWO)
Onderzoeks-onderwerp: Voorspelling van vormen van kristallen met behulp van computerprogramma's in verband met technische zuiveringsmethodes
Promotor: Prof. dr. P. Bennema

Onderwijstaken:
- Assistent practicum Synthese II (1991)
- Assistent practicum Fysische Chemie (1992)
- Werkcollege-assistent (1994-1997)
- Begeleiding van een hoofdvakstudente (1996/1997)

Per 1 maart 1998 werkzaam bij de sectie FC-DT van DSM Research in Geleen